Engineered Approaches to Querying the Microenvironment of Cancer Metastasis

by

Nathan E. Reticker-Flynn

B.S. Mechanical Engineering
Tufts University, 2006

S.M. Mechanical Engineering
Massachusetts Institute of Technology, 2008

SUBMITTED TO THE HARVARD-MIT DIVISION OF HEALTH SCIENCES AND TECHNOLOGY IN PARTIAL FULFILLMENT OF THE REQUIREMENTS FOR THE DEGREE OF

DOCTOR OF PHILOSOPHY IN BIOMEDICAL ENGINEERING
AT THE
MASSACHUSETTS INSTITUTE OF TECHNOLOGY
JUNE 2013

Signature of Author: Signature redacted

Harvard-MIT Division of Health Sciences and Technology
May 20, 2013

Certified by: Signature redacted

Sangeeta N. Bhatia, MD, PhD
John J. and Dorothy Wilson Professor of Health Sciences and Technology &
Electrical Engineering and Computer Science, MIT
Thesis Supervisor

Accepted by: Signature redacted

Emery N. Brown, MD, PhD
Professor of Health Sciences and Technology and
Professor of Computational Neuroscience, MIT
Director, Harvard-MIT Program in Health Sciences and Technology

Engineered Approaches to Querying the Microenvironment of Cancer Metastasis

by Nathan E. Reticker-Flynn

Submitted to the Harvard-MIT Division of Health Sciences and Technology on May 28, 2013 in Partial Fulfillment of the Requirements for the Degree of Doctor of Philosophy in Biomedical Engineering

Abstract

Cancer metastasis is the underlying mechanism of 90% of cancer-related deaths, yet few therapeutics exist that directly target it. Part of this scarcity is attributable to a general lack of knowledge with regards to the underlying mechanisms that mediate traversal of the sequential steps required for malignant dissemination. Recently, biologists and clinicians have gained appreciation for the role that the microenvironment plays in promoting or inhibiting metastasis.

This thesis sought to expand our understanding of the involvement of extracellular matrix (ECM) interactions during metastasis through the development and use of a novel ECM microarray screening platform. This platform consists of 768 unique single and pairwise combinations spotted in quintuplicate as 150μm features onto polyacrylamide coated glass slides. Cells are seeded onto these arrays and queried for their adhesion, proliferation, and marker expression using automated fluorescence microscopy in conjunction with automated cell counting and image analysis. In the first part of this thesis, this platform is used in conjunction with a mouse model of lung adenocarcinoma metastasis ($Kras^{LSL\text{-}G12D/+};p53^{flox/flox}$) where distinct stages of metastasis are defined by characteristic cell lines derived from these mice. Hierarchical clustering of the adhesion profiles revealed conserved alterations in ECM adhesion signatures that correlate with metastasis. Additionally, they identify a role for combinations of ECM composed of fibronectin with any of galectin-3, galectin-8, or laminin. In the next part of this thesis, these molecules are investigated for their involvement in mice bearing the autochthonous tumors or in humans with lung cancer. The integrin $\alpha 3\beta 1$ is found to mediate adhesion to the fibronectin-galectin combinations *in vitro* and promote metastasis *in vivo.* Subsequently, this thesis investigates the role of carbohydrate-mediated interactions in promoting galectin adhesion. The oncofetal T-Antigen glycan motif is found to be increasingly expressed on cells with elevated metastatic potential, and is found to be the result of aberrant glycosyltransferase activity. Finally the role of galectin-3 in the metastatic niche and its presentation on bone marrow derived cells recruited to tumors is investigated.

The results of this thesis suggest a role for novel phenotypic screening platforms in investigating regulation of the cancer microenvironment. Additionally, we extend these studies to the role of ECM in the epithelial-mesenchymal transition (EMT) and lay the groundwork for the development of nanoparticle-based therapeutics targeting the conserved glycan-ECM interactions. Such technologies will likely prove useful to study other disease mechanisms as well as identify novel biomarkers.

Thesis Supervisor: Sangeeta N. Bhatia
Title: John J. and Dorothy Wilson Professor of Health Sciences and Technology & Electrical Engineering and Computer Science

Acknowledgements

I am deeply thankful for the amazing support that I have received over my graduate career at MIT. I would like to start by thanking my incredibly inspiring mentor, Sangeeta Bhatia. As is evident to anyone who meets her, Sangeeta is an incredibly bright researcher and professor whose enthusiasm for science is immediately evident. I cannot speak highly enough about the degree to which Sangeeta has fostered my development toward becoming an independent scientist. Her support, mentorship, feedback, and ability to know when to let me fail and when to intervene is something I will cherish and continue to benefit from for the rest of my life.

I have been incredibly fortunate to have one of the most insightful committees possible. I will not speak to their brilliance or the significance of their contributions to science, as much of this is evident simply from perusing the 'Introductions' and 'References' sections of this thesis. What has been most outstanding, however, has been their complete willingness to provide extensive feedback on my research despite their many obligations. Dr. Richard Hynes has opened his lab to me and provided me with feedback not only on the details of metastasis and ECM, but also general research philosophies. Dr. J. Christopher Love has provided me with much useful advice particularly with regards to the platform development, and Dr. Daniel Haber has provided insights both from a clinical standpoint and a basic research standpoint. Furthermore, his kind demeanor has helped to bolster my confidence starting from the early days of my involvement with Stand Up to Cancer.

In addition to her many obvious skills and contributions, is Sangeeta's, perhaps overlooked, ability to identify incredible scientists who are also outstanding human beings. As a result, I have been blessed to work with some of the greatest labmates a PhD student could ask for. To Geoff and Alice, thanks for being amazing role models and friends. To Kartik, Kevin, Cheri, and Meghan, thanks for always keeping it fun since the day we all got here. To the younger graduate students – Shengyong, Justin, Alex, Andrew, and Vyas – you guys are amazingly brilliant despite your humility. I can't wait to see how you change the world. To the many postdocs who have helped guide me over the years especially Dave, Gabe, Kelly, Sandra, Greg, and Rob, you have taught me so much despite never having any official collaborations. To the newer postdocs – Ester, Arnout, Sabine, Tal, and Kathleen – thanks for all of the fun we've had and for even pretending that I know anything of value to help out your projects once every blue moon. To Salil, thanks for being another companion lunatic trained in microfabrication who wanders too far into the depths of biology. To the amazing lab managers, technicians, and support staff – Heather, Lia, Emma, Ani, Liz, Sue, and especially Steve – thank you for being the real ones that make any of this research happen and for your friendships. Most importantly, thanks to David Braga Malta for being the best collaborator anyone could ask for and truly the most thoughtful caring friend I've had here. To all of you in the lab, I'm incredibly thankful for the relationships that I've had with each of you. You make me truly love this place.

I would also like to thank Dr. John Lamar and Dr. Monte Winslow for being outstanding collaborators and unofficial mentors. Their guidance has inspired me and given me the confidence to pursue important biological questions. Additionally, I would like to thank the many members of the Koch Institute who have helped train and guide me throughout this research including Dr. Tyler Jacks, Glenn Paradis, Charlie Whittaker, Mike Brown, and Stuart Levine. I would also like to thank the many members of the MTL including Dennis, Kris, Kurt, Dave, and Donal.

I have been blessed to work with and learn from a fantastic group of undergraduates. Much of this work would not have been possible without the contributions of Liz Tsai, Mary Xu, Peijie Ong, Jenn Kao, Camille Sullivan, and (unofficially) Luvena Ong. I am deeply thankful for all of

their help and for teaching me so much. They will undoubtedly have outstanding careers as physicians, scientists, and whatever else they may choose to pursue.

Thanks to the band, Ames and Main, for providing me a musical outlet during my PhD. Steve, Michel, Phil, and Jon, you guys are outstanding musicians and scientists alike.

HST is a truly unique program to be a part of, and I am incredibly thankful for the opportunities it has given me. In addition to all of the medical coursework, I am especially grateful for the opportunity to practice medicine in our clinical clerkship. I learned a tremendous amount from Dr. Charles Hatem, Dr. Xaviour Walker, Dr. Ahmet Toprak, and Dr. Tafadzwa Muguwe during my time at Mount Auburn Hospital. I will cherish these teachings about medicine and humanity as I move forward in the worlds of medicine, biology, and engineering.

I would like to thank my previous PIs Dr. Sang-Gook Kim (MIT) and Dr. Gary Leisk (Tufts) for teaching me a tremendous amount about research. Their guidance helped initiate the passion that I have for this profession. Additionally, I would like to thank my previous educators for encouraging and developing my constant quest for knowledge. In particular, I would like to thank Peter Atlas (CCHS), Andrei Joseph (CCHS), and Alfonse Litz (Willard). It is precisely because my exposure to these outstanding educators that I have achieved this accomplishment.

As a Boston native, I have had many friends in the area who have supported me and tolerated my frequent absences over the past years. You all are outstanding people. In particular, to Todd, Ellie, Zac, Eric, and Emily, thanks for always being there for me and for keeping me standing when my legs seemed to give up. To Aaron, thanks for being my heart and motivation. You're the reason I'll never give up.

As someone who was born in Cambridge and has lived in and around this city my whole life, the events of this past April were both shocking and heartbreaking. I want to thank the members of this community and the city for the incredible way they handled the tragedy. In particular, I would like to thank Officer Sean Collier for his dedication to this city and this university. His character epitomizes the numerous members of this community whose selfless dedication to this place enables all of the achievements that come out of it. As a member of this city and this university, I would not be here, if not for people like Sean, and I am incredibly thankful for all that he and others have done for us.

I have been blessed to have the greatest family that I could imagine. My parents have always supported me. They have encouraged my growth in a way that has never felt forced yet still managed to elicit my greatest efforts. I want to thank them for always supporting me and for always giving me confidence in everything that I cared to pursue. Even when I don't deserve it, they have always showered me with praise for whatever I attempt to achieve. It is undoubtedly because of their faith in me that I will so blindly charge into the investigations of sciences that I have no official training in. My sister Julia, while always competitive, has been an amazing source of inspiration. Her success in everything that she does dwarfs anything that I have achieved academically, and I am constantly humbled by her accomplishments. I am in awe of all of you and love you very much.

Finally, I would like to thank Pamela Basto for being my lifeboat, inspiration, and greatest companion in life. Pam, you have helped me more than you will ever know. You're knowledge of biology, chemistry, medicine, and engineering is astounding. I love every minute we spend discussing science and everything else in life. Thanks for always making me laugh, for supporting me when I need it, and keeping my enthusiasm in check when my overzealous excitement for glycan structures gets carried away. I am forever thankful for all that you've done for me, and I love you.

Table of Contents

List of Figures

the slides sit such that their top surface is flush with the remainder of the bottom of the chamber. A vacuum port exists at the bottom of each chamber and connects to a central vacuum line. The vacuum acts to hold the slides in place and prevents media from leaking onto the backs of the slides. (b) CAD schematic depicting the four chambers of the seeding device.

Figure 2.4. *Cells Adhered to ECM Microarrays.* Representative images of cells adhered to ECM spots demonstrating selective adhesion to the regions where ECM has been deposited. Nuclei (blue) are stained with Hoechst. Leftmost image is of five replicate spots. Scale bar on five-spot image is 200μm. Scale bars on single-spot images are 50μm.

Figure 2.5. *Combinatorial Adhesion Profiles are Generated using ECM Microarrays.* (a) Nuclear stain of cells seeded on the ECM microarrays. (b) Identification of individual nuclei on one spot using CellProfiler[3]. (c) Quantification of adhesion to all molecule combinations for one cell line. (d) Selected adhesion profiles for three molecules: Collagen I (blue), Collagen IV (green), and Fibronectin (red) in combination with all other molecules. Dashed blue lines represent adhesion to that molecule alone. Arrows denote combinations with the other two molecules or alone. Error bars are s.e.m. of three replicate slides. (e) Comparisons of three replicate slides for two representative cell lines. Scale bars in (a) and (b) are 450μm and 100μm, respectively.

Table 2.2. *Cell lines screened.* This table lists the cell lines screened on the arrays and their classifications. Cell lines derived from primary lung tumors that did not give rise to metastases (T_{nonMet}), did give rise to metastases (T_{Met}), lymph node metastases (N/LN), and distant metastases (M/Met).

Figure 2.6. *ECM Microarrays Demonstrate Conserved Changes in Adhesion that Correlate with Metastasis.* Unsupervised hierarchical clustering of adhesion profiles generated by the ECM microarrays. Vertical axis represents different ECM combinations. Horizontal axis represents different cell lines. Yellow bars indicate primary tumors (T_{nonMet} and T_{Met} lines). Red bars indicate nodal (N) or distant metastases (M). T_{nonMet} lines are in blue text, T_{Met} lines are in green text, N lines are in orange text, and M lines are in red text. The dendogram at the top represents the results of the clustering based on Euclidean distances.

Figure 2.7. *Gene Expression Clustering.* Unsupervised hierarchical clustering of gene expression microarrays. All probesets displaying a variance>0.5 and expression>3.0 were included. Yellow bars demote primary tumor-derived cell lines (T_{nonMet} and T_{Met}) and red bars denote metastasis-derived cell lines (N and M). Clustering is performed using complete linkage analysis with a half square Euclidean distance and average value ordering weight.

Figure 2.8. *Identification of metastasis-associated ECM molecules.* (a) Average adhesion of metastatic cell lines (M) to each combination compared to those of the metastatic primary tumor cell lines (T_{Met}). (b) Comparison of 393M1 adhesion for each combination to its clonally related primary tumor line, 393T5. Red dots indicate top ECM combinations exhibiting preferential adhesion by metastatic lines over the metastatic primary tumor lines. (c) Top three combinations exhibiting the greatest increase in adhesion across tumor progression as represented by the four classes of cell lines (T_{nonMet}, T_{Met}, N, and M). Error bars in (c) are s.e.m. of the different cell lines of each class (n = 3 cell lines per class) with the exception of the M class where there are two lines, and thus the error bars are the range of the means.

Figure 2.9. *Changes in adhesion correlate with metastatic progression.* Molecules to which there is a loss of adhesion (blue) or gain of adhesion (red) between the T_{nonMet} (n = 3), T_{Met} (n = 3), N (n = 3), and M (n = 2) cell lines when examined alone (a) or as an average of all combinations containing them (b). Combinations that exhibited the greatest gains (red) or losses in adhesion (blue) as determined by linear regression are depicted in (c). Combinations were selected based on the magnitude of the slopes provided that the regressions had r^2 values greater than 0.9. Y-axes represent normalized adhesion. Values less than ~0.5 represent very minimal adhesion. Error bars are s.e.m. of the different cell lines of each class with the exception of the M class where there are two lines, and thus the error bars are the range of the means.

Figure 2.10. *ECM combinations can have anti-adhesive effects when compared to single molecules.* (a) Heat map depiction of adhesion profile of the M line 393M1 for each ECM combination. (b) All combinations of molecules containing fibronectin. Fibronectin alone is depicted in blue. Four combinations that exhibited significantly decreased adhesion when compared to fibronectin alone are depicted in red. CSP: chondroitin sulfate proteoglycan; AGR: aggrecan; MUC: mucin; HSP: heparin sulfate proteoglycan. The three metastasis-associated ECM combination hits are also denoted (LAM: laminin; GAL3: galectin-3; GAL8: galectin-8). Error bars are s.e.m. of three replicate slides. (c) Verification of anti-adhesive effects of the molecules highlighted in (b) was performed by coating 96-well plates with the molecules and examining adhesion of the 393M1 cell line. Error bars are standard error. $***P < 0.001$; $**P < 0.01$; $*P < 0.05$. Significance was determined using one-way ANOVA with Tukey's Multiple Comparisons post-test.

Scheme 3.1. *The galectin family.* (a) The three types of galectins: prototype, chimera type, and tandem repeat type. (b) Structure of human galectin-3.

Figure 3.1. *Identified ECM molecules are present in primary tumors and metastases.* (a) Staining on lungs containing primary lung tumors from *Kras*$^{LSL\text{-}G12D/+}$;*p53*$^{flox/flox}$ mice. (b) Staining of lymph node metastases from the mice. Red arrowheads denote

tumor front exhibiting high osteopontin staining. (c) IHC of primary tumor-associated ECM in the lung and lymph node. Black arrowheads: collagen I, open black arrowheads: collagen VI. (d) Summary of IHC results. 'H&E': Hematoxylin and eosin. 'Trichrome': Masson's trichrome. 'Hmga2': High-mobility group AT-hook 2 (marker of metastatic/invasive tumor cells). 'T': primary lung tumor. 'N': lymph node metastasis. 'M': distant metastasis. Scale bars: (a) low magnification: 1mm; high magnification: 100μm; (b) low magnification: 500μm; high magnification: 50μm; (c) 50μm.

Figure 3.2. *Metastasis-associated ECM molecules are present in the sites of metastases but not primary tumors.* Immunostaining of the metastasis-associated ECM molecules in the lungs, lymph nodes, and distant metastases of mice bearing endogenous lung adenocarcinomas (*Kras*$^{LSL\text{-}G12D/+}$;*p53*$^{flox/flox}$ mice). Insets are magnified views of boxed areas showing ECM molecule fibrils. Number of tissues examined for each organ: Lungs: 10; lymph nodes: 5; livers/kidneys: 22. 'T': tumor. Dotted line depicts edge of tumor and normal kidney. Scale bars are 50μm.

Figure 3.3. *ECM production by cell lines has minimal correlation with adhesion.* Western blot analysis of the metastasis- and primary tumor-associated ECM molecules produced by the 393T5 (T_{Met}) and 393M1 (M) cell lines. 'Gal-3' Galectin-3; 'Gal-8' Galectin-8; 'FN' fibronectin; 'Lam' laminin; 'Coll I' collagen I, 'OPN' osteopontin.

Figure 3.4. *ECM adhesion does not correlate with integrin gene expression.* (a) Comparison of ECM adhesion for all cell lines to gene expression of the cognate integrins from gene expression microarray data. GeneGO software was used to identify reported interactions between integrins and ECM molecules contained on the ECM microarrays. For each reported interaction, the adhesion value from the ECM arrays was plotted on the ordinate and the gene expression was plotted along the abscissa. (c) Integrin subunit mRNA expression of the cognate integrins for the metastasis-associated ECM molecules from Affymetrix microarray analysis in 393T5 (T_{nonMet}) and 393M1 (M) cell lines.

Figure 3.5. *Integrin Surface Expression Correlates with ECM binding profiles.* (a) Flow cytometry of integrin surface expression in 393T5 (T_{Met}) and 393M1 (M) cell lines. Integrin subunits that bind to metastasis-associated molecules show increased surface presentation in the metastatic line (α5, αv, α6, α3), while those that bind to primary tumor-associated molecules show decreased presentation (α1 and α2). (b) IHC for metastasis-associated integrins in mice bearing autochthonous tumors with spontaneous metastases to the liver and lymph nodes. Scale bars are 100μm.

Figure 3.6. *Flow cytometry analysis of surface integrin expression.* (a) Median values for fluorescence intensity of each of the T_{Met} (blue) and M (red) cell lines for the metastasis-associated molecule cognate integrins and primary tumor-associated molecule cognate integrins. (b) Multicolor flow analysis of integrin profiles in the 393M1

(M) and 393T5 (T_{Met}) for the metastasis-associated molecule cognate integrins shows a lack of discrete subpopulations.

Figure 3.7. *Lung adenocarcinoma metastasis (LAM) network identified α3β1.* GeneGO software (Metacore) allows for the generation of *in silico* network maps depicting known interactions between molecules as established in the literature. This manually curated database generated networks based upon the most closely related molecules. Networks were generated by seeding an autoexpand algorithm with the metastasis-associated ECM molecules (fibronectin, laminins, galectin-3, and galectin-8) (a,b). (c) This network was queried for the diseases most highly associated with it. P-values determined by hypergeometric test. (b,d) Analysis of the network reveals that integrin α3β1 is the surface receptor with the most edges.

Figure 3.8. *Primary tumor network map.* Here, GeneGO (Metacore) was used in an equivalent manner as performed for the LAM network generated in Fig. 3.7 with the exception that the autoexpand algorithm was seeded with the primary-tumor associated ECM molecules (collagen I, IV, VI and osteopontin) (a). (b) Disease association rank of the primary tumor molecule network shown in (a). P-values determined by hypergeometric test.

Figure 3.9. *Integrin α3β1 mediates adhesion and seeding* in vitro *and* in vivo. (a,b) Flow cytometry analysis of integrin surface expression following retroviral transduction of short hairpins targeting the integrin subunits. (a) knockdown of ITGB1; (b) knockdown of ITGA3. Black: control hairpin against firefly luciferase; red: hairpin against integrin subunits. Knockdown of both α3 and β1 integrin subunits by shRNA reduces adhesion to metastasis-associated molecules *in vitro* (b) and prevents metastatic seeding *in vivo* (c,d). shFF is the control hairpin targeting firefly luciferase. One-way ANOVA with Tukey's Multiple Comparison Test was used to analyze the data in figure (b). Error bars in (b) represent standard error ($n = 3$). (c) Number of liver tumor nodules of the surface of livers 2.5 weeks after intrasplenic injection. Mann-Whitney (non-parametric) test was used to analyze significance. (d, top) Fluorescence imaging of whole livers after resection. Cell lines express nuclear-excluded ZSGreen. Scale bars are 0.5cm. (d, bottom) Hematoxylin and eosin stain of liver slices. Scale bars are 2mm. Blue data points in (c) correspond to images in (d). All results shown are representative of multiple independent experiments.

Figure 3.10. *Metastasis-associated molecules are present in the metastases of human lung cancers* (a-d) Oncomine[4] results for human lung cancer expression of LGALS3 and LGALS8. (a) LGALS3 Expression in Hou Lung: Large Cell Lung Carcinoma – Advanced Stage. (b) LGALS3 Expression in Bild Lung: Lung Adenocarcinoma – Advanced Stage. (c) LGALS8 Expression in Hou Lung: Large Cell Lung Carcinoma – Advanced Stage. (d) LGALS8 Copy Number in TCGA Lung 2: Lung Adenocarcinoma –

Advanced M Stage. LGALS3 and LGALS8 are overexpressed in Stage II lung cancer compared to stage I (P = 0.018 and 9.72E-4, respectively)(a,c). Microarray data source GSE19188[5]. (b) LGALS3 is overexpressed in Stage IV lung cancer compared to other stages (P = 0.040). Microarray data source GSE3141[6]. (d) LGALS8 has increased copy number in advanced M stage lung cancer (P = 0.013) in the "Lung Carcinoma DNA Copy Number Data" dataset available from The Cancer Genome Atlas website (https://tcga-data.nci.nih.gov/tcga/tcgaHome2.jsp). (e) Representative images of human tissue microarray staining results for galectin-3 presence or absence in the primary sites and lymph nodes. Scale bars are 500μm. Box and whisker plots in (a-d): dots represent maximum and minimum values, whiskers show 90th and 10th percentiles, boxes show 75th and 25th percentiles, and line shows median. P-values in (a-d) were computed by Oncomine software using Student's t-test (a, c-d) or Pearson's correlation analysis (b).

Figure 4.1. *Glycan-galectin interactions in lung cancer metastasis.* (a) Schematic depicting the mouse model used in these studies. Cell lines are generated from *Kras*$^{LSL\text{-}G12D/+}$;*p53*$^{flox/flox}$ mice following tumor development from the primary tumors that did not metastasize (T_{nonMet}), primary tumors that did give rise to metastases (T_{Met}), and distant metastases (M). (b) Potential glycan ligands for the galectin-3 CRD. The T-Antigen (Galβ1-3GalNac-α1-O-S/T) is specific for the carbohydrate recognition domain (CRD) of galectin-3 and -8. *N*-Acetyllactosamine (LacNAc) binds the CRD of all galectins and exhibits increased affinities when in a polymeric form. The A- B- Type 2 blood group antigens have reported affinities for a variety of galectins, including galectin-3, by glycan array analysis.

Figure 4.2. *T-Antigen expression increases with metastatic progression.* Peanut agglutinin (PNA) exhibits a strong specific affinity for the T-Antigen. (a) Flow cytometry analysis of lines 802T4 (T_{nonMet}), 393T5 (T_{Met}), and 393M1 (M) for binding of PNA. Cells were incubated with PNA conjugated to AlexaFluor 647 for 30 minutes prior to washing and analysis by flow cytometry. (b) Staining by PNA (green) on 393T5 and 393M1 cells. Cells were cultured on tissue-culture-plastic, fixed, and stained with PNA conjugated to AlexaFluor 647. Nuclei (blue) were stained with Hoechst.

Figure 4.3. *T-Antigen expression on human NSCLC patients.* Human tissue microarrays were stained with peanut agglutinin (PNA) for presence of the T-Antigen. (a) Sample images of PNA stains from human tissue microarrays. Quantitation of staining of lung (b) and lymph node (c) samples looking at diffuse positive staining and membrane-specific staining. (d) Results from (c) with representation of the subtypes of NSCLC. Scale bars in (a) are 200μm and 100μm on the inset images. P values were determined using Fisher's Exact Test. PNA: peanut agglutinin; N: non-cancerous tissue; C: cancerous tissue; Adeno: adenocarcinoma; LCC: large cell carcinoma; SCC: squamous cell carcinoma.

Figure 4.4. *Galectin-3 adhesion is carbohydrate mediated.* (a) Incubation of 393M1 cells with LacNAc (red) or Sucrose (black) prior to staining with fluorescent galectin-3. LacNAc inhibition reduces galectin-3 adhesion in a carbohydrate-dependent manner. (b) Short-hairpin knockdown of $\alpha 3$ and $\beta 1$ integrin subunits (or control firefly luciferase) in the 393M1 cell line followed by PNA staining for the T-Antigen.

Figure 4.5. *T-Antigen presentation increases with metastatic progression on a variety of proteins.* Surface proteins were isolated from T_{nonMet}, T_{Met}, and M cell lines and run on SDS-PAGE gels. PNA lectin blots of cell surface proteins (a) and whole cell lysates (b). Ponceau S stains show total protein.

Figure 4.6. *Glycosyltransferase gene expression.* (a) Gene expression microarray analysis of known glycosyltransferase expression reveals minimal alterations in global gene expression profiles between cell lines of the different stages. (b) Gene expression microarray analysis of select genes predicted to generate the galectin-3 binding partners (see Fig. 4.1b). All data is $\log_2$ mRNA expression.

Figure 4.7. Gcnt3 *and* St6galnac4 *are differentially regulated during metastasis.* (a) Comparison of the average primary tumor (all T_{nonMet} and T_{Met} lines) gene expression by the average metastases (all N and M lines) gene expression for all glycosyltansferases. (b) Expression of *Gcnt3* and *St6galnac4* in the three representative lines by qRT-PCR. (c) Schematic depicting the glycosylation resulting from C2GNT2 and ST6GALNAC4 activity. (d) Gene expression microarray analysis for all cell lines for select glycosyltransferase activity and the resulting structures. Size of spots in (a) refers to the absolute difference between the clonally related 393T5 and 393M1 pair. *P*-values in (a) are calculated between each class of lines (i.e. T_{nonMet} vs. T_{Met}, T_{Met} vs. N, N vs. M). Error bars in (b) are s.e.m. of separate RNA isolations and in (d) are s.e.m. of different cell lines of the same type. *P*-values in (b) and (d) were determined by one-way ANOVA followed by Tukey's multiple comparison post-test. * $P < 0.05$; ** $P < 0.01$; *** $P < 0.001$.

Figure 4.8. Gcnt3 *downregulation and* St6galnac4 *upregulation promote galectin-3 adhesion. St6galnac4* was knocked down by retroviral transduction of short hairpins. Galectin-3 (a) and PNA (b) staining of 393M1-shSt6galnac4 and 393M1-shLuc control cells. Galectin-3 (a) and PNA (b) staining of 393M1 cells transfected with *Gcnt3* plasmid. (e,f) Quantitation of (c,d). *GCNT3* copy number in human tissue taken from blood, normal lungs, or lung adenocarcinoma.

Figure 5.1. *Galectin-3 is expressed on CD11b$^+$ peripheral blood leukocytes in mice bearing tumors.* Peripheral blood was harvested by cardiac puncture from mice implanted with subcutaneous flank tumors derived from various cell lines. Cells were gated based on their FSC and SSC profiles. (a,b) Galectin-3/Mac-2 staining of all

peripheral blood cells. (c,d) CD11b staining of all peripheral blood cells. (e,f) Gating for CD11b$^+$Mac-2$^+$ double-positive cells. (g) FSC vs. SSC for all cells (red) and galectin-3/Mac-2$^+$ cells (blue). 'NT' no tumor; 'T_{nonMet}' mice bearing the 802T4 cell line; 'M' mice bearing the 393M1 cell line. *** $P < 0.001$. NT: no tumor.

Figure 5.2. *Tumor-bearing mice have enriched galectin-3$^+$ CD11b$^+$Gr-1$^+$ and CD11b$^+$Ly6C^{hi} cells.* Mice bearing no tumors (NT), T_{nonMet} tumors, or M tumors injected into their rear flanks were analyzed for CD11b$^+$ subsets by flow cytometry. (a) Staining for Gr-1$^+$ cells. (b) Staining for CD115$^+$ monocytes. (d,e) Mice with tumors have elevated levels of Ly6C^{hi} monocytes. (f) Fluorescence intensity of galectin-3 staining on monocytes from mice with and without tumors. Intensity of galectin-3 staining on (g) all CD11b$^+$ cells and (h) Gr-1$^+$ cells. (i) Percentage of all monocytes that are galectin-3$^+$. ** $P < 0.01$; *** $P < 0.001$. NT: no tumor.

Figure 5.3. *Galectin-3 expression in cell lines and mice.* (a) Gene expression microarray mRNA levels of *Lgals3* (galectin-3) and *Lgals8* (galectin-8) for cell lines from each of the four classes: T_{nonMet} (n=3), T_{Met} (n=3), N (n=3), and M (n=2). (b) Western blot analysis of protein levels of galectin-3 and -8 for three representative lines: 802T4 (T_{nonMet}), 393T5 (T_{Met}), and 393M1 (M). (c) ELISA analysis of serum levels of circulating galectin-3 in mice bearing T_{nonMet} and T_{Met} cell lines. (d) Western blot analysis of galectin-3 and -8 levels of the livers of mice bearing tumors but no detectable metastases. (e) Flow cytometry of galectin-3 levels on CD11b$^+$ cells of mice bearing tumors following MACS separation in the presence of 200mM lactose or sucrose. **** $P < 0.0001$; n.s. not significant. RM resident monocyte; IM inflammatory monocyte; MDSC myeloid-derived suppressor cell.

Figure 5.4. *Mice bearing the metastatic tumor line have galectin-3$^+$ macrophages in accumulation in the tumors.* Mice were implanted with the 393M1 (M) tumor cell line. Tumors were harvested and stained for macrophages (F4/80, green) and galectin-3 (pink). Nuclei (blue) are stained with Hoechst. Scale bars on the top and bottom rows are 100μm. Scale bars on the middle row are 25μm. Middle row is zoom of the dashed white box from the top row. IgG: isotype control.

Figure 5.5. *Mice bearing tumors exhibit accumulation of galectin-3$^+$ macrophages in their livers.* Staining of livers from transplanted tumor-bearing mice prior to the detection of metastatic cells for macrophages (F4/80) and galectin-3. Nuclei are stained with Hoechst. Scale bars on the top and bottom rows are 50μm. Scale bars on the middle row are 25μm. IgG: isotype control.

Figure 5.6. *Conditioned medium from tumor lines induces rapid recruitment of CD11b$^+$Mac-2$^+$ leukocytes into circulation.* Fresh medium (white), 393M1 conditioned medium (red), or fresh medium with 20μg/mL recombinant galectin-3 (Gal-3, gray) was

injected into circulation of naïve mice. Peripheral blood, harvested two hours after media injections, was analyzed by flow cytometry for (a) the percentage of all cells CD11b$^+$, (b) the percentage of all cells galectin-3$^+$, (c) the percentage of all cells CD11b$^+$ and galectin-3$^+$, (d) the percentage of all cells CD11b$^+$Gr-1$^+$, (e) the ratio of inflammatory to resident monocytes, and (f) the expression levels of galectin-3. (g) Luminex ELISA analysis of cytokine levels in the fresh (white) and conditioned (black) medium. (h) Galectin-3 levels of medium supernatant from 393M1 lines transduced with hairpins against galectin-3 (shGal3) or firefly luciferase (shLucMis) by ELISA. *** $P < 0.001$; N.D. not detected.

Figure 6.1. *Profiling adhesion of cells undergoing EMT.* (a) Schematic of the screening workflow: (I) ECM microarrays are spotted, (II) wild-type HMLERs, HMLERs expressing *TWIST*, or a 1:1 ratio of both are prepared, and (III) seeded onto the ECM arrays. (b) Micrographs of cells on individual spots stained for E-cadherin or N-cadherin (top). Epithelial and mesenchymal cells were stained with green and orange Calcein AM, respectively and seeded on the arrays after mixing (middle and bottom).

Figure 6.2. *Identification of ECM combinations yielding the greatest adhesion.* Rank ordered cell counts for all of the combinations on the ECM microarrays for both the wild-type (a) and *TWIST*-expressing (b) HMLERs four hours following seeding of the arrays. Red bars and inset graphs indicate the top 2.5% of combinations.

Figure 6.3. *EMT induces differential adhesion to ECM.* (a) Unsupervised hierarchical clustering of replicate slides for both the wild-type and *TWIST*$^+$ cells depicts conserved differences in adhesion profiles. (b) Normalized adhesion values for all of the ECM combinations on the arrays plotted as wild-type cells (abscissa) versus the *TWIST*$^+$ cells (ordinate). Black line depicts equivalent adhesion values (x = y). (c) Top differential adhesion values between the two cell states. Combinations listed as "1" (blue) represent elevated adhesion by the wild-type cells and "2" (red) represent those to which the mesenchymal cells exhibit greater adhesion. (d) Top differential hits as calculated by the absolute value of the difference between the wild-type and *TWIST*$^+$ cells. Blue bars depict combinations to which the epithelial values are higher and red bars refer to those to which the mesenchymal values are higher.

Figure 6.4. *EMT induces differential proliferative responses to ECM.* Rank ordered population doublings for the top ECM combinations as quantified by the ratio of day 2 counts to day 0 counts for the (a) mesenchymal and (b) epithelial cells. (c) Top differential counts following normalization to the non-zero means of the slides. Combinations listed under "1" (red) are those to which the mesenchymal cells had higher counts and those under "2" (blue) represent the epithelial hits. (d) The same as (c) but where the counts have not been normalized. Here "1" (blue) refers to the epithelial hits and "2" (red) represents the mesenchymal hits.

Figure 6.5. *Galectin-3 induces increased E-cadherin expression.* (a,c) E-cadherin expression measured as fluorescent intensity and normalized to cell counts per spot for all combinations where the standard deviation is less than 2×10^6 (a) or 1×10^5 (c). (a) depicts values for the wild-type cells and (c) depicts *TWIST*$^+$ cells. (b) Top 10 combinations with the highest E-Cadherin staining from (a). Combinations listed in red contain galectin-3 as one of their components. Blue dots in (c) represent combinations that contain galectin-3 or its cleaved form galectin-3c. Error bars in (b) are s.e.m.

Scheme 7.1. *ECM interactions in metastasis.* This schematic depicts the working model of ECM interactions during metastasis as explored in this thesis. Primary tumors exhibit adhesion to a variety of collagens and osteopontin. These tumors also secrete collagens. They express high levels of integrin α1 and α2 subunits on their surfaces. These tumors express high levels of *Gcnt3* and low levels of *St6galnac4* in a manner that promotes *O*-glycan extension and branching. Both the primary and metastatic tumors secrete galectin-3 and -8, which can be found in the circulation. The metastatic tumors exhibit increased adhesion to fibronectin, laminins, galectin-3, and galectin-8. Additionally, they secrete osteopontin. These tumors exhibit elevated surface presentation of integrin α3, α5, α6, and αv subunits. Furthermore, they have elevated T-Antigen presentation, which is a result of downregulation of *Gcnt3* and upregulation of *St6galnac4* and that mediates galectin-3 adhesion. Early in tumorigenesis, CD11b$^+$ leukocytes are recruited to the blood and sites of metastases. These cells exhibit high levels of galectin-3 on their surfaces.

Scheme A.1. *Nanoparticle Synthesis.* Iron oxide nanoparticles have dextran coatings crosslinked by epichlorohydrin. The nanoparticles are aminated using ammonium hydroxide. The free amines are first reacted with the NHS esters on the SIA crosslinkers. The iodoacetyl groups are then reacted with the end-terminal cysteines on the peptides to generate particles presenting T-Antigen-specific peptides in a multivalent fashion.

Figure A.1. *Nanoparticle Characterization.* (a) Dynamic light scattering (DLS) measurements of nanoparticle diameters. (b) Flow cytometry analysis of nanoparticle binding and T-Antigen inhibition on 393M1 cells. Nanoparticles incubated with no (blue) or 20μM (red) concentrations of nanoparticles. PE monitors nanoparticle TAMRA fluorescence, and APC measures PNA binding. (c) Nanoparticle titration and quantification of parameters measured in (b).

Figure A.2. *Nanoparticles bind the T-Antigen and prevent lectin interactions.* Cell lines from the T_{nonMet} (802T4), T_{Met} (393T5), and M (393M1) lines were incubated with fluorescent PNA in the presence of nanoparticles and analyzed for PNA binding by flow cytometry. (b,c) Cells were cultured with nanoparticles and washed and imaged to query uptake. Error bars represent s.e.m.

Figure A.3. *Nanoparticles bind tumors* in vivo. Mice are injected into contralateral flanks with tumor cells lines from different classes (i.e. T_{nonMet} vs. T_{Met} vs. M). (a,b) IVIS quantification of fluorescence in tumors excised from mice 3.5 hours after injection of nanoparticles into systemic circulation. (c) Fluorescence of tumor lysates 30 hours after injection of nanoparticles or PBS control.

Chapter 1. Introduction

1.1 Scope

Cancer is the second leading cause of death in the United States following heart disease and accounts for roughly 23.3% of all deaths[7]. It kills 580,350 people domestically (estimated for 2013)[8] and 7.6 million people worldwide (2008)[9] per year. Of those deaths, 90% are thought to be the result of metastasis, the process by which cancer spreads throughout the body, rather than outgrowth of the primary tumor[10-11]. In order for this process to occur, cancer cells must alter the way they interact with their microenvironments through *de novo* mutations, alterations in regulatory mechanisms, or cooption of existing programs. These alterations allow tumor cells to break free from their sites of origin, survive the circulatory and lymphatic transport systems, take root at a distant site, and ultimately colonize that tissue. Despite many recent advances in the field, this driver of morbidity is a poorly characterized process. In particular, the study of how cells interact with the dynamic molecules of the extracellular matrix (ECM) throughout the metastatic cascade has yet to benefit from systematic unbiased large-scale characterization. **Thus, the overall goal of this thesis is to improve our understanding of the role of ECM in cancer metastasis through the use of engineering approaches.**

1.2 Lung Cancer

1.2.1 Incidence

With an estimated US death toll of 159,480 in 2013, lung cancer is the largest killer among all neoplasms[8]. It far surpasses both breast (40,030) and prostate (29,720) cancers despite having less than half the incidence rates[8]. Nonetheless, while $15,690

and $9,376 research dollars were spent per cancer death in 2010 for those two cancer types, respectively, only $1,792 was spent per lung cancer death[12], and it is considered one of the most underfunded cancers both within the US and abroad[13]. Furthermore, while a reduction in tobacco use within the US has resulted in a slight decline in deaths, the mortality rates of lung cancer still far surpass any of the other cancers (Fig. 1.1a-c), and the survival from time of diagnosis is one of the shortest of all malignancies (Fig. 1.1d-f). The brevity of this survival time is primarily due to the existence of distant overt metastases at the time of diagnosis for which no curative treatment can be provided.

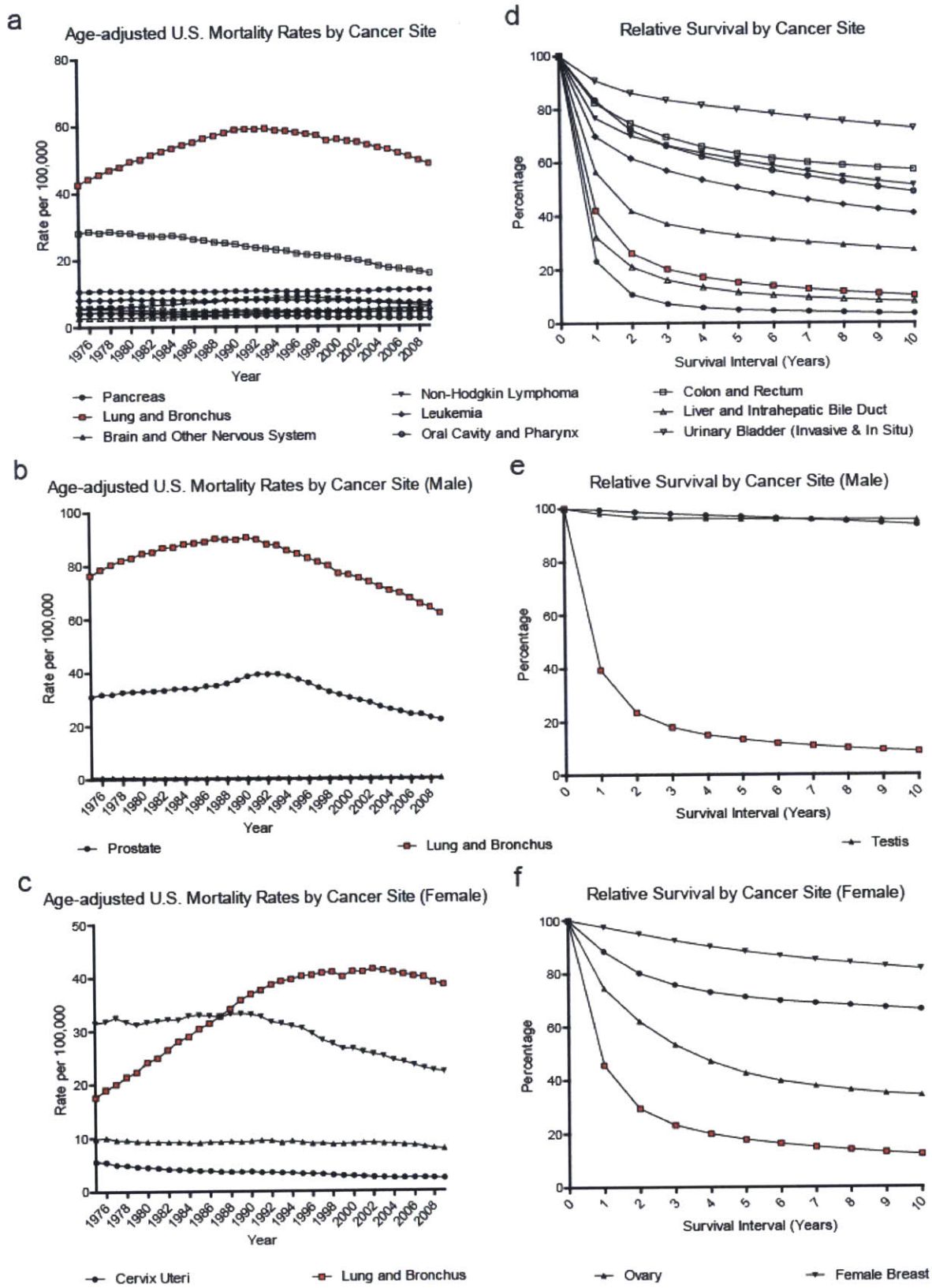
a
Age-adjusted U.S. Mortality Rates by Cancer Site
Rate per 100,000
Year
d
Relative Survival by Cancer Site
Percentage
Survival Interval (Years)
Pancreas
Lung and Bronchus
Brain and Other Nervous System
Non-Hodgkin Lymphoma
Leukemia
Oral Cavity and Pharynx
Colon and Rectum
Liver and Intrahepatic Bile Duct
Urinary Bladder (Invasive & In Situ)
b
Age-adjusted U.S. Mortality Rates by Cancer Site (Male)
Rate per 100,000
Year
e
Relative Survival by Cancer Site (Male)
Percentage
Survival Interval (Years)
Prostate
Lung and Bronchus
Testis
c
Age-adjusted U.S. Mortality Rates by Cancer Site (Female)
Rate per 100,000
Year
f
Relative Survival by Cancer Site (Female)
Percentage
Survival Interval (Years)
Cervix Uteri
Lung and Bronchus
Ovary
Female Breast

Figure 1.1. *Cancer Survival Statistics.* Age-adjusted U.S. mortality rates by cancer site for both genders (a), males (b), and females (c). Relative survival by survival time by cancer site for both genders (a), males (b), and females (c). Red squares are for cancers of the lung and bronchus. Statistics are for all ages and all races. Data in (a)-(c) is from US Mortality Files and (d)-(f) is from 1988-2008 SEER 9. Graphs were generated from data provided by the NCI Surveillance and Epidemiology End Results (SEER) at http://seer.cancer.gov/statistics/ Accessed 21 April 2013.

1.2.2 Etiologies

The primary cause of the majority of lung cancers is tobacco smoking. Epidemiological studies are perhaps the most convincing evidence with 87% of lung cancers arising in current or recent smokers[14]. Additional causes include other environmental exposures such as asbestos[15] and radon[16] and genetic alterations, which will be discussed below.

1.2.3 Genetics

Like all cancers, lung cancer is an inherently genetic disease. Perhaps, the most common genetic alteration that occurs in lung cancers are mutations in the tumor suppressor gene p53[14, 17]. Patients bearing germline p53 mutations have increased incidences of lung cancer[18] that is exacerbated by smoking[19]. Other major tumor suppressor genes commonly altered in lung cancer include *RB1*, *p16(INK4a)*, *FHIT*, and *LKB1*[19-21]. Additionally, genome-wide association scans of SNPs in lung cancer patients identified a variation at 15q25.1, the location of *PSMA4* and subunits of the nicotinic acetylcholine receptor[22]. These SNPs showed a weak correlation with smoking behavior, but a strong correlation with lung cancer susceptibility. As nicotine stimulates the cholinergic receptors, these findings may help to explain the correlation between smoking and lung cancer incidence[22].

In addition to alterations in tumor suppressor activities, lung cancers typically harbor one or more mutations in oncogenes. These alterations typically vary depending on the lung cancer subtypes. In particular, small-cell lung cancers (SCLC) often present alterations in *C-KIT*, *MYCN*, and *MYCL*, while non-small-cell lung cancers (NSCLC) are typically accompanied by alterations in *EGFR* or *KRAS*[14, 17] (Table 1.1). While the latter two are common to NSCLC, they are nearly mutually exclusive with *EGFR* mutations occurring most commonly in non-smokers, particularly Asian females[23-24]. These *EGFR* mutations sensitize patients to gefitinib, whereas patients without the mutations have no response[25-26]. Additionally, the *EML4-ALK* fusion protein occurs in 7% of adenocarcinomas[17].

Abnormality	SCC	Adeno	SCLC
KRAS mutation	very rare	10 to 30%	very rare
BRAF mutation	3%	2%	very rare
EGFR			
kinase domain mutation	very rare	10 to 40%	very rare
amplification	30%	15%	very rare
variant III mutation	5%	very rare	very rare
HER2			
kinase domain mutation	very rare	4%	very rare
amplification	2%	6%	unknown
ALK fusion	very rare	7%	unknown
MET			
mutation	12%	14%	13%
amplification	21%	20%	unknown
TITF-1 amplification	15%	15%	very rare
p53 mutation	60 to 70%	50 to 70%	75%
LKB1 mutation	19%	34%	very rare
PIK3CA			
mutation	2%	2%	very rare
amplification	33%	6%	4%

Table 1.1. *Genetic abnormalities in lung cancer*. This table lists the common genetic abnormalities found in human lung cancer. SCC: squamous cell carcinoma; Adeno: adenocarcinomas; SCLC: small cell lung cancer. Table is adapted from reference [17].

1.2.4 Diagnosis and Staging

Clinical presentation of lung cancers can result from features related to the primary tumor, local or distant metastases, or paraneoplastic syndromes. Patients will often present with cough, dyspnea (shortness of breath), hemoptysis (blood stained sputum), cachexia, or chest pain related to pleural involvement[14, 27]. Typical sites of metastases for lung cancer include the brain, pleura, bone, liver, adrenals, contralateral lung, and skin, and the presenting symptoms may be related to involvement of these sites rather than the primary tumors[27]. At the time of initial diagnosis, only 15% of patients have resectable early stage disease for which the survival rate is 48%[14]. All other patients have metastases, and are primarily treated with palliative care. Survival rates for patients with NSCLC are shown in Table 1.2 (adapted from ref [1]). While a range of paraneoplastic syndromes occur with lung cancer ranging from coagulopathies to glomerulonephritis to Cushing syndrome to neurological syndromes[28], only a small number of patients will first present with symptoms related to them rather than the tumors themselves[27].

Stage	TNM	1yr Survival	5yr Survival
Local			
IA	T1N0M0	94	67
IB	T2N0M0	87	57
IIA	T1N1M0	89	55
Locally Advanced			
IIB	T2N1M0 T3N0M0	73	39
IIIA	T1N2M0 T2N2M0 T3N1M0 T3N2M0	64	23
IIIB	AnyTN3M0	32	3
Advanced			
IIIB	T4AnyNM0	37	7
IV	AnyTAnyNM1	20	1

Table 1.2. *Lung Cancer Survival by Stage.* Survival rates at 1 and 5 years for NSCLCs according to clinical stage. Adapted from reference [1]. 'TNM' refers to the TNM stage as defined by the AJCC Cancer Staging Manual[2], where 'T' refers to the characteristics of the primary tumor, 'N' refers to the involvement of lymph node metastases, and 'M' refers to the absence (0) or presence (1) of distant metastases.

Screening approaches for detection of lung cancer have been generally unsuccessful. Screening by chest radiography and sputum cytology did not show a significant reduction in deaths. Screening using high-resolution computed tomography (CT) scanning is still considered controversial, but may be beneficial in high-risk patients[29].

Diagnosis of lung cancer is typically made through a combination of imaging and histological evaluations. Imaging typically includes chest X-ray and chest CT scans. Fiberoptic bronchoscopy is used for visualization of central lesions. For peripheral lesions, CT-guided fine-needle aspiration is highly effective[27]. The use of positron-emission tomography (PET) in combination with CT can be more effective than the use of either alone for diagnosing mediastinal disease[30]. Evaluation of node involvement

allows for staging and determination of management. Patients with node-positive disease will typically undergo bone scans and brain MRI imaging prior to pursuing aggressive local therapy[1].

Lung cancers are typically classified as either SCLC or NSCLC. SCLCs make up approximately 13.7% and 18.3% of lung cancers in men and women, respectively[31], and occur almost exclusively in smokers[14]. Of NSCLCs, adenocarcinomas are the most common (37.5%) followed by squamous cell carcinomas (26.8%) other histologies (26.5%), large-cell carcinomas (5.7%), and bronchioalveolar carcinomas (3.5%)[32].

NSCLC is staged following the TNM staging guidelines according to the AJCC Cancer Staging Manual[2]. The 'T' stage, graded 1 to 4, refers mainly to the size of the primary tumor nodule and its invasive characteristics. The 'N' stage, graded 0 to 3, refers to the number and identity of lymph nodes involved, and the 'M' stage, graded 0, 1a, or 1b, refers to the existence of metastases. Accurate staging of lung cancers is essential for proper management of the disease.

Metastasis occurs early in SCLC making TNM staging an uninformative method for staging this type of disease. Instead clinicians typically categorize the disease state as either 'limited' or 'extensive' disease. Limited disease is defined as a tumor burden that is confined to the ipsilateral hemithorax within one radiation port (i.e. one treatment field) and represents approximately one-third of all presenting patients[1]. All other disease is defined as extensive.

1.2.5 Management

Whenever possible the primary choice of NSCLC patients with early disease is surgical resection. It is currently thought that patients with stage I to IIIA have potentially resectable disease and are good candidates for surgical treatment. Even so, the propensity for lung cancers to metastasize early results in, at best, a 67% survival rate at 5 years (Stage IA) and drops to 23% for stage IIIA[1, 33]. Surgery includes either lobectomies or pneumonectomies with removal of any involved mediastinal nodes. The role of either adjuvant chemotherapy or adjuvant radiation in the post-operative setting is less clear. Most studies of adjuvant radiotherapy show no improvement in survival time and some indicate increased relative risk of death[34]. While the use of adjuvant chemotherapy in this setting is still under debate, the use of platinum-based chemotherapy for these patients may have some marginal benefits[35].

In patients with stage III nonresectable (Stage IIIB) or resectable but locally advanced (Stage IIIA) disease, the use of neoadjuvant therapy may be advantageous. Neoadjuvant therapy refers to the use of non-surgical therapy as the initial treatment. Using this approach, treatment may shrink the tumors resulting in increased survival and clean margins following surgery. Studies have shown that while radiotherapy alone provides little survival benefit, combined radiation and chemotherapy can increase survival significantly, in this setting[36-37], and even in the context of nonresectable disease[38].

While patients with advanced stage NSCLC (Stage IIIB or IV) will not be cured, there are benefits to the use of chemotherapy. Stage IV patients represent 40%-50% of patients presenting with lung cancer[27]. Use of chemotherapy can increase survival two to four

months and may improve quality of life[1]. Surgical approaches have no benefit to this patient cohort.

Chemotherapy regimens for advanced stage NSCLC are typically two-drug platinum-based regimens. The choice of agents (i.e. cisplatin, paclitaxel, gemcitabine, docetaxel, or carboplatin) does not appear to have significant effects on outcome, but the use of two drugs does improve survival over conventional one-drug regimens[39].

Chemotherapy can be highly effective in patients with SCLC despite an earlier propensity for metastatic dissemination than NSCLC. While surgical resection is not typically used in these patients, it can be performed on those with stage I or II disease. Typical chemotherapy regimens for patients with limited disease include the use of irinotecan and cisplatin with a marginal benefit over etoposide and cisplatin[40], which can benefit from the addition of radiotherapy[41]. Patients with extensive disease receive etoposide with either cisplatin or carboplatin. Despite the initial benefits of chemotherapy in patients with SCLC the 5 year survival rates are only 15-25% in patients with limited disease and less than 5% in patients with extensive disease[1].

Overall, survival rates of all patients with lung cancer are poor. That even stage I patients have only a 60-70% 5 year survival rate combined with the improved survival benefits with chemotherapy at all stages of the disease suggest that metastatic dissemination of the tumors prior to diagnosis is the major contributor to morbidity. While chemotherapy and some prophylactic radiotherapy, such as whole brain radiation, are beneficial for reducing metastatic burden, no specific targeted therapeutics exist for treating metastases in the context of lung cancer.

1.3 Cancer Metastasis

While cancer metastasis is responsible for 90% of cancer-related deaths[10-11], the programs that govern this process are still poorly understood. As a result few therapeutic targets have been identified and even fewer have seen realization[42]. Increasing our understanding of the biology of metastasis will not only improve our diagnostic and prognostic toolsets, but also promote the development of therapeutics for currently incurable disease states.

1.3.1 Biology of Metastasis and the Metastatic Cascade

In order for malignant neoplasms to spread throughout the body and develop into clinically relevant metastases, they must traverse the highly inefficient process known as the metastatic cascade (Scheme 1.1). This process consists of loss of cell-cell adhesion, local invasion, intravasation, survival and transit in the blood or lymphatics, extravasation, and colonization of the distant tissue[43-44].

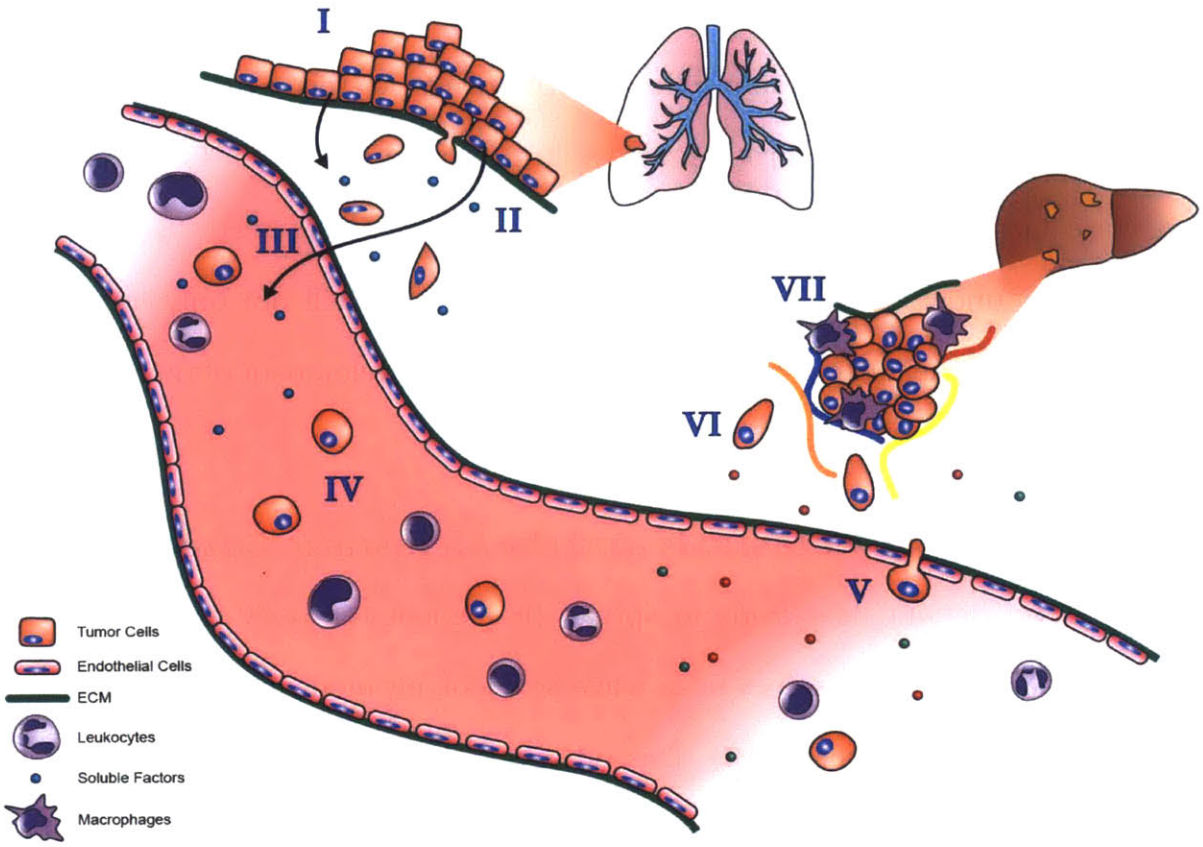

Scheme 1.1. *The metastatic cascade.* (I) Outgrowth of the primary tumor; (II) Invasion through basement membrane and interstitium; (III) Intravasation into the blood or lymphatics; (IV) Survival in circulation; (V) Extravasation; (VI) Survival and migration at a secondary site; (VII) Colonization.

The first step of this cascade, known as local invasion, relates to the ability of primary tumor cells to break free from their local microenvironment and invade into adjacent stroma. To achieve this ability, cells will downregulate the adhesion molecules that attach to their neighboring cells (i.e. cell junction proteins such as cadherins, occludins, and connexins) and to the underlying basement membrane (i.e. specific integrins). They also must break through that basement membrane, which is typically achieved through the expression of matrix metalloproteinases or downregulation of their inhibitors, TIMPs[45]. This local invasion can occur in a cohesive multicellular fashion "collective invasion" or at a single-cell level in either a adhesion-dependent manner known as

"mesenchymal invasion" or an adhesion-independent manner known as "amoeboid invasion"[46-47].

After invading through the basement membrane and local stroma, cancer cells must invade blood vessels and lymphatics to travel to distant sites. During growth of the primary tumor, blood vessels are recruited following activation of the "angiogenic switch"[48-49]. Metastasizing tumor cells must degrade the basement membrane surrounding these vessels and cross the endothelial barrier in order to gain access to the lumens of these vessels. While this process is still poorly understood, it is thought that the leaky vasculature coupled with a general lack of pericytes in the newly recruited vessels aids in the process of intravasation[50-51].

The next phase of metastasis involves survival in circulation. Recent clinical evidence has shown that circulating tumor cells exist in the blood of patients with cancer and can be a useful biomarker of disease progression as well as represent the diverse biology of these cells[52-56]. In this anchorage-independent state, circulating tumor cells (CTCs) must avoid anoikis. Furthermore, they must evade immune surveillance by cells such as natural killer (NK) cells. In some instances, this evasion may be achieved through binding to platelets in a manner that shields them from NK cells[57-59]. Furthermore, signaling from platelets to tumor cells can promote metastasis through the induction of epithelial-mesenchymal transitions[60] or generation of tumor thrombi[61-62].

Eventually, CTCs will arrest within blood vessels and subsequently extravasate. The timeframe within which a given CTC is in circulation is still debated, but considerations of capillary lumen size (~8μm) compared to tumor cells size (~20-30μm) along with data from experimental metastasis assays suggest that it is unlikely that most CTCs have

more than one pass through circulation[43]. Nonetheless, organ-specific metastasis is a clinical reality, and while microenvironment effects on colonization are likely the main agents of this specificity, elements of the vasculature may also play a role. Increased exposure to basement membrane proteins in the context of inflammation may permit increased adhesion of tumor cells. Tumor cells expressing $\alpha 3\beta 1$ integrin have been shown to bind laminin-5 in vascular basement membrane[63]. Metadherin expression may also potentiate adhesion specifically to pulmonary vasculature by breast cancer cells[64].

Following arrest, tumor cells can extravasate immediately or continue to grow in the lumen prior to extravasation[65]. The ability for cells to extravasate at distant sites can be challenging in the absence of the same vascular permeability available during intravasation. Thus, it is now suggested that CTCs may re-seed the initial tumor while slowly undergoing whatever alterations are necessary to extravasate or colonize distant sites[66]. Alternatively, establishment of a pre-metastatic niche wherein recruited myeloid cells secrete factors such as VEGF may also potentiate increased extravasation[67-68].

Following extravasation, disseminated tumor cells (DTCs) can survive as micrometastases for extensive time periods without colonizing distant tumors. Clinically, it is not infrequent to see breast cancer patients survive ten years without any recurrence following surgical resection of their primary tumor only to later find outgrowth at distant sites. Experimental evidence suggests that tumor cells can survive as dormant micrometastases without colonizing the tissue[69]. Thus, it is now appreciated that all of the prior stages of the metastatic cascade occur early in tumor

progression, and that colonization is the rate-limiting step in the development of clinically detectable metastases[70-74]. This transition from latency to overt metastases is likely governed by the ability of the DTCs to interact with their microenvironment. These interactions will be discussed in more detail in subsequent sections.

1.3.2 Metastasis as a Therapeutic Target

Despite the well characterized effects of metastasis on disease prognosis, few therapeutics exist that directly address this phase of the disease progression. Challenges range from detection to delivery of therapy to heterogeneity of the tumors to resistance against conventional drugs. Nonetheless, a variety of gene expression studies have helped to elucidate changes that occur during metastatic progression and have resulted in signatures that have significant clinical utility[75-80]. While these signatures have provided useful biomarkers for disease progression, they still do not provide a means to treat the disease.

Conventional treatment regimens for cancer typically consist of the use of chemotherapy and radiation. These approaches target rapidly dividing cells by preventing cell division or inducing DNA damage. It is now appreciated that there may be a subset of slow-growing cells that maintain the ability to repopulate the tumors. The self-renewal capability of these cells has led some to label them as 'cancer stem cells' (CSCs)[81-83]. In addition to their ability to drive tumor heterogeneity and self-renewal, these populations are typically resistant to radiation and chemotherapy[84-87]. Recent studies have linked CSCs to the embryonic program known as the epithelial-mesenchymal transition (EMT)[88]. This process is thought to play a role in metastasis. Subsequent studies have shown that these cells are not only resistant to conventional

chemotherapies, but have identified alternate small molecule inhibitors that have little effect on the primary tumor cells, but are highly effective against this CSC population[89]. Such screening approaches may help identify new classes of inhibitors that selectively target metastatic populations.

Recent advances in RTK inhibitors and biological therapeutics provide an alternative to conventional therapeutics in treating cancer. While these approaches often suffer from a lack of a durable response and eventual recurrence of the disease, their specificity often yields incredible initial responses with relatively few side effects. Just as metastatic cells often behave differently than their primary tumor counterparts, the genes that regulate and inhibit this phase of the disease are also different. Recently a class of genes, known as metastasis-suppressor genes (MSGs), have emerged that act to prevent metastasis formation[90]. These roughly twenty genes act to suppress the various components that promote metastasis. NM23, PEBP1, RECK, CTGF, KAI1, KISS1, RHOGD12, MAP2K4, BRMS1, and CASP8 have all been useful as prognostic indicators of metastasis[90-92]. In addition to their prognostic value, a variety of approaches can be taken to utilize MSGs. These approaches include the use of exogenous gene expression, induction of upstream activators, pharmacologic induction of expression, altering epigenetic regulation, exogenous introduction of the proteins, and inhibiting downstream targets[90, 93-99].

As systemic spread likely occurs early in metastatic progression, the most advantageous steps of the cascade to target are probably those of extravasation and colonization[100]. Thus, approaches that target the microenvironment of the metastases may be beneficial. Stromal cells such as osteoclasts and myeloid-derived cells (discussed in the next

section) may serve as good targets. Inhibition of additional angiogenesis can be achieved with anti-VEGF therapies such as Bevacizumab.

Perhaps, the most effective treatment against metastases may prove to be an increase in immune surveillance for cancer cells. Recent treatments aimed at reducing regulatory immune phenotypes through inhibition of CTLA4 and PD-1 have proved highly effective in patients with advanced stage melanoma and other cancers[101-102]. Unlike approaches that target BRAF activation[103-104] where patients eventually relapse, these immunotherapies have the potential to elicit complete responses. These responses may, in part, be due to the ability of the immune system to target dormant cells in combination with their recognition of broad antigen presentations.

1.4 Effects of the Microenvironment on Tumor Progression

The role of the microenvironment on promoting normal tissue homeostasis was elegant demonstrated in 1975 when malignant teratoma cells were reprogrammed by an embryonic blastocyst to generate normal chimeric mice[105]. Recently, it has become apparent that the tumor microenvironment dramatically impacts metastatic progression[106]. These effects range from interactions with other cell types such as fibroblasts or recruited myeloid cells to alterations in the extracellular components such soluble factors and extracellular matrix. These factors affect the ability of cells to traverse each step of the metastatic cascade and ultimately colonize distant organ sites where the microenvironment is vastly different from the tissue of origin.

In 1889 Stephen Paget first presented his theory of "Seed and Soil" as it pertains to metastasis suggesting that the relationship between the migrating cells and the microenvironment of the secondary site is a key factor in the ability of a tumor to

spread[107]. While some of the differential tissue specificity observed in different cancers may be attributed to the locations of capillary beds during hematogenous dissemination, this fluid mechanics argument cannot fully explain the patterns observed clinically. The diversity of molecules and cells in different organs is likely to play a role in why some cancers preferentially spread to particular tissues over others. A variety of studies have aimed to elucidate the regulatory networks that promote tissue-specific metastasis[66, 108-111].

Changes in cancer cell-extracellular matrix (ECM) interactions likely influence each stage of the metastatic cascade, starting with the loss of basement membrane adhesion to colonization of distant sites. Furthermore, alterations in matrix production and crosslinking can promote metastasis[112-114]. Consequently, inhibiting interactions of tumor cells with their microenvironments by targeting adhesion molecules is an area of active investigation[115-116]. In addition to their effects on cell adhesion, ECM molecules contain many domains capable of binding other ECM molecules and growth factors in a manner that can yield synergistic signaling events in cells[117]. This synergy highlights the importance of studying multiple ECM components simultaneously.

In addition to the role of altered ECM, a variety of cells are frequently recruited to promote metastasis. Recently, it has become appreciated that paracrine signaling loops between cancer cells and other cell types are acting to establish microenvironments that are conducive to metastasis[106]. Recruitment of mesenchymal stem cells through CCL5[118] and bone marrow stromal cells by osteopontin[119] or VEGFR1/VLA-4[67] signaling has been shown to promote metastasis. Furthermore, increased osteoclast activity in bone metastases through activation by soluble VCAM-1[120] and TGFβ[121]

promotes establishment of a metastatic niche and the RANKL cytokine promotes migration in bone by the cancer cells[122]. Tenascin-C has been found to act both in an autocrine fashion and from the tumor stroma to promote metastatic outgrowth[114]. Secretion of LOX by premetastatic cells can crosslink collagen IV at metastatic sites and induce recruitment of bone marrow derived cells to establish the metastatic niche[123]. It is now understood that macrophages help establish the metastatic niche[124]. Recent evidence suggests that these cells are likely recruited through CCL2 signaling to inflammatory monocytes that subsequently promote extravasation of tumor cells by secretion of VEGFA[68]. Many of these paracrine loops involve direct alterations of ECM or integrin presentation, while others result in indirect presentation through the cells that they recruit. In general, chemokine signaling plays a large role in recruitment of stromal cells and conferring tumor cell homing in a manner that helps explain tissue specificity of metastasis[125].

In general, the majority of the cellular interactions involve leukocytes that either stimulate or perpetuate an inflammatory microenvironment or discourage cytolytic adaptive immune responses through the recruitment of regulatory leukocytes. T_H2 $CD4^+$ T-cells prevent anti-tumor activity by $CD8^+$ T-Cells and NK cells[106]. Tumor-associated macrophages (TAMs) have been found to promote tumor growth and metastasis in animal models, and have shown correlations to poor prognosis, clinically[126-127]. Secretion of factors such as CSF1 by cancer cells can attract TAMs in a paracrine fashion[128-129]. Furthermore, intravital imaging studies have revealed that TAMs can act to promote intravasation of tumor cells[130]. In addition to TAMs,

myeloid-derived suppressor cells (MDSCs) promote tumor progression and metastasis through inhibition of anti-tumor responses[131-132].

1.5 Extracellular Matrix and Integrins

At each step of the metastatic cascade, cells must alter their interactions with extracellular matrix and integrins. Appropriate modifications of these interactions are necessary for the traversal of these stages, and failure to adapt is likely at the root of the inefficiencies of this process. In this section, these classes of molecules are briefly reviewed.

1.5.1 Extracellular Matrix

Extracellular matrix plays essential roles in maintaining tissue homeostasis as well as permitting the evolution of disease states. ECM provides a scaffold on which individual cells can migrate and, in the context of the basement membrane, upon which layers of epithelial cells can form. At a tissue level, it provides structural support for organs and helps organize groups of cells within tissues to coordinate their functions. Modulations of the mechanical properties of ECM can affect cellular responses[133-134]. Through integrins (discussed in the next section), this diverse set of dynamically-regulated molecules helps to control the responses and fates of cells that make up our tissues in a manner that may exceed those of soluble factors[117].

In addition to its role in cellular adhesion, ECM affects a wide range of cellular responses. Patterning of ECM has been shown to guide the orientation of the cell division axis[135]. Basement membranes, composed primarily of collagen IV, laminin, nidogen, and perlecan, act not only to support parenchymal epithelial sheets, but also

support blood vessels and angiogenesis[136]. ECM molecules contain a variety of growth factor binding domains. Heparan sulfate proteoglycans bind FGF and this complex is what is recognized by FGFR[137]. Furthermore, sequestration of TGF-β by ECM molecules such as fibrillins controls its activity. As a result, Marfan's patients, who have mutations in the fibrillin gene, suffer from aberrant TGF-β signaling, which results in a number of adverse pathologies once thought to be a direct effect of altered mechanical properties of fibrillin[138]. ECM molecules often contain EGF-like domains[139-140], which may themselves be capable of ligating EGFR and inducing signaling[117]. That ECM molecules typically contain multiple domains capable of binding cells, growth factors, and other ECM molecules suggests an attractive model of these molecules as signal integrators that act to induce localization and synergistic activation of growth factor receptors and integrins in a spatially constrained manner[117].

While ECM proteins play important roles in maintaining normal tissue physiology, their contributions to malignancy cannot be ignored. Frequently, alterations in MMP and cathepsin activity in cancer are observed, suggesting a role for matrix degradation in tumor progression[141-144]. Additionally, matrix crosslinking by lysyl oxidase[123] promotes development of the premetastatic niche, and TG2-induced crosslinking may inhibit tumor growth[145]. Just as heparan-sulfate PGs can promote FGF signaling, improper regulation of HSGAGs can promote tumor growth and assist in immune evasion[146-147]. Production of tenascin-C and osteopontin, as discussed previously, has been shown to assist in establishment of the metastatic niche[114, 119, 148-149]. Alterations in laminin isoforms are evident at the invading front of carcinomas[150].

Elegant animal models based on human tissue neoplasia have identified a temporal regulation of ECM-related genes during squamous cell carcinoma progression[151]. Production of type VI collagen by adipocytes has been shown to promote mammary tumor progression[152]. Galectins, a family of β-galactoside binding lectins and the subject of later chapters in this thesis, have a diverse set of roles in tumorigenesis[153]. The importance of ECM in cancer is so profound that it has even elicited recommendations of tissue engineering approaches to cancer therapy that aim to normalize the mechanical properties of the ECM[154]. As an immense body of literature has aimed to characterize the role of ECM in neoplasia, the aforementioned findings represent only a small sampling of its diverse roles in this disease.

1.5.2 Integrins

The identification of fibronectin (originally termed "LETS protein") as an extracellular matrix molecule by Richard Hynes and others in the mid-1970s initiated a considerable interest in identifying its corresponding surface receptor[155-158]. Its significant effects on adhesion and migration[159-160] coupled with its association with viral transformation[155, 158] highlighted its relevance in normal physiology and, potentially, disease states. The identification of the minimal fibronectin-derived binding sequence, RGDS, by Erkki Ruoslahti's group[161] in conjunction with the recognition of GPIIb/IIIa as a fibronectin receptor[162] led to the eventual cloning and classification of the integrin receptor[163-164].

Integrins, named after their recognition as an integral membrane protein capable of linking ECM to the cytoskeleton, are the main class of adhesion molecules. Integrins are heterodimers that consist of an α chain and a β chain. There are 18 unique α and 8

unique β subunits that dimerize to form 24 distinct integrins[165]. In addition to their roles as ECM adhesion molecules, many of the integrins are present on leukocytes and potentiate their ability to home to sites of inflammation through interactions with VCAM-1 ($\alpha 4\beta 1$) and ICAMs ($\alpha L\beta 2$), binding complement through C3b ($\alpha M\beta 2$), and binding E-Cadherin and intestinal microvasculature($\alpha E\beta 7$)[166-168].

Integrins serve both as signaling molecules and force transducers, and these roles are not wholly independent. Their ~50 amino acid long cytoplasmic tails interact directly with the actin-based microfilament system. In order to bind their corresponding ligands, integrins typically must be activated by inside-out signaling. This phenomena is readily apparent on leukocytes and platelets, where activation mediates a switch toward inflammation and coagulation, respectively[165]. Regulation of activation of integrins on epithelial cells likely also plays a role in adhesion and migration[169]. This activation can result in altered positioning of the metal in the metal ion-dependent adhesion site within the I/A domain in integrins with α-I/A domains[170] or separation of the β-I/A domain from the 7-bladed β-propeller in the α subunit of integrins lacking α-I/A domains[171]. The activation state of the integrins is controlled by the localization of their C-terminal ends, wherein only upon separation of these tails can the integrins be activated[172-174]. In addition to inside-out signaling that mediates integrin activation states, integrins also potentiate outside-in signaling upon ligation in a manner that can promote survival, growth, and migration and that is typically dependent upon recruitment of focal adhesion kinases (FAK) or Src family kinases (SFK).

As might be expected from their roles in adhesion, proliferation, and migration, regulation of integrin activity can have profound effects on tumor progression[115, 175].

Loss of α2β1 is found in many tumors and its re-expression in mammary tumor cells reduces their malignant phenotype[176]. Anchorage-independent growth is a hallmark of cancers, as most epithelial cells will undergo anoikis in the absence of integrin-mediated contacts. Furthermore, it has been claimed that unligated integrins may promote apoptosis[177]. In many tumor cells, however, unligated αvβ3 promotes survival[178]. Integrin signaling by both tumor cells and endothelial cells can promote angiogenesis. Furthermore, αv integrins have been shown to work in concert with growth factor receptors to promote activation of angiogenesis pathways[179]. Similarly, integrin-growth factor complexes can form within tumor cells to mediate cooperative signaling[180-182]. Mutant p53 can induce constitutive activation of EGFR/integrin signaling by promoting integrin recycling in a manner that increases invasion[183]. Integrins promote recruitment of bone marrow-derived cells that are pro-tumorigenic[184-185], and interactions between VCAM-1 on tumor cells and α4β1 on leukocytes promote tumor growth and metastasis[120, 186]. FAK signaling has been found to be necessary for tumor progression in breast cancer[187] in a manner that acts through Ras and PI3K[188]. MMP-2 can interact with αvβ3 on invasive cells to promote ECM degradation during invasion[189]. As integrins have many roles in tumor progression, targeting these interactions can inhibit malignancy. Valerie Weaver and Mina Bissell used a 3-dimensional culture system to demonstrate the efficacy of a β1 inhibitory antibody to revert the malignant phenotype of breast cancer cells[116]. Subsequently, a variety of antibodies and peptides targeting integrins have been developed and are currently undergoing clinical trials[115, 190].

1.6 Phenotypic Screening

Phenotypic screening approaches have gained recent popularity, particularly by pharmaceutical companies, in order to assess the effects of small molecules or RNA interference during drug discovery. Traditional genetic screens have been useful in identifying candidate genes, elucidating signaling pathways, and associating genes of similar function through transcriptional profiling. Such approaches have been implemented in the study of normal cell function and disease mechanisms. In particular, a variety of gene expression screens have been utilized for cancers of the lung and other tissues[76-77, 109-110, 151, 191-194]. While these screens have identified a diversity of candidate effector genes and gene sets, the disparity between these profiles implies a lack of conserved mechanistic alterations that occur at the gene expression level to confer malignancy. Phenotypic screening has the added advantage of the ability to assess a diversity of functional responses beyond alterations in gene expression. Using such approaches, one can uncover conserved phenotypic responses that are not reflected by transcriptional profiling. Nonetheless, many phenotypic screens are based on RNAi, and while they measure functional responses rather than transcriptional ones, they still suffer from the reliance on genetic perturbations [195-198]. Other phenotypic screens utilize small molecules and automated microscopy to determine drug effects on cellular responses[199-200]. While these screens can provide insights beyond alterations in expression, the measured phenotypes are often confined to viability or morphological changes.

Despite its drawbacks, phenotypic screening has still exhibited a large degree of success in the pharmaceutical industry. Genetic and other approaches have been useful in

identifying a variety of targets whose underlying molecular mechanisms make them strong candidate targets for therapeutics. As a result target-based screens are frequently used to discover new drugs. While such approaches appear, theoretically, to be a superior method for drug discovery, phenotypic screening has proved more effective in delivering first-in-class small-molecule drugs than existing target-based approaches[201]. Despite its successes, however, attrition rates are still exceedingly high using phenotypic screening. Advances in high-content screening, will likely improve these screening techniques by allowing investigators to query many diverse readouts instead of simple measures such as cell death[202]. Additionally, novel screening technologies that permit investigation of interactions beyond solution-phase administration of small molecules, short RNAs, and peptides will likely reveal a variety of cellular responses that cannot currently be queried with existing technologies. Such advances in technologies and approaches will be essential for the development of additional first-in-class drugs that can sustain the patent expirations[203].

Chapter 2. Development of an Extracellular Matrix Screening Platform

Adapted from: Reticker-Flynn, N.E., *et al.* "A combinatorial extracellular matrix platform identifies cell-extracellular matrix interactions that correlate with metastasis." *Nat Commun* **3**, 1122 (2012).

2.1 Introduction

Cancer metastasis is a poorly understood multistep process that results in 90% of cancer-related deaths[10-11]. At the time of initial diagnosis, almost half of lung adenocarcinoma patients have detectable metastases and the majority of the remaining half will relapse with metastatic disease after surgical removal of the primary tumor and adjuvant chemotherapy[27]. Despite the ominous nature of metastatic disease, the molecular mechanisms that drive each step are poorly characterized and few effective therapies exist[42]. Recently, it has become apparent that the tumor microenvironment dramatically impacts metastatic progression[106]. Changes in cancer cell-extracellular matrix (ECM) interactions likely influence each stage of the metastatic cascade, starting with the loss of basement membrane adhesion to colonization of distant sites. Furthermore, alterations in matrix production and crosslinking can promote metastasis[112-114]. Consequently, inhibiting interactions of tumor cells with their microenvironments by targeting adhesion molecules is an area of active investigation[115-116].

While a variety of techniques exist for studying microenvironmental interactions, it has been challenging to date to interrogate the functional implications of specific cell-ECM interactions in a high-throughput manner. Microinjection of Rous sarcoma virus into embryos documented the anti-tumor effects of the embryonic microenvironment[204-

205], and coculture studies have identified the roles of carcinoma-associated fibroblasts on tumor progression[206]. ECM-coated transwells have been used to study the effects of small numbers of individual candidate ECM molecules on 2D invasion[207], and 3D collagen gels have been useful particularly in the study of matrix metalloproteinase activity[144]. *In vivo* studies using gene-targeted mice have documented the importance of several ECM molecules and their receptors in transplant-based models of cancer and metastasis[208-209]. Each of these techniques has documented key microenvironmental regulators of metastasis, but they have not allowed an unbiased systematic evaluation of the role that ECM components play.

Cell-ECM interactions are particularly difficult to study due to their complexity of synergistic and antagonistic interactions *in vivo*[117]. Experiments targeting integrins, a central family of cell surface receptors that mediate ECM interactions, have implicated integrin-ECM interactions as important regulators of cancer progression[115, 151, 190]. However, in addition to adhesion, integrins regulate stress transmission and bidirectional signaling, and typically bind multiple ECM molecules[165]. Furthermore, transmembrane collagens, syndecans, lectins, carbohydrates, gangliosides, glycolipids, CD44, and dystroglycans are among a host of non-integrin ECM receptors. Thus, techniques that allow the specific unbiased interrogation of cell-ECM adhesion are required to directly query the diversity of potential interactions.

In this chapter, we describe a high-throughput platform capable of systematically uncovering cell-ECM interactions, and use this method to characterize the global changes in ECM adhesion in a model of cancer progression. We previously described a first-generation platform that utilized robotic spotting technology to generate arrays

with combinations of five ECM molecules found in normal basement membrane and connective tissue[210]. Since then, others have utilized similar platforms to investigate ECM responses[211-214]. While these platforms have demonstrated feasibility of such approaches in physiologic processes such as differentiation of stem cells, they have not yet been applied to increase our understanding of disease states. Furthermore, their limited size (typically five different ECM molecules) has prevented them from querying the diversity of ECM interactions present in the human body. Here, we present an expanded ECM microarray platform containing 768 unique pairwise ECM molecule combinations expressed differentially in development, regeneration, and disease including an expanded representation of proteoglycans and glycosaminoglycans which are difficult to study through integrin manipulation alone, and apply them to investigate changes in adhesion throughout metastatic progression. We have established a high-throughput pipeline to generate these microarrays that utilizes liquid handlers for mixing of source ECM, optimized cell-seeding devices, and automated image capture and analysis. We studied the adhesion profiles of lung adenocarcinoma cell lines generated from a genetically engineered mouse model where discrete stages of metastatic progression have been defined, and correlated the findings with *in vivo* ECM distributions in mice and humans with metastatic lung cancer[194, 215-216]. This approach is easily extensible to other disease states, ECM combinations, and phenotypic readouts.

2.2 Results

2.2.1 Extracellular Matrix Microarrays to Probe Cell-ECM Adhesion

To allow the unbiased study of the ECM adhesion characteristics of any cells-of-interest, we developed a novel high-throughput platform. We expanded, automated, and optimized our adhesion platform[210-211] to include every single and pairwise combination of 38 unique ECM molecules (Table 2.1). Thus, these arrays contain 768 different combinations in quintuplicate and 160 control spots, for a total of 4000 arrayed features.

ECM Molecules		
Collagen I	Keratin	Thrombospondin-4
Collagen II	Mucin	Osteopontin
Collagen III	Superfibronectin	Osteonectin
Collagen IV	F-Spondin	Testican 1
Collagen V	Nidogen-2	Testican 2
Collagen VI	Heparan Sulfate Proteoglycan (Perlecan)	Fibrin
Fibronectin	Biglycan	Tenascin-C
Laminin	Decorin	Nidogen-1
Laminin α2	Galectin-1	Vitronectin
Tenascin-R	Galectin-3	Agrin
Chondroitin Sulfate Proteoglycans	Galectin-3c	Hyaluronan
Aggrecan	Galectin-4	Brevican
Elastin	Galectin-8	

Table 2.1. *ECM Microarray Molecule List.* This table lists all of the molecules included in the ECM Microarray platform.

To fabricate the arrays, the slides are first prepared by coating with a polyacrylamide gel approximately 100μm thick. To achieve this coating, fresh prepolymer solution consisting of 10%(w/v) acrylamide, 0.5%(w/v) bis-acrylamide, and 20%(w/v) Irgacure 2951 is prepared. 100μL of the prepolymer solution is pipetted onto acrylated glass slides. A number 1 coverslip it placed on top of the prepolymer, ensuring an even distribution of solution between the slide and the coverslip, and the slides are exposed to UV irradiation for 5 minutes. The slides are then allowed to soak in ddH_2O for one

minute prior to removal of the coverslip. The slides are then left in new water for two days with four changes of the water to completely remove any unreacted monomer. Slides are then dehydrated on a hotplate and stored at room temperature prior to printing.

To print the slides, the 38 ECM molecules and rat tail collagen I controls are transferred from a 96-well source plate to two low-volume 384-well plates and mixed thoroughly using a Tecan robotic liquid handler. These 384-well plates are then used as source plates for deposition of the matrix combinations onto the slides by a DNA microarray spotter. The dehydrated hydrogel acts to entrap molecules without requiring their chemical modification (Fig. 2.1a). Our data indicate that molecules larger than ~10kDa can be robustly entrapped in the hydrogel (Fig. 2.1b), and we verified their entrapment using NHS-Fluorescein labeling or antibody-mediated detection after entrapment (Fig. 2.1c). Of the 38 molecules that we tested by these methods, all showed excellent reproducibility and uniformity within the expected region of printing (Fig. 2.1c and data not shown). Furthermore, the positive controls allow for monitoring of spatial effects during seeding.

It should be noted that, while these data demonstrate entrapment of all of the ECM molecules, a variety of factors may prevent their appropriate presentation. Differences in spotting buffer pH or steric hindrance imposed by the hydrogel pore size may prevent the orientation or conformation of molecules to allow cellular interactions in a manner analogous to *in vivo* interactions. Furthermore, the purity of the molecules is likely not 100%, suggesting the possibility of additional unknown ECM interactions during the screening. Finally, these slides are briefly sterilized by exposure to ultraviolet light. This

UV exposure may induce radiation damage to the ECM molecules. All of these effects may play a role in the cell-ECM interactions measured on the arrays, and should be taken into consideration when evaluating the relevance of negative results.

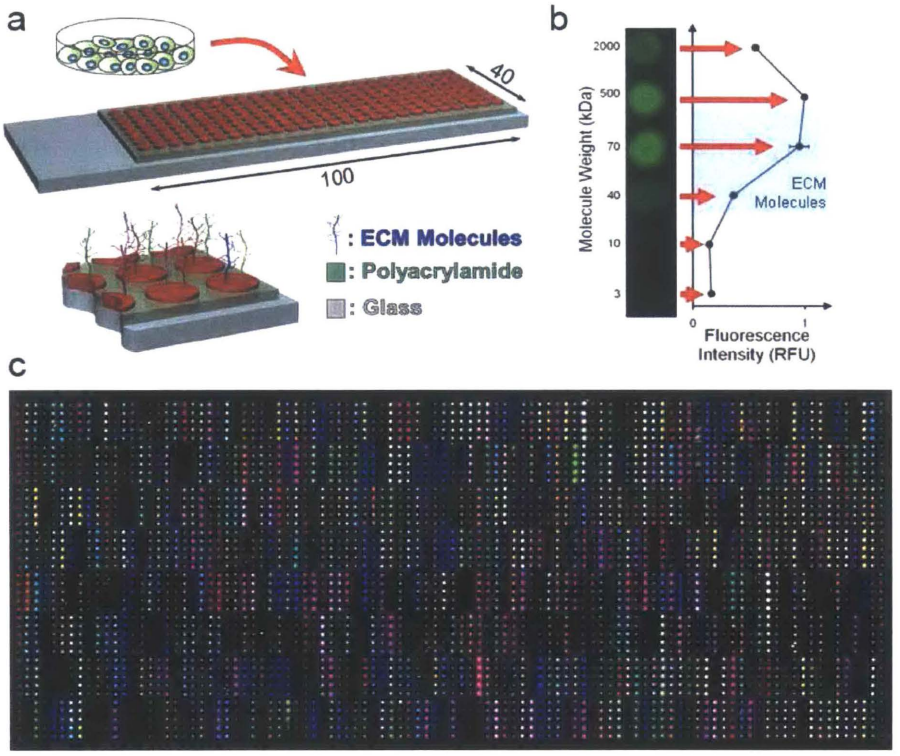

Figure 2.1. *Extracellular Matrix Microarray Platform Presents Combinations of ECM Molecules for Cell Attachment* (a) ECM microarrays are generated by spotting 768 unique combinations of ECM molecules on glass slides coated with polyacrylamide followed by seeding of cells onto the slides. (b) Fluorescence intensity of Rhodamine-labeled dextran of various molecular weights spotted onto polyacrylamide-coated slides. Slides were incubated in media at 37°C overnight and washed with PBS prior to imaging. (c) Verification of presentation of all molecules by immunolabeling (colored spots) or NHS-fluorescein labeling (grayscale spots) of all molecules subsequent to array generation and rehydration.

To measure cell-ECM interactions, cells are seeded onto the arrays in serum-free medium and allowed to adhere for 1.5 hours at 37°C (Fig. 2.2). Prior to seeding the

arrays, the slides are rehydrated in PBS and sterilized by UV exposure for ten minutes. The PBS is then replaced with medium for five minutes, which is then aspirated and the cells are seeded. To ensure uniform seeding, the slides are agitated every fifteen minutes. Furthermore, the top surfaces of the slides are held flush with the bottom of the plate through the use of a custom-designed seeding device that employs a vacuum seal (Fig. 2.3). This device minimizes seeding variability between experiments and avoids cell loss by preventing cells from settling below the slide surface or on the backs of the slides. For cancer cell experiments, cells are seeded at a concentration of 4×10^5 cells in six milliliters of serum-free medium per slide. Following initial seeding, the arrays are washed once and placed in medium with serum in 4-well tissue culture plates. The arrays are left at 37°C prior to staining. Uniformity of seeding across individual arrays and between replicate arrays was confirmed using test slides composed of only one matrix molecule (data not shown).

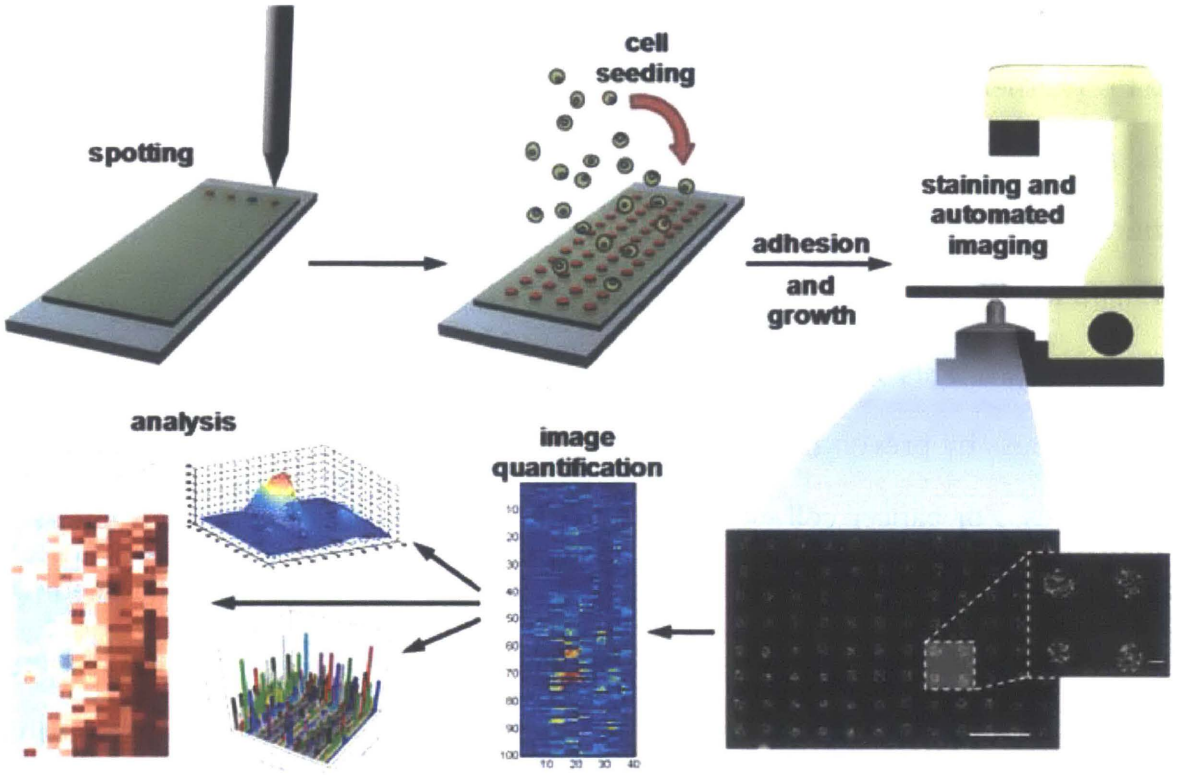

Figure 2.2. *Process Flow for ECM Microarray Experiments.* Slides are prepared by spotting ECM onto polyacrylamide-coated slides; cells are seeded onto slides; following adhesion and growth of cells, slides are stained and imaged on an automated epifluorescence microscope; images are quantified and analyzed using custom software.

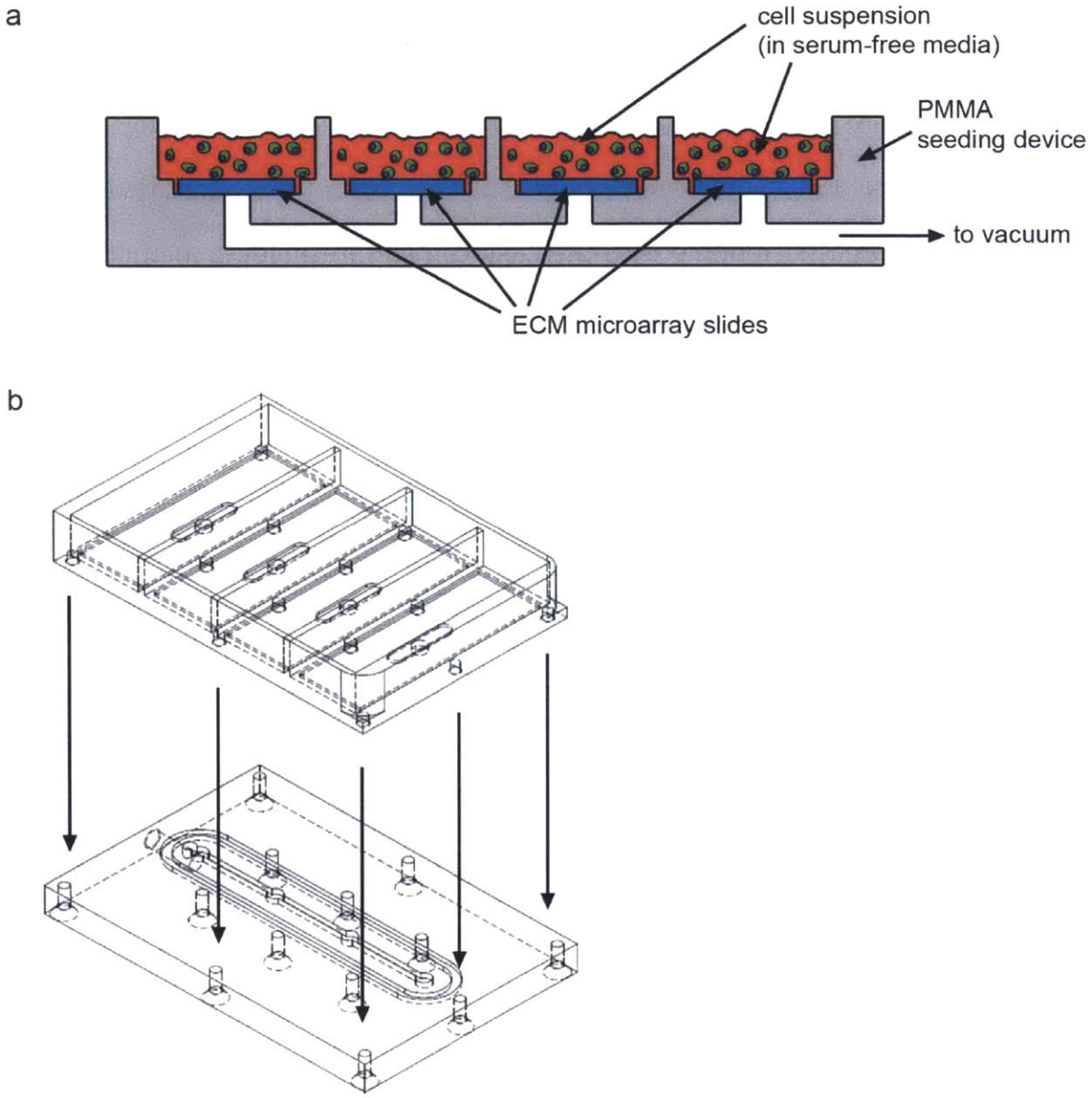

Figure 2.3. *Seeding Devices for ECM Microarrays.* (a) Cross-sectional schematic of seeding device. The device consists of four chambers each of which holds a single ECM microarray slide. The bottom of each chamber consists of a recessed region into which the slides sit such that their top surface is flush with the remainder of the bottom of the chamber. A vacuum port exists at the bottom of each chamber and connects to a central vacuum line. The vacuum acts to hold the slides in place and prevents media from leaking onto the backs of the slides. (b) CAD schematic depicting the four chambers of the seeding device.

To quantify cells bound to each spot, nuclei are stained according to conventional fluorescence staining protocols, and the slides are imaged using an automated inverted

epifluorescence microscope with NIS Elements software (Fig. 2.2 and 2.4). Large images are cropped to individual spots and indexed using MATLAB (Mathworks). Regions outside of the ECM spots are masked, and adhesion is quantified using CellProfiler software to detect and count nuclei (Fig. 2.5b)[3]. Nuclei are identified using the "IdentifyPrimaryObjects" module with the Otsu Global thresholding method. Clumped objects are distinguished using "Intensity". Subsequent image and data analysis are performed in MATLAB.

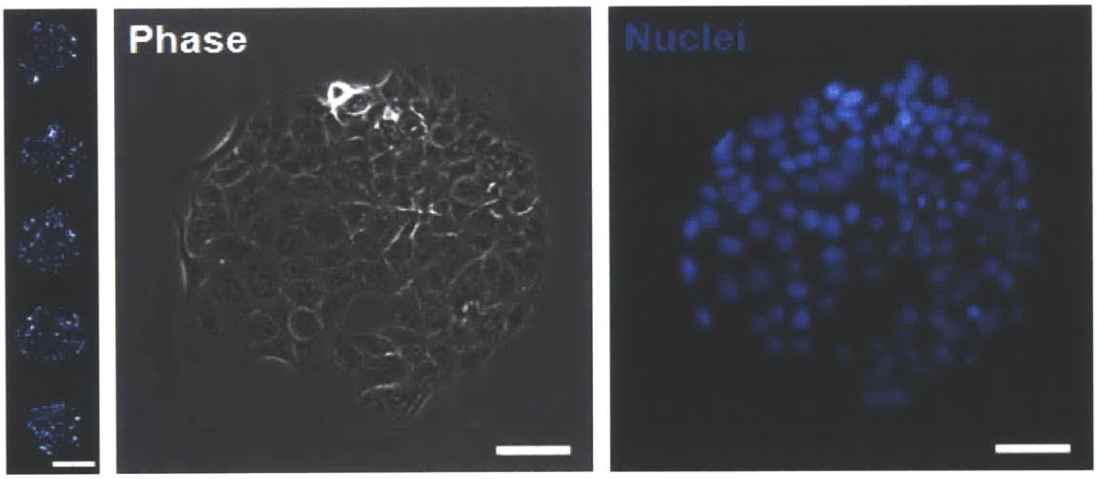

Figure 2.4. *Cells Adhered to ECM Microarrays.* Representative images of cells adhered to ECM spots demonstrating selective adhesion to the regions where ECM has been deposited. Nuclei (blue) are stained with Hoechst. Leftmost image is of five replicate spots. Scale bar on five-spot image is 200μm. Scale bars on single-spot images are 50μm.

Comparisons of adhesion signatures are performed using the following approach. The average and standard deviation of counts on replicate spots are quantified. Spots for which the count is greater or less than one standard deviation above or below the mean, respectively, are discarded, and the average of the remaining counts is computed (x). Each slide is then normalized by first computing the average count across all ECM combinations on the slide for which the count is greater than zero (X). The normalized

adhesion value for each combination is then computed by dividing the average of the raw counts for the combination by the average of the non-zero counts for the slide (x/X).

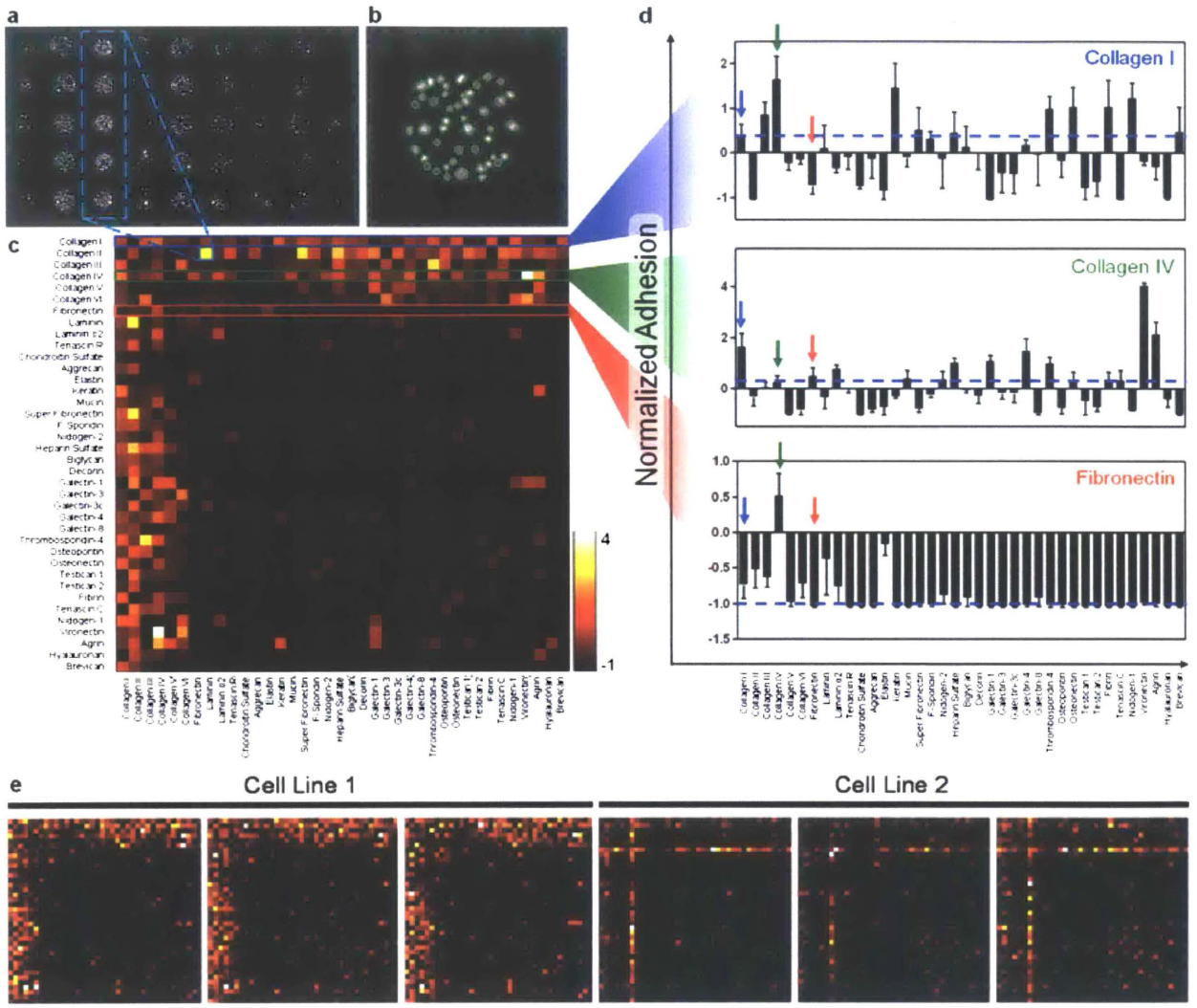

Figure 2.5. *Combinatorial Adhesion Profiles are Generated using ECM Microarrays.* (a) Nuclear stain of cells seeded on the ECM microarrays. (b) Identification of individual nuclei on one spot using CellProfiler[3]. (c) Quantification of adhesion to all molecule combinations for one cell line. (d) Selected adhesion profiles for three molecules: Collagen I (blue), Collagen IV (green), and Fibronectin (red) in combination with all other molecules. Dashed blue lines represent adhesion to that molecule alone. Arrows denote combinations with the other two molecules or alone. Error bars are s.e.m. of three replicate slides. (e) Comparisons of three replicate slides for two representative cell lines. Scale bars in (a) and (b) are 450μm and 100μm, respectively.

2.2.2 *ECM Microarrays Identify Distinct Adhesion Profiles During Metastatic Progression*

To uncover changes in the global adhesion profile of cancer cells during cancer progression and metastatic spread, we analyzed a panel of murine lung adenocarcinoma cell lines derived from non-metastatic primary tumors (T_{nonMet}), primary tumors that metastasized (T_{Met}), or lymph node (N) and liver (M) metastases (Table 2.2)[194]. These cell lines were derived from a genetically engineered mouse model of metastatic lung adenocarcinoma in which tumors were initiated in *Kras*$^{LSL\text{-}G12D/+}$;*p53*$^{flox/flox}$ mice with lentiviral-Cre vectors. The stable and random integration of the lentiviral vector allowed the clonal relationship between the multifocal primary tumors and metastases to be established[194]. Previous gene expression analysis revealed conserved alterations in expression patterns between the T_{nonMet} and T_{Met} lines, but not the T_{Met} and N/M lines. These studies revealed a role for *Nkx2-1* and *Hmga2* in discouraging and promoting metastasis, respectively[194].

Cell Line	Classification
368T1	TnonMet
394T4	TnonMet
802T4	TnonMet
389T2	TMet
393T5	TMet
482T1	TMet
389N1	LN
482N1	LN
2691N1	LN
393M1	Met
2691M1	Met

Table 2.2. *Cell lines screened.* This table lists the cell lines screened on the arrays and their classifications. Cell lines derived from primary lung tumors that did not give rise to metastases (T_{nonMet}), did give rise to metastases (T_{Met}), lymph node metastases (N/LN), and distant metastases (M/Met).

To determine whether conserved alterations in adhesion correlate with metastatic progression, we ran these cell lines on the ECM microarrays. Analysis of the adhesion profiles of these cell lines highlighted the diversity in adhesion of a given line to different ECM combinations (Fig. 2.5c). Our analysis of these cell lines revealed highly reproducible adhesion between replicate spots and arrays, confirming the quantitative nature of the assay (Fig. 2.5e and data not shown). We examined the profiles to interrogate whether various populations exhibit enhanced adhesion to combinations of ECM molecules, relative to the same molecules spotted in isolation. This analysis revealed that different pairwise combinations of ECM molecules result in additive, synergistic, and antagonistic effects on adhesion. For example, for the T_{nonMet} cell line shown in Figures 2.5c and 2.5d, many molecules improve adhesion to collagen I, while others reduce cell binding in comparison to the molecule in isolation (blue line, Fig. 2.5d top panel). A similar range of responses was observed for other molecules, including collagen IV and fibronectin (Figure 2.5d middle and bottom panels, respectively). These types of combinatorial effects were present for many molecules and, while the specific patterns varied, all cell lines tested exhibited examples of increased and reduced binding to various ECM combinations (data not shown). For each of the fifteen murine lung adenocarcinoma cell lines tested, distinct profiles that were highly reproducible across replicate slides were obtained (Fig. 2.5e).

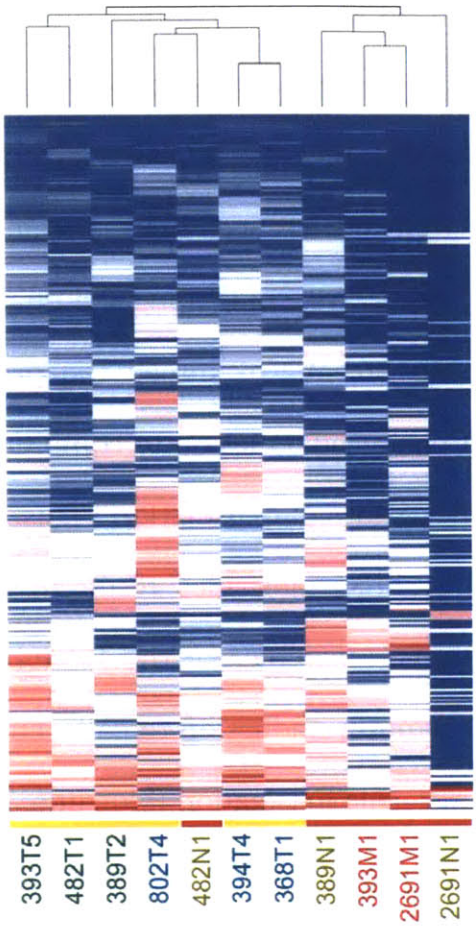

Figure 2.6. *ECM Microarrays Demonstrate Conserved Changes in Adhesion that Correlate with Metastasis.* Unsupervised hierarchical clustering of adhesion profiles generated by the ECM microarrays. Vertical axis represents different ECM combinations. Horizontal axis represents different cell lines. Yellow bars indicate primary tumors (T_{nonMet} and T_{Met} lines). Red bars indicate nodal (N) or distant metastases (M). T_{nonMet} lines are in blue text, T_{Met} lines are in green text, N lines are in orange text, and M lines are in red text. The dendogram at the top represents the results of the clustering based on Euclidean distances.

We used the ECM microarrays to compare the adhesion profiles of populations from each of the T_{nonMet}, T_{Met}, N, and M classes of cell lines. We applied unsupervised hierarchical clustering analysis of the adhesion values in a manner analogous to clustering of gene expression microarray data. Of note, all the cell lines derived from metastases (N or M), save for one lymph node line, clustered independently from the cell lines derived from primary lung tumors (T_{nonMet} or T_{Met}) (Fig. 2.6). This result is particularly notable, since two of the metastatic lines (393M1 and 389N1) were generated from metastases that originated from two of the primary tumors (393T5 and 389T2, respectively), yet clustered more closely to the other metastases than the lines derived from those primary tumors. Thus, there is a conserved change in the ECM

adhesion profile of cancer cells present in a metastatic site compared to those that remain in the primary tumor. Furthermore, this differential clustering was not evident from unsupervised hierarchical clustering of the gene expression of these lines (ref[194] and Fig. 2.7), suggesting that the metastasis-specific adhesion phenotype provides a complementary, non-overlapping view of the molecular mediators that influence metastatic progression.

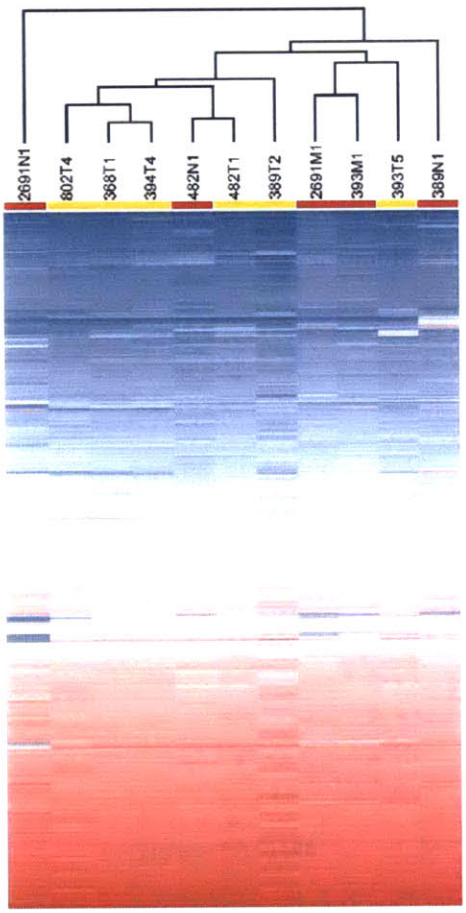

Figure 2.7. *Gene Expression Clustering.* Unsupervised hierarchical clustering of gene expression microarrays. All probesets displaying a variance>0.5 and expression>3.0 were included. Yellow bars demote primary tumor-derived cell lines (T_{nonMet} and T_{Met}) and red bars denote metastasis-derived cell lines (N and M). Clustering is performed using complete linkage analysis with a half square Euclidean distance and average value ordering weight.

2.2.3 *Identification of Metastasis-Associated ECM Molecules*

In light of the hierarchical clustering results, we asked whether there were particular combinations of molecules that are favored by metastatic cells rather than by cells from primary tumors. Thus, we compared the average adhesion of the liver metastasis-

derived cell lines (M) for each ECM combination to the average adhesion of the T_{Met} lines (Fig. 2.8a). While many of the M lines exhibit elevated binding to combinations containing fibronectin, pairings that combined fibronectin with any of galectin-3, galectin-8, or laminin had the highest differential adhesion between the T_{Met} and M lines. To explore changes in adhesion that specifically correlated with changes in metastatic progression, we compared the T_{Met} cell line 393T5 and the clonally-related liver metastasis-derived cell line 393M1. This pair of lines was derived from a primary tumor and a metastasis that disseminated from that tumor, as confirmed by examination of the lentiviral integration site[194]. Furthermore, the differential adhesion to the aforementioned ECM combinations was clear in both the group-wise comparison (Fig. 2.8a) and in the direct comparison of this primary tumor-liver metastasis pair (Fig. 2.8b).

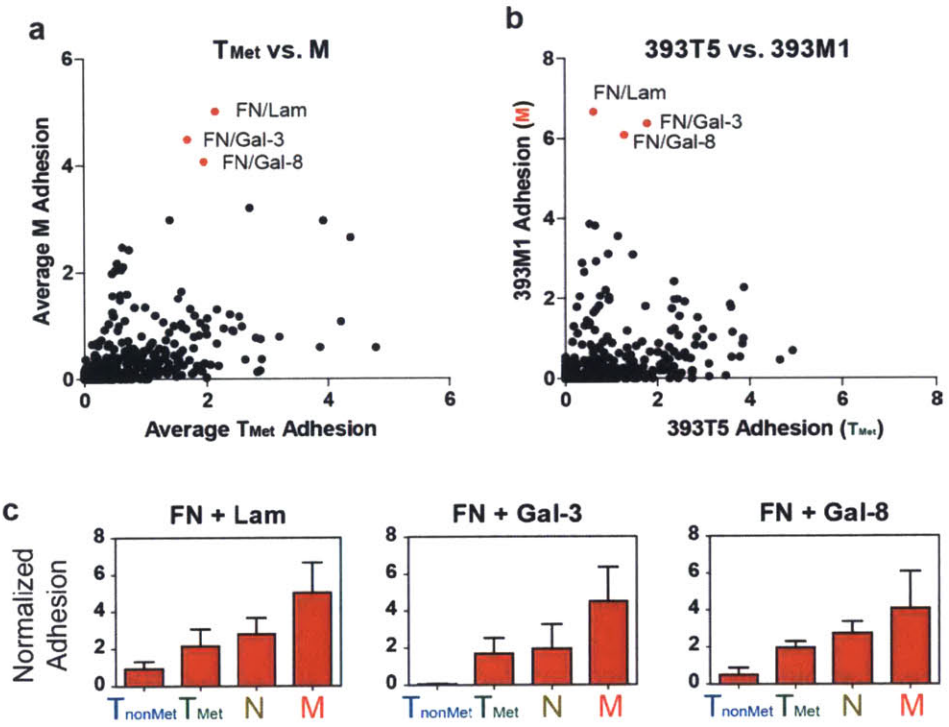

Figure 2.8. *Identification of metastasis-associated ECM molecules.* (a) Average adhesion of metastatic cell lines (M) to each combination compared to those of the metastatic primary tumor cell lines (T_{Met}). (b) Comparison of 393M1 adhesion for each combination to its clonally related primary tumor line, 393T5. Red dots indicate top ECM combinations exhibiting preferential adhesion by metastatic lines over the metastatic primary tumor lines. (c) Top three combinations exhibiting the greatest increase in adhesion across tumor progression as represented by the four classes of cell lines (T_{nonMet}, T_{Met}, N, and M). Error bars in (c) are s.e.m. of the different cell lines of each class ($n = 3$ cell lines per class) with the exception of the M class where there are two lines, and thus the error bars are the range of the means.

Collectively, the patterns observed suggest that combinations of molecules may play a more significant role in the adhesion profile of a given population than the tendency to bind to any of the ECM molecules alone. Interestingly, the trend towards increased binding to fibronectin/galectin-3, fibronectin/laminin, and fibronectin/galectin-8 combinations was consistent across tumor progression when we compared the average adhesion of all T_{nonMet}, T_{Met}, N, and M cell lines (Fig. 2.8c). Binding to these molecules, when presented alone, showed minimal (fibronectin) or no trend (laminin, galectin-3, and galectin-8) across the four groups of cell lines (Fig. 2.9a, red bars). When in combination, however, these pairs demonstrated enhanced effects that exceed the additive values of their individual adhesion.

In contrast to the increases in adhesion on the metastasis-associated combinations, other combinations demonstrated a reduced adhesion trend in relatively more metastatic populations, including a variety of collagens and osteopontin (Fig. 2.9a-c, blue bars). Taken together, these data suggest that adhesion to fibronectin in combination with any of galectin-3, galectin-8, or laminin is highly associated with tumor progression in this model system. Furthermore, a loss of adhesion to a variety of combinations containing collagen correlates well with metastatic progression. These

gain and loss of adhesion trends are particularly enhanced in combinations of ECM molecules over presentation of their individual constituents.

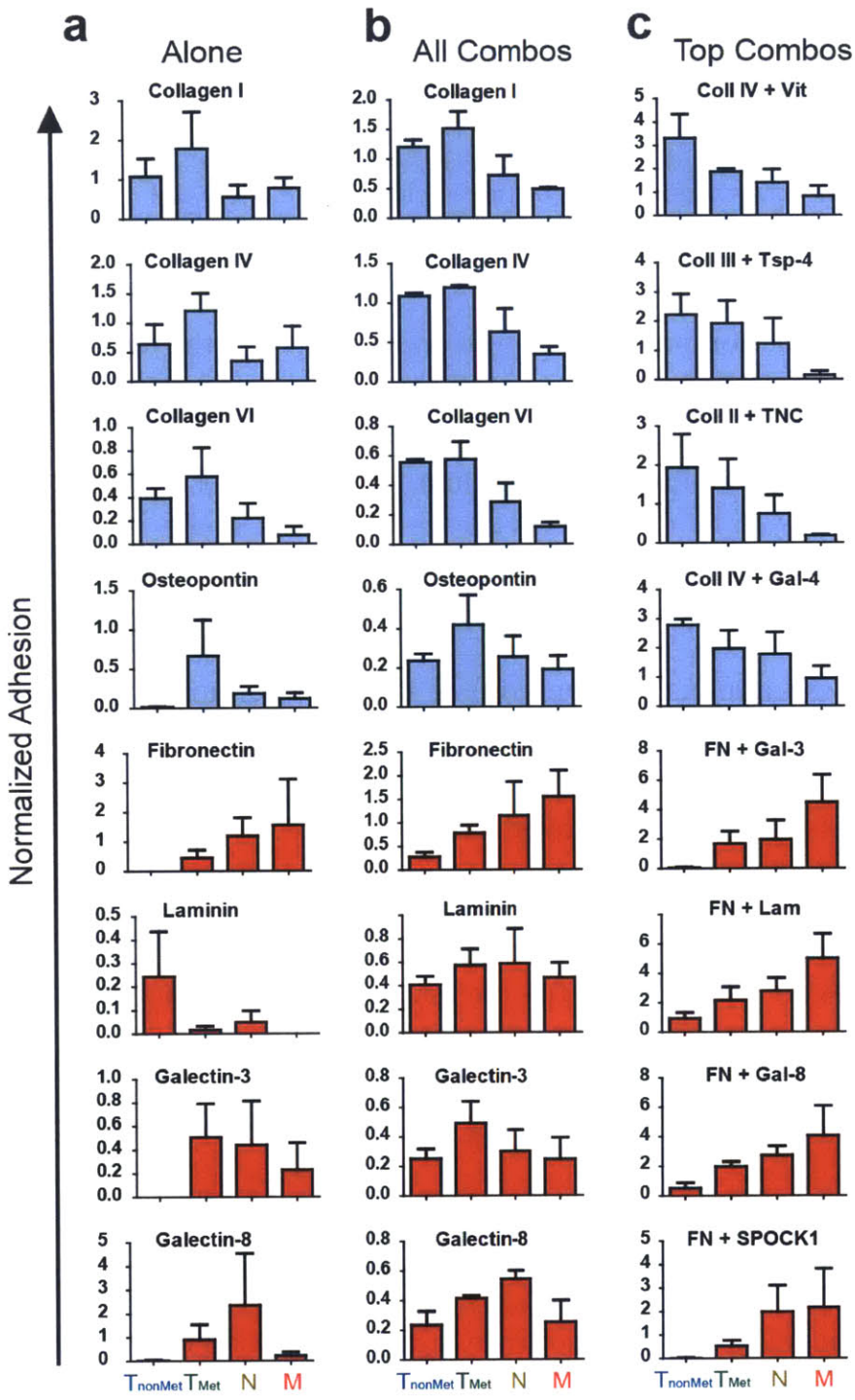

Figure 2.9. *Changes in adhesion correlate with metastatic progression.* Molecules to which there is a loss of adhesion (blue) or gain of adhesion (red) between the T_{nonMet} ($n = 3$), T_{Met} ($n = 3$), N ($n = 3$), and M ($n = 2$) cell lines when examined alone (a) or as an average of all combinations containing them (b). Combinations that exhibited the greatest gains (red) or losses in adhesion (blue) as determined by linear regression are depicted in (c). Combinations were selected based on the magnitude of the slopes provided that the regressions had r^2 values greater than 0.9. Y-axes represent normalized adhesion. Values less than ~0.5 represent very minimal adhesion. Error bars are s.e.m. of the different cell lines of each class with the exception of the M class where there are two lines, and thus the error bars are the range of the means.

In addition to the additive and synergistic effects of combining multiple ECM molecules, we noted that some combinations of molecules appear to elicit antagonistic effects on adhesion. We looked more closely at the adhesion profile of the M line 393M1 (Fig. 2.10a) and observed that, while the metastasis-associated molecules laminin, galectin-3, and galectin-8 all increase adhesion to fibronectin, other molecules appeared to decrease adhesion to it (Fig. 2.10b). *In vitro* adhesion assays using co-adsorbed ECM to multiwell polystyrene plates confirmed that the addition of these molecules does exhibit decreased adhesion of this line when compared to fibronectin alone(Fig. 2.10c). Possible explanations for this decrease in adhesion could include hindrance of access to binding domains within fibronectin by these high molecular weight proteoglycans or inhibition of adsorption of fibronectin to the plates through its interactions with these molecules. Collectively, the existence of both synergistic and antagonistic effects highlights the importance of investigating combinations of ECM molecules rather than isolated components.

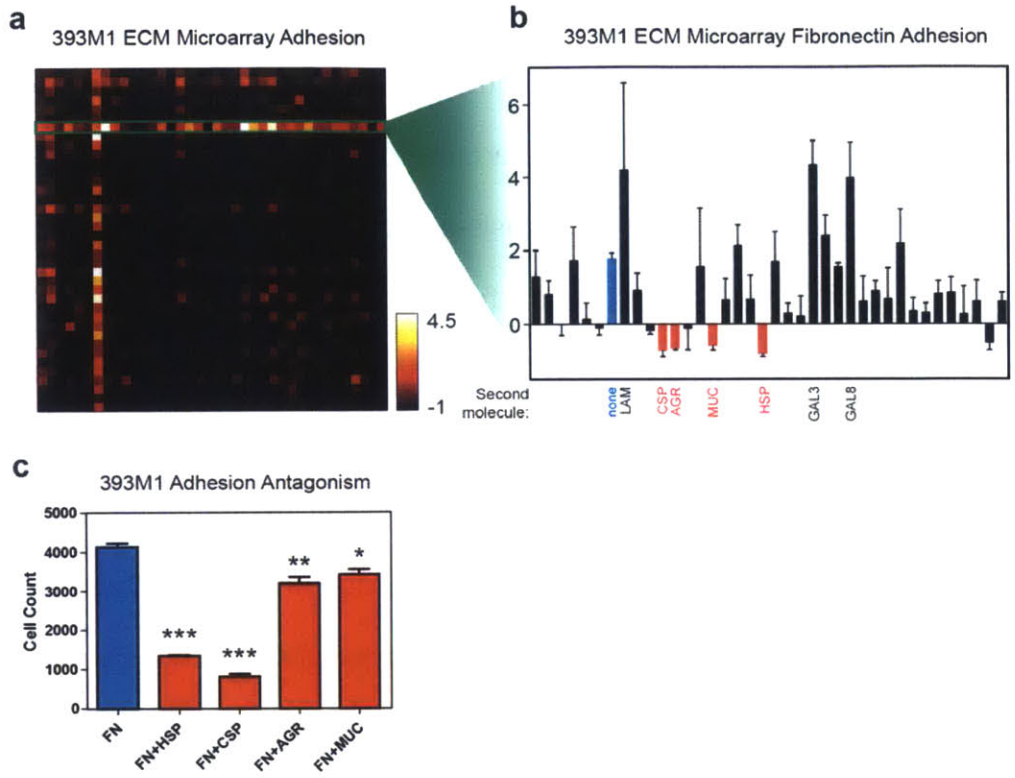

Figure 2.10. *ECM combinations can have anti-adhesive effects when compared to single molecules.* (a) Heat map depiction of adhesion profile of the M line 393M1 for each ECM combination. (b) All combinations of molecules containing fibronectin. Fibronectin alone is depicted in blue. Four combinations that exhibited significantly decreased adhesion when compared to fibronectin alone are depicted in red. CSP: chondroitin sulfate proteoglycan; AGR: aggrecan; MUC: mucin; HSP: heparin sulfate proteoglycan. The three metastasis-associated ECM combination hits are also denoted (LAM: laminin; GAL3: galectin-3; GAL8: galectin-8). Error bars are s.e.m. of three replicate slides. (c) Verification of anti-adhesive effects of the molecules highlighted in (b) was performed by coating 96-well plates with the molecules and examining adhesion of the 393M1 cell line. Error bars are standard error. $^{***}P < 0.001$; $^{**}P < 0.01$; $^{*}P < 0.05$. Significance was determined using one-way ANOVA with Tukey's Multiple Comparisons post-test.

2.3 Discussion

Our ECM microarrays provide a high-throughput multiplexed platform capable of measuring a variety of cellular responses to ECM. Here, we show they are capable of identifying adhesion patterns that differentiate metastatic populations from primary tumors. We found that metastatic lung cancer cells preferentially bind to fibronectin in

combination with laminin, galectin-3, or galectin-8 compared to cells derived from primary tumors. It is worth noting that the combinations of these ECM components elicited the strongest effects, highlighting the importance of using a platform that is capable of measuring responses to more than individual molecules.

The use of gene expression signatures for patient stratification in the clinic has become more widespread[76, 191, 217-219], but while genomic approaches have been beneficial for identifying candidate genes, the diversity of findings makes the development of broad therapeutic options seem nearly impossible. By assaying for conserved mechanisms at the phenotypic level, however, relevant targets can be identified and therapeutics can be developed for a broad spectrum of patients. Our results highlight the utility of phenotypic screening approaches for identifying clinical biomarkers. We demonstrate that the adhesion signatures generated by the ECM microarrays are capable of differentiating between genetically similar populations with varying metastatic potential. The signatures gleaned from this platform may provide a complementary set of biomarkers that could assist conventional and genetic biomarkers in staging patients and deciding upon treatment options.

The value of the ECM microarray platform extends beyond the specific application of cancer metastasis. While this study documents the ability to profile adhesion patterns, cells bound to the arrays can be kept in culture for multiple days to monitor long-term responses to ECM such as cell death, proliferation, and alterations in gene or protein expression. Toward that end, one could use multiplexed antibody staining to probe the effects of ECM on stem cell differentiation or activation. Orthogonal screens can be performed to look at the effects of growth factors, small molecules, or RNA-interference

agents in the context of ECM. Reduction of requisite cell numbers can be achieved using miniaturized arrays to screen rare cell populations such as circulating tumor cells or cancer stem cells and to help expand those populations *in vitro* for further biological studies. Overall, the ECM microarrays will enhance our ability to study a host of questions as they pertain to both basic biological and clinical settings.

2.4 Methods

Murine Lung Adenocarcinoma cell lines

Cell lines have been described[194]. Briefly, tumor initiation was achieved using intratracheal injection of lentiviral Cre recombinase. Tumors were resected, digested, and plated onto tissue culture treated plastic to generate cell lines[194]. Cell lines were subsequently cultured in DMEM, 10% FBS, penicillin/streptomycin, and glutamine. These lines were derived from both primary lung tumors and their metastases. See Table 2.2 for nomenclature regarding cell line origins.

Extracellular Matrix Microarrays Preparation

Vantage acrylic slides (CEL Associates VACR-25C) were coated with polyacrylamide by depositing prepolymer containing Irgacure 2959 photoinitiator (Ciba) between the slide and a glass coverslip[210]. Following polymerization, slides were soaked in ddH_2O and the coverslips were removed. Slides were allowed to dry prior to molecule deposition. Slides were spotted using a DNA Microarray spotter (Cartesian Technologies Pixsys Microarray Spotter and ArrayIt 946 Pins). 768 combinations were spotted in replicates of five. Rhodamine dextran (Invitrogen) was spotted as negative controls and for use in image alignment. The following molecules were used: Collagen I (Millipore), Collagen II (Millipore), Collagen III (Millipore), Collagen IV (Millipore), Collagen V (BD

Biosciences), Collagen VI (BD Biosciences), Fibronectin (Millipore), Laminin (Millipore), Merosin (Millipore), Tenascin-R (R&D Systems), Chondroitin Sulfate (Millipore), Aggrecan (Sigma), Elastin (Sigma), Keratin (Sigma), Mucin (Sigma), Superfibronectin (Sigma), F-Spondin (R&D Systems), Nidogen-2 (R&D Systems), Heparan Sulfate (Sigma), Biglycan (R&D Systems), Decorin (R&D Systems), Galectin 1 (R&D Systems), Galectin 3 (R&D Systems), Galectin 3c (EMD Biosciences), Galectin 4 (R&D Systems), Galectin 8 (R&D Systems), Thrombospondin-4 (R&D Systems), Osteopontin (R&D Systems), Osteonectin (R&D Systems), Testican 1 (R&D Systems), Testican 2 (R&D Systems), Fibrin (Sigma), Tenascin-C (R&D Systems), Nidogen-1 (R&D Systems), Vitronectin (R&D Systems), Rat Agrin (R&D Systems), Hyaluronan (R&D Systems), Brevican (R&D Systems). The laminin used is Millipore Catalog No. AG56P, and is a mixture of human laminins that contain the β1 chain. Source plates used in the spotter were prepared using a Tecan liquid handler. Molecules were prepared at a concentration of 200μg/mL using a buffer described previously [210]. Slides were stored in a humidity chamber at 4°C prior to use.

Extracellular Matrix Microarray Seeding and Analysis

Slides were washed in PBS and treated with UV prior to seeding cells. They were placed in a seeding device that holds the top surface of the slides flush with bottom of the well. 400,000 cells were seeded on each slide in 6mL of serum-free medium (DMEM and penicillin/streptomycin). Cells were allowed to attach for two hours at 37°C. After attachment, slides were washed three times, transferred to quadriperm plates (NUNC, 167063), and new medium was added (DMEM, 10%FBS, penicillin/streptomycin, and glutamine). Slides were left at 37°C for two additional hours prior to removal for

staining. Slides were washed twice with PBS and fixed with 4% paraformaldehyde. Nuclei were stained using Hoechst (Invitrogen) in combination with 0.1% Triton-X and PBS. Slides were mounted with Fluoromount-G (Southern Biotech 0100-01) and stored at 4°C prior to imaging. Slides were imaged using a Nikon Ti-E inverted fluorescence microscope and NIS Elements Software (Nikon). The entire slide was scanned and images stitched using that software. Image manipulation and analysis were performed in MATLAB (Mathworks) and quantification of nuclei was performed using CellProfiler [3]. Clustering analysis was performed using Spotfire (Tibco). Replicate spots on each slide were averaged and those whose values were greater than one standard deviation above or below the mean of the replicates were excluded. Slides were normalized to the mean of their non-zero adhesion values. Clustering was performed based on Euclidean distances using Spotfire (TIBCO) with the Hierarchical Clustering algorithm (normalized adhesion > 0.01).

In vitro Adhesion Seeding

in vitro ECM adhesion tests were performed using 96-well-plates (Corning 3603). Plates were coated with 20μg/mL of fibronectin alone or 20μg/mL of fibronectin and 20μg/mL of the second molecule in PBS overnight at 4°C. Plates were then blocked with 1%(w/v) BSA at room temperature for one hour. Plates were allowed to dry prior to adding 2×10^4 cells/well in warm serum-free DMEM. Cells were allowed to adhere for one hour at 37°C and shaken every fifteen minutes to ensure uniform seeding. Cells were washed, fixed with 4% paraformaldehyde, and stained with Hoechst (invitrogen). Wells were imaged using a Nikon Ti-E inverted epifluorescence microscope and analyzed with Nikon Elements software.

RNA Isolation and Expression Profiling

Cell lysates were harvested using Trizol (Sigma). Chloroform extraction was performed followed by RNA cleanup using Qiagen RNeasy spin columns. Lysates were analyzed for RNA integrity and prepared with Affymetrix GeneChip WT Sense Target Labeling and Control Reagents kit, followed by hybridization to Affymetrix Mouse 3' Arrays (Mouse 430A 2.0). Lysates used for gene expression microarrays were harvested at the same time as the ECM microarrays were seeded to ensure minimal variability introduced by cell culture. R/Bioconductor software was used to process array images. Unsupervised hierarchical clustering analysis was performed in Spotfire (Tibco) for all probesets with variance>0.5 and expression>3.0 using Euclidean distances. Datasets are publically available from NCBI under accession number GSE40222.

Chapter 3. Functional Relevance of Metastasis-Associated ECM Combinations

Adapted from: Reticker-Flynn, N.E., *et al.* "A combinatorial extracellular matrix platform identifies cell-extracellular matrix interactions that correlate with metastasis." *Nat Commun* **3**, 1122 (2012).

3.1 Introduction

The role of extracellular matrix (ECM) and its binding receptors in tumor progression has been an area of active investigation since the identification of reductions in membrane-bound fibronectin on transformed cells[155]. Adhesion to fibronectin has been associated with tumor progression and metastasis[220-223] as has its integrin receptors α5β1[224-227], α4β1[228], and the αv family[115, 178, 189]. Similarly, laminins have been associated with invasion and metastasis[142, 150, 229] through interactions with α3β1 and α6 family integrins[63, 180, 230]. These studies suggest that alterations in cell-ECM interactions are necessary in order for tumor cells to invade and metastasize throughout the body.

While perhaps less studied than the other canonical laminin receptors, α3β1 has been shown to be an important mediator of adhesion to laminin-1, laminin-5, galectin-3, and galectin-8[231-234]. It is important in wound healing and regulation of basement membranes[235-236]. Furthermore, it has been implicated in a variety of carcinomas as a regulator of metastasis[237-241]. In addition to the prototypical binding of integrins, α3β1 is heavily *N*-glycosylated[242-243], which may mediate its adhesion to galectins[244]. Indeed, the glycosylation profile of VLA-3 is altered with tumor progression[245-246].

Galectins are a family of β-galactoside binding lectins with a diverse set of functions in normal physiology and tumorigenesis. Galectins are classified based on their membership in one of three groups: those that contain only one carbohydrate recognition domain (CRD) known as prototype galectins (galectin-1, 2, 5, 7, 10, 11, 13, 14, and 15), chimera-type galectins that contain one CRD with an extended N-terminal composed of tandem-repeats of amino acids (galectin-3), and tandem repeat type galectins that contain two CRDs linked by a short peptide sequence (galectin-4, 6, 8, 9, 12) (Scheme 3.1a).

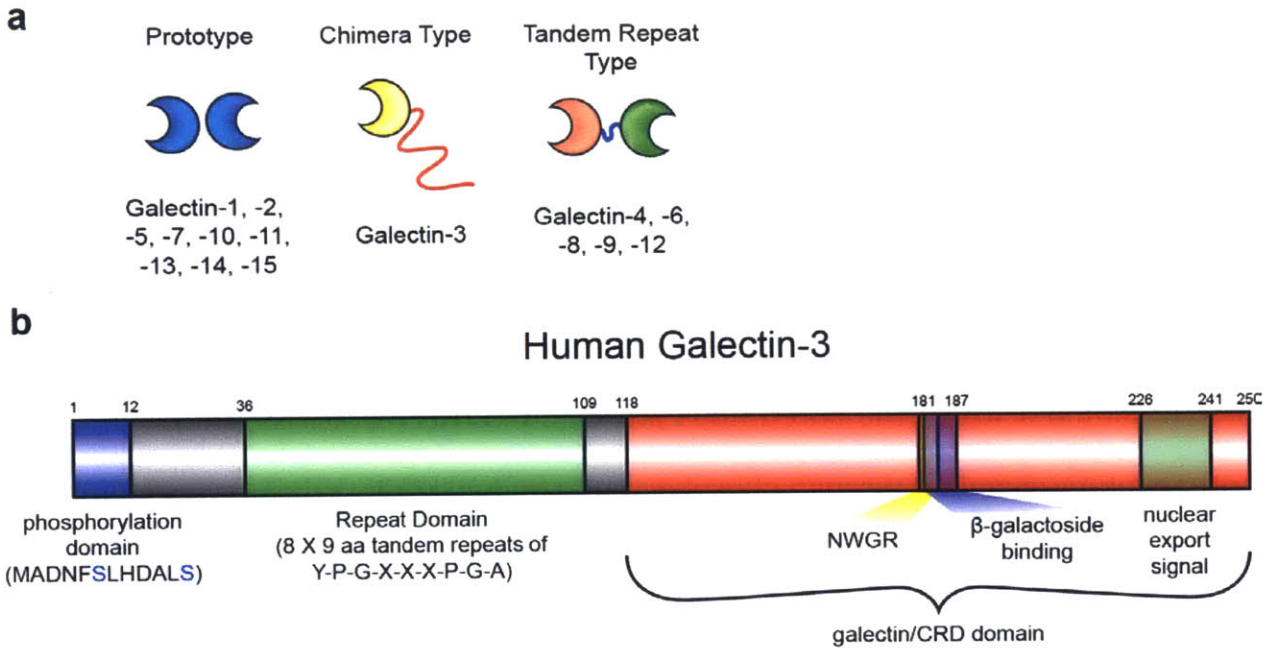

Scheme 3.1. *The galectin family.* (a) The three types of galectins: prototype, chimera type, and tandem repeat type. (b) Structure of human galectin-3.

Galectins were first identified in the electric eel[247] and subsequently in mammals[248] and can be found in sponges, fungi, nematodes, vertebrates, and viruses[249]. They were named and classified into a family in 1994 after recognition of this family of S-type lectins that bound β-galactosides and had conserved CRD sequence

similarity[250]. Galectins are found both intracellularly and extracellularly despite their ubiquitous absence of a signal sequence[251-252]. Furthermore, they readily oligomerize to potentiate multivalent binding of ligands, presumably to compensate for the lower affinity of glycan-protein interactions. While all galectins bind lactose, they exhibit non-overlapping specific affinities for other glycan motifs as well.

Galectin-3 is the only member of the chimera-type galectins and is perhaps the most well studied member of the galectin family. It was originally identified on the surface of murine macrophages[253] and is now appreciated to be expressed by many tissue types[254-255]. The structure of human galectin-3 is depicted in Scheme 3.1b. The N-terminal domain of galectin-3 contains multiple repeats of Pro-Gly-Ala-Tyr-Pro-Gly-X-X-X and shares significant homology to the internal domain of the N-terminus of the collagen α1 (II) chain[256]. The N-terminal domain also mediates oligomerization[257] and can be cleaved by MMP-2 and MMP-9 at Ala^{62}-Tyr^{63} in a manner that prevents multimerization but retains the carbohydrate-binding function of the CRD[258]. The first 12 amino acids of the N-terminus are highly conserved across species and elicit anti-apoptotic signaling through phosphorylation of Ser^{6}[259]. X-Ray crystallography of the 130 amino acid CRD of galectin-3 reveals structural similarities to galectin-1 and -2 in that it contains 5- and 6-stranded β-sheets that form a β-sandwich arrangement[260]. In addition to its carbohydrate-binding properties the CRD contains within it the BH1 (NWGR) motif of the BCL-2 family[261], which can act as an anti-apoptotic signal in the cytosol.

Galectin-3 exhibits a plethora of functions in normal physiology and disease states. Its role in mediating immune responses is discussed in Chapter 5. Galectin-3 can bind a

variety of ECM proteins including fibronectin, laminin, tenascin-C and -R, and elastin[262-265]. It has been suggested that laminin and fibronectin may contain polylactosamine chains that potentiate galectin-3 adhesion[266]. Intracellularly, galectin-3 has been reported to affect pre-mRNA splicing[267], interact with oncogenic Ras and promote RAF1 and PI3K signaling[268], and prevent apoptosis in a manner that alters tumor cell susceptibility to chemotherapies[269-271]. Galectin-3 also appears to affect the growth kinetics of tumors. Inhibition of galectin-3 reduces growth of breast cancer cell *in vivo*[272], and the ambiguous MDA-MB-435 cell line exhibits reduced proliferation when transfected with anti-sense galectin-3 cDNAs[273]. The effects of galectin-3 on cell growth are also thought to be dependent on subcellular localization[274], and has been claimed to be mediated by interactions with TTF1[275] or through interactions with cell-cycle regulators[276]. Galectin-3 may also promote angiogenesis *in vitro* and *in vivo*[277] and may alter integrin endocytosis[278]. It has even been utilized as a biomarker for a variety of cancers[279]. In light of the suggested pleiotropic roles of galectin-3 in many cancer phenotypes, a variety of reagents aimed at inhibiting and detecting galectins are being developed[280].

Galectin-3, in particular, has been associated with metastasis. Galectin-3 interactions with the Thomsen-Friedenreich Antigen (T-Antigen) promote attachment of breast cancer cells to the endothelium[281]. Furthermore, galectin-3 and -8 bind integrins including $\alpha 3\beta 1$[232-233], $\alpha 6\beta 1$[282], and αM[283-284], and galectin-3 has been suggested to upregulate integrin expression[285]. Galectin-3 can promote migration of breast cancer lines[286] and lung cancer lines[287] *in vitro* and metastasis of colon cancer *in vivo*[288]. Its inhibition with antibodies also inhibits liver metastasis

formation from xenografts of human adenocarcinomas[289], and synthetic galectin-3 inhibitors have been shown to increase chemosensitivity of metastatic cells[290].

In the previous chapter, we demonstrate that lung adenocarcinoma cells gain adhesion to combinations of ECM containing fibronectin with any of laminin, galectin-3, or galectin-8 as they become more metastatic. In this chapter, we confirm the presence of these molecules in mice bearing autochthonous tumors and humans with metastatic disease. Furthermore, we establish a functional role for α3β1 in adhesion to the fibronectin/galectin combinations *in vitro* and metastatic seeding *in vivo*.

3.2 Results

3.2.1 ECM Molecules are Present in Sites of Endogenous Tumors

We sought to correlate our *in vitro* adhesion profiles with ECM expression *in vivo*. To investigate whether the identified ECM molecules may be important in natural tumorigenesis, organs containing primary autochthonous tumors and their metastases were resected from $Kras^{LSL\text{-}G12D/+};p53^{flox/flox}$ mice and stained for those molecules. Trichrome staining of lungs with extensive tumor burden revealed a significant presence of ECM deposition in the tumor-bearing lung (Fig. 3.1a and ref [291]). Previously, Winslow, *et al.* found that primary tumors that have acquired the ability to metastasize (T_{Met} tumors) upregulate the chromatin-associated protein Hmga2[194]. Therefore, we used Hmga2 immunohistochemistry in addition to histological characteristics to identify areas of highly aggressive cancer cells (Fig. 3.1a).

As anticipated, primary lung tumors were positive for collagen I (black arrowheads), collagen VI (open black arrowheads), and osteopontin (red arrowheads), with the most

intense staining overlapping with the high-grade tumor areas (Fig. 3.1a,c). In particular, osteopontin staining strongly co-localized with Hmga2^{pos} regions, suggesting that increased osteopontin production is associated with metastatic primary lung tumors. Furthermore, little to no laminin, galectin-3, or galectin-8 staining was detected in the primary tumors (Fig. 3.2). Of note, fibronectin staining in the tumor was strong, revealing a correlation between increasingly metastatic populations and the presence of fibronectin early in the metastatic cascade (Fig. 3.2).

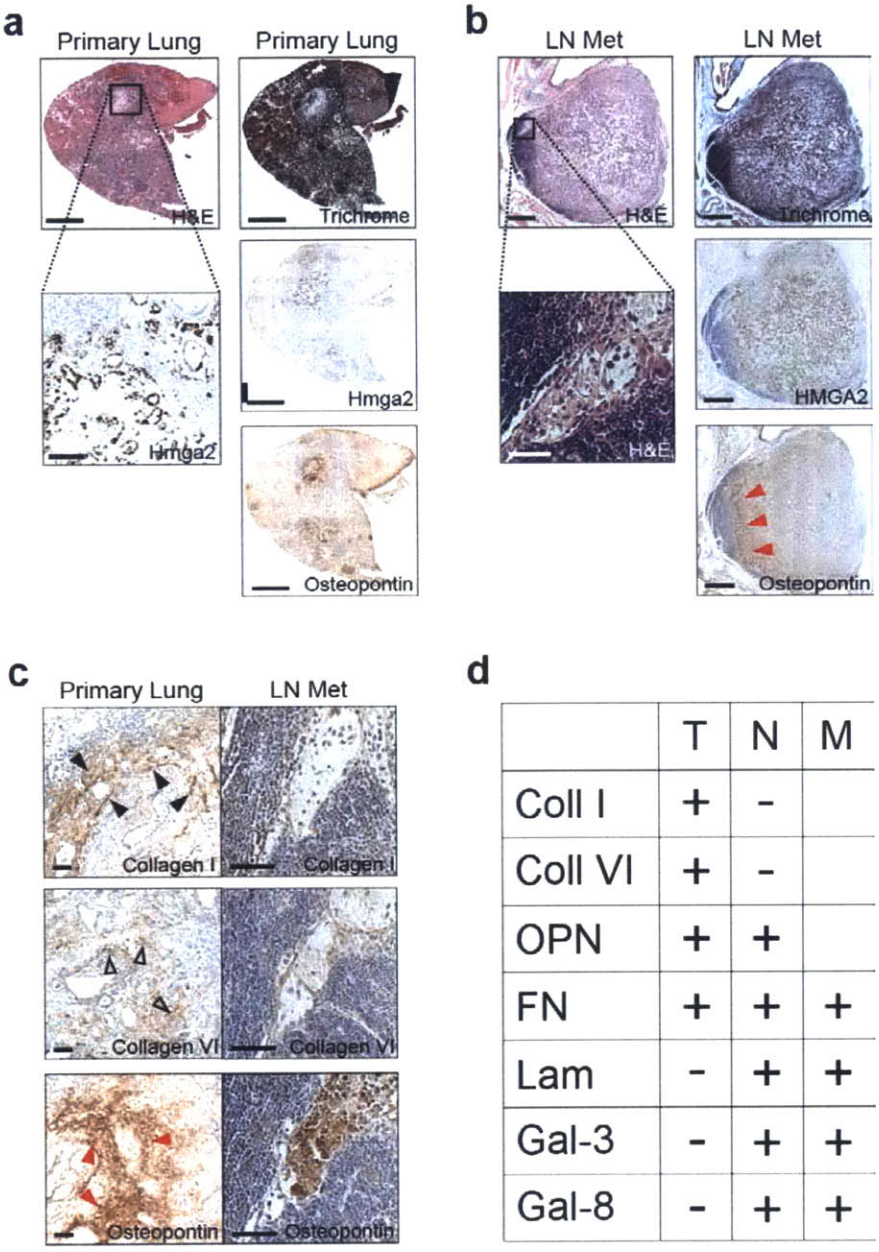

	T	N	M
Coll I	+	-	
Coll VI	+	-	
OPN	+	+	
FN	+	+	+
Lam	-	+	+
Gal-3	-	+	+
Gal-8	-	+	+

Figure 3.1. *Identified ECM molecules are present in primary tumors and metastases.* (a) Staining on lungs containing primary lung tumors from $Kras^{LSL\text{-}G12D/+};p53^{flox/flox}$ mice. (b) Staining of lymph node metastases from the mice. Red arrowheads denote tumor front exhibiting high osteopontin staining. (c) IHC of primary tumor-associated ECM in the lung and lymph node. Black arrowheads: collagen I, open black arrowheads: collagen VI. (d) Summary of IHC results. 'H&E': Hematoxylin and eosin. 'Trichrome': Masson's trichrome. 'Hmga2': High-mobility group AT-hook 2 (marker of metastatic/invasive tumor cells). 'T': primary lung tumor. 'N': lymph node metastasis. 'M': distant metastasis. Scale bars: (a) low magnification: 1mm; high magnification: 100μm; (b) low magnification: 500μm; high magnification: 50μm; (c) 50μm.

We next asked whether the lymph node and distant organ metastases contained the metastasis-associated ECM molecules. Again, trichrome staining revealed the presence of significant matrix deposition within the lymph nodes (Fig. 3.1b). As expected, the entirety of the lymph node tumors were histologically high-grade and were $Hmga2^{pos}$

(Fig. 3.1b). There was also clear expression of all four of the metastasis-associated molecules (fibronectin, laminin, galectin-3, and galectin-8) within the lymph node metastases (Fig. 3.2). Furthermore, there was essentially no collagen I or collagen VI (Fig. 3.1b). Interestingly, osteopontin was present in the metastases (Fig. 3.1c) and had its highest expression along the invasive front (Fig. 3.1a,b).

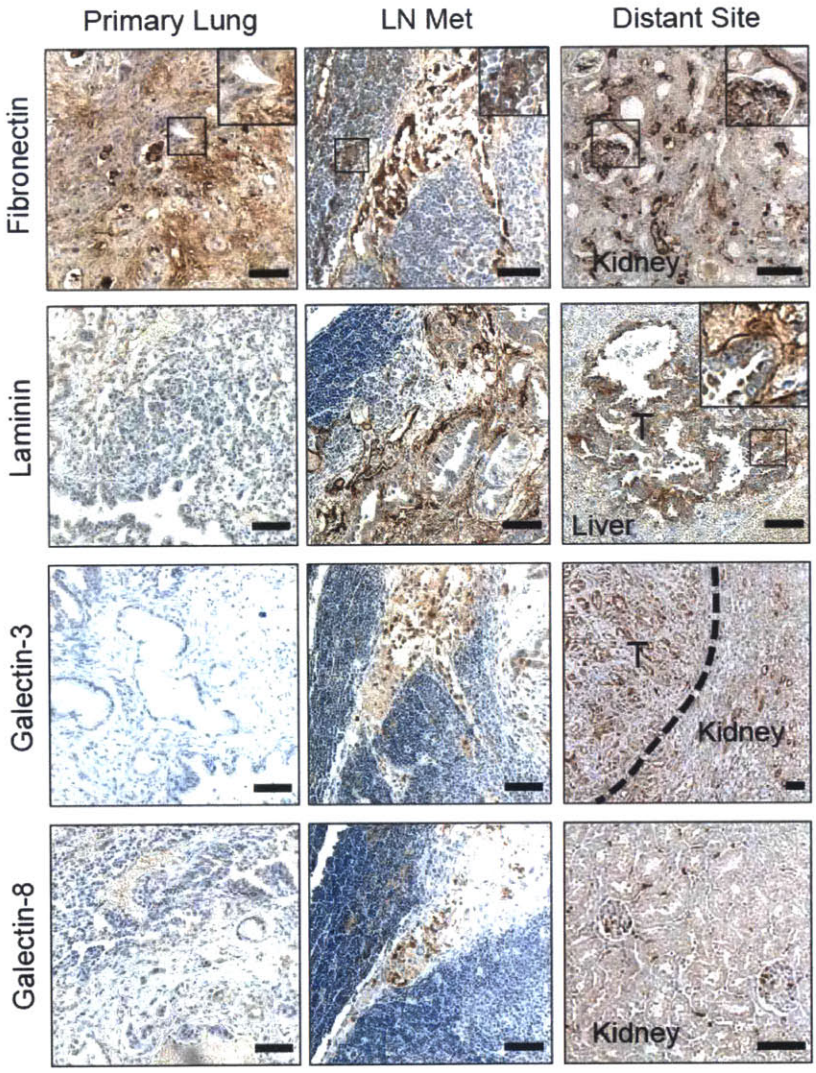

Figure 3.2. *Metastasis-associated ECM molecules are present in the sites of metastases but not primary tumors.* Immunostaining of the metastasis-associated ECM molecules in the lungs, lymph nodes, and distant metastases of mice bearing endogenous lung adenocarcinomas (*Kras*$^{LSL\text{-}G12D/+}$;*p53*$^{flox/flox}$ mice). Insets are magnified views of boxed areas showing ECM molecule fibrils. Number of tissues examined for each organ: Lungs: 10; lymph nodes: 5; livers/kidneys: 22. 'T': tumor. Dotted line depicts edge of tumor and normal kidney. Scale bars are 50μm.

We also examined common metastatic sites for the presence of the metastasis-associated molecules (Fig. 3.2). Both galectin-3 and galectin-8 were distinctly visible in these sites. Laminin and fibronectin both appeared to line the sinusoids of the livers of the mice and were also present in the metastases formed there. To determine whether these differences between the primary and metastatic sites were due to altered matrix production by the tumor cells, we performed immunoblots on the 393T5 and 393M1 T_{Met} and M cell lines. While the M line showed slight increases in fibronectin and laminin production compared to the T_{Met} line, production of both galectins was constant (Fig. 3.3). Furthermore, collagen I production was constant, and osteopontin production was actually increased in the M line. Taken together, these data suggest that the ECM microarrays identified molecules that were found within the physiologically relevant sites of mice bearing autochthonous tumors, and that the differential adhesion to these molecules is not solely reflected by differences in matrix production by the tumor cells, themselves.

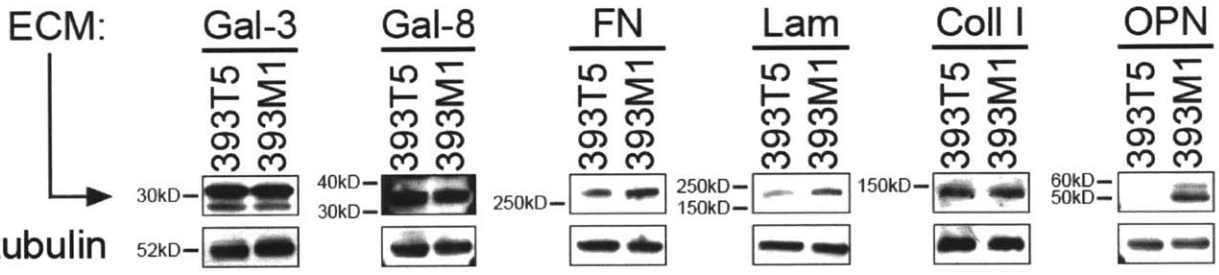

Figure 3.3. *ECM production by cell lines has minimal correlation with adhesion.* Western blot analysis of the metastasis- and primary tumor-associated ECM molecules produced by the 393T5 (T_{Met}) and 393M1 (M) cell lines. 'Gal-3' Galectin-3; 'Gal-8' Galectin-8; 'FN' fibronectin; 'Lam' laminin; 'Coll I' collagen I, 'OPN' osteopontin.

3.2.2 Integrin surface expression correlates with ECM binding profiles

We asked whether the changes in adhesion found by the ECM microarrays could have been predicted by transcriptional profiling of the genes encoding the cognate integrins. Analysis of gene expression microarray data revealed that adhesion trends on our ECM arrays did not necessarily correlate with transcriptional profiles of those integrins (Fig. 3.4a). Thus, to correlate our findings with the presence of receptors for these metastasis-associated ECM molecules, we examined the clonally-related pair of representative T_{Met} and M cell lines for surface expression of their cognate integrins. While the mRNA expression patterns did not show significant alterations in integrin gene expression (Fig. 3.4b), flow cytometry analysis of the integrin subunits corresponding with either the primary tumor-associated molecules or metastasis-associated molecules revealed that the receptor expression trends were consistent with the observed binding patterns. Specifically, integrin subunits known to bind fibronectin ($\alpha 5$ and αv), laminin ($\alpha 6$ and $\alpha 3$), and galectins ($\alpha 3$) were all more prevalent on the metastasis-derived line, while those associated with collagens ($\alpha 1$ and $\alpha 2$) were relatively higher on the primary tumor-derived line (Fig. 3.5a). These surface expression trends were consistent for the other T_{Met} and M lines as well (Fig. 3.6a). Furthermore, within a given cell line, we observed relatively homogeneous surface expression of the metastasis-associated integrins (Fig. 3.6b) suggesting that variations in adhesion between lines are due to global increases in surface receptor expression, rather than binding patterns of select subpopulations.

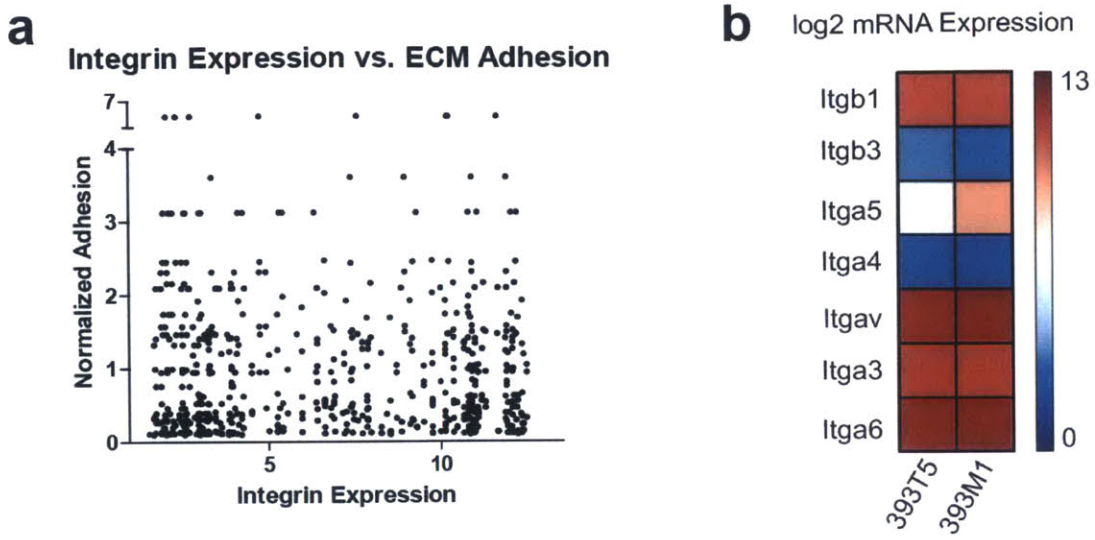

Figure 3.4. *ECM adhesion does not correlate with integrin gene expression.* (a) Comparison of ECM adhesion for all cell lines to gene expression of the cognate integrins from gene expression microarray data. GeneGO software was used to identify reported interactions between integrins and ECM molecules contained on the ECM microarrays. For each reported interaction, the adhesion value from the ECM arrays was plotted on the ordinate and the gene expression was plotted along the abscissa. (c) Integrin subunit mRNA expression of the cognate integrins for the metastasis-associated ECM molecules from Affymetrix microarray analysis in 393T5 (T_{nonMet}) and 393M1 (M) cell lines.

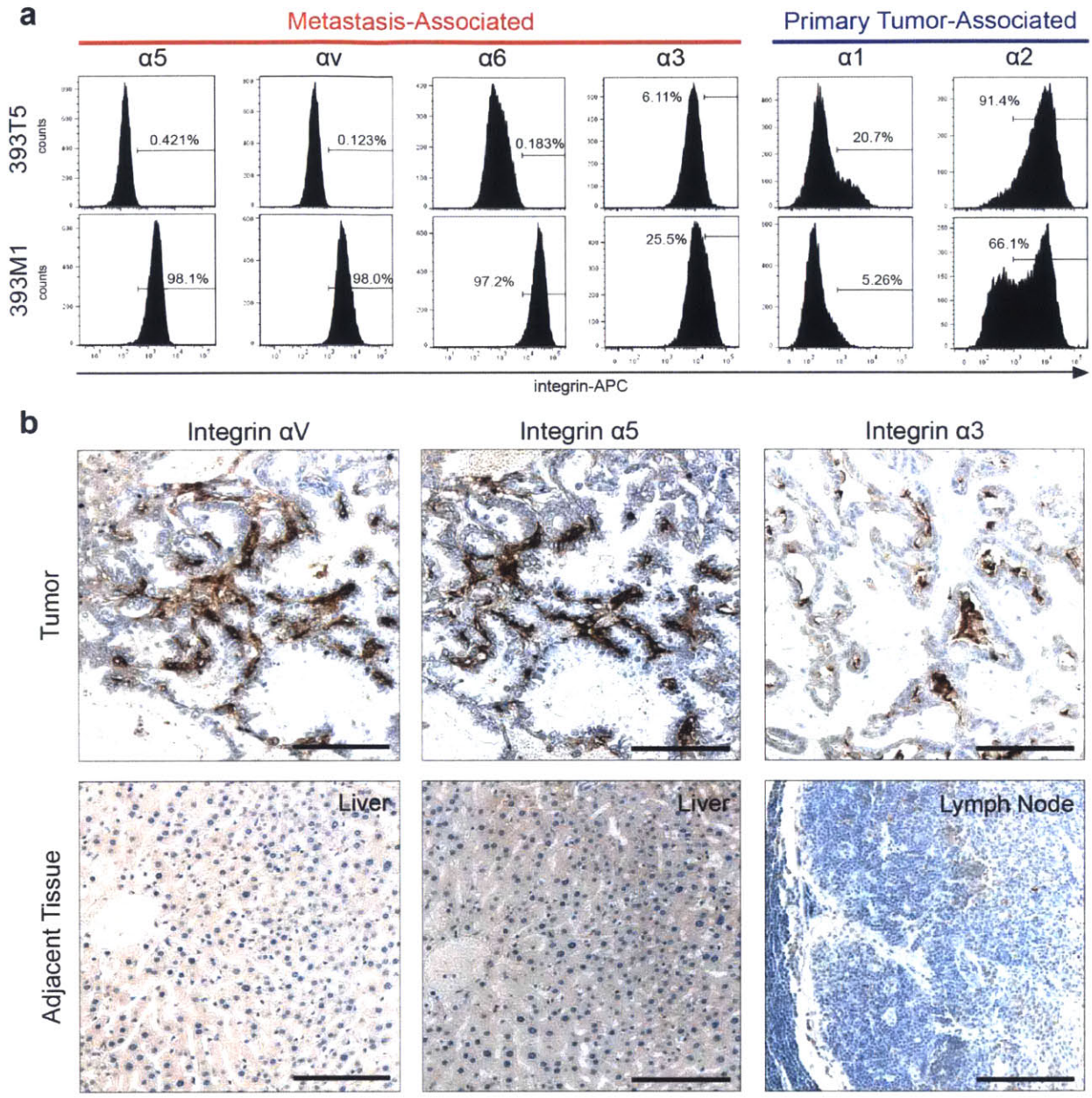

Figure 3.5. *Integrin Surface Expression Correlates with ECM binding profiles.* (a) Flow cytometry of integrin surface expression in 393T5 (T_{Met}) and 393M1 (M) cell lines. Integrin subunits that bind to metastasis-associated molecules show increased surface presentation in the metastatic line (α5, αv, α6, α3), while those that bind to primary tumor-associated molecules show decreased presentation (α1 and α2). (b) IHC for metastasis-associated integrins in mice bearing autochthonous tumors with spontaneous metastases to the liver and lymph nodes. Scale bars are 100μm.

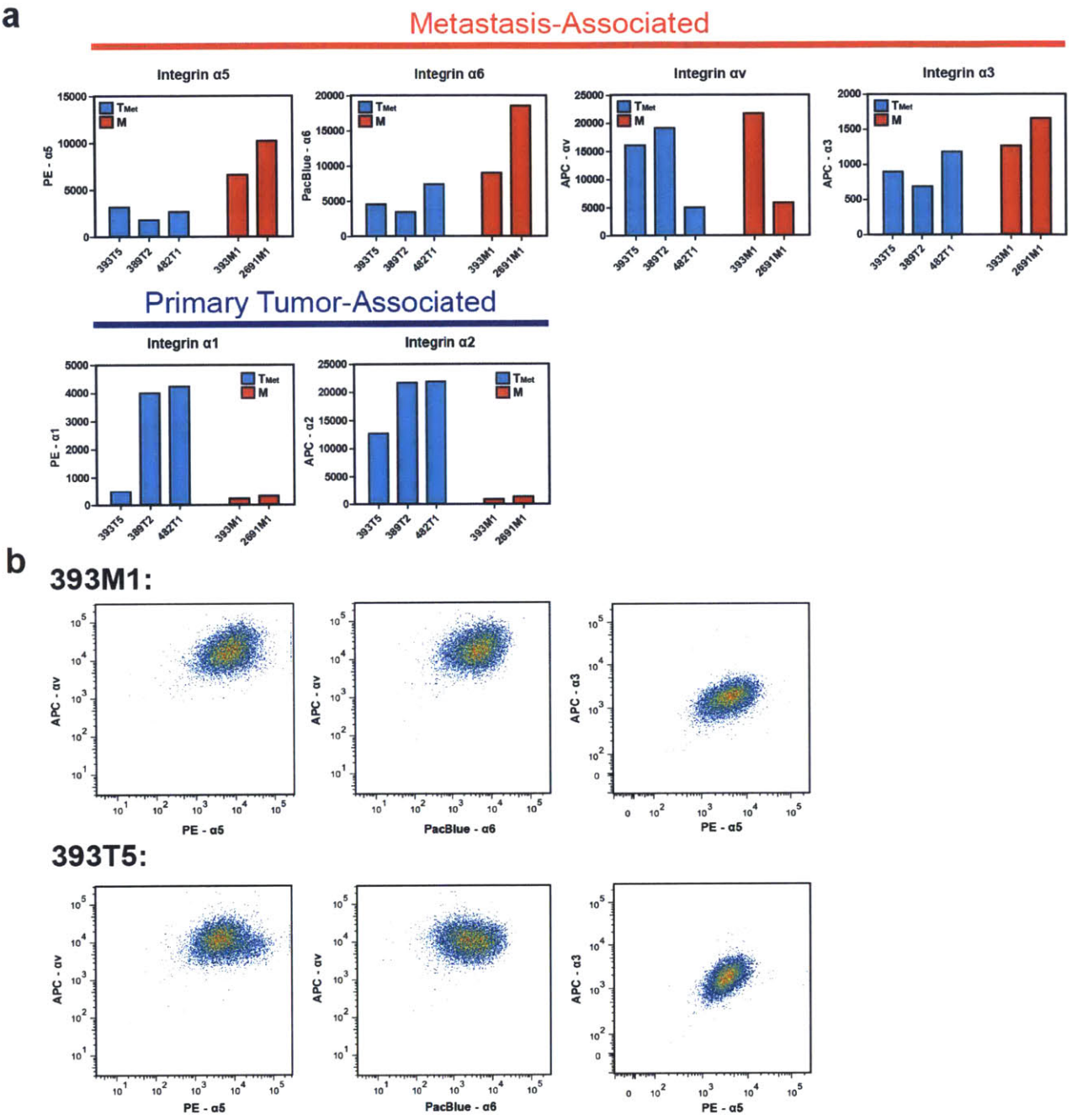

Figure 3.6. *Flow cytometry analysis of surface integrin expression.* (a) Median values for fluorescence intensity of each of the T_{Met} (blue) and M (red) cell lines for the metastasis-associated molecule cognate integrins and primary tumor-associated molecule cognate integrins. (b) Multicolor flow analysis of integrin profiles in the 393M1 (M) and 393T5 (T_{Met}) for the metastasis-associated molecule cognate integrins shows a lack of discrete subpopulations.

Immunohistochemistry revealed that these integrins were also present in the metastases of mice bearing autochthonous tumors, but not the adjacent tissue (Fig. 3.5b). The finding that the transcriptional levels of the integrins do not agree with the adhesion trends suggests that post-transcriptional regulation, post-translational modifications such as altered glycosylation, or alterations in membrane trafficking or activation state of the integrins are likely responsible for the changes in adhesion. Thus, by utilizing our platform that investigates specific ECM binding rather than receptor gene or protein expression, we are able to identify candidate ECM interactions that might otherwise have been overlooked.

3.2.3 *Integrin α3β1 mediates adhesion and seeding in vitro and in vivo*

To examine which candidate receptor/ECM interactions may participate in the observed binding patterns, we performed *in silico* network mapping of the metastasis-associated ECM molecules using GeneGO software (Metacore) of manually curated molecular interactions. Networks were generated by initiating expansion around the metastasis-associated ECM molecules. We generated a network map that we termed the Lung Adenocarcinoma Metastasis (LAM) network that has a greatest disease association with 'Neoplasm Metastasis' ($P = 1.094 \times 10^{-45}$, hypergeometric test, Fig. 3.7a-c). A network generated using the same parameters but with the primary-tumor-associated molecules did not exhibit any disease association with metastasis (Fig. 3.8). Analysis of the LAM network identified integrin α3β1 as the surface receptor with the greatest number of edges (Fig. 3.7b,d). Based on this finding, we performed a knockdown of both the α3 and β1 subunits (ITGA3 and ITGB1, respectively) using short-hairpin-mediated RNA-

interference (Fig. 3.9a). Knockdown of these genes in the metastatic line, 393M1, resulted in reduced adhesion to the metastasis-associated molecules *in vitro* when compared to the control hairpin targeting the firefly luciferase gene (Fig. 3.9b).

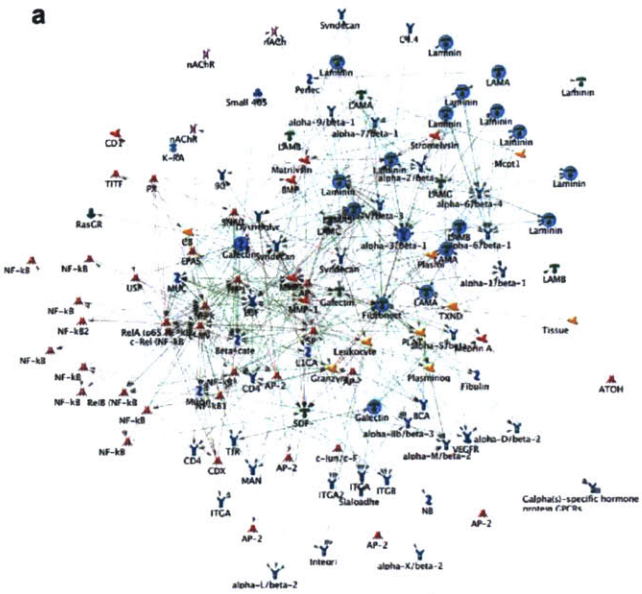

c

LAM Network

#	Disease	%	p-Value
1	**Neoplasm Metastasis**	**55.28**	**1.094E-45**
2	Neoplastic Processes	55.28	5.054E-44
3	Pathologic Processes	80.49	2.373E-41
4	Genital Diseases, Male	74.8	1.289E-36
5	Skin Diseases	79.67	2.990E-36

d

#	Receptor Name	Edges
1	**α3β1**	**14**
2	Syndecan-4	12
3	α6β1	10
4	α6β4	10
5	CD44	10

Figure 3.7. *Lung adenocarcinoma metastasis (LAM) network identified α3β1.* GeneGO software (Metacore) allows for the generation of *in silico* network maps depicting known interactions between molecules as established in the literature. This manually curated database generated networks based upon the most closely related molecules. Networks were generated by seeding an autoexpand algorithm with the metastasis-associated ECM molecules (fibronectin, laminins, galectin-3, and galectin-8) (a,b). (c) This network was queried for the diseases most highly associated with it. P-values determined by hypergeometric test. (b,d) Analysis of the network reveals that integrin α3β1 is the surface receptor with the most edges.

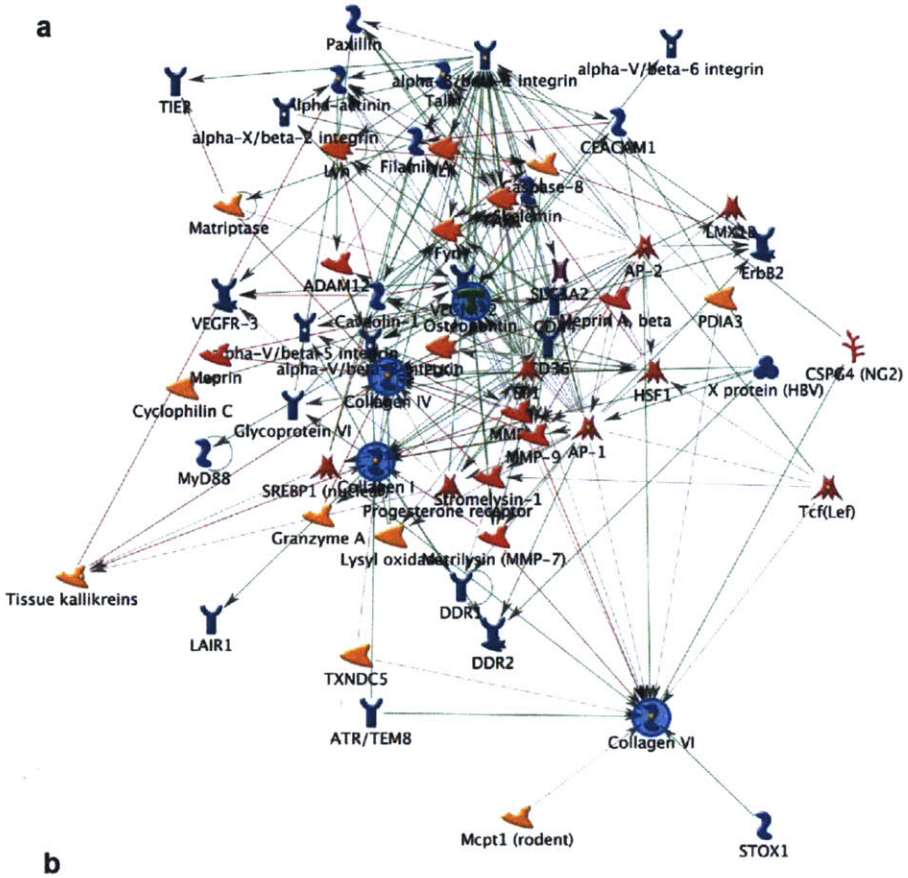

#	Disease	%	p-Value
1	Wounds and Injuries	56.64	2.507E-41
2	Osteosarcoma	36.28	1.811E-37
3	Neoplasms, Bone Tissue	36.28	4.663E-37
4	Neoplasms, Connective and Soft Tissue	47.79	2.067E-33
5	Neoplasms, Connective Tissue	39.82	1.052E-32

Figure 3.8. *Primary tumor network map.* Here, GeneGO (Metacore) was used in an equivalent manner as performed for the LAM network generated in Fig. 3.7 with the exception that the autoexpand algorithm was seeded with the primary-tumor associated ECM molecules (collagen I, IV, VI and osteopontin) (a). (b) Disease association rank of the primary tumor molecule network shown in (a). P-values determined by hypergeometric test.

We next assessed whether this integrin dimer plays a role in metastatic seeding *in vivo*. As the 393M1 cell line was derived from a liver metastasis, we chose to use an experimental metastasis model of hematogenous seeding of the liver. Thus, we conducted experimental metastasis assays by intrasplenic injection of 393M1-shα3 or 393M1-shFF cells into wild-type mice, and monitoring for liver tumor formation. We found that mice injected with the 393M1-shα3 cells formed fewer tumor nodules than the controls (Fig. 3.9c,d). Taken together, these findings suggest that the α3β1 integrin

dimer plays a role in adhesion of metastatic cells to the metastasis-associated ECM molecules and in metastatic seeding.

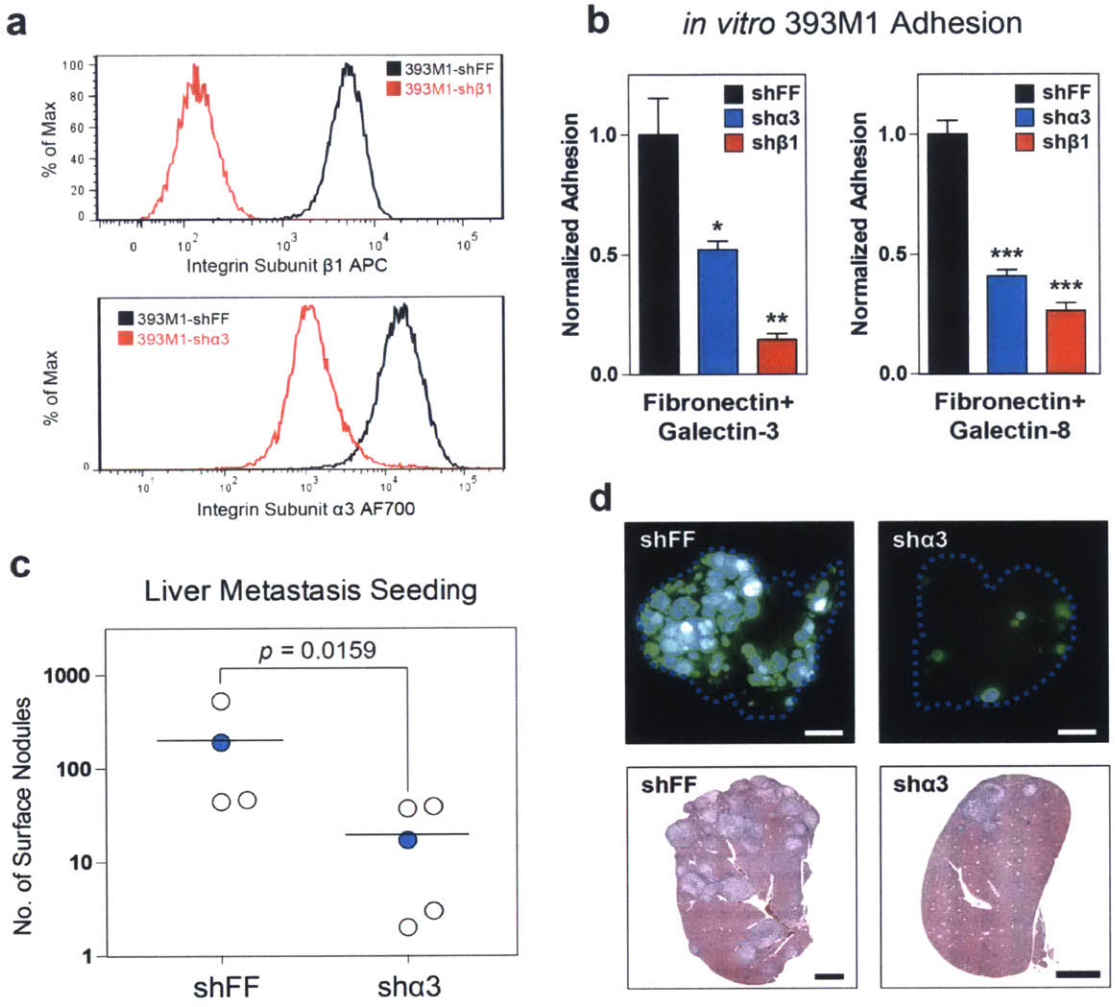

Figure 3.9. *Integrin α3β1 mediates adhesion and seeding* in vitro *and* in vivo. (a,b) Flow cytometry analysis of integrin surface expression following retroviral transduction of short hairpins targeting the integrin subunits. (a) knockdown of ITGB1; (b) knockdown of ITGA3. Black: control hairpin against firefly luciferase; red: hairpin against integrin subunits. Knockdown of both α3 and β1 integrin subunits by shRNA reduces adhesion to metastasis-associated molecules *in vitro* (b) and prevents metastatic seeding *in vivo* (c,d). shFF is the control hairpin targeting firefly luciferase. One-way ANOVA with Tukey's Multiple Comparison Test was used to analyze the data in figure (b). Error bars in (b) represent standard error ($n = 3$). (c) Number of liver tumor nodules of the surface of livers 2.5 weeks after intrasplenic injection. Mann-Whitney (non-parametric) test was used to analyze significance. (d, top) Fluorescence imaging of whole livers after resection. Cell lines express nuclear-excluded ZSGreen. Scale bars are 0.5cm. (d, bottom) Hematoxylin and eosin stain of liver slices. Scale bars are 2mm. Blue data points in (c)

correspond to images in (d). All results shown are representative of multiple independent experiments.

3.2.4 *Galectin-3/8 are present in human lung cancer metastases*

Based on the *in vitro* adhesion data and *in vivo* mouse findings, we sought to explore the role of the metastasis-associated ECM molecules in human samples. Using Oncomine[4], a human genetic dataset analysis tool, we examined the correlation of ECM gene expression and disease severity (e.g. clinical stage or the presence of metastases). Results of these queries demonstrate that increased expression of LGALS3 or LGALS8 (galectin-3 and galectin-8, respectively) correlate with increased clinical stage or the presence of metastases (Fig. 3.10a-d).

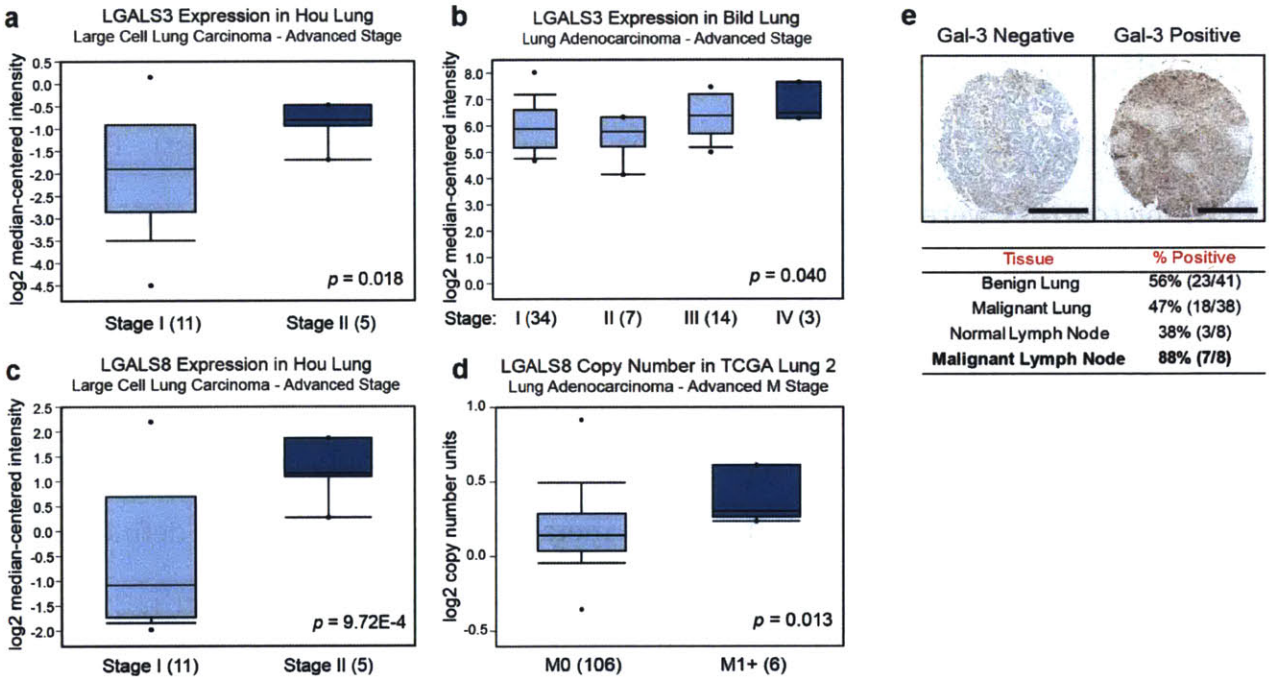

Figure 3.10. *Metastasis-associated molecules are present in the metastases of human lung cancers* (a-d) Oncomine[4] results for human lung cancer expression of LGALS3 and LGALS8. (a) LGALS3 Expression in Hou Lung: Large Cell Lung Carcinoma – Advanced Stage. (b) LGALS3 Expression in Bild Lung: Lung Adenocarcinoma – Advanced Stage. (c) LGALS8 Expression in Hou Lung: Large Cell Lung Carcinoma – Advanced Stage. (d) LGALS8 Copy Number in TCGA Lung 2: Lung Adenocarcinoma – Advanced M Stage. LGALS3 and LGALS8 are overexpressed in Stage II lung cancer compared to stage I (P = 0.018 and 9.72E-4,

respectively)(a,c). Microarray data source GSE19188[5]. (b) LGALS3 is overexpressed in Stage IV lung cancer compared to other stages ($P = 0.040$). Microarray data source GSE3141[6]. (d) LGALS8 has increased copy number in advanced M stage lung cancer ($P = 0.013$) in the "Lung Carcinoma DNA Copy Number Data" dataset available from The Cancer Genome Atlas website (https://tcga-data.nci.nih.gov/tcga/tcgaHome2.jsp). (e) Representative images of human tissue microarray staining results for galectin-3 presence or absence in lung tissue. Quantification of positive and negative galectin-3 staining in lung and lymph node tissues with and without tumors. Scale bars are 500μm. Box and whisker plots in (a-d): dots represent maximum and minimum values, whiskers show 90th and 10th percentiles, boxes show 75th and 25th percentiles, and line shows median. P-values in (a-d) were computed by Oncomine software using Student's t-test (a, c-d) or Pearson's correlation analysis (b).

We next investigated whether galectin-3 protein is present at higher levels in malignant human lung tumors compared to benign non-neoplastic human lung tissue using samples taken from lungs and lymph nodes of patients. Staining for galectin-3 in human tissue microarrays revealed a higher presence of the molecule in lymph nodes of patients with malignant disease (88%) compared to those without cancer (38%) (Fig. 3.10e). Furthermore, there was a higher fraction of galectin-3-positive lymph nodes (88%) than positive primary lung tumor samples (47%), confirming its association with the metastatic site over the primary tumor ($P < 0.05$, Fisher's Exact Test). Thus, the ECM microarrays were capable of identifying interactions associated with metastasis in human lung cancer.

3.3 Discussion

In the previous chapter, we used our ECM microarrays to identify conserved changes in ECM adhesion that occur with lung cancer metastasis. In particular, we defined three combinations of ECM (fibronectin/laminin, fibronectin/galectin-3, and fibronectin/galectin-8) as being highly associated with the metastatic populations. Here, we show that these changes in adhesion correlate with changes in surface presentation of various integrins. In particular, α3β1 mediates adhesion to these molecules *in vitro* and permits metastatic seeding *in vivo*. Furthermore, metastases derived from both a

genetically-engineered mouse lung cancer model and from human lung cancers express the metastasis-associated ECM molecules.

Galectins are a class of lectins that bind β-galactosides and can associate with other ECM molecules such as fibronectin[153]. Galectin-3 is associated with metastasis in a variety of cancers[292-293] and can bind to the oncofetal Thomsen-Friedenreich antigen, a carbohydrate antigen overexpressed by many carcinomas[294]. Our platform confirmed its importance in lung adenocarcinoma, and also identified galectin-8 as having similar importance. While galectin-8 is known to affect adhesion of cells to other matrix molecules, its role in cancer and metastasis has been less clear as it has been found to have both a positive and negative association with adhesion and tumorigenesis[295-296]. Using the ECM microarrays, we showed that binding to galectin-8 in combination with fibronectin is strongly associated with metastatic progression in lung adenocarcinoma.

Furthermore, in addition to many collagens, we found that loss of adhesion to osteopontin accompanied metastatic progression (Fig. 2.9a-c). Osteopontin levels correlate with prognosis in patients with metastatic disease[149], and secretion of osteopontin by primary tumors results in mobilization of bone marrow-derived stromal precursors that help establish the metastatic niche[119]. In addition to confirming the presence of the metastatic molecules at the sites of metastases, we found that the invasive portions of primary tumors and the invasive front of the metastases secrete osteopontin (Fig. 3.1b). A metastatic tumor line also produces more osteopontin than its corresponding primary (Fig. 3.3). These findings suggest that while some primary tumors may activate bone marrow cells by secreting osteopontin, in our model

metastatic cells may contribute to this recruitment at a comparable or higher level than the instigating primaries, despite their own loss of adhesion to the immobilized molecule.

Just as the adhesion signatures described in the previous chapter may provide useful biomarkers of tumor progression, their associated receptors are likely to be useful in a similar capacity. Such changes in the presentation of these receptors was not readily evident by analysis of transcriptional activity, yet clear discrepancies in presentation of integrins on the surfaces of the cells was apparent through flow cytometry, highlighting the utility of phenotypic screening. While targeting ECM can be a difficult therapeutic approach, drugs that target increases in surface receptors during the progression of many pathologies provide an attractive avenue for targeted therapies. In particular, a variety of therapeutics targeting integrins have been developed and are currently undergoing clinical trials[115, 190]. Utilizing the differential expression of these receptors will not only enable selective targeting of malignancies, but will also interfere with their ability to spread and colonize distant sites. By knocking down $\alpha 3\beta 1$, we demonstrated a reduction in metastasis formation. While such a genetic approach may be difficult to realize in humans with this disease, monoclonal blocking antibodies against this or other integrin pairs may be able to achieve similar results in humans with lung cancer.

3.4 Methods

Murine Lung Adenocarcinoma cell lines

Cell lines have been described[194]. Briefly, tumor initiation was achieved using intratracheal injection of lentiviral Cre recombinase. Tumors were resected, digested,

and plated onto tissue-culture-treated plastic to generate cell lines[194]. Cell lines were subsequently cultured in DMEM, 10% FBS, penicillin/streptomycin, and glutamine. These lines were derived from both primary lung tumors and their metastases. See Supplementary Table S2 for nomenclature regarding cell line origins.

Cell Transplantation Assays

All animal procedures were performed in accordance with the MIT Institutional Animal Care and Use Committee under protocol 0211-014-14. Cell injection studies were performed in B6129SF1/J mice (Jackson Laboratory, Stock Number 101043). Intrasplenic injections were performed using 5×10^5 cells resuspended in 100μL of PBS and injected into the tip of the spleen following existing protocols[194]. Animals were anesthetized with avertin prior to surgery. Fur was removed from the animals and they were sterilized with Betadine and 70% ethanol. The spleen was exteriorized following incisions in the skin and body wall. Cells were injected into the end of the spleen with a 27gauge syringe and allowed to travel into circulation for two minutes. Spleens were then excised from the animals following cauterization of the splenic vessels. The muscle wall was closed using 5-0 dissolvable sutures, and the skin was closed using 7mm wound clips (Roboz). Mice were euthanized 2.5-4 weeks following injection, and their livers were excised. Quantification of surface nodules and imaging of livers was performed using a dissection microscope. Tissues were embedded in paraffin following fixation in 4% paraformaldehyde and stained using hematoxylin and eosin.

Protein Analysis

Western blot analysis of ECM molecules was performed with the following antibodies: galectin-3 (Abcam ab53082, 1:500), galectin-8 (Abcam ab69631, 1:500), osteopontin

(Abcam ab8448, 1:2000), fibronectin (Abcam ab2413, 1:1000), laminin (Abcam b11575, 1:1000), collagen I (Abcam ab34710, 1:5000), and α-tubulin (Cell Signaling 2125, 1:1000). Immunohistochemistry of ECM molecules was performed with the following antibodies: galectin-3 (Abcam ab53082, 1:500), galectin-8 (Abcam ab69631, 1:75), osteopontin (Abcam ab8448, 1:200), laminin (Abcam ab11575, 1:100), fibronectin (Millipore AB2033, 1:80), Hmga2 (Biocheck 59170AP, 1:1000), collagen I (Abcam ab34710, 1:500),collagen VI (Abcam ab6588, 1:100). Integrin staining was performed using the following antibodies: integrin αv (Millipore AB1930, 1:200), integrin α5 (Chemicon AB1928, 1:200), integrin α3 antibody was a gift from JML. Tissue microarrays were acquired from LifeSpan Biosciences (LS-SLUCA50), and were stained with the same galectin-3 antibody. Murine tissues were harvested from *Kras*$^{LSL\text{-}G12D}$, *p53*$^{flox/flox}$ mice[194, 215-216]. IHC was performed following resection from mice, fixation in formalin, and embedding in paraffin. Flow cytometry analysis of integrin expression was performed using the following antibodies: integrin α5 (Abcam and BioLegend-clone 5H10-27, 1:100), integrin αv (BD-clone RMV-7, 1:100), integrin α6 (BD and BioLegend-clone GoH3, 1:100), integrin α3 (R&D, 1:100), integrin α1 (BD-clone Ha31/8 and BioLegend-clone HMα1, 1:100) and integrin α2 (BD-clone HMα2, 1:100).

Retroviral shRNA Constructs

miR30-based shRNAs targeting integrins β1 (TGCTGTTGACAGTGAGCGCGGCTCTC AAACTATAAAGAAATAGTGAAGCCACAGATGTATTTCTTTATAGTTTGAGAGCCTTGCC TACTGCCTCGGA), α3 (TGCTGTTGACAGTGAGCGCCGGATGGACATTTCAGAG AAATAGTGAAGCCACAGATGTATTTCTCTGAAATGTCCATCCGTTGCCTACTGCCTCGG

A), or control firefly luciferase (AAGGTATATTGCTGTTGACAGTGAGCGAGCTCCC GTGAATTGGAATCCTAGTGAAGCCACAGATGTAGGATTCCAATTCAGCGGGAGCCTGC CTACTGCCTCG) were designed using the shRNA retriever software (http://katahdin.cshl.edu/homepage/siRNA/RNAi.cgi?type=shRNA), synthesized (IDT, Coralville, Iowa), and then cloned into the MSCV-ZSG-2A-Puro-miR30 vector[297]. Packaging of retrovirus and transduction of cells was done as described previously[298].

Chapter 4. Aberrant O-glycosylation mediates increased galectin-3 interactions in metastasis

4.1 Introduction

Altered glycosylation states have long been associated with malignant progression[299-302]. Even in the early days of transformed cells, evidence of altered glycosylation was apparent by lectin staining[303]. This aberrant glycosylation is ubiquitous across human cancers and likely plays a key role in invasion and metastasis. MUC1, a heavily *O*-glycosylated glycoprotein is frequently upregulated in carcinomas[304-305], and knockdown of this protein reduces migratory behavior of cancer cell lines in an E-cadherin-dependent manner[306]. Considerable work has been initiated to elicit immune responses to the protein, and these vaccines typically show greater efficacy when the glycosylated form is presented[307-309]. Clinically, many cancer biomarkers are carbohydrate antigens (e.g. CA19-9, CA125, DUPAN-II, AFP-L3, etc.) owing to the conserved alterations in glycosylation that accompanies malignancy[310].

One particular glycan antigen expressed on as many as 90% of cancers is known as the Thomsen-Friedenreich Antigen (T-Antigen)[294, 311]. This glycan epitope is the core 1 *O*-linked disaccharide, Galβ1-3GalNAc, upon which further *O*-glycosylation occurs. In healthy tissues, this motif is masked by further glycosylation. Its expression, as evidenced by lectin staining, in cancer cells, however, is widely apparent[312-316]. Furthermore, it has been strongly associated with metastasis in experimental models[317-320]. Its naked presentation in normal tissue is so rare that all humans have low titers of IgM against it[316], and vaccination strategies have proved useful in humans with cancer[321-324].

Aside from its affinity for lactosamines, galectin-3 exhibits the ability to bind the T-Antigen[318, 325-327]. This recognition provides an attractive model for binding of T-Antigen-expressing tumor cells to galectin-3 expressed on the endothelium[318, 328]. In the previous chapter, we find that metastatic lung adenocarcinoma cells have elevated adhesion to combinations of galectin-3 and -8 when presented in the context of fibronectin, and that these molecules are present in the metastases of mice and humans. Given the association of galectin-3 with the T-Antigen, this chapter investigates the regulation of this glycan motif on metastatic cells and the mechanisms underlying its presentation.

4.2 Results

4.2.1 Increased T-Antigen Expression Correlates with Increases in Metastatic Progression

Previously, we found that adhesion to galectin-3 and -8, in the context of fibronectin, correlated strongly with metastasis of lung adenocarcinoma[329]. We used a genetic mouse model of lung cancer wherein mice bearing an oncogenic Kras allele at the endogenous locus downstream of a lox-stop-lox element as well as loxP sites flanking both endogenous p53 alleles ($Kras^{LSL\text{-}G12D/+};p53^{flox/flox}$) are administered a lentiviral Cre-recombinase through inhalation, resulting in the formation of multifocal autochthonous lung tumors[194, 215-216]. These mice develop distant metastases that can be correlated to their specific primary tumors of origin through examination of their lentiviral integration sites. Cell lines were developed from these tumors representing primary tumors that did not metastasize (T_{nonMet}), those that did give rise to metastases (T_{Met}), and distant metastases (M) (Fig. 4.1a)[194]. Previously, we found that the $\alpha3\beta1$ integrin was, in part, responsible for adhesion to these ECM molecule

combinations[329]. As galectin-3 and -8 are part of the galectin family of β-galactoside-binding lectins, we asked whether carbohydrate-mediated interactions might also have a role in the increases in adhesion.

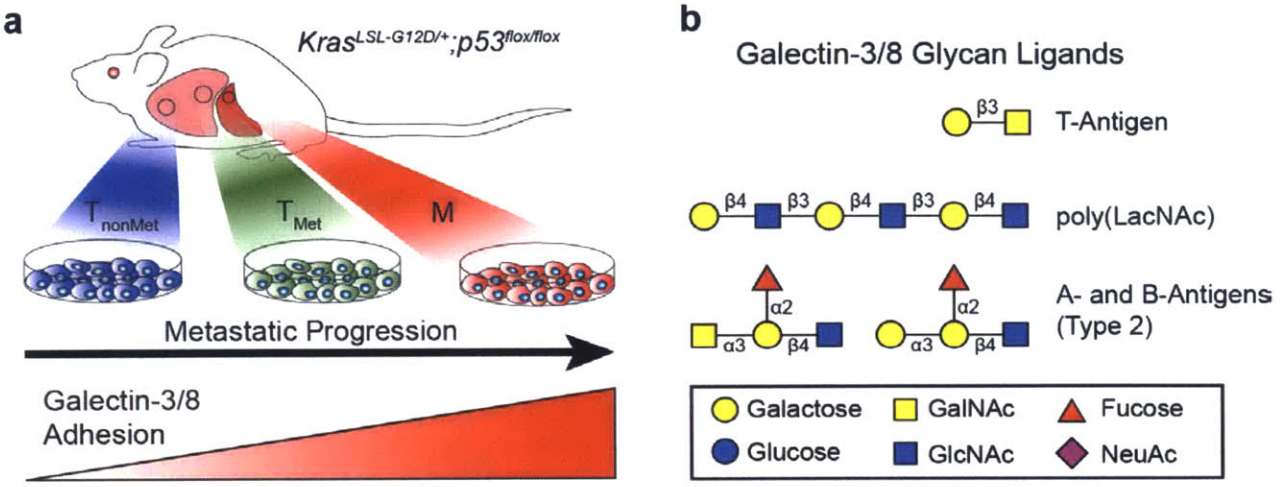

Figure 4.1. *Glycan-galectin interactions in lung cancer metastasis.* (a) Schematic depicting the mouse model used in these studies. Cell lines are generated from *Kras*$^{LSL\text{-}G12D/+}$;*p53*$^{flox/flox}$ mice following tumor development from the primary tumors that did not metastasize (T_{nonMet}), primary tumors that did give rise to metastases (T_{Met}), and distant metastases (M). (b) Potential glycan ligands for the galectin-3 CRD. The T-Antigen (Galβ1-3GalNac-α1-O-S/T) is specific for the carbohydrate recognition domain (CRD) of galectin-3 and -8. *N*-Acetyllactosamine (LacNAc) binds the CRD of all galectins and exhibits increased affinities when in a polymeric form. The A-B- Type 2 blood group antigens have reported affinities for a variety of galectins, including galectin-3, by glycan array analysis.

Examination of existing studies and publicly available glycomics databases[330] reveal a variety of glycan motifs recognized by the carbohydrate recognition domains (CRDs) of galectin-3 and -8 (Fig. 4.1b). While N-acetyllactosamine (LacNAc) shows a strong affinity to all galectins as a disaccharide and, to a greater extent, as repeated units, galectin-3 shows a specific affinity for motifs such as the Thomsen-Friedenreich Antigen (T-Antigen). The T-Antigen is an oncofetal O-linked disaccharide thought to be overexpressed on as many as 90% of carcinomas[294, 311, 316]. To determine the degree of T-Antigen presentation throughout metastatic progression, we performed microscopy and flow cytometry analysis on cell lines from the T_{nonMet}, T_{Met}, and M

classes following staining with peanut agglutinin (PNA), a plant lectin with specificity for the Gal-β(1-3)-GalNAc (T-Antigen) motif (Fig. 4.2a,b). These analyses revealed a strong increase in T-Antigen presentation as the cells become more metastatic.

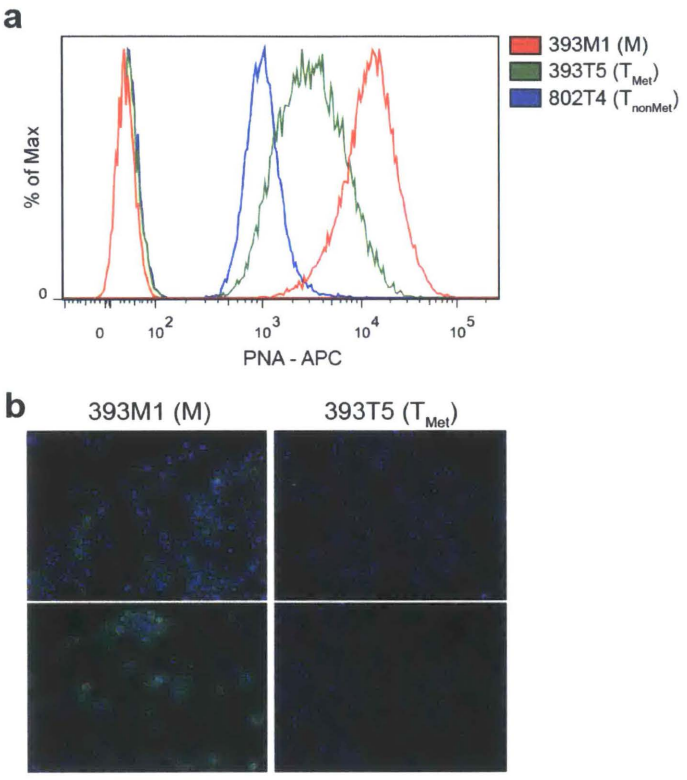

Figure 4.2. *T-Antigen expression increases with metastatic progression.* Peanut agglutinin (PNA) exhibits a strong specific affinity for the T-Antigen. (a) Flow cytometry analysis of lines 802T4 (T_{nonMet}), 393T5 (T_{Met}), and 393M1 (M) for binding of PNA. Cells were incubated with PNA conjugated to AlexaFluor 647 for 30 minutes prior to washing and analysis by flow cytometry. (b) Staining by PNA (green) on 393T5 and 393M1 cells. Cells were cultured on tissue-culture-plastic, fixed, and stained with PNA conjugated to AlexaFluor 647. Nuclei (blue) were stained with Hoechst.

To determine whether these changes occur in humans with lung cancer we stained human tissue microarrays for the T-Antigen. We observed that 60.5% of primary lung tumors stained positive for PNA (as compared to 13.0% of non-cancerous lung tissue, $P = 4.9\times10^{-6}$, Fisher's Exact Test) and 31.6% had distinct membrane PNA staining (as compared to 0% of non-cancerous lung, $P = 2.4\times10^{-5}$, Fisher's Exact Test) (Fig. 4.3a,b,d). Typically, activated germinal centers will stain positive for PNA. Nonetheless, we saw distinct differences in PNA staining between lymph nodes with cancer and normal lymph nodes. 100% of lymph node metastases stained positive for PNA (as compared to 12.5% of non-cancerous nodes, $P = 0.0007$, Fisher's Exact Test), and 50%

had membrane-specific staining (as compared to 0% of non-cancerous, $P = 0.0385$, Fisher's Exact Test) (Fig. 4.3a,c,d). These trends were consistent across a variety of NSCLC types (Fig. 4.3d).

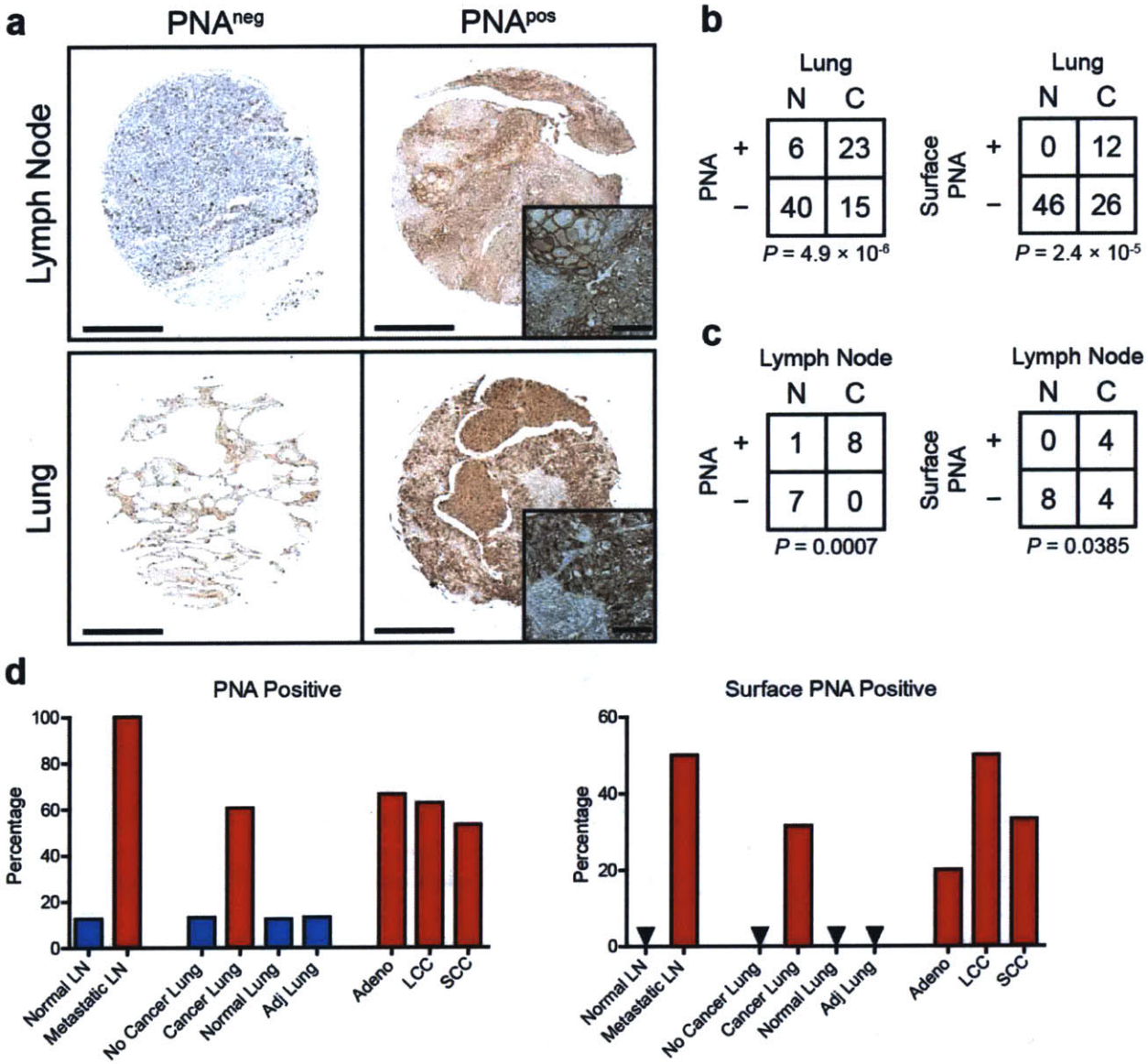

Figure 4.3. *T-Antigen expression on human NSCLC patients.* Human tissue microarrays were stained with peanut agglutinin (PNA) for presence of the T-Antigen. (a) Sample images of PNA stains from human tissue microarrays. Quantitation of staining of lung (b) and lymph node (c) samples looking at diffuse positive staining and membrane-specific staining. (d) Results from (c) with representation of the subtypes of NSCLC. Scale bars in (a) are 200μm and 100μm on the inset images. *P* values were determined using Fisher's Exact Test. PNA: peanut agglutinin; N: non-cancerous tissue; C: cancerous tissue; Adeno: adenocarcinoma; LCC: large cell carcinoma;

SCC: squamous cell carcinoma.

4.2.2 Galectin-3 Adhesion is Carbohydrate Mediated

Previously, we showed that knockdown of the α3 and β1 integrin subunits reduced adhesion of the metastatic cells to combinations of fibronectin with either galectin-3 and galectin-8[329]. Furthermore, α3β1 has been reported to bind galectin-8[233, 331] and may interact with galectin-3, as well[232, 332]. Thus, it is possible that the galectin-3 adhesion is a reflection of protein-protein interactions rather than the changes in cell-surface glycans. To determine whether adhesion of the metastatic cells to galectin-3 was truly carbohydrate-mediated, we incubated the cells (393M1) with fluorescent galectin-3 in the presence of LacNAc, a potent binder to the CRD of galectins (Fig. 4.1a), or a control disaccharide (sucrose) prior to flow cytometric analysis (Fig. 4.4a). Indeed, incubation with LacNAc inhibited galectin-3 adhesion to the metastatic cells confirming the functional relevance of the aberrant glycosylation in galectin adhesion.

Since knockdown of the α3 and β1 integrin subunits appeared to have an effect on galectin-3 and -8 adhesion, we asked whether this might be due to presentation of the T-Antigen on the integrin dimer. α3β1 is known to be heavily *N*-glycosylated, and it is thought that this glycosylation may promote its adhesion to galectin-3 or promote malignant progression[243, 245, 332-334]. Thus, we asked whether it may also present the *O*-glycans such as the T-Antigen. We analyzed PNA staining of the α3 and β1 knockdown lines by flow cytometry to determine whether removal of the integrin subunits reduced the T-Antigen presentation. While knockdown of β1 did not affect the degree of PNA staining, knockdown of the α3 subunit yielded a somewhat reduced

degree of staining (Fig. 4.4b), suggesting the possibility for *O*-glycosylation and T-Antigen presentation on the α3 integrin subunit. Furthermore, this finding suggests a possible synergistic role for protein- and glycan- recognition by single cell surface glycoproteins. Such results, however, would be best accompanied by validation with a second hairpin and immunoprecipitation of the α3 integrin subunit followed by lectin blotting with PNA.

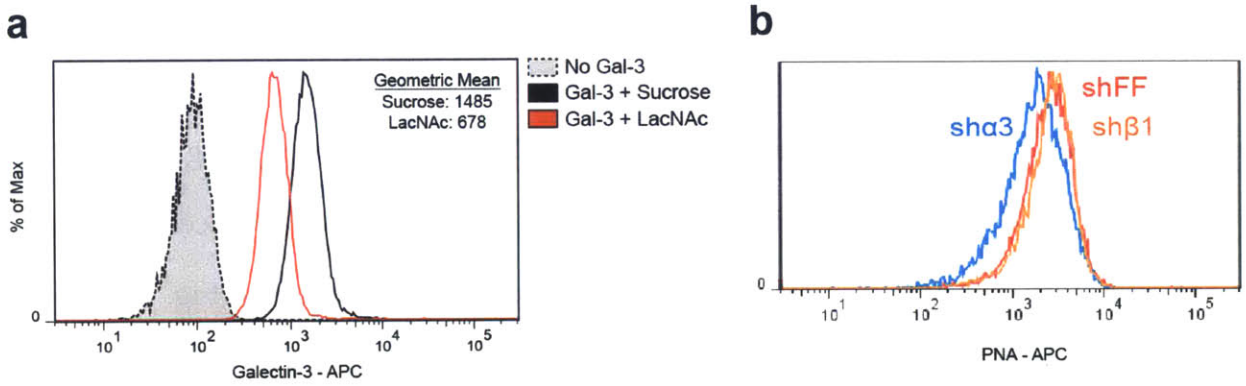

Figure 4.4. *Galectin-3 adhesion is carbohydrate mediated.* (a) Incubation of 393M1 cells with LacNAc (red) or Sucrose (black) prior to staining with fluorescent galectin-3. LacNAc inhibition reduces galectin-3 adhesion in a carbohydrate-dependent manner. (b) Short-hairpin knockdown of α3 and β1 integrin subunits (or control firefly luciferase) in the 393M1 cell line followed by PNA staining for the T-Antigen.

4.2.3 Changes in glycosylation are mediated by altered glycosyltransferase activity

We next asked whether changes in T-Antigen presentation were the result of increased expression of an individual glycoprotein or to global changes in glycosylation. Thus, we performed lectin blotting of cell surface proteins by isolating those proteins, running them on PAGE gels, and blotting PNA. We found that while specific bands were strongly enriched, there is a significant increase in global glycan presentation correlating with metastatic progression (Fig. 4.5a).

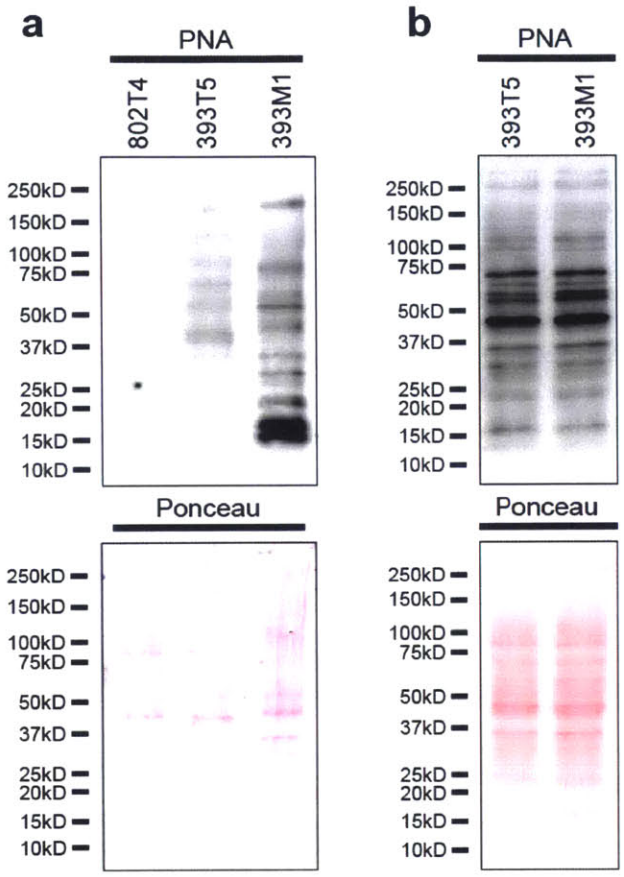

Figure 4.5. *T-Antigen presentation increases with metastatic progression on a variety of proteins.* Surface proteins were isolated from T_{nonMet}, T_{Met}, and M cell lines and run on SDS-PAGE gels. PNA lectin blots of cell surface proteins (a) and whole cell lysates (b). Ponceau S stains show total protein.

In light of this apparent global alteration in T-Antigen presentation, we asked whether regulation of specific glycosyltransferases induced these changes. Analysis of gene expression microarrays for 216 glycosyltransferase genes did not show widespread shifts in expression, nor were there significant changes in genes coding for transferases specific for generation of the galectin-3 ligands (Fig. 4.6a,b). Comparisons between the average primary tumor and metastasis-derived cell lines, however, did identify *Gcnt3* and *St6galnac4* as being under- and over-expressed in the metastatic lines, respectively (Fig. 4.7a), and these alterations were confirmed by RT-PCR in the representative cell lines (Fig. 4.7b). C2GNT2 (*Gcnt3*) induces the addition of a β(1-6)GlcNAc to the T-

Antigen, whereas St6galnac4 adds a α(2-6)NeuAc to the sialyl-T-Antigen (Fig. 4.7c). As further elongation of the core-1 disaccharide prevents recognition by galectin-3, these changes in Gcnt3 and St6galnac4 expression promote T-Antigen presentation through prevention of branching and capping of elongation, respectively. Similar trends were seen across all of the cell lines analyzed by gene expression microarrays (Fig. 4.7d). Lectin blotting of whole-cell lysates also revealed no differences in T-Antigen expression between the lines (Fig. 4.5b). This similarity is likely due to the nature of the changes in glycosylation. Generation of the disaccharide occurs in the endoplasmic reticulum (ER) and Golgi [335-336]. Thus, this similarity between the lines is likely a reflection of equivalent generation of the disaccharide within the Golgi, and further suggests that the differences in surface glycosylation observed are a result of decreased glycan extension rather than reduced generation of the disaccharide.

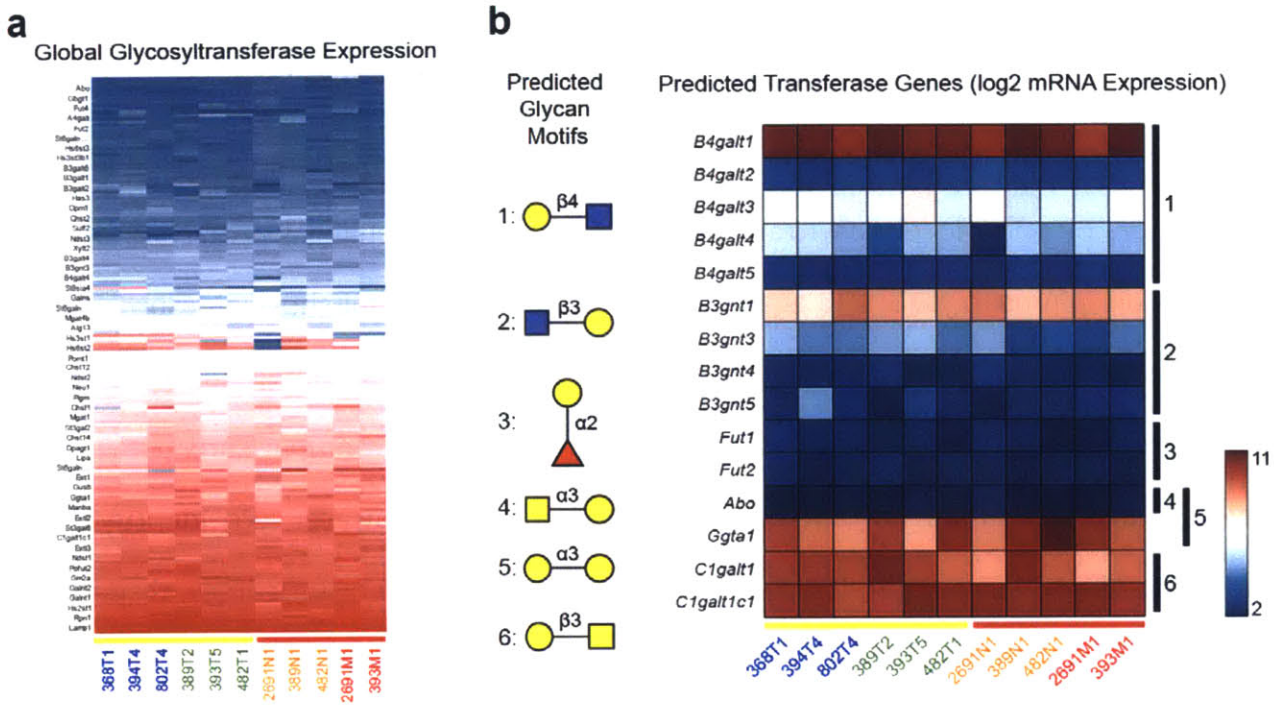

Figure 4.6. *Glycosyltransferase gene expression.* (a) Gene expression microarray analysis of

known glycosyltransferase expression reveals minimal alterations in global gene expression profiles between cell lines of the different stages. (b) Gene expression microarray analysis of select genes predicted to generate the galectin-3 binding partners (see Fig. 4.1b). All data is log_2 mRNA expression.

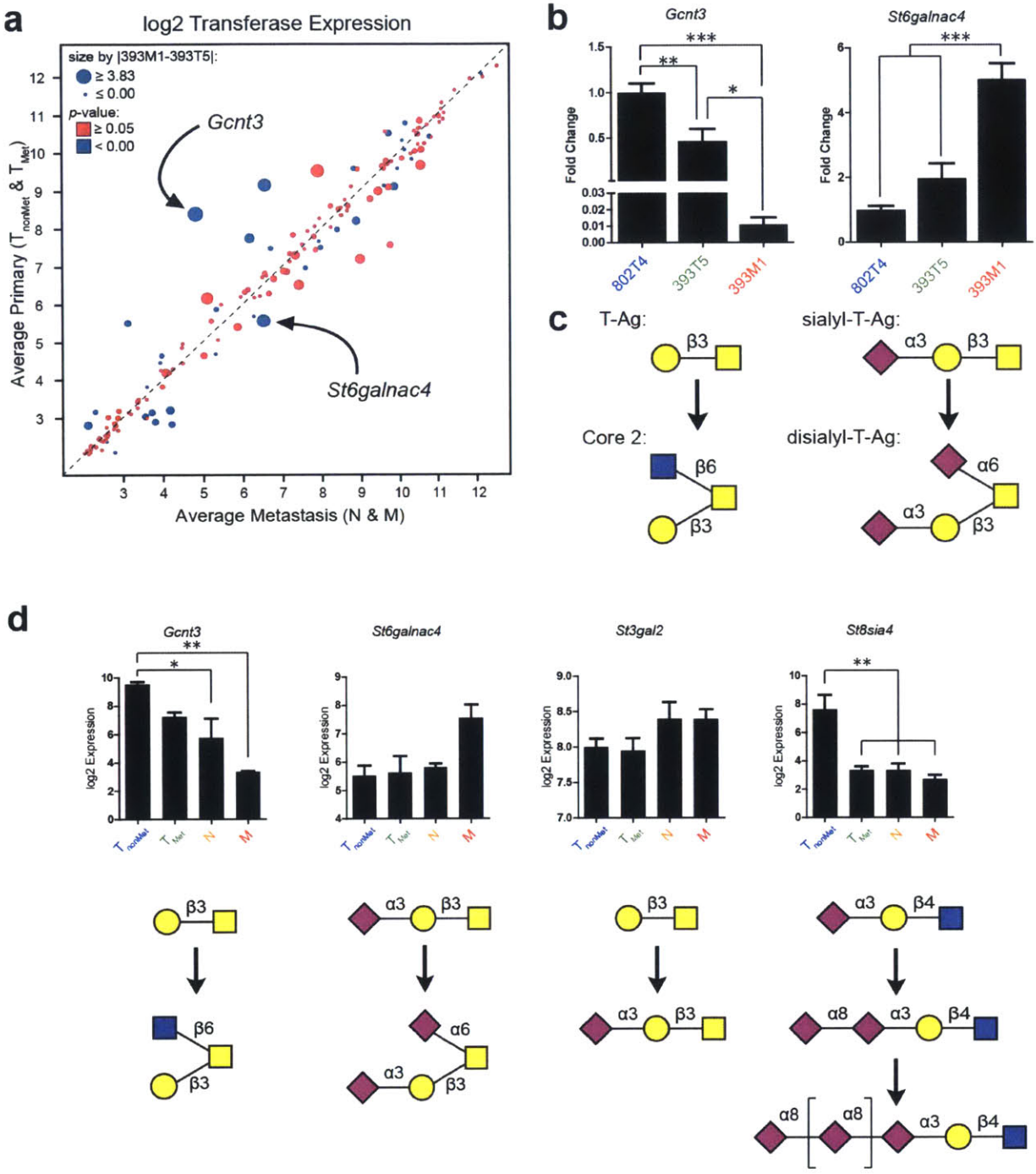

Figure 4.7. Gcnt3 *and* St6galnac4 *are differentially regulated during metastasis.* (a)

Comparison of the average primary tumor (all T_{nonMet} and T_{Met} lines) gene expression by the average metastases (all N and M lines) gene expression for all glycosyltansferases. (b) Expression of *Gcnt3* and *St6galnac4* in the three representative lines by qRT-PCR. (c) Schematic depicting the glycosylation resulting from C2GNT2 and ST6GALNAC4 activity. (d) Gene expression microarray analysis for all cell lines for select glycosyltransferase activity and the resulting structures. Size of spots in (a) refers to the absolute difference between the clonally related 393T5 and 393M1 pair. *P*-values in (a) are calculated between each class of lines (i.e. T_{nonMet} vs. T_{Met}, T_{Met} vs. N, N vs. M). Error bars in (b) are s.e.m. of separate RNA isolations and in (d) are s.e.m. of different cell lines of the same type. *P*-values in (b) and (d) were determined by one-way ANOVA followed by Tukey's multiple comparison post-test. * $P < 0.05$; ** $P < 0.01$; *** $P < 0.001$.

To determine whether the loss of the N-acetylglucosaminyltransferase C2GNT2 (*Gcnt3*) or gain of the sialyltransferase ST6GALNAC4 affect T-Antigen presentation and galectin-3 binding, we expressed and knocked down those genes in the metastatic line, respectively. Knockdown of *St6galnac4* using retroviral transduction of short hairpins targeting the gene resulted in reduced galectin-3 binding (Fig. 4.8a). PNA does not bind to the sialylated T-Antigen. Correspondingly, no differences in PNA staining were observed with this knockdown, confirming that its effects are specific to the sialylated form of the carbohydrate (Fig. 4.8b). Transfection of a *Gcnt3* ORF into the metastatic cells also reduced galectin-3 adhesion (Fig. 4.8c,e) and PNA staining (Fig. 4.8d,f), suggesting that its activity does indeed reduce T-Antigen presentation and, consequently, galectin-3 binding. Given these findings, we asked whether the alterations glycosyltransferase activity occurs in humans with lung cancer, as well. Analysis of *GCNT3* copy number in the cancer genome atlas [337] revealed a significant loss of copy number lung adenocarcinoma when compared to normal lung or blood (Fig. 4.8g, $P = 1.44 \times 10^{-11}$)[4].

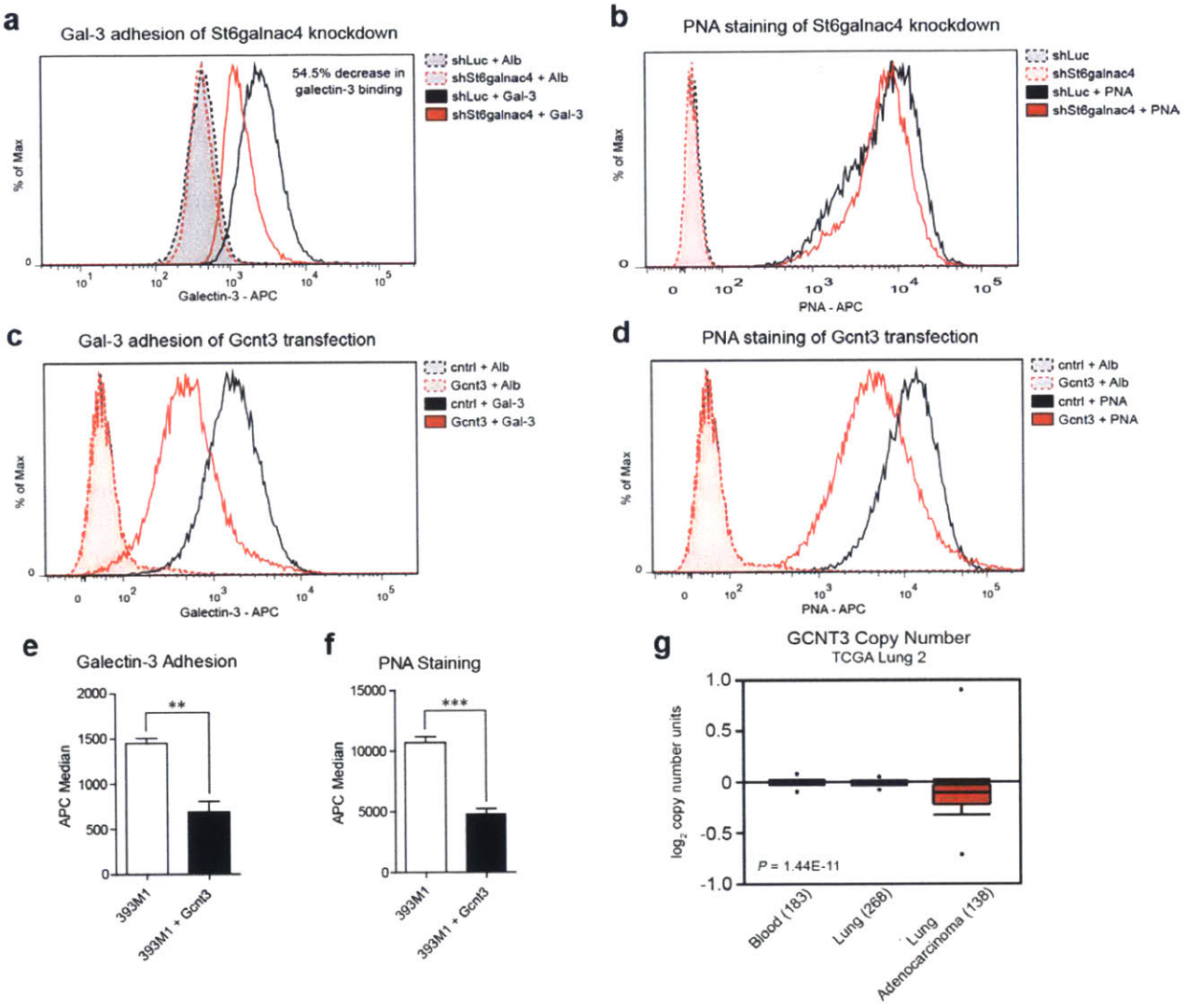

Figure 4.8. Gcnt3 *downregulation and* St6galnac4 *upregulation promote galectin-3 adhesion. St6galnac4* was knocked down by retroviral transduction of short hairpins. Galectin-3 (a) and PNA (b) staining of 393M1-shSt6galnac4 and 393M1-shLuc control cells. Galectin-3 (a) and PNA (b) staining of 393M1 cells transfected with *Gcnt3* plasmid. (e,f) Quantitation of (c,d). *GCNT3* copy number in human tissue taken from blood, normal lungs, or lung adenocarcinoma.

4.3 Discussion

In this chapter we explore the role of carbohydrate interactions with galectins as potential mediators of adhesion by the metastatic cells. We found that in this model of lung adenocarcinoma, the tumor cells increase their presentation of the core 1 O-linked disaccharide known as the Thomsen-Friedenreich Antigen (T-Antigen). This motif is

rarely exposed on normal cells as further glycosylation and branching extend the glycans. Galectin-3 specifically binds the T-Antigen when exposed on cell surfaces as a disaccharide. Here, we show that the metastatic cells bind galectin-3 in a carbohydrate-specific manner. We also show that these changes are the result of altered expression of specific glycosyltransferases that mediate extension of the glycan chains beyond the core 1 disaccharide. Genetic perturbation of these transferases prevents T-Antigen presentation and reduces galectin-3 adhesion.

While the role of glycans in tumorigenesis and metastasis remain an understudied component of cancer biology, they represent an attractive target due to their conserved representation and disregulation during neoplasia. In fact, in addition to many other glycoproteins and glycans, MUC1 was recently listed by the National Cancer Institute as the second of 75 highest ranked cancer antigens to prioritize for targeting [338]. MUC1 is a highly *O*-glycosylated glycoprotein that is frequently overexpressed on many carcinomas. Its widespread expression on carcinomas has prompted many to investigate its use for a cancer vaccine[307-309, 339]. Importantly, recognition of the glycosylated peptides on MHC molecules confers increased recognition by CD4 and CD8 T-Cells and improved tumor responses[307, 340]. Thus, significant research to enhance glycoprotein antigen responses is being pursued[341-344].

While these approaches hold great promise for generating immune responses against tumors, they rely upon some degree of peptide recognition and loading onto MHC molecules. Our data suggest that T-Antigen presentation is likely not restricted to single glycoproteins but rather represents global changes in glycosylation. Previous work has suggested that another α2,6-sialyltransferase, ST6GALNAC5, promotes breast cancer

metastasis to the brain through increased adhesion to endothelium and traversal of the blood-brain barrier[110]. While targeting specific transferase activity (e.g. ST6GALNAC4, ST6GALNAC5, or C2GNT2) may be a viable approach, those specific changes are not likely to be conserved across cancers in the same manner as the T-Antigen epitope itself, and thus, may represent targets for which resistance could easily develop.

Much of the initial work done on the T- and Tn- (GalNAc-α_1-*O*-Ser/Thr) Antigens, particularly in the context of eliciting anti-cancer immune responses was performed by Georg F. Springer[311, 316, 345]. Springer developed a vaccine by purifying T- and Tn-Antigens from the surfaces of erythrocytes and combining them with phosphoglycolipid A hyperantigen (*S. typhi* vaccine) and $Ca_3(PO_4)_2$ as adjuvants. Though his patient studies were significantly underpowered and lacked any appropriate control arm, the 5- and 10-year survival rates for his breast cancer patients were significantly above national averages[311]. Thus, targeting the T-Antigen itself may prove to be an effective therapy.

Interactions between glycans and galectins likely provide a means for CTCs to form metastases. This process may be mediated by accumulation of galectin-3 upon the endothelium during cancer progression, thus aiding in arrest and extravasation[318, 325, 346]. The interactions may also promote integrin interactions that promote migration or colonization[332]. Galectins are also appreciated to be potent immune modulators[347], suggesting that galectin-glycan interactions may be promoting metastasis through modulation of pro- and anti-tumor immune responses.

4.4 Methods

Cell Lines

Cell lines (a gift from Tyler Jacks and Monte Winslow, Massachusetts Institute of Technology, Cambridge, MA) were described previously[194] and were cultured in DMEM with 10% (vol/vol) fetal bovine serum and 1% L-glutamine.

Western and Lectin Blot Analysis

Cell lysates were harvested in RIPA buffer (Sigma) containing Complete Protease Inhibitor (Roche) and Phospho Stop (Roche) on ice and run on SDS-PAGE gels. PVDF membranes were stained for galectin-3 (Abcam, ab53082, 1:500), galectin-8 (Abcam, ab69631, 1:500), and α-tubulin (Cell Signaling, 2125, 1:1000). Lectin blotting for glycans was performed using PNA-Biotin (Sigma) followed by detection using the ABC Elite Kit (Vector Labs, PK-6100) or PNA-Peroxidase conjugates (Sigma). Ponceau S solution (Thermo) was used for total protein detection following transfer to PVDF membranes.

Cell Surface Protein Isolation

Cell surface proteins were isolated prior to Western blot analysis using Thermo Scientific kit 89881 following the manufacturer's instructions. Briefly, cells are washed followed by biotinylation of the surface proteins by a Sulfo-NHS-Biotin through conjugation to free amines. The reaction is quenched and cells are harvested and lysed. Lysate is washed through a column containing a neutravidin resin to capture the biotinylated surface proteins. Finally, the disulfide linkage is reduced through incubation with 50mM DTT and the proteins are captured.

Flow Cytometric Analysis

Peanut agglutinin staining was performed by incubating 3×10^5 cells in PBS with 10µL PNA-AlexaFluor 647 (invitrogen) on ice for 30 minutes. Fluorescent galectin-3 was produced by reacting recombinant murine galectin-3 (R&D Systems) with DyLight 650 NHS Ester (Thermo Pierce). Conjugated protein was purified by FPLC and concentrated to 0.5mg/mL using 3,000 MWCO Amicon centrifugal filter units (Millipore). Cells were stained by incubating 3×10^5 cells in PBS with 10µL of the fluorescent galectin-3 on ice for 30 minutes. For galectin-3 binding inhibition experiments, cells were incubated with galectin-3, as described above in the presence of 20mM *N*-Acetyl-D-lactosamine (Carbosynth) or sucrose (Sigma). Flow cytometry was performed on a LSR Fortessa (BD Biosciences) and analyzed using Flowjo (Tree Star).

RNA Isolation and Expression Profiling

Gene expression microarray analysis was described previously[329] and is available from NCBI under accession number GSE40222. RNA was isolated using RNeasy mini kits (Qiagen) according to the manufacturer's instructions. cDNA reactions were performed using iScript cDNA synthesis kit (Bio-Rad). qRT-PCR was performed using IQ SYBR Green Supermix (Bio-Rad). Fold change is reported following analysis using the $\Delta\Delta C_t$ method where genes were normalized to *Hprt* housekeeping control. Primers were: *St6galnac4* forward 5'-GGTTGGTTCACCATGATTCTG-3', *St6galnac4* reverse 5'-GGAGCGGGGACTCTTCTC-3', *Gcnt3* forward 5'-GCAGCCAAGAAGGTACCAAA-3', *Gcnt3* reverse 5'-ACAGGCGAGGACCATCAA-3', *Hprt* forward 5'-GTCAACGGGGGACATAAAAG-3', *Hprt* reverse 5'-CAACAATCAAGACATTCTTTACA-3'. Gene expression analysis and visualizations were performed using Spotfire (Tibco) and MATLAB (Mathworks).

Cell and Tissue Staining

For immunocytochemical analysis of T-Antigen presentation, cells were stained with PNA-AlexaFluor 647 (invitrogen). All paraffin sections were developed using DAB and counterstained with hematoxylin. Carbo-Free Blocking Solution (Vector Laboratories) was used for all staining involving the use of peanut agglutinin. Endogenous peroxidase activity was blocked using the Dual Endogenous Enzyme Block (Dako). PNA staining of human tissue microarrays was performed with PNA-HRP (Sigma, 4µg/mL) following antigen retrieval in citrate buffer. Staining of the Human Lung Cancer and Normal Tissue Microarray (US Biomax, Inc) was scored blinded.

Hairpins and Plasmids

Knockdown of St6galnac4 was performed using short-hairpin RNA (5'-TTCTGCTCCTCACACTGTGCATCTTGACA-3') or a control hairpin targeting firefly luciferase in the pGFP-V-RS vector (Origene, TG502032 and TR30002). Plasmids were packaged into retroviruses using the Phoenix-Eco system. Viral supernatant was filtered using 0.45µm syringe filters and cultured with 393M1 cells at no dilution. Transduced cells were selected with puromycin (Invitrogen), and knockdown efficiency was determined by qRT-PCR following four weeks of culture. Tansfection of *Gcnt3* was performed using Lipofectamine (Invitrogen) according to the manufacturer's instructions with plasmids purchased from Origene (MC215765).

Chapter 5. Presentation of Galectin-3 in the Metastatic Niche

5.1 Introduction

5.1.1 The role of hematopoietic cells in the tumor microenvironment

The establishment of pro-tumor microenvironments not only within the site of the primary tumor, but also the metastases is now well-appreciated[106]. These microenvironments consist of a variety of extracellular matrix molecules[112] and stromal cell types[348]. Many of the ECM molecules have been found to specifically promote metastasis rather than growth of the primary tumors. ECM molecules such as fibronectin have long been associated with invasion and metastasis in both *in vitro* and *in vivo* settings[221, 224, 349]. Recently, a variety of ECM molecules have been suggested to play a role in establishment of the metastatic niche. Lysyl oxidase (LOX) induces crosslinking of collagen IV in the lungs of mice with breast cancers[123], tenascin-C[114] produced by both cancer cells and the stroma support metastasis, and osteopontin can promote not only adhesion but also act in an endocrine fashion to mobilize pro-tumorigenic bone marrow-derived cells (BMDCs) to the sites of metastases[119, 148].

Many of these ECM molecules and other secreted molecules promote establishment of the metastatic site through recruitment of pro-tumorigenic leukocytes. Many tumors elicit inflammatory responses, which in turn, recruit inflammatory cells[350]. Many of the BMDCs act to promote angiogenesis[351-354]. In particular tumor-associated macrophages (TAMs) exhibit a phenotype similar to M2 alternatively activated

macrophages and exhibit both immune suppressive and pro-tumor activities[124, 355-356]. As macrophages typically express CSF1-R (colony-stimulating factor-1 receptor, CD115), they are frequently recruited by CSF1 signaling circuits. Consequently, genetic ablation of CSF1 reduces tumor growth and metastasis[357] and TAMs that are recruited by CSF1 secrete EGF to tumor cells to establish a paracrine signaling loop that promotes invasion[128]. In addition to TAMs, myeloid-derived suppressor cells (MDSCs) are a diverse group of $CD11b^{+}Gr\text{-}1^{+}$ leukocytes capable of suppressing anti-tumor T and NK cell activity, frequently infiltrate tumors[358-359], and can promote metastasis[360]. Furthermore, TNF-α secretion by endothelial and stromal cells following chemotherapy results in increased CXCL1/2 expression by cancer cells and consequently enhanced MDSC recruitment to the tumors and metastases[361]. In addition to TAMs, we now appreciate that there is a distinct subset of macrophages that appear to specifically promote metastases (metastasis-associated macrophages, MAMs)[362]. These cells, and their precursor inflammatory monocytes, are recruited specifically to metastases by tumor- and stroma- secreted of CCL2[68].

Recently, multiple groups have reported evidence of the establishment of a 'pre-metastatic' niche that is conducive to tumor seeding and colonization even prior to the arrival of tumor cells. As previously mentioned in the context of collagen IV[123], these signaling networks often involve ECM molecules, soluble factors, and BMDCs. LOX secretion is induced by hypoxia of the primary tumors and induces crosslinking of collagen IV in the basement membranes of the lungs. This crosslinking results in $CD11b^{+}$ cell recruitment, and these cells, in turn, degrade the collagen IV into peptides that act to recruit more BMDCs and CTCs. Similarly, tumor-secreted factors induce fibronectin

presentation in the pre-metastatic niche, resulting in recruitment of VEGFR1$^+$ BMDCs and, subsequently, the tumor cells[67]. Secretion of chemoattractants S100A8 and S100A9 by tumors acts to recruit BMDCs to the lungs through their induction of serum amyloid A 3[363-364]. Thus, a variety of signaling loops appear to exist where primary tumors secrete chemokines[365] and other factors, many of which are ECM molecules, that act to establish a pre-metastatic niche through the recruitment of CD11b$^+$ leukocytes.

5.1.2 The role of galectins in adaptive immunity

In addition to the roles of galectins discussed in the previous chapter, galectins have significant roles in modulating immune responses[347]. Frequently, galectins modulate these responses by oligomerizing and clustering specific glycoproteins on cell surfaces into lattices capable of affecting downstream signaling[366-367].

With regards to the T-cell compartments, galectin-1 induces apoptosis of activated T-cells by binding and clustering CD45[368-369]. Galectin-9 is a Tim-3 ligand that acts through that receptor specifically to induce an intracellular calcium flux and cell death of T_H1 cells[370]. Galectin-1 binding[371] and intracellular galectin-10[372] have both been shown to promote anergy and contribute to the immunosuppressive activity of regulatory T-cells (T_{Reg}). Demetriou and colleagues showed that *Mgat5* driven *N*-glycosylation of the T-Cell Receptor (TCR) normally heightens the T-cell activation threshold and its absence leads to autoimmune disease. They show that the resultant glycans interact with galectin-3 to generate a lattice that limits TCR recruitment to the site of antigen presentation[373]. More generally, galectin-glycan interactions restrict lateral movement of the TCR and CD45 to prevent aberrant TCR activation[374]. While

galectin-1 can induce apoptosis in T_H1 and T_H17 cells, differential α2,6 sialylation prevents galectin-1-induced apoptosis in T_H2 cells[375]. Importantly, galectin-3 can induce anergy in tumor-specific CTLs by segregating CD8 from the TCR[376]. Furthermore, extracellular galectin-3 can induce T-cell apoptosis in an independent manner from galectin-1 by binding CD45 and CD71[377] or CD7 and CD29 (β1 integrin)[378].

In a manner similar to T-cells, galectins help modulate B-cells and the humoral immune response. Galectin-1 promotes interactions at the pre-B cell-stromal synapse through interactions with integrins[379-380]. Galectin-3 promotes B-cell survival and differentiation towards memory cells[381], and may, in addition to galectin-1, promote anergy[382].

The activities of antigen presenting cells (APCs) are also frequently regulated by galectin-glycan interactions. Galectin-3 can form lattices on APCs that retain cytokine receptors on cell surfaces to enhance signaling[383]. Dendritic cells from galectin-3 knockout mice have a reduced ability to prime T- and B-cells[384], and galectin-1 inhibits macrophages from activating T-cells[385].

The roles of galectins in modulating immune responses are important for maintaining normal physiological responses to disease. These mechanisms, however, can be utilized by tumors to prevent immune responses to the malignancies[153, 347]. The galectins can promote anergy and the generation of T_{reg}s. Furthermore, tumors often secrete high levels of galectin-1 to induce effector T-cell apoptosis.

5.1.3 The role of galectins in innate immunity

In addition to their roles in recognition of self-glycans on immune cells, galectins may act as pattern recognition receptors and initiate danger signals[386]. Galectin-3 was the first of such examples as it was reported to recognize LPS through both its glycan and non-glycan structures[387-388]. These findings provide potential justification for the evolutionary conservation of the galectins and their CRDs.

One essential component of both adaptive and innate immune responses is the ability of leukocytes to home to sites of inflammation. Galectins are often expressed on vascular endothelium and contribute to leukocyte extravasation[389-390]. Galectin-1 and -3 have been reported to influence resident DC migration into the draining lymphatics[391-392]. Essentially all leukocytes that enter into tissues and exit into the lymphatics express galectins, and thus many galectins have been reported in a variety of inflammatory disease states[393].

In addition to their effects on regulating specific interactions with the endothelium, galectins can act as chemokines that drive migration of leukocytes. Importantly, galectin-3 acts as a chemoattractant for neutrophils, eosinophils, monocytes, and macrophages *in vitro*[394-395] and *in vivo*[395], and it promotes migration of granulocytes, monocytes, and lymphocytes into inflamed tissues[396-399]. It can act as a damage-associated molecular pattern (DAMP) to recruit neutrophils to parasitic infections[400]. Galectin-9 is a chemoattractant for eosinophils[401]. Unlike galectin-3 and -9, however, galectin-1 inhibits leukocyte recruitment. In particular it prevents neutrophil entry in acute peritonitis and edema[402-403] and lymphocytes in the context of contact hypersensitivity[404]. Nonetheless, galectin-1 and -3 may both promote exit from tissue into the lymphatics[393].

In addition to its role as a chemoattractant, galectin-3 has a variety of effects on peripheral blood monocytes and neutrophils. It can induce superoxide anion production by both of these cell types[405-406]. It also appears to activate NAPDH-oxidase specifically in primed neutrophils taken from inflamed tissue, but not peripheral blood[407]. Once exposed to stimuli, however, peripheral blood neutrophils can generate respiratory bursts[407-408]. Galectin-3 also promotes phagocytosis in neutrophils, and many of these responses may be mediated by CD66[409-410]. Furthermore, galectin-3 promotes neutrophil adhesion to laminin, and to a lesser extent, fibronectin[411]. It is important to note that while galectin-3 induces phophatidylserine exposure and subsequent apoptosis of T-cells, no such effect is observed on neutrophils, suggesting it has differential effects depending on immune cell subset[412].

Galectin-3 has a variety of effects on macrophages as well. Similarly to PMNs, galectin-3 knockout mice have reduced phagocytosis of apoptotic cells and microorganisms by macrophages[413]. MacKinnon and Farnworth *et al.* recently found that galectin-3 promotes IL-4/IL-13 alternative macrophage activation in an independent manner from classical activation, and that signals through CD98[414]. They show that IL-4 stimulates galectin-3 expression. It is worth noting that CD98, a galectin-3 receptor, can promote integrin activation following dimerization via ligation of the heavy chains by galectin-3[415]. CD98 is one of multiple cell surface glycoproteins on macrophages capable of binding galectin-3. Dong and Hughes characterized these receptors by galectin-3 affinity chromatography of murine macrophages and found the following molecules to associate with galectin-3: CD11b, LAMP1, LAMP2, Mac-3, and the CD98 heavy chain[284].

Furthermore, galectin-8 promotes superoxide production by neutrophils through its interactions with CD11b[416].

Taken together, these findings suggest a potential role for inflammatory immune cell presentation of galectin-3 in the tumor microenvironment. These cell types are frequently upregulated in cancer, and we have previously seen a strong correlation between metastatic progression and galectin-3 adhesion. In this chapter we explore the role of the metastatic microenvironment as it pertains to presentation of galectin-3 and galectin-8.

5.2 Results

5.2.1 Mice bearing tumors exhibit elevated galectin-3 positive populations in their peripheral blood

To address the role of galectin-3 in the pro-tumorigenic immune response, we asked whether circulating inflammatory populations present galectin-3 (also known as Mac-2). Flow analysis of peripheral blood leukocytes showed a strong enrichment for galectin-3$^+$ cells in mice bearing either T_{nonMet} (802T4) or M (393M1) tumors when compared to mice without tumors (Fig. 5.1a-b). Furthermore, these mice have highly elevated numbers of CD11b$^+$ cells (Fig. 5.1c-d), and the majority of galectin-3$^+$ cells are also CD11b$^+$ (Fig. 5.1e-f). Examination of the scatter profile suggests that the galectin-3 expressing cells are likely myeloid neutrophils and monocytes (Fig. 5.1g).

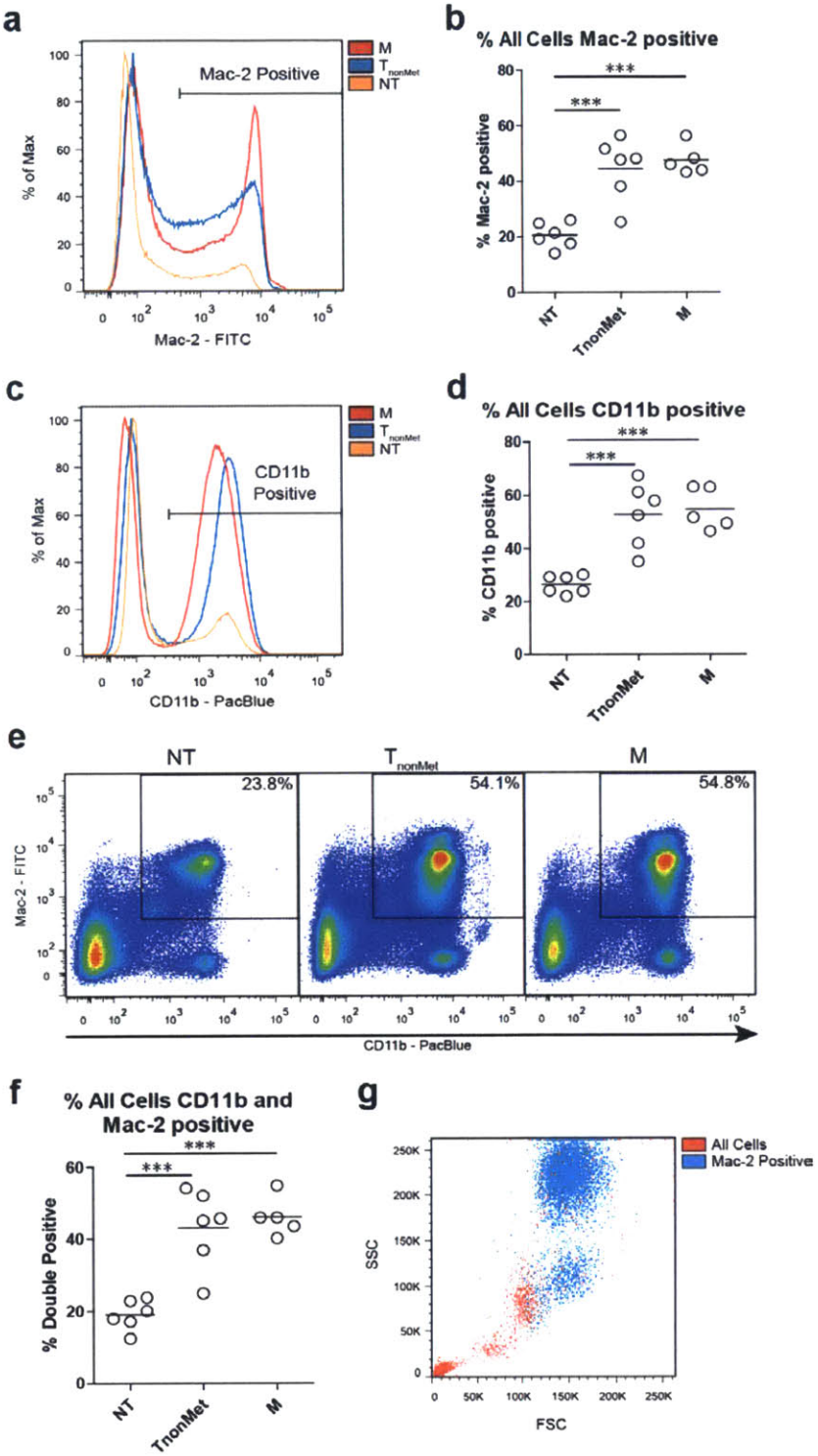

Figure 5.1. *Galectin-3 is expressed on CD11b⁺ peripheral blood leukocytes in mice bearing tumors.* Peripheral blood was harvested by cardiac puncture from mice implanted with subcutaneous flank tumors derived from various cell lines. Cells were gated based on their FSC and SSC profiles. (a,b) Galectin-3/Mac-2 staining of all peripheral blood cells. (c,d) CD11b staining of all peripheral blood cells. (e,f) Gating for CD11b⁺Mac-2⁺ double-positive cells. (g) FSC vs. SSC for all cells (red) and galectin-3/Mac-2⁺ cells (blue). 'NT' no tumor; 'T_{nonMet}' mice bearing the 802T4 cell line; 'M' mice bearing the 393M1 cell line. *** $P < 0.001$. NT: no tumor.

CD11b is the α subunit of the αMβ2 integrin dimer, is a complement receptor (CR3), and is found on the surfaces of neutrophils, monocytes, macrophages, and natural killer cells. We found that mice bearing tumors had elevated numbers of $CD11b^{+}Gr\text{-}1^{+}Ly6C^{mid}$ cells (many of which are likely neutrophils, Fig. 5.2a,b) and $CD11b^{+}CD115^{+}$ monocytes (Fig. 5.2c). In agreement with previous reports, we found that mice bearing tumors had elevated ratios of $Ly6C^{hi}$ inflammatory monocytes (IMs) to $Ly6C^{lo}$ residential monocytes (RMs) (Fig. 5.2d,e). Furthermore, we found that, particularly in mice bearing the metastatic cell line, galectin-3 levels were much higher in the IMs than RMs (Fig. 5.2f). Of note, the galectin-3 levels on individual $CD11b^{+}$ cells were not strongly increased in mice bearing tumors (Fig. 5.2g-i), suggesting that the increases in galectin-3^{+} cells is likely due to increased inflammatory cell recruitment or production rather than their degree of galectin-3 presentation.

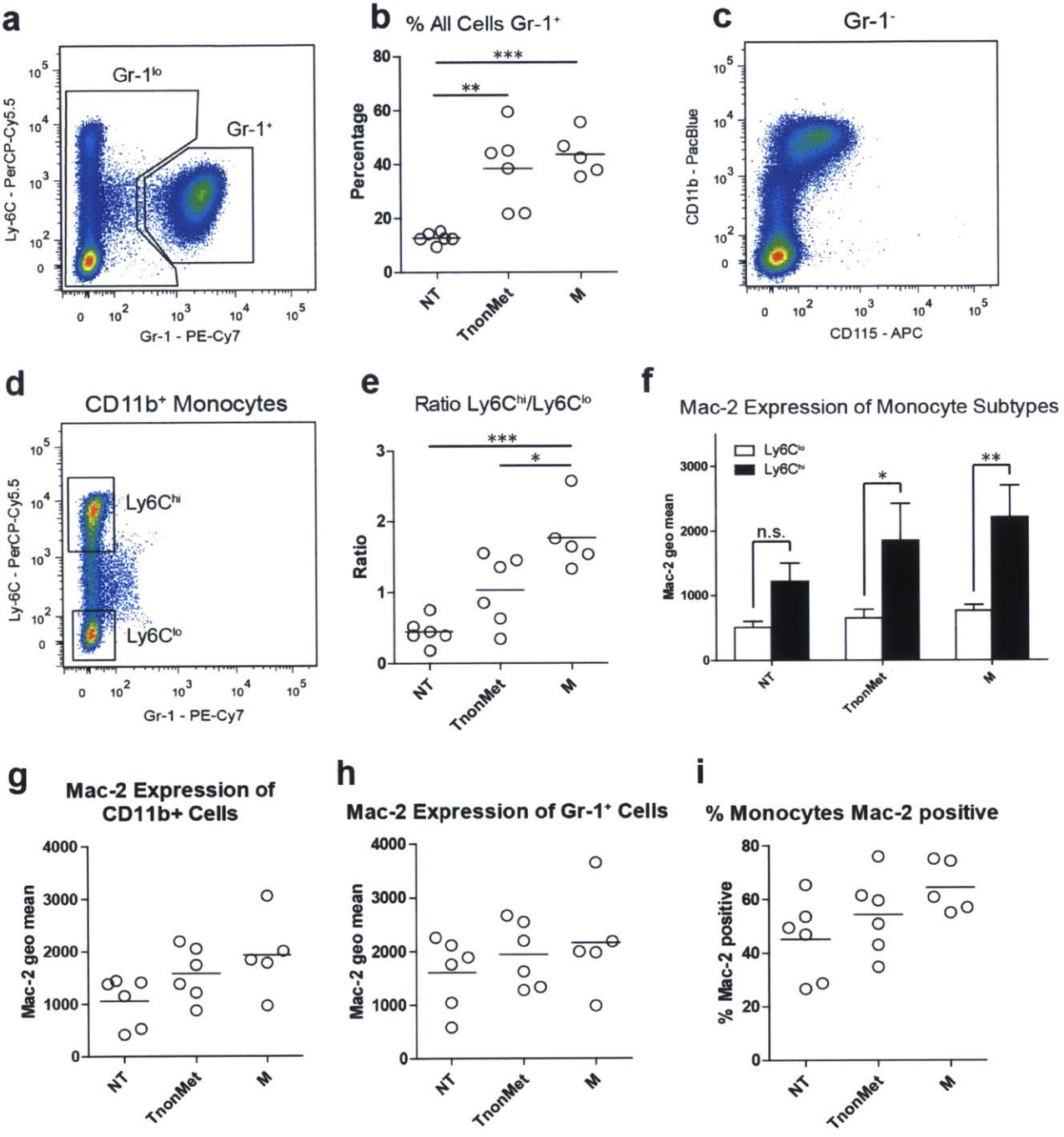

Figure 5.2. *Tumor-bearing mice have enriched galectin-3⁺ CD11b⁺Gr-1⁺ and CD11b⁺Ly6C^{hi} cells.* Mice bearing no tumors (NT), T_{nonMet} tumors, or M tumors injected into their rear flanks were analyzed for CD11b⁺ subsets by flow cytometry. (a) Staining for Gr-1⁺ cells. (b) Staining for CD115⁺ monocytes. (d,e) Mice with tumors have elevated levels of Ly6C^{hi} monocytes. (f) Fluorescence intensity of galectin-3 staining on monocytes from mice with and without tumors. Intensity of galectin-3 staining on (g) all CD11b⁺ cells and (h) Gr-1⁺ cells. (i) Percentage of all monocytes that are galectin-3⁺. ** $P < 0.01$; *** $P < 0.001$. NT: no tumor.

5.2.2 *Tumor-specific production of galectin-3 is constant throughout metastatic progression*

Previously, we observed that strong differences in adhesion to galectin-3 and galectin-8 existed between the T_{nonMet} and M cell lines (see Chapter 2)[329]. Nonetheless, recruitment of $CD11b^{+}Mac\text{-}2^{+}$ cells into peripheral blood seemed relatively constant between the different stages. Thus, we asked whether tumor-specific production of galectin-3 remained constant throughout metastatic progression. Indeed, transcriptional levels of *Lgals3* and *Lgals8* by gene expression microarray for all lines as well as protein levels for the three representative lines remained constant (Fig. 5.3a,b). Since, for galectin-3, these levels may represent intracellular activity as well, we examined whether the tumors secreted galectin-3 in a manner that could interact with circulating immune cells or travel to other organs. Thus, we examined serum levels of circulating galectin-3 in mice bearing tumors (T_{nonMet} and T_{Met}) compared to naïve mice. Analysis of serum-levels revealed a strong increase in circulating galectin-3 in mice bearing tumors (Fig. 5.3c).

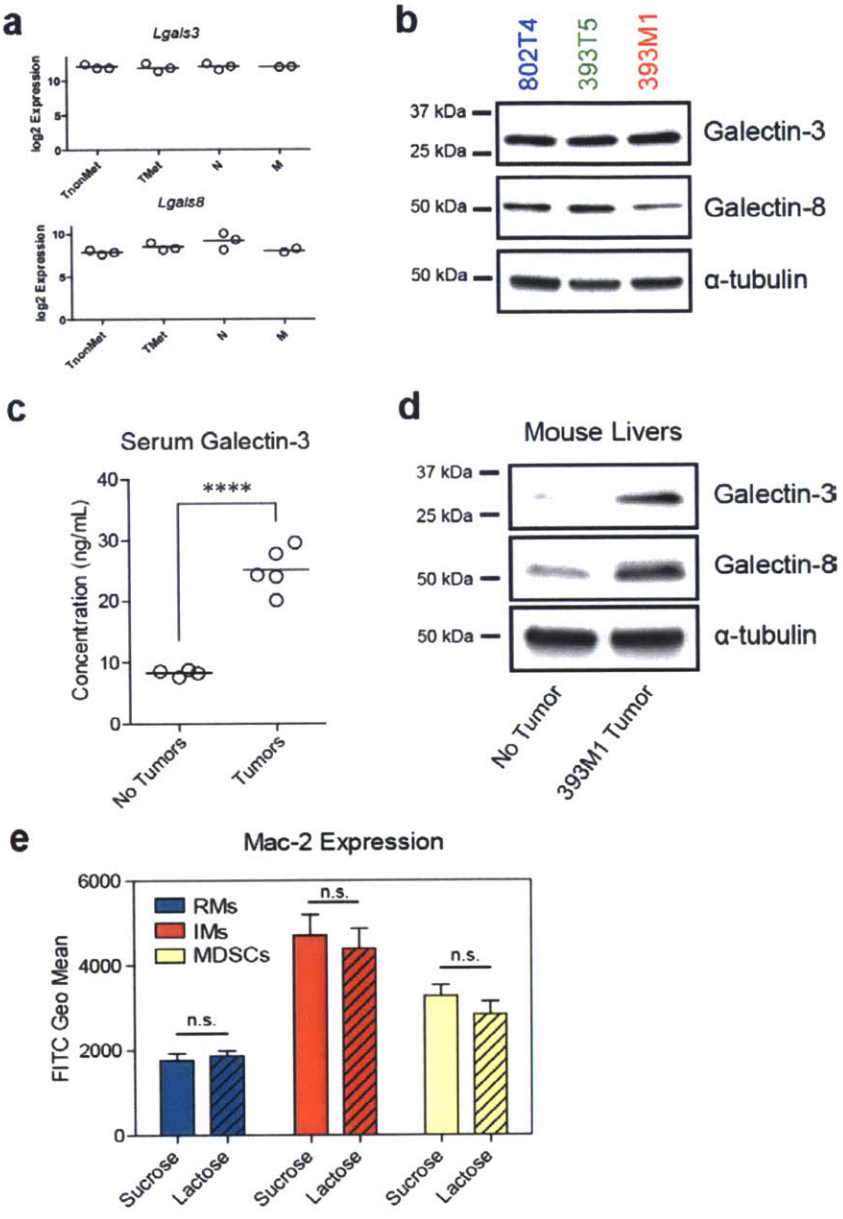

Figure 5.3. *Galectin-3 expression in cell lines and mice.* (a) Gene expression microarray mRNA levels of *Lgals3* (galectin-3) and *Lgals8* (galectin-8) for cell lines from each of the four classes: T_{nonMet} (n=3), T_{Met} (n=3), N (n=3), and M (n=2). (b) Western blot analysis of protein levels of galectin-3 and -8 for three representative lines: 802T4 (T_{nonMet}), 393T5 (T_{Met}), and 393M1 (M). (c) ELISA analysis of serum levels of circulating galectin-3 in mice bearing T_{nonMet} and T_{Met} cell lines. (d) Western blot analysis of galectin-3 and -8 levels of the livers of mice bearing tumors but no detectable metastases. (e) Flow cytometry of galectin-3 levels on $CD11b^+$ cells of mice bearing tumors following MACS separation in the presence of 200mM lactose or sucrose. **** $P < 0.0001$; n.s. not significant. RM resident monocyte; IM inflammatory monocyte; MDSC myeloid-derived suppressor cell.

5.2.3 *Galectin-3 is present in the metastatic niche*

Previously, we found that mice bearing autochthonous tumors had galectin-3 and -8 in their metastatic sites, but not their primary tumors. To establish a role for presentation of galectin-3 in the metastatic niche, we asked whether the metastatic tumors also had the inflammatory infiltrates. We found that the $Kras^{G12D/+};p53^{\Delta/\Delta}$ mice do indeed have

these infiltrates at the sites of metastases. Furthermore, tumors from mice bearing the metastatic line stain positive for F4/80$^+$ macrophages that frequently co-localize with galectin-3 (Fig. 5.4). Given the high circulating galectin-3 levels and CD11b$^+$Mac-2$^+$ leukocytes in the blood, we asked whether mice bearing tumors can establish galectin-3-positive niches prior to the arrival of circulating tumor cells (CTCs). We found that, in mice bearing the primary tumor lines, F4/80$^+$ macrophages were readily visible within their livers that co-stained for galectin-3 (Fig. 5.5). Furthermore, we harvested livers of tumor-bearing mice prior to the development of metastases and analyzed whole tissue lysates following homogenization. Elevated levels of galectin-3 were present in the livers of mice bearing tumors (Fig. 5.3d), suggesting that galectin-3 is being presented at the sites of metastases prior to the detection of metastases.

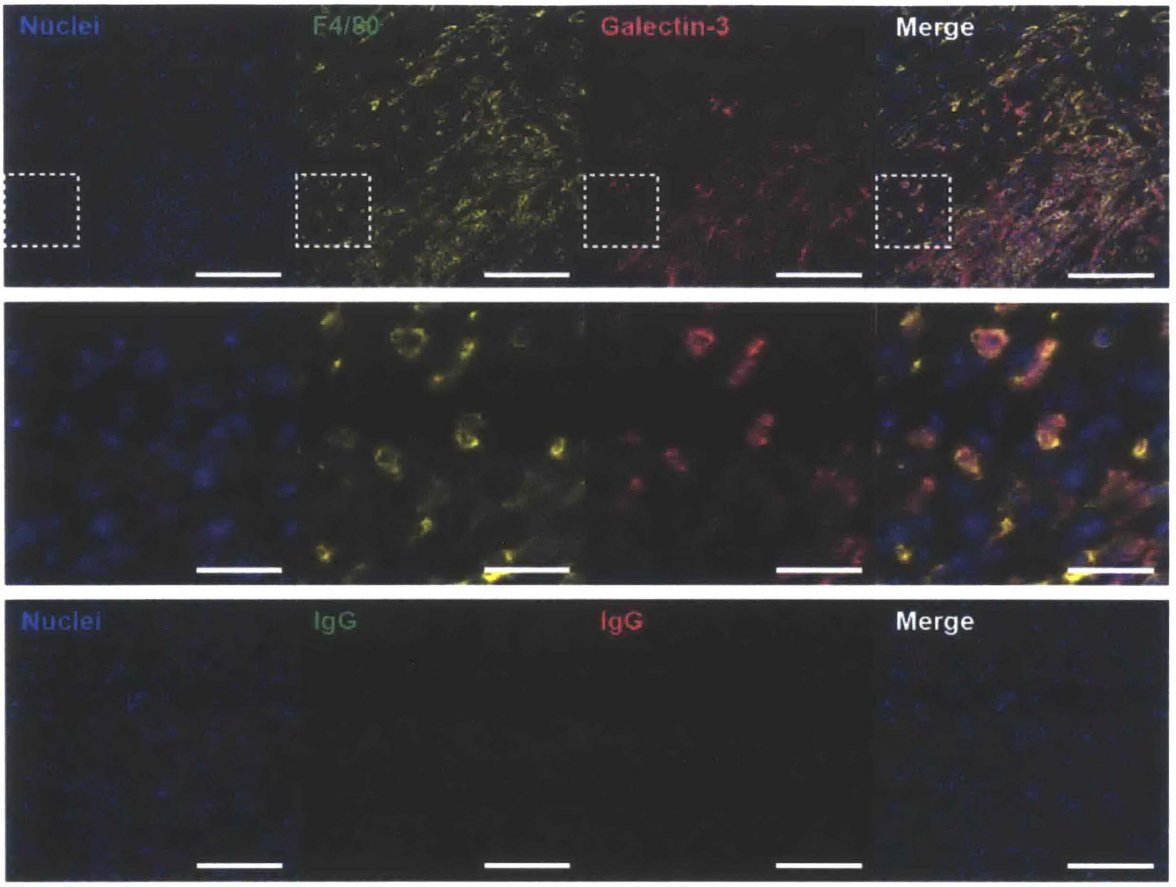

Figure 5.4. *Mice bearing the metastatic tumor line have galectin-3⁺ macrophages in accumulation in the tumors.* Mice were implanted with the 393M1 (M) tumor cell line. Tumors were harvested and stained for macrophages (F4/80, green) and galectin-3 (pink). Nuclei (blue) are stained with Hoechst. Scale bars on the top and bottom rows are 100μm. Scale bars on the middle row are 25μm. Middle row is zoom of the dashed white box from the top row. IgG: isotype control.

As the reported macrophage galectin-3 surface receptors are glycoproteins, it has been suggested that galectin-3 binding is carbohydrate-mediated[284]. Our previous findings, however, suggest that tumor cell adhesion to galectin-3 is mediated by its CRD (Fig. 4.4a). If the CD11b cells in the metastatic niche are binding galectin-3 through its CRD, it may inhibit tumor cell binding. Thus, we asked whether galectin-3 surface expression on CD11b⁺ cells from mice bearing tumors is truly carbohydrate mediated. We harvested peripheral blood from tumor-bearing mice, and incubated the CD11b⁺ cells with lactose. Flow cytometry analysis revealed no reduction of galectin-3 staining

following lactose treatment, suggesting that the lectin is, at least in part, bound to the surface through protein-protein interactions (Fig. 5.3e). While MACS separation of the CD11b$^+$ cells may have affected the carbohydrate-bound galectin-3, these findings suggest that a considerable amount of galectin-3 is presented in a manner that leaves the CRD exposed for additional interactions.

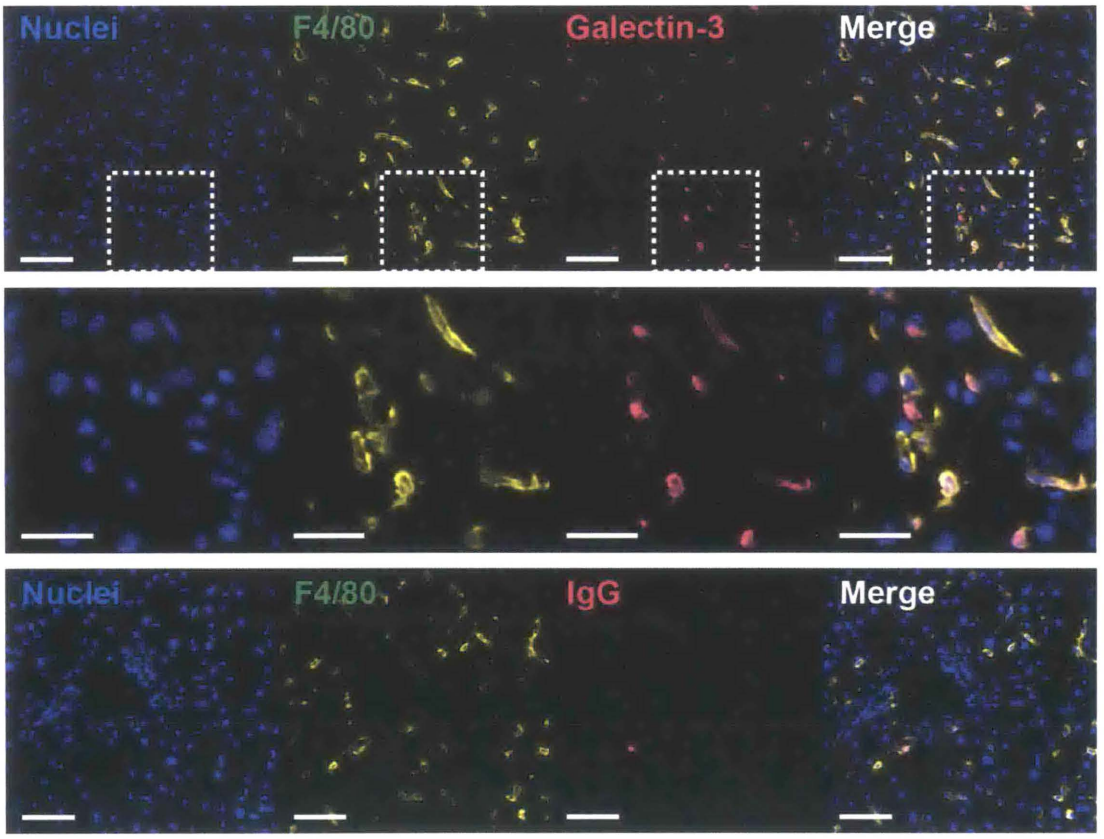

Figure 5.5. *Mice bearing tumors exhibit accumulation of galectin-3$^+$ macrophages in their livers.* Staining of livers from transplanted tumor-bearing mice prior to the arrival of metastatic cells for macrophages (F4/80) and galectin-3. Nuclei are stained with Hoechst. Scale bars on the top and bottom rows are 50μm. Scale bars on the middle row are 25μm. IgG: isotype control.

5.2.4 Presence of galectin-3$^+$CD11b$^+$ cells is a result of acute recruitment

As galectin-3 is known to activate neutrophils and act as a chemoattractant for monocytes and macrophages, we asked whether tumor-secreted galectin-3 or other

secreted factors could induce acute recruitment of these cell types. We harvested conditioned media from metastatic cell cultures and injected these into the circulation of naïve mice. Two hours following the injection we harvested peripheral blood samples and analyzed them for the galectin-3^{+}-positive populations. Surprisingly, the conditioned media elicited strong CD11b^{+}Mac-2^{+} recruitment that was analogous to the blood of tumor-bearing mice (Fig. 5.6a-f). Thus, we asked whether galectin-3 alone would be sufficient to account for this myeloid cell recruitment. Injections of fresh media supplemented with recombinant murine galectin-3, however, was unable to induce the response exhibited by the conditioned media (Fig. 5.6a-f, gray circles). Again, these differences were a result of increased recruitment without any additional galectin-3 expression on an individual cell basis (Fig. 5.6f).

Previous work has shown a role for interleukin signaling in enhancing galectin-3 expression and alternative macrophage activation[414]. Thus, we asked whether any cytokines were highly expressed in the conditioned media. Luminex cytokine profiling of the conditioned media from the M cell line found only IL-6 to be differentially expressed in the conditioned media compared to the control media (Fig. 5.6g). IL-6 has been found to correlate with tumor progression and metastasis[417-420]. Thus, it may be possible that it acts in conjunction with galectin-3 to recruit these pro-metastatic myeloid-derived cells.

To address whether galectin-3 is necessary for the recruitment of the galectin-3^{+}CD11b^{+} myeloid cells we have initiated a variety of studies. We knocked down galectin-3 in the 393M1 metastatic cell line by transduction of short hairpins targeting *Lgals3*. This knockdown resulted in an approximately 50% reduction in secreted galectin-3 for three

hairpins (Fig. 5.6h). To test whether the reduction in galectin-3 alters myeloid cell recruitment we implanted the lines into mice. Once the tumors have reached an appropriate size, peripheral blood will be harvested from these mice and queried for the presence of galectin-3^{+} cells. Additionally, conditioned media will be harvested from these lines and tested for its ability to recruit these populations upon intravenous injection. If these knockdowns yield galectin-3 levels that are still too high to test its effects *in vivo*, an alternate approach would be to remove the galectin-3 from the conditioned media by affinity chromatography using anti-galectin-3 antibody coated resins. These experiments will help elucidate the specific role of galectin-3 on the direct recruitment of these hematopoietic populations.

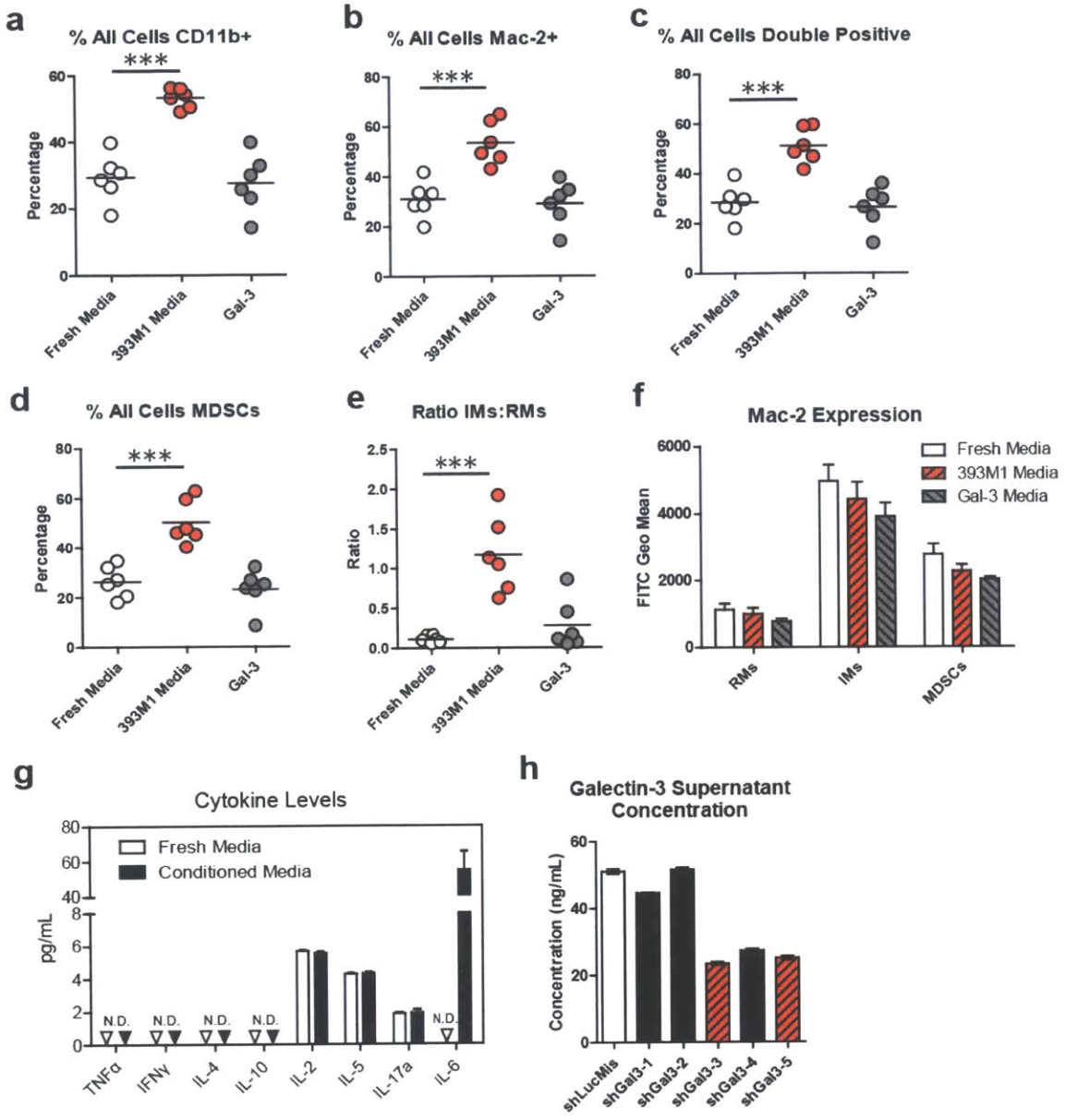

Figure 5.6. *Conditioned medium from tumor lines induces rapid recruitment of CD11b⁺Mac-2⁺ leukocytes into circulation.* Fresh medium (white), 393M1 conditioned medium (red), or fresh medium with 20μg/mL recombinant galectin-3 (Gal-3, gray) was injected into circulation of naïve mice. Peripheral blood, harvested two hours after media injections, was analyzed by flow cytometry for (a) the percentage of all cells CD11b⁺, (b) the percentage of all cells galectin-3⁺, (c) the percentage of all cells CD11b⁺ and galectin-3⁺, (d) the percentage of all cells CD11b⁺Gr-1⁺, (e) the ratio of inflammatory to resident monocytes, and (f) the expression levels of galectin-3. (g) Luminex ELISA analysis of cytokine levels in the fresh (white) and conditioned (black) medium. (h) Galectin-3 levels of medium supernatant from 393M1 lines transduced with hairpins against galectin-3 (shGal3) or firefly luciferase (shLucMis) by ELISA. *** $P < 0.001$; N.D. not detected.

5.3 Discussion

Inflammatory leukocytes are now understood to play a role in metastasis in a variety of cancers and the cytokine crosstalk involved in their promotion of the disease is being rapidly uncovered. The identification of intimate interactions between these populations within the blood vessels and colonized tissues suggests a role for conserved increases in an adhesion-receptor molecule axis during metastatic progression. Previously, we have shown a role for galectin-3 binding during metastatic progression. Here, we uncover a population of cells, known to be involved in metastasis, that display galectin-3 on their surfaces and that are rapidly recruited during tumorigenesis. It appears that these $CD11b^{+}Mac\text{-}2^{+}$ leukocytes are likely recruited early in the metastatic cascade as the non-metastatic primary tumor line efficiently produced these cells in the blood. The equivalent recruitment of these cells is mirrored by the equivalent production of galectin-3 and -8 across all of the lines representing different stages of tumor progression. Thus, it is reasonable to suspect that deposition of galectin-3 in the pre-metastatic site and recruitment of the leukocytes is an early step in tumor progression. To confirm this hypothesis, one could examine the presence of these cells in the peripheral blood of mice bearing autochthonous tumors that have yet to metastasize. Regardless of the exact timing of this recruitment, lung adenocarcinomas clearly have the ability to recruit $galectin\text{-}3^{+}CD11b^{+}$ cells into circulation and to the sites of metastases.

Furthermore, injection of tumor secreted factors rapidly recruited these leukocytes into the blood. This suggests that a pool of $galectin\text{-}3^{+}$ MDSCs, monocytes, or their progenitors exists in lymphoid organs of healthy animals. Lung and breast cancers

frequently metastasize to the bones of patients early in tumor progression[47, 111]. This phenomenon may be, in part, a result of decreased barriers to extravasation (e.g. fenestrated endothelium) and increased growth factors in the hematopoietic niche. The role of macrophages in this process, however, is also a likely contributor to this process[120, 421-422]. As the myeloid cells found to express galectin-3 are bone-marrow-derived, it is reasonable to expect that they are present in the bone prior to exposure to the tumor-secreted factors. That these cells express galectin-3 on their surfaces may explain why these cancers metastasize to the bones so readily in a clinical setting.

Among the secreted cytokines in the conditioned media, we found IL-6 to be significantly expressed. IL-4 has been shown to promote establishment of the tumor microenvironment through induction of cathepsin activity by TAMs[423]. Similarly, tumor-derived IL-6 may act to promote cathepsin B secretion by monocytes in the context of breast cancer cells[424]. The effects of galectin-3 on alternative macrophage activation was found to be IL-4-dependent[414]. Thus, it is possible that, in our model, IL-6 plays a similar role in sensitizing bone-marrow-derived cells to galectin-3 and initiating their rapid recruitment into circulation.

While some evidence has been reported that supports the existence of a pre-metastatic or early-metastatic niche, its precise role in tumor progression is incompletely understood. Animal models demonstrate deposition of ECM and recruitment of myeloid cells to these sites in a manner that appears to affect tumor seeding, but the significance of these experimental models on the human disease is difficult to decipher as clinical evidence of this nature is nearly impossible to ascertain. Our data suggest that galectin-3

may be present in the early-metastatic sites and upon the myeloid cells recruited to those sites. Clinical evidence shows that cancer patients have elevated levels of galectin-3 in circulation and within the tumor tissue[425]. Thus, it is possible that galectin-3 may be acting to promote metastasis through its immunomodulatory activities and tumor adhesion potential at the pre-metastatic sites.

5.4 Methods

Cell Lines and Mouse Transplantation Assays

Cell lines (a gift from Tyler Jacks and Monte Winslow, Massachusetts Institute of Technology, Cambridge, MA) were described previously[194] and were cultured in DMEM with 10% (vol/vol) fetal bovine serum and 1% L-glutamine.

All animal procedures were performed in accordance with the MIT Institutional Animal Care and Use Committee under protocol 0211-014-14. Cell injection studies were performed in B6129SF1/J mice (Jackson Laboratory, Stock Number 101043). Mice were injected with 3×10^5 cells resuspended in 100μL of PBS into the subcutaneous region of flanks of mice, while anesthetized with isofluorane. Tumors and peripheral blood were harvested 5-8 weeks following injections. Approximately 1mL of peripheral blood was harvested by cardiac puncture, while mice were anesthetized with isofluorane and used for flow cytometric analysis. Mice were immediately euthanized following recovery of the blood and their tumors were harvested.

Immunohistochemical and Immunocytochemical Analysis

Following necropsy, tumors and livers were fixed overnight in 4% paraformaldehyde at 4°C. Tissues used for paraffin embedding were transferred to cassettes and placed in 70% ethanol. Those used for frozen sections were placed in 30% sucrose overnight at 4°C. Tissues were then transferred to O.C.T. compound (Tissue-Tek) for 4 hours at room temperature followed by freezing in isopentane (Sigma) placed in a liquid nitrogen bath. Co-staining of galectin-3 and F4/80 was performed on frozen sections using antibody clones M3/38 (BioLegend) and CI:A3-1 (BioLegend), respectively. Nuclei were stained with Hoechst (Invitrogen).

Western and Eastern Blot Analysis

Cell lysates were harvested in RIPA buffer (Sigma) containing Complete Protease Inhibitor (Roche) and Phospho Stop (Roche) on ice and run on SDS-PAGE gels. PVDF membranes were stained for galectin-3 (Abcam, ab53082, 1:500), galectin-8 (Abcam, ab69631, 1:500), and α-tubulin (Cell Signaling, 2125, 1:1000).

Galectin-3 ELISA

Peripheral blood was harvested from mice without tumors or bearing contralateral flank tumors of both 802T4 and 393T5 cell lines by cardiac puncture as described above. Blood was collected in serum collection tubes (Capiject) and allowed to clot for 30 minutes prior to centrifugation and removal of serum. The galectin-3 ELISA kit (R&D Systems) was used according to the manufacturer's instructions.

Liver Galectin-3 Western Blots

Mice bearing 393M1 flank tumors or no tumors were perfused by intracardiac injection of 20mL of phosphate buffered saline. Livers were then excised and 50mg portions were added to gentleMACS M tubes (Miltenyi Biotech) in 4.5mL of RIPA (Sigma) with Complete Protease Inhibitors (Roche). Tissue was dissociated using the gentleMACS Octo Dissociator (Miltenyi Biotech) and run on polyacrylamide gels as described above.

Flow Cytometric Analysis and Antibodies

Peripheral blood was drawn by cardiac puncture and transferred to K2 EDTA 5.4mg Plus Blood Collection Tubes (BD Vacutainer, BD Biosciences). Red blood cells were lysed using RBC lysis buffer (eBiosciences). Cells were fixed in 4% paraformaldehyde and washed prior to staining. Cells were blocked using anti-mouse CD16/CD32 antibody clone 2.4G2 (BD Biosciences). Antibodies against mouse antigens were: CD11b (M1/70, BD Biosciences), CD115 (AFS98, eBiosciences), Mac-2 (M3/38, BioLegend), Ly-6C (HK1.4, BioLegend), and Gr-1 (RB6-8C6, BioLegend). Flow cytometry was performed on a LSR Fortessa (BD Biosciences) and analyzed using Flowjo (Tree Star). Peanut agglutinin staining was performed by incubating 3×10^5 cells in PBS with 10µL PNA-AlexaFluor 647 (invitrogen) on ice for 30 minutes. *Also add alpha3 and beta1 Abs if included.*

Magnetic separation of $CD11b^+$ cells was performed using CD11b MACS microbeads (Miltenyi). Following collection of peripheral blood by cardiac puncture and lysis of erythrocytes, cells were incubated with the MACS beads following the manufacturer's instructions. $CD11b^+$ cells were isolated using MACS MS Collection Columns (Miltenyi).

Galectin-3 binding inhibition

For competition of galectin-3 presentation on leukocytes, peripheral blood was harvested from mice bearing 393M1 flank tumors, as described above. Cells were incubated with 200mM β-lactose (Sigma) or sucrose (Sigma) in 2% FBS for 30 minutes on ice. Cells were then fixed, stained, and analyzed by flow cytometry.

Conditioned Media Experiments

Twenty-five milliliters of conditioned medium was harvested from one T150 flask of 393M1s following three days of culture. This medium (or fresh control medium) was filtered through 0.2μm filters and concentrated 15-fold using 3,000 MWCO centrifugal filters (Amicon). 200μL of medium was injected into the lateral tail vein of mice. Two hours after injections, peripheral blood was harvested from the mice by cardiac puncture, as described above, followed by fixation, staining, and flow cytometric analysis.

RNA isolation and Expression Profiling

Gene expression microarray analysis was described previously[329] and is available from NCBI Gene Expression Omnibus under accession number GSE40222. For quantitative PCR, RNA was harvested using RNEasy Mini Kits (Qiagen). RNA was reverse transcribed using the iScript cDNA Synthesis Kit (Bio-Rad). qPCR reactions were performed using 2μL of cDNA, 12.5μL of IQ SYBR Green Supermix (Bio-Rad), and 1μmol of each primer.

Chapter 6. Involvement of ECM during epithelial-mesenchymal transitions

6.1 Introduction

The epithelial-mesenchymal transition (EMT) is an embryonic program that permits the acquisition of a mesenchymal phenotype by cells that were previously epithelial[426-428]. While this process performs essential roles in normal physiology including both development and wound healing, it has recently been appreciated to be involved in various disease states[429-431]. In particular, it has been suggested to be a driving force behind the acquisition of migratory and invasive phenotypes in tumors, thus, promoting cancer metastasis. In this model of cancer dissemination, cells within the primary tumors activate transcriptional programs that induce EMT. This induction is characterized by a downregulation of cell-cell junction proteins such as E-cadherin, changes in β-catenin localization and signaling, and production of vimentin and fibronectin. Furthermore, the plasticity conferred upon these cells appears to induce a stem-cell-like phenotype as is evident from their ability to form mammospheres (in the context of mammary cells), expression of surface markers such as elevated CD44 and decreased CD24, and an increased ability to generate tumors[88]. These highly invasive cells can use EMT to traverse the many stages of the metastatic cascade, from migration upon and degradation of extracellular matrix (ECM), to survival in the bloodstream, to extravasation and migration within distant organs. Nonetheless, it is now appreciated that colonization of a distant organ is likely the rate-limiting step in the metastatic cascade[43, 69, 71]. In this model of metastasis, the cells likely undergo a reverse

transition, mesenchymal-epithelial transition (MET), that allows them to regain their epithelial phenotype and colonize a distant site[432].

Intracellular promoters of EMT include transcription factors such as TWIST and SNAIL, in addition to ZEB family proteins and miR-200 family microRNAs[433-435]. Upstream activation of these pathways can be conferred by a variety of signaling molecules, the best-established being transforming growth factor beta (TGF-β). While the roles of these proteins have been thoroughly investigated in their mechanisms of inducing EMT, the factors promoting MET are less well-understood.

While molecules such as fibronectin have been implicated in EMT, the influence of extracellular matrix (ECM) molecules in inducing EMT and MET is still largely unappreciated. Interactions between integrins and TGF-β have been reported[436] and pathologies resulting from improper sequestration of TGF-β by ECM molecules have been well-characterized[138, 437]. Nonetheless, the majority of alterations in cell-ECM interactions during EMT are uncharacterized. Furthermore, a role for ECM in inducing MET at the site of metastasis has not been revealed.

In this work, we use our previously-described ECM microarray platform[329], to screen for changes in cell-ECM interactions during EMT. We establish adhesion and proliferation profiles for Human Mammary Epithelial Cells harboring the Ras oncogene (HMLER) that are in their normal epithelial state or following activation of an EMT program. Furthermore, we investigate the role of particular ECM molecules for inducing increased E-Cadherin expression and a MET.

6.2 Results

6.2.1 *Epithelial and mesenchymal cells exhibit differential adhesion signatures*

To study differences in cell-ECM interactions between epithelial and mesenchymal cells, we used Human Mammary Epithelial Cells harboring the Ras oncogene (HMLER)[433, 438] in either their wild-type state or following introduction of constitutive *TWIST* activation. To determine the effects of EMT on adhesion, we screened these cells on our ECM microarray platform. This platform consists of 768 unique single and pairwise combinations of 38 ECM molecules spotted onto a glass slide coated with polyacrylamide. The dehydrated hydrogel entraps the ECM molecules after spotting and prevents cells from adhering to the slide in locations where there is no ECM. Following spotting of the molecules, cells are seeded onto the arrays in serum-free medium. Quantification of their adhesion is performed following fixation and staining using automated microscopy combined with CellProfiler analysis tools, as previously described[3, 329].

The wild-type or TWIST$^+$ cells were seeded onto the arrays separately or following labeling and mixing at equal ratios (Fig. 6.1a,b). While many combinations of ECM demonstrate shared adhesion between both the epithelial and mesenchymal states, distinct combinations reveal increased adhesion by cells of one of the two states when compared to the other (Fig. 6.1b). Figure 6.2a and b show adhesion to all combinations by the wild-type and *TWIST*$^+$ cells, respectively. The top 2.5% of combinations (Fig. 6.2a and b, red bars) share many similarities between both cell types including adhesion to combinations containing galectin-8 and some collagens, perhaps, reflecting an adhesion

signature characteristic of all breast tissue. Nonetheless, clear differences in adhesion were apparent between the epithelial and mesenchymal cells.

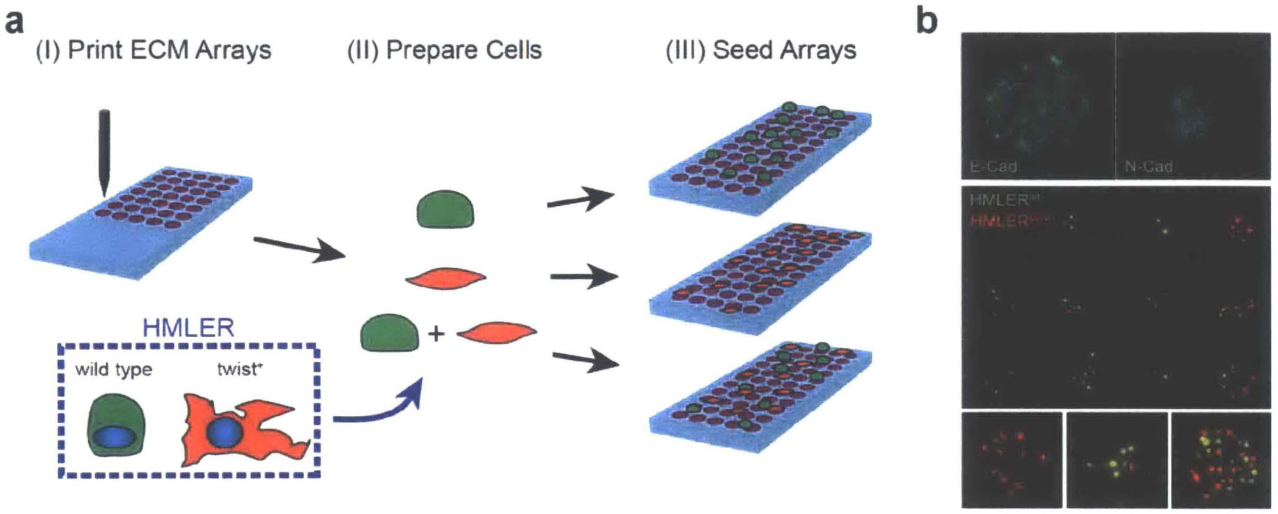

Figure 6.1. *Profiling adhesion of cells undergoing EMT.* (a) Schematic of the screening workflow: (I) ECM microarrays are spotted, (II) wild-type HMLERs, HMLERs expressing *TWIST*, or a 1:1 ratio of both are prepared, and (III) seeded onto the ECM arrays. (b) Micrographs of cells on individual spots stained for E-cadherin or N-cadherin (top). Epithelial and mesenchymal cells were stained with green and orange Calcein AM, respectively and seeded on the arrays after mixing (middle and bottom).

To ensure the differences between the two cell types are real, we performed unsupervised hierarchical clustering of the adhesion signatures generated from all replicate arrays that we ran (Fig. 6.3a). Indeed, the mesenchymal signatures all clustered together and separately from the epithelial arrays. We next asked to what degree the adhesion values differed between the cell types for each combination. While one might expect that the adhesion values would be similar for most combinations, we found that a significant number of combinations yielded a strong preference by one of the two cell types (Fig. 6.3b).

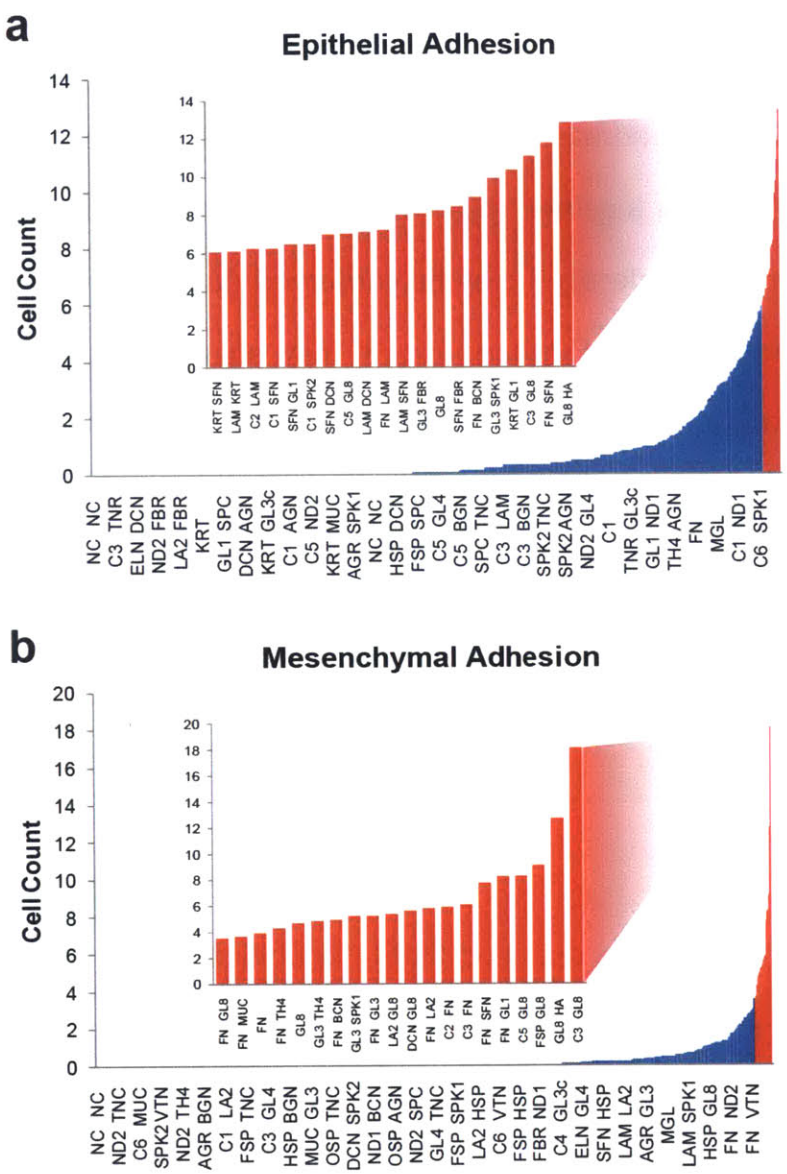

Figure 6.2. *Identification of ECM combinations yielding the greatest adhesion.* Rank ordered cell counts for all of the combinations on the ECM microarrays for both the wild-type (a) and *TWIST*-expressing (b) HMLERs four hours following seeding of the arrays. Red bars and inset graphs indicate the top 2.5% of combinations.

We generated an adhesion signature based upon the top differential hits from the replicate arrays (Fig. 6.3c) as well as ranked the top differential adhesion combinations (Fig. 6.3d). These analyses predictably suggest an enhanced adhesion to combinations containing fibronectin by the mesenchymal cells. Furthermore, the wild-type cells exhibited higher adhesion to combinations containing basement membrane proteins

including laminins, nidogen, and collagen IV. It is worth noting that combinations of fibronectin and galectin-3 are among the top hits for the mesenchymal cells. Previously, we found that metastatic lung adenocarcinomas have greatly increased adhesion to this combination[329](see Chapter 2). Taken together, these findings may suggest that this increased adhesion to fibronectin with galectin-3 may be conserved during metastatic progression for a variety of tumor types. Furthermore, it may suggest a role for previously unappreciated EMT programs within this lung cancer model as well.

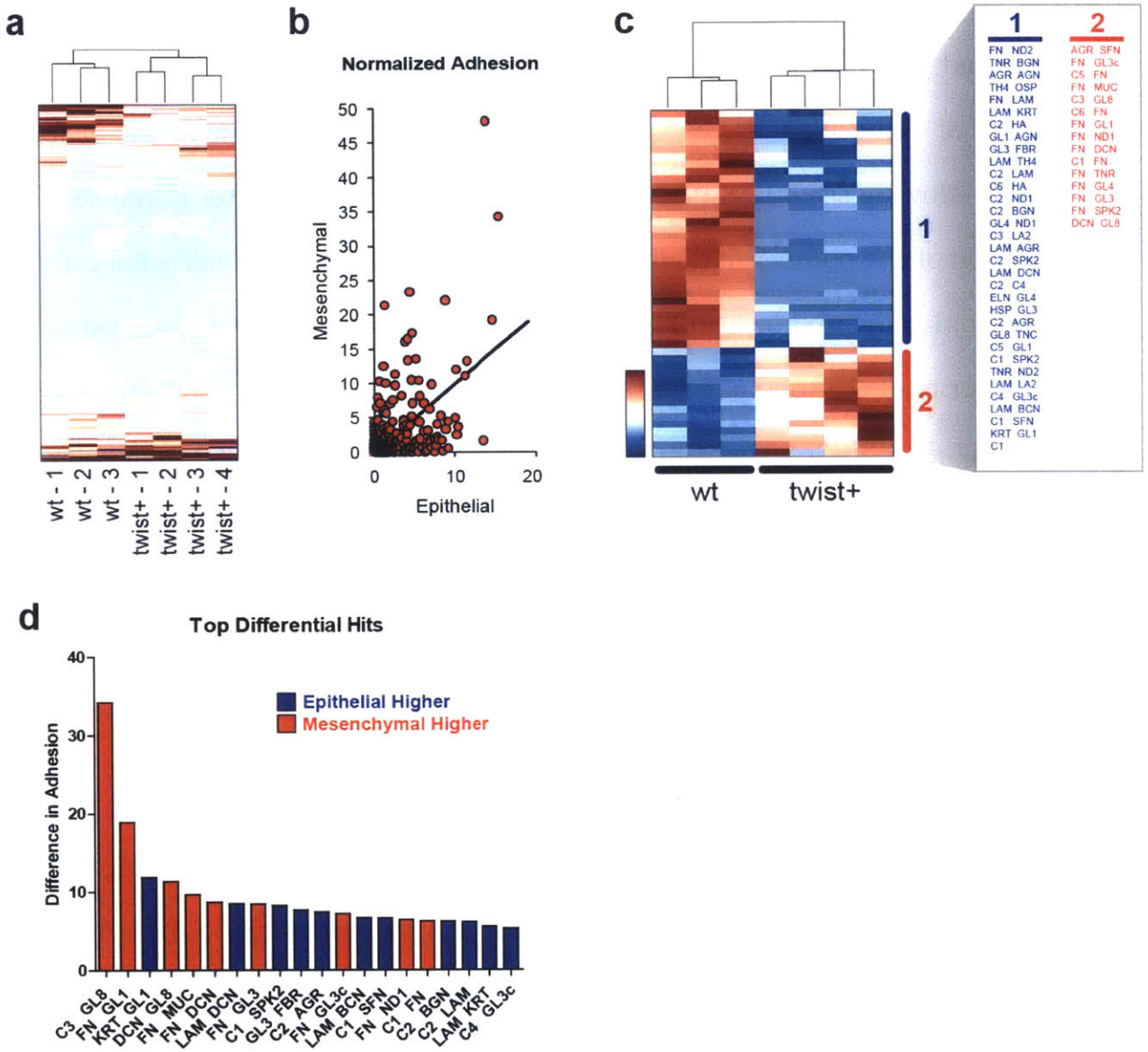

Figure 6.3. *EMT induces differential adhesion to ECM.* (a) Unsupervised hierarchical clustering of replicate slides for both the wild-type and *TWIST*+ cells depicts conserved differences in adhesion profiles. (b) Normalized adhesion values for all of the ECM combinations on the arrays plotted as wild-type cells (abscissa) versus the *TWIST*+ cells (ordinate). Black line depicts equivalent adhesion values (x = y). (c) Top differential adhesion values between the two cell states. Combinations listed as "1" (blue) represent elevated adhesion by the wild-type cells and "2" (red) represent those to which the mesenchymal cells exhibit greater adhesion. (d) Top differential hits as calculated by the absolute value of the difference between the wild-type and *TWIST*+ cells. Blue bars depict combinations to which the epithelial values are higher and red bars refer to those to which the mesenchymal values are higher.

6.2.2 *Galectin-3 promotes increased proliferation*

We next asked whether specific ECM combinations are capable of inducing increased proliferation of either type. We examined the quantity of cells on our arrays at forty-eight hours following seeding and compared these counts to those after initial seeding. Quantification of the number of doublings for the mesenchymal and epithelial cells for the top combinations is shown in Figures 6.4a and b, respectively. Of note, we found that the majority of the top combinations for both cell types included galectin-3 or its cleaved form galectin-3c. This finding suggests that while galectin3 may play an important role in metastasis through its increased affinity for metastatic cells in the context of fibronectin, it may also play a role in promoting tumor outgrowth regardless of the cell type interacting with it.

In an analogous manner to the adhesion studies, we asked whether certain combinations exhibited differential proliferative responses. Figures 6.4c and d show heatmaps of differential cell counts on arrays either normalized to the average of the non-zero values of the arrays (Fig. 6.4c) or un-normalized (Fig. 6.4d). While the normalization accounts for experimentally introduced differences in seeding concentrations or global shifts in adhesion profiles between cellular states (e.g. if the mesenchymal cells have a global reduction in adhesion to all combinations), its use may be limited for later timepoints due to the confounding effects of proliferative differences. Nonetheless, both the raw and normalized counts suggest a role for combinations containing fibronectin as promoting, not only adhesion, but proliferation of the mesenchymal cells when compared to their epithelial counterparts.

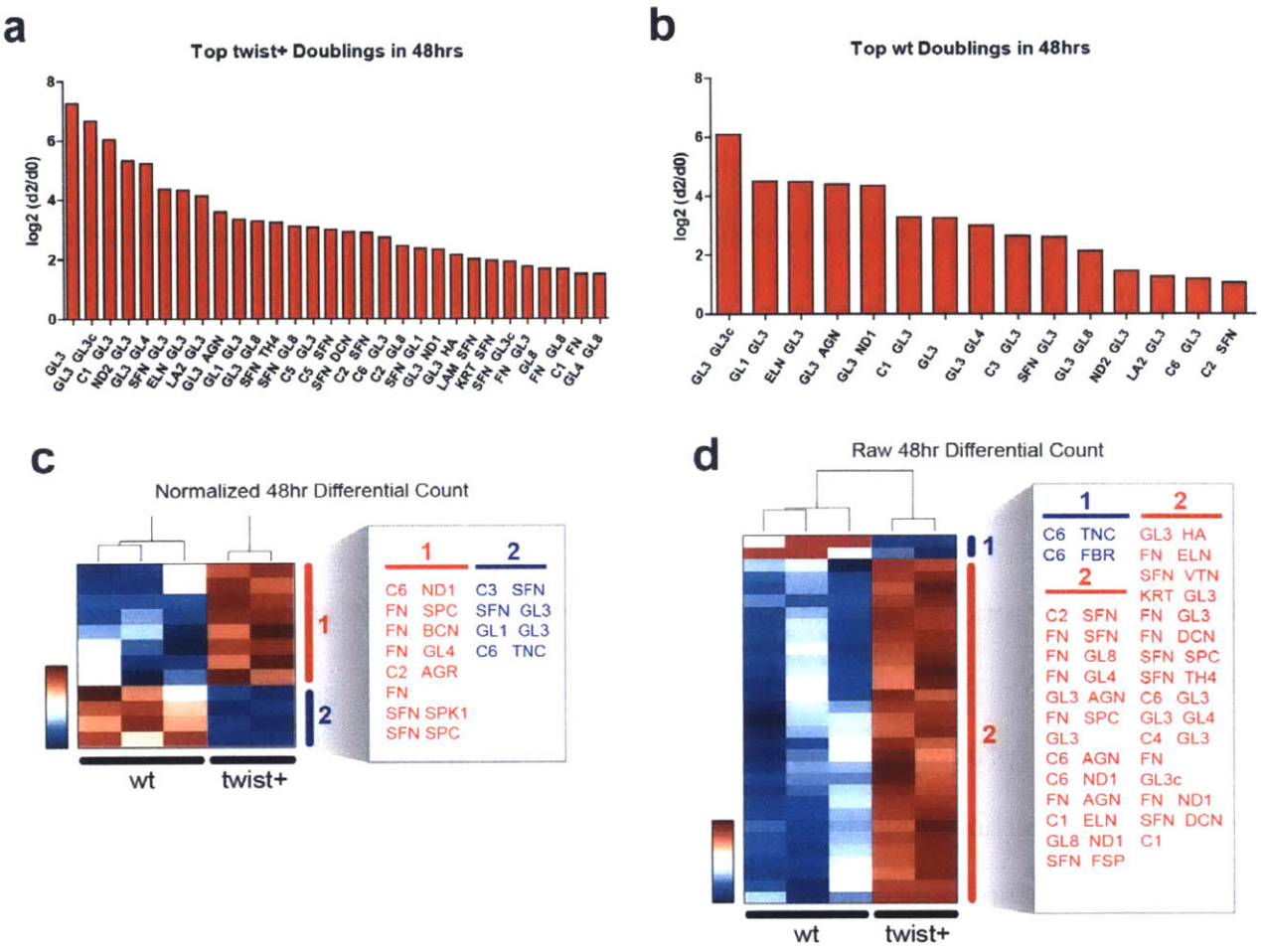

Figure 6.4. *EMT induces differential proliferative responses to ECM.* Rank ordered population doublings for the top ECM combinations as quantified by the ratio of day 2 counts to day 0 counts for the (a)mesenchymal and (b) epithelial cells. (c) Top differential counts following normalization to the non-zero means of the slides. Combinations listed under "1" (red) are those to which the mesenchymal cells had higher counts and those under "2" (blue) represent the epithelial hits. (d) The same as (c) but where the counts have not been normalized. Here "1" (blue) refers to the epithelial hits and "2" (red) represents the mesenchymal hits.

6.2.3 Galectin-3 promotes mesenchymal-epithelial transitions (MET)

In order for disseminated tumor cells (DTCs) that have undergone EMT to colonize a distant site and establish clinically relevant metastases, it is suggested that they likely undergo the reverse transition: mesenchymal-epithelial transition (MET). Thus, we

asked whether certain ECM combinations could promote this transition through their induction of an epithelial phenotype.

We stained cells on our arrays for E-cadherin forty-eight hours after initially seeding them on the arrays. E-cadherin intensity was calculated for each spot and normalized to the number of cells on that spot. Figure 6.5a shows the E-cadherin intensity for each combination on the arrays for the wild-type cells. Of note, the combination exhibiting the greatest E-cadherin staining was pure galectin-3. Furthermore, six of the top ten combinations, based on E-cadherin staining, contained galectin-3 (Fig. 6.5b).

Because the mesenchymal cells constitutively overexpress *TWIST*, it is unlikely that an exogenous ECM molecule will induce signaling capable of overriding the induced transcriptional program. Nonetheless, analysis of the top E-cadherin expressing combinations, although far lower than their epithelial counterparts, reveals a number of combinations containing galectin-3 or -3c (Fig. 6.5c). Taken together, these data suggest that galectin-3 may play a role in inducing an MET and an epithelial phenotype.

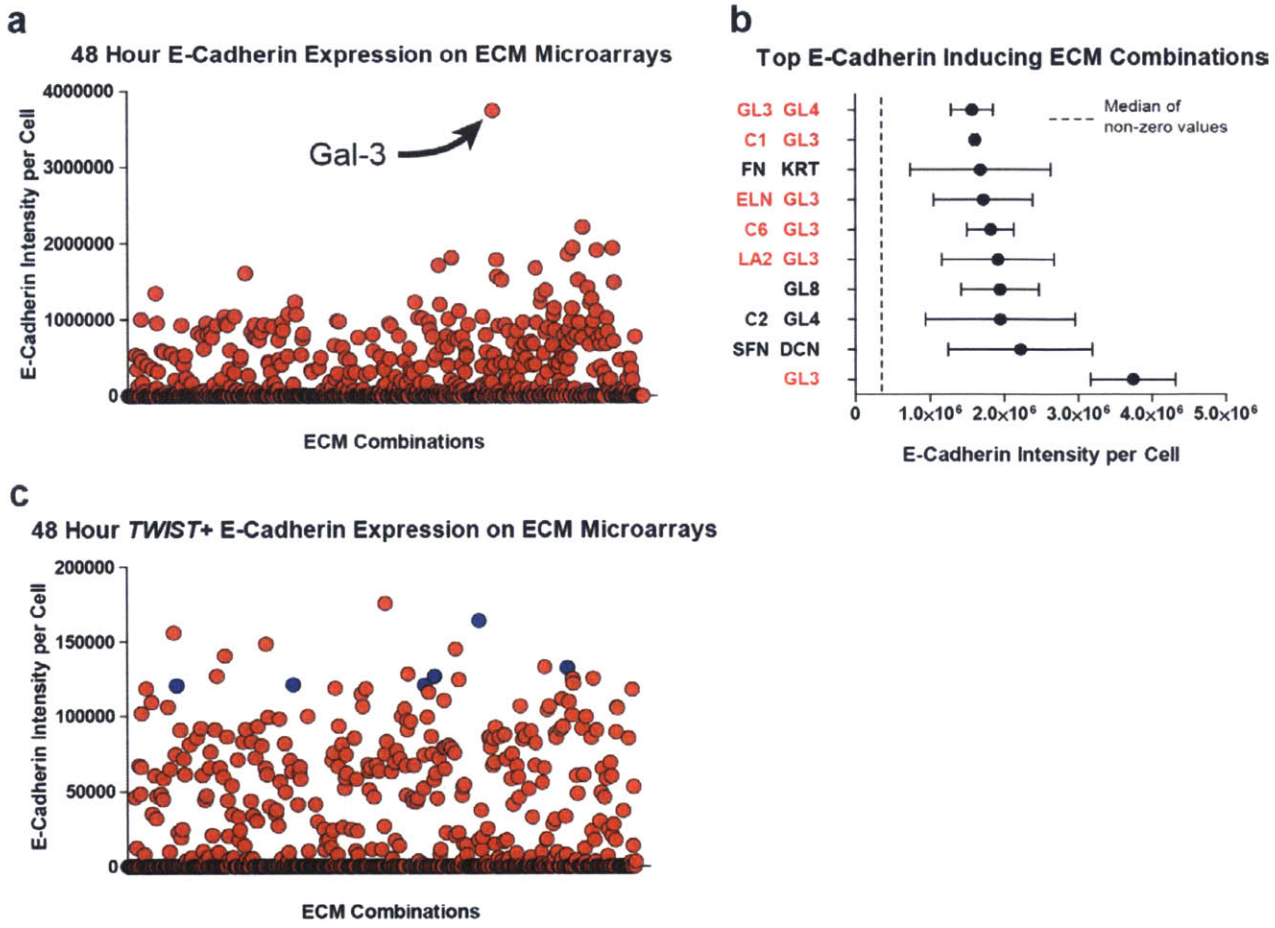

Figure 6.5. *Galectin-3 induces increased E-cadherin expression.* (a,c) E-cadherin expression measured as fluorescent intensity and normalized to cell counts per spot for all combinations where the standard deviation is less than 2×10^6 (a) or 1×10^5 (c). (a) depicts values for the wild-type cells and (c) depicts *TWIST*$^+$ cells. (b) Top 10 combinations with the highest E-Cadherin staining from (a). Combinations listed in red contain galectin-3 as one of their components. Blue dots in (c) represent combinations that contain galectin-3 or its cleaved form galectin-3c. Error bars in (b) are s.e.m.

6.3 Discussion

The roles of ECM and the microenvironment are now appreciated to be driving forces that influence all stages of metastasis (see Chapter 1). While EMT is appreciated as one of the major mechanisms by which tumors gain metastatic potential, there is much to learn about the changes in interactions with ECM during this transition outside of an increased production and adhesion to fibronectin and altered MMP activity. Alterations

in the expression and signaling of a variety of integrins during EMT have been reported[439-442]. Nonetheless, the role that these interactions play in promoting EMT or, perhaps more importantly, MET is still unclear. Through the use of our ECM microarrays, we found alterations in both adhesion and proliferation of breast cancer cells between their native state and following an EMT. Furthermore, we find that galectin-3 appears to promote both proliferation and expression of E-Cadherin, suggesting that it may play a role in MET at the distant site.

As has been extensively discussed in this thesis, galectin-3 has been reported to possess a wide variety of intracellular and extracellular functions that are mediated through both protein-protein and protein-glycan interactions. That galectin-3 may promote proliferation and an MET is an attractive concept as it, coupled with our previous findings in lung cancer, provides a means by which presentation of this protein in distant tissues and upon the endothelium could allow traversal of most of the rate-limiting steps in the metastatic cascade. Recent studies have suggested a role for altered glycosylation during EMT[443-446]. Perhaps, these altered glycosylation states promote interactions with galectin-3 in the distant tissues and stimulate an MET and subsequent colonization.

Previously, we showed that metastatic lung cancer cells exhibited the highest adhesion to combinations of fibronectin with galectin-3. Fibronectin has long been associated with metastasis[208, 222, 447-450] and EMT. Accordingly, we found mesenchymal cells to have an enhanced adhesion to combinations with fibronectin. This phenotype, however, after 48 hours appeared to switch to that of growth on combinations containing galectin-3. Perhaps these molecules work in a synergistic fashion: fibronectin

acting to permit migration within tissues and galectin-3 acting to promote an MET. While additional studies will be necessary to elucidate the mechanisms mediating this potential induction, its potential role as a conserved means of promoting colonization provides an attractive target for therapeutic approaches to this rate-limiting step in metastasis.

6.4 Methods

Cell Lines

Cell lines (a gift from Frank Gertler, Massachusetts Institute of Technology, Cambridge, MA) were described previously[433, 438] and were cultured in 1:1:2 DMEM:F12:MEGM.

Extracellular Matrix Microarray Seeding and Analysis

ECM microarray analysis was performed as described previously[329]. Slides were seeded with 4×10^5 cells per slide in 6mL of serum-free DMEM:F12 (1:1) for two hours prior to washing. Slides were then transferred into their normal culture medium and allowed to sit for two additional hours prior to fixation and staining for day zero analysis. Alternatively, slides were cultured for 48 hours prior to fixation.

Analysis was performed as previously described. Analysis of E-cadherin expression was performed by normalizing whole spot fluorescence intensities to the number of cells on those spots following quantification of nuclei. Top differential combinations were selected based upon statistical significance between replicate slides. All hierarchical clustering analysis was performed in Matlab (Mathworks) using the Bioinformatics

Toolbox. Slide normalization is performed by dividing each value by the average of all non-zero values on the arrays. Prior to any normalization or analysis, individual spots with values greater or less than one standard deviation from the mean of the replicate spots on a single array were discarded. Proliferation was determined by taking the $\log_2$ of the quotient of day two to day zero values.

Immunocytochemistry and Antibodies

Slides were fixed with 4% PFA (Electron Microscopy Sciences) and stained for E-cadherin (BD Biosciences, clone 36/E-Cadherin, 1:100) following permeabilization with 0.1% (v/v) Triton-X (Sigma). Slides were mounted with Fluoromount-G (Southern Biotech) and imaged on a Nikon Ti-E inverted epifluorescence microscope.

RNA Isolation and Expression Profiling

mRNA was harvested from cells using RNEasy mini kits (Qiagen). Lysates were analyzed for RNA integrity and prepared with Affymetrix GeneChip WT Sense Target Labeling and Control Reagents kit, followed by hybridization to Affymetrix Mouse 3' Arrays (Mouse 430A 2.0). R/Bioconductor software was used to process array images.

Chapter 7. Perspectives and Future Directions

Increasing our understanding of the biological processes that influence cancer metastasis has been the focus of extensive studies in the field of cancer biology. Genomic approaches in mice and men have identified a plethora of genes that both correlate with and play functional roles in promoting this devastating march toward malignancy[76-77, 108-110, 151, 193-194, 451-452]. Nonetheless, the knowledge gleaned from these studies and the targets identified have shown little clinical utility outside of their use as biomarkers. Developing targeted therapies for inappropriate gene regulation is challenging, and in the cases where this has been achieved (e.g. EGFR, BCR-ABL, HER2/neu, $BRAF^{V600E}$, etc.), eliciting robust durable responses has been nearly impossible. This failure is largely due to the mutational potential and heterogeneity of tumors that allow them to adapt in a manner that is no longer reliant upon the particular gene mutation targeted. Perhaps, to this day, the most broadly effective therapeutics available for the treatment of cancer are chemotherapy and radiation. These therapies take advantage of phenotypes of the disease rather than particular gene mutations (e.g. reliance upon cell division, lack of proper DNA repair responses, and reliance upon continued nutrients). Thus, tumors cannot evade their effects by activating alternative pathways.

Despite the obvious benefits of chemotherapy and radiation, they are ill-poised to treat metastatic disease for a variety of reasons outlined in Chapter 1. In particular, a lack of an ability to identify the locations of the metastases prior to extensive outgrowth makes radiation therapy near impossible. Chemotherapy can, in select situations, marginally

improve survival times of patients with metastatic disease due to its systemic administration, however, it suffers from systemic toxicity, poor targeting, and chemoresistance of the disseminated tumor populations particularly to the drugs typically used on primary tumors. Thus, an understanding of conserved phenotypic mechanisms that mediate metastasis is needed. Cancer biologists now appreciate that interactions with the microenvironment can promote or discourage traversal of the metastatic cascade and outgrowth of secondary tumors. Even with our continually developing understanding of these processes, conserved phenotypes are emerging that highlight some potential targets.

Taking into consideration the importance of elucidating conserved specific phenotypic mechanisms that underlie the rate-limiting steps of metastasis, this thesis aimed to develop a screening approach capable of revealing interactions between metastasizing cells and their microenvironments, with a focus on cell-ECM interactions. Using the ECM microarray platform that we developed in conjunction with a mouse model of lung cancer and a human model of breast cancer, we have identified particular ECM interactions that may be conserved within many instances of metastasis. In particular, we identified interactions between increasingly metastatic cells with galectins as being potential involved in cancer metastasis.

These interactions are likely a result of perturbed glycosylation on metastatic populations. Such changes would have been difficult to elucidate using conventional genetic approaches given the diversity of genes encoding glycosyltransferases and glycosidases that can give rise to particular glycan structures. As is the case for many cellular phenotypes, an enormity of individual genetic alterations could occur that yield

the same phenotypic responses. This principle is especially the case for glycosylation where there is not only transcriptional and translational regulation of the structures, but localization of enzymes, availability of molecules, transport of proteins to cell surfaces, extracellular concentrations of additional transferases and glycosidases, and many other factors that dynamically control the presentation of particular carbohydrates on the surfaces of cells. In an analogous manner, integrins are another family of cell-surface receptors that bind ECM. They too exhibit a variety of regulatory mechanisms that affect their activity beyond transcription and translation ranging from bidirectional signaling responses, to membrane localization, to activation, and even to glycosylation.

By identifying conserved phenotypes, new targets can be identified that may hold significant therapeutic value. Interrupting conserved cell-cell or cell-ECM interactions that promote metastasis may avoid the poor recurrence rates seen with the current targeted therapies while providing a specificity that prevents the systemic toxicity experienced with conventional chemotherapies. Integrins have begun to be used as therapeutic targets in cancer[115, 190], and the continued development of these approaches will undoubtedly result in efficacious therapies. Nonetheless, challenges, especially related to delivery, may retard these efforts. Thus, in the Appendix of this thesis, we present preliminary work focusing on the use of multifunctional nanoparticles capable of targeting and disrupting cells expressing the T-antigen.

7.1 Conclusions

Understanding the role of the microenvironment in cancer metastasis is important both for our understanding of the underlying mechanisms of disease and for developing therapeutics. The aims of this thesis were to develop new techniques to learn about this

complex process and to identify conserved mechanisms of disease progression that provide viable therapeutic targets. To achieve these goals we developed a phenotypic screening platform capable of interrogating cell-ECM interactions. This platform has allowed us to query a variety of cellular responses to their ECM microenvironments, many of which are outside of the scope of this thesis. In addition to our work on lung and breast cancer metastasis, we have investigated the role of ECM in promoting lineage specific differentiation of induced pluripotent stem cells (iPSCs) and embryonic stem cells (ESCs)[453], hepatocyte maintenance, heat shock factor responses, growth of primary tumor cells, adhesion and growth of many other cancer cell lines, interactions with cells expressing different Mena isoforms, growth of embryoid bodies, and responses by many other cell types.

In the context of cancer metastasis, this platform helped elucidate the importance of particular ECM interactions. That these interactions were conserved across naturally arising tumors in distinct mice lends credence to their conserved importance in lung adenocarcinoma metastasis, a finding that is bolstered by their presence in the human disease. Thus, this thesis begins to construct a picture for potential mechanisms of metastasis (Scheme 7.1). In this model, primary tumors secrete a variety of molecules into circulation including galectin-3 and galectin-8. As, they progress, they increase their secretion of osteopontin while simultaneously decreasing their adhesion to it as well as to a variety of collagens. This decreased adhesion correlates with diminished presentation of integrins $\alpha 1\beta 1$ that appears not to be a result of transcriptional regulation. Furthermore, as these cells become more invasive they begin to increase their presentation of specific glycan structures such as the Thomsen-Friedenreich

Antigen. This difference in glycan presentation is not due to increases in the transferases that mediate core 1 *O*-glycosylation, but rather through regulation of transferases that prevent or permit additional glycan chain extension or branching (e.g. ST6GALNAC4 and C2GNT2). Furthermore, secretion of tumor-derived factors from primary tumors recruits bone-marrow-derived cells that express galectin-3 on their surfaces into circulation. These cells appear to accumulate at the sites of metastases even prior to the formation of identifiable metastases. The increased T-Antigen presentation in combination with increased integrin presentation mediates adhesion to galectin-3, -8, and fibronectin permitting the adhesion to, and perhaps colonization of, these distant sites.

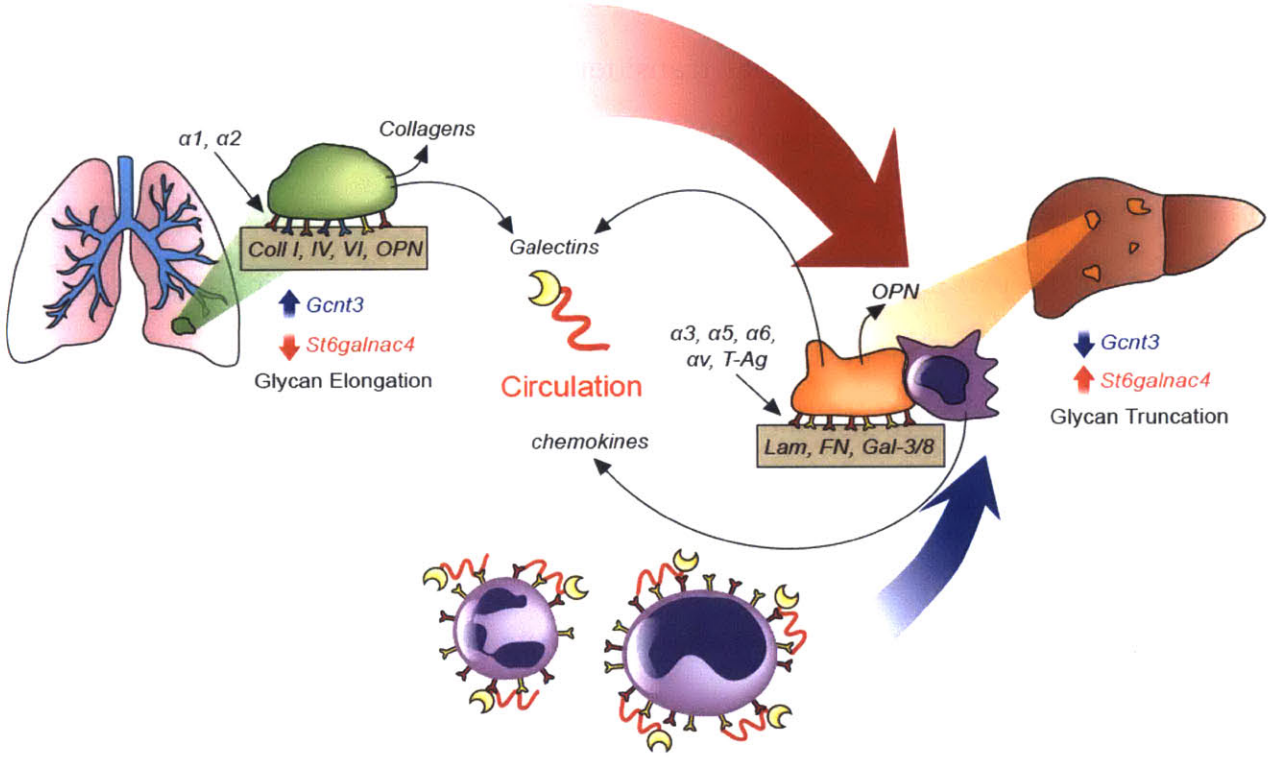

Scheme 7.1. *ECM interactions in metastasis.* This schematic depicts the working model of ECM interactions during metastasis as explored in this thesis. Primary tumors exhibit adhesion to a variety of collagens and osteopontin. These tumors also secrete collagens. They express high levels of integrin α1 and α2 subunits on their surfaces. These tumors express high levels of

Gcnt3 and low levels of *St6galnac4* in a manner that promotes *O*-glycan extension and branching. Both the primary and metastatic tumors secrete galectin-3 and -8, which can be found in the circulation. The metastatic tumors exhibit increased adhesion to fibronectin, laminins, galectin-3, and galectin-8. Additionally, they secrete osteopontin. These tumors exhibit elevated surface presentation of integrin α3, α5, α6, and αv subunits. Furthermore, they have elevated T-Antigen presentation, which is a result of downregulation of *Gcnt3* and upregulation of *St6galnac4* and that mediates galectin-3 adhesion. Early in tumorigenesis, CD11b$^+$ leukocytes are recruited to the blood and sites of metastases. These cells exhibit high levels of galectin-3 on their surfaces.

This thesis has contributed additional implications of the role of galectin-3 in cancer metastasis to an already growing literature describing its pleiotropic roles in disease pathologies. In particular, we describe its role in adhesion of metastatic cells through integrin and glycan interactions, its presentation within the early metastatic niche, its expression upon CD11b$^+$ leukocytes within the peripheral blood, tumors, and early metastatic niches, its secretion into circulation by primary and metastatic tumors, and even its ability to induce E-cadherin expression in a manner that may implicate its role in inducing mesenchymal-epithelial transitions. While its involvement is certainly a conserved correlative event, the exact roles that galectin-3 plays in all of these interactions remains to be fully elucidated. We show strong evidence for increased adhesion to the extracellular form of the molecules with metastatic progression in a manner that appears to be dependent upon binding to the Thomsen-Friedenreich carbohydrate antigen. We also show that galectin-3 is being presented on the surfaces of macrophages within tumors and livers of mice bearing tumors. The exact role that galectin-3 plays in this context may range from adhesion to promotion of survival to clustering of integrins to chemoattractant effects upon other CD11b$^+$ cells to the suppression of anti-tumor adaptive immune responses, among many other potential roles. It is the opinion of this author that its roles in metastatic cell adhesion and promotion of interactions between metastatic tumor cells and TAMs or MAMs strongly

promote metastatic colonization. The extent to which its other functions or suggested capacities play within this process are yet to be determined, but will undoubtedly improve our understanding of the mechanisms behind this disease.

It is worth highlighting that our model of ECM interactions in metastasis was the product of insights gained through the development of novel tools. As the majority of these effects were not readily evident from transcriptional profiling, the pursuit of understanding of the roles of these molecules in this disease process would not have been initiated without the findings gleaned from this platform. Thus, it is the belief of this author that the development of novel technologies capable of investigating biological mechanisms and providing clinical insights is one of the most enabling approaches to science. Much of our understanding of immunology can be credited to the development of flow cytometry, genomics to sequencing technologies, and molecular biology to polymerase chain reactions (PCR). Imaging modalities such as X-Rays, CT, PET, and MRI have revolutionized our ability to diagnose and treat cancers and other diseases. While the ECM microarrays pale in comparison to such enabling technologies, they highlight the importance of technological development in understanding disease mechanisms. Future iterations could include the incorporation of protease-cleavable readouts, in-situ hybridization, high-content imaging for morphological studies, variable stiffnesses, inclusion of growth factors, higher-order combinations, inclusion of orthogonal screens (e.g. small molecules, RNAi, TKIs, etc.), or even the adaptation to three-dimensional ECM screens *in vitro* or *in vivo*. Such advances would undoubtedly provide additional insights into the mechanisms of cancer metastasis and the methods used to treat it.

Appendix

Multifunctional nanoparticle-based approaches for identifying and targeting metastatic populations

A.1 Introduction

Therapeutic targeting of metastases carries a number of innate obstacles discussed previously. In this work we aim to utilize our identification of galectin-3 – T-antigen interactions in lung cancer metastasis to target metastatic populations. Targeting of tumor surface molecules typically requires identification of binding partners. There exist a variety of targeting moieties typically used for targeting of tumor cells: proteins/antibodies, peptides, nucleic acids/aptamers, small molecules, and other structures such as glycans[454]. The most common approach to generating targeting moieties is through the use of monoclonal antibodies. Such approaches have generated many of the current successful targeted therapies including Trastuzumab and Bevacizumab. While antibody development can be an efficient way to generate binding partners, they are less effective against pure glycan structures. As glycans cannot be presented in an MHC fashion in the absence of a peptide conjugate, T-helper activity cannot be elicited and class switching and somatic cell hypermutation cannot take place. Thus, resultant antibodies are typically of the IgM isotype and lack the high affinity and specificity that might be necessary for a targeted therapeutic. Identification of previously unknown small molecules capable of binding particular structures typically involves screening extensive libraries in a manner that can be resource-intensive. Aptamers are short nucleic acid sequences capable of forming three-dimensional structures with binding capacities for protein targets. Their small size and simple structures often make them more attractive than protein-based moieties. Nonetheless,

aptamers are susceptible to nucleases and renal filtration and can stimulate immune responses through TLR activation[455]. Peptides, by comparison, exhibit low immunogenicity, can be easily synthesized, and are easily screened for binding affinities by techniques such as phage display.

In 1996, Thomas Quinn's group reported studies in which they used bacteriophage peptide display libraries to identify peptide sequences capable of binding the T-Antigen[456-457]. In these studies, and others from his group, they show that these peptides are capable of binding to the T-Antigen and inhibiting binding of other lectins including galectin-3[318, 458]. Furthermore, in a subsequent study, they use combinatorial evolution to improve affinity and solubility of their peptide sequence to yield an improved version of this peptide that they term "P30-1"[459]. These peptides exhibit reported dissociation constants for the T-Antigen, when presented on asialofetuin, on the order of 1μM[457]. Thus, targeting of T-Antigen presenting cells using peptides may be a reasonable approach for detecting and treating metastases.

Recently, a variety of nanoparticle formulations have been developed for the diagnosis and treatment of cancer[454, 460]. The use of nanoparticles has a variety of benefits including passive targeting through the enhanced permeability and retention (EPR) effect, active targeting through multivalent display of ligands, improved circulation times, the ability to carry a therapeutic payload, and delivery of materials whose properties can be exploited for imaging purposes. Clinically, the most common imaging modalities for diagnosing and monitoring cancer include magnetic resonance imaging (MRI), X-Ray computed tomography (CT), and positron emission tomography (PET), and recent advances in technologies have allowed for the use of these modalities in

experimental settings for imaging small animals[461-462]. While PET is frequently used for monitoring and detecting metastases its poor resolution prevents its utility in early detection. MRI is particularly useful for imaging soft tissue, but can be difficult to use for detecting tumors in a variety of tissues. Therefore, contrast agents have been developed to improve MRI-based imaging techniques. Dextran-coated iron oxide nanoparticles have been developed and used clinically for imaging tumors in lymph nodes of patients with prostate cancer[463].

Protein-glycan interactions suffer from reduced affinities compared to protein-protein interactions and, in particular, those of antibodies. Increased valency can yield increased avidities and improve the binding of proteins and peptides to glycan structures. Thus, in this work, we aim to take advantage of the multivalent display capabilities of nanoparticles in conjunction with their other tumor-targeting properties to develop vehicles capable of specific targeting of metastases. We conjugate the previously identified peptides to dextran-coated iron oxide nanoparticles in an attempt to improve the clinical imaging detection limits of metastases as well as provide a therapeutic benefit through inhibition of T-Antigen – galectin interactions.

A.2 Preliminary Results

Peptides were synthesized to contain terminal cysteines (HGRFILPWWYAFSPSK(TAMRA)GGC). Tetramethylrhodamine (TAMRA) tags were added to the lysine in order to determine conjugation efficiency and to track uptake *in vitro* and *in vivo*. Peptides were reconstituted at 20mM concentrations in dimethylformamide (DMF). The terminal cysteine permits conjugation through a sulfhydryl iodoacetyl reaction. Nanoparticles were synthesized by crosslinking dextran

onto iron oxide nanoparticles (Ocean Nanotech) with epichlorohydrin. The nanoparticles were then aminated in ammonium hydroxide. The NHS-iodoacetyl heterobifunctional crosslinker SIA was used to conjugate the nanoparticles to the cysteines on the peptides (Scheme A.1). Following conjugation, nanoparticles were purified by FPLC to remove any unconjugated peptide and concentrated in centrifugal spin filters to a concentration of 5mg/mL.

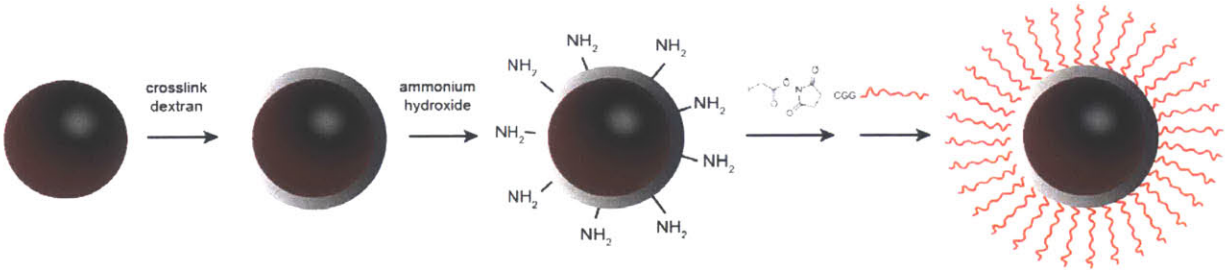

Scheme A.1. *Nanoparticle Synthesis.* Iron oxide nanoparticles have dextran coatings crosslinked by epichlorohydrin. The nanoparticles are aminated using ammonium hydroxide. The free amines are first reacted with the NHS esters on the SIA crosslinkers. The iodoacetyl groups are then reacted with the terminal cysteines on the peptides to generate particles presenting T-Antigen-specific peptides in a multivalent fashion.

Absorbance measurements reveal a molar ratio of peptides to nanoparticles of 80.6. Dynamic light scattering (DLS) measurements of size showed a major peak at 68.5nm (Fig. A.1a). An additional peak at ~380nm may indicate a tendency for the nanoparticles to aggregate.

To determine the ability of the nanoparticles to inhibit T-Antigen binding, the metastatic cell line 393M1 was incubated with fluorescent PNA in the presence of varying concentrations of nanoparticles on ice prior to washing. Binding of nanoparticles can be monitored through the fluorescence of the TAMRA label. Flow cytometry analysis revealed binding of the nanoparticles when in low micromolar to nanomolar concentrations, with an inverse correlation between nanoparticle and PNA

binding (Fig. A.1b,c). Thus, the nanoparticles appear to inhibit binding of the T-Antigen to lectins when presented on cells.

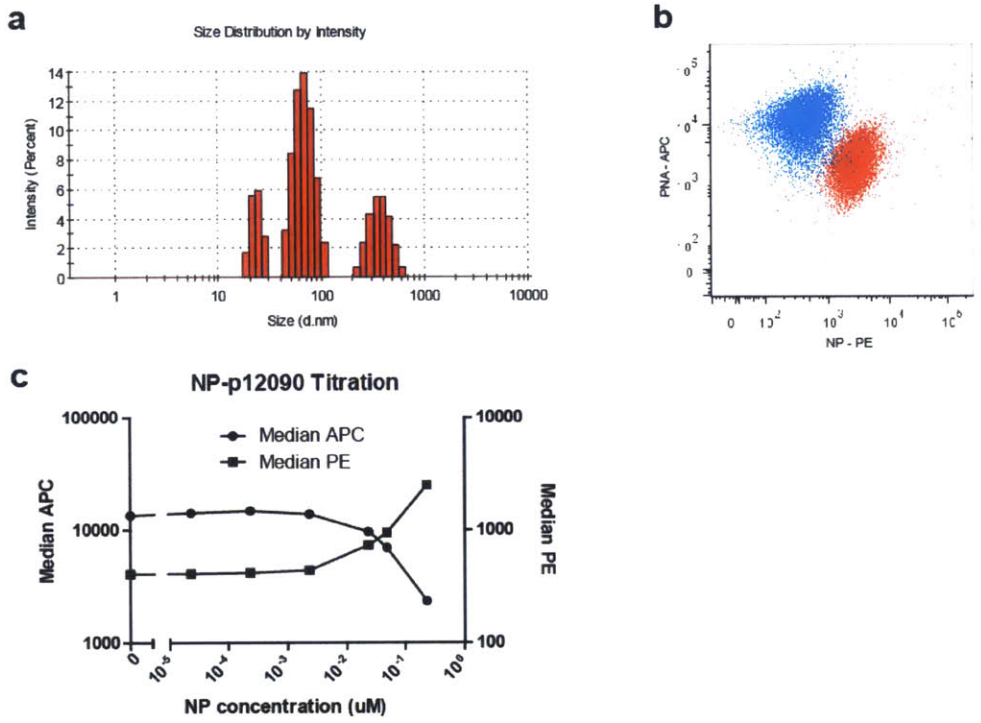

Figure A.1. *Nanoparticle Characterization.* (a) Dynamic light scattering (DLS) measurements of nanoparticle diameters. (b) Flow cytometry analysis of nanoparticle binding and T-Antigen inhibition on 393M1 cells. Nanoparticles incubated with no (blue) or 20μM (red) concentrations of nanoparticles. PE monitors nanoparticle TAMRA fluorescence, and APC measures PNA binding. (c) Nanoparticle titration and quantification of parameters measured in (b).

Previously, we demonstrated that, as tumors become more metastatic, they increase presentation of the T-Antigen (see Chapter 4). Thus, lines from the T_{nonMet}, T_{Met}, and M classes were incubated with the nanoparticles and queried for their ability to bind peanut agglutinin. Analysis by flow cytometry revealed that even for the line expressing the lowest amount of T-Antigen (802T4), the nanoparticles were still effective in reducing PNA binding (Fig. A.2a). To determine the degree of nanoparticle uptake by

these cells, nanoparticles were added to these three lines in culture and allowed to incubate with the cells for twelve hours at 37°C. After this period, cells were washed and stained. Accumulation of the nanoparticles was measured using epifluorescence microscopy (Fig. A.2b,c).

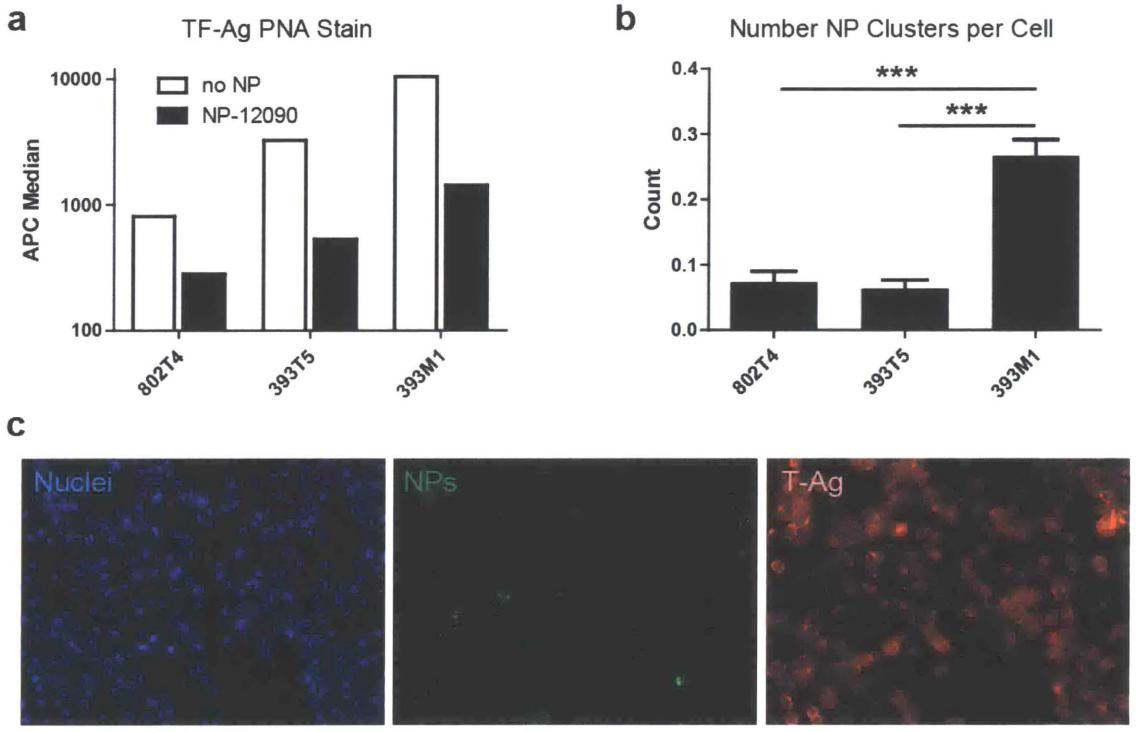

Figure A.2. *Nanoparticles bind the T-Antigen and prevent lectin interactions.* Cell lines from the T_{nonMet} (802T4), T_{Met} (393T5), and M (393M1) lines were incubated with fluorescent PNA in the presence of nanoparticles and analyzed for PNA binding by flow cytometry. (b,c) Cells were cultured with nanoparticles and washed and imaged to query uptake. Error bars represent s.e.m.

The ability of these nanoparticles to selectively target metastases *in vivo* was next assessed. Wild-type mice were injected with contralateral flank tumors of the different cell lines (i.e. 802T4/393T5, 393T5/393M1, or 802T4/393M1). Following significant tumor growth, nanoparticles were injected into the lateral tail veins of mice. 3.5 hours after the injections, mice were euthanized and tumors were harvested. IVIS imaging was performed to determine the amount of fluorescence and nanoparticle accumulation

(Fig. A.3a,b). While the tumors exhibited significantly higher fluorescence than the control PBS injections, there appeared to be greater nanoparticle accumulation in the tumors with less T-Antigen. This discrepancy, however, may be a result of differential vascularization or differences in surface fluorescence compared to what had accumulated in the bulk of the tumor.

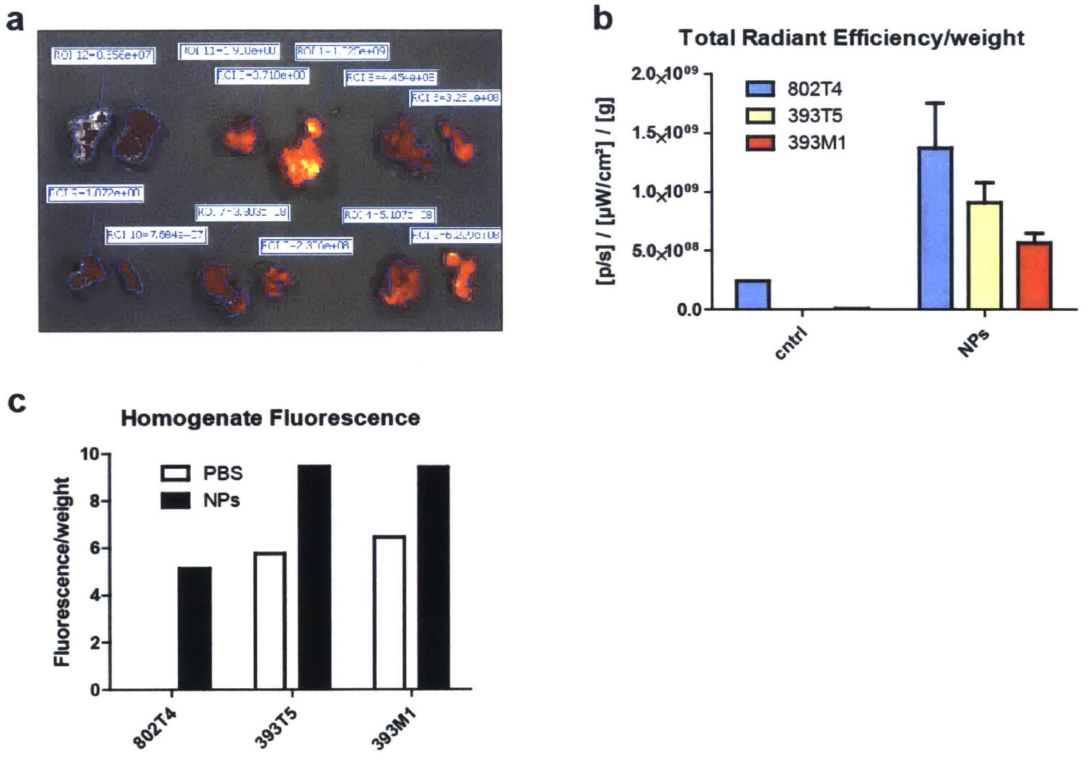

Figure A.3. *Nanoparticles bind tumors* in vivo. Mice are injected into contralateral flanks with tumor cells lines from different classes (i.e. T_{nonMet} vs. T_{Met} vs. M). (a,b) IVIS quantification of fluorescence in tumors excised from mice 3.5 hours after injection of nanoparticles into systemic circulation. (c) Fluorescence of tumor lysates 30 hours after injection of nanoparticles or PBS control.

As nanoparticle accumulation and tumor cell uptake may require additional time, these experiments were repeated with a 30 hour time period between injections and tumor harvesting. To account for variability in tumor size and surface accumulation of nanoparticles, tumors were homogenized in 10mM Tris solutions containing 0.1% SDS

and boiled at 95°C for ten minutes to ensure the nanoparticles were removed from cells. Homogenates were spun down to pellet debris and supernatants were analyzed by fluorescence spectrometry. These experiments revealed a relatively elevated accumulation of nanoparticles in the tumors expressing the T-Antigen compared to the T_{nonMet} line and compared to the PBS injections (Fig. A.3c). Thus, these nanoparticles may possess T-Antigen specific targeting properties *in vivo*.

A.3 Improvements and Future Experiments

Initial experiments using nanoparticles containing peptides that bind the T-Antigen lend encouraging data that such an approach may be effective for targeting metastases *in vivo*. Many additional experiments need to be performed to improve their function and thoroughly characterize the robustness of such an approach. Firstly, control nanoparticles presenting scrambled peptide sequences should be used. These particles would not only help account for non-specific binding in the *in vitro* experiments but also would help control for effects such as differences in vascularization of the different tumor lines, which may be resulting in differential accumulation simply through the EPR effect. Additionally, these peptides are highly insoluble. To address this constraint, we have designed newer versions of their revised peptides. This peptide (C-K-K-K(TAMRA)-I-V-W-H-R-W-Y-A-W-S-P-A-S-R-PEG2-K-K) includes additional hydrophilic residues for improved solubility and compatibility with conjugation chemistries.

In addition to demonstration of *in vivo* targeting and disruption of T-Antigen – galectin-3 interactions, the iron-oxide core provides a means to image tumors. Recent studies have demonstrated the utility of these approaches in the clinic and small animal

models[463-465]. Characterization of the MR properties *in vitro* and *in vivo* for these nanoparticles will be essential for determining their clinical utility. It is worth noting that, in addition to iron-oxide, a wide variety of other materials could be easily used following similar conjugation schemes. These materials could allow for the use of additional imaging modalities that provide a more sensitive and comprehensive evaluation of metastatic tumor burden.

It is worth noting that lymph-node positive disease where no metastases have been identified (N≥1, M0) carries the most variable prognoses for patients. This variability could be the result of numerous factors. One such factor, however, may be our inability to differentiate between patients with micrometastases or generally small metastases from patients who truly only have lymph node involvement. Thus, the development of more sensitive imaging techniques, specifically for metastatic disease, may provide great improvements in our diagnostic and prognostic capabilities. Indeed, we may even find that a certain burden of micrometastases is treatable in an aggressive non-palliative manner. Reports of oligometastases, single metastases that can be treated with curative intent by surgery or radiation, support such a philosophy[466-469].

References

1. Spira, A. and D.S. Ettinger, Multidisciplinary Management of Lung Cancer. New England Journal of Medicine, 2004. 350(4): p. 379-392.
2. Edge, S.B., Byrd, D.R., Compton, C.C., Fritz, A.G., Greene, F.L., Trotti, A., AJCC Cancer Staging Manual. 2010.
3. Carpenter AE, J.T., Lamprecht MR, Clarke C, Kang IH, Friman O, Guertin DA, Chang JH, Lindquist RA, Moffat J, Golland P, Sabatini DM, CellProfiler: image analysis software for identifying and quantifying cell phenotypes. Genome Biology, 2006. 7: p. R100.
4. Rhodes, D.R., et al., ONCOMINE: a cancer microarray database and integrated data-mining platform. Neoplasia, 2004. 6(1): p. 1-6.
5. Hou, J., et al., Gene expression-based classification of non-small cell lung carcinomas and survival prediction. PLoS ONE, 2010. 5(4): p. e10312.
6. Bild, A.H., et al., Oncogenic pathway signatures in human cancers as a guide to targeted therapies. Nature, 2006. 439(7074): p. 353-7.
7. Leading Causes of Death. Centers for Disease Control and Prevention, 2013. http://www.cdc.gov/nchs/fastats/lcod.htm.
8. Cancer Facts and Figures. American Cancer Society, 2013.
9. Globocan, Fast Stats. http://globocan.iarc.fr/factsheets/populations/factsheet.asp?uno=900, 2008.
10. Gupta, G.P. and J. Massagué, Cancer Metastasis: Building a Framework. Cell, 2006. 127(4): p. 679-695.
11. Mehlen, P. and A. Puisieux, Metastasis: a question of life or death. Nat Rev Cancer, 2006. 6(6): p. 449-458.
12. Cancer Research Funding. National Cancer Institute, 2010. http://www.cancer.gov/cancertopics/factsheet/NCI/research-funding.
13. Carter, A.J. and C.N. Nguyen, A comparison of cancer burden and research spending reveals discrepancies in the distribution of research funding. BMC Public Health, 2012. 12: p. 526.
14. Robbins, S.L., V. Kumar, and R.S. Cotran, Robbins and Cotran pathologic basis of disease. 8th ed. 2010, Philadelphia, PA: Saunders/Elsevier. xiv, 1450 p.
15. Hammond, E.C., I.J. Selikoff, and H. Seidman, Asbestos exposure, cigarette smoking and death rates. Ann N Y Acad Sci, 1979. 330: p. 473-90.
16. Pershagen, G., et al., Residential radon exposure and lung cancer in Sweden. N Engl J Med, 1994. 330(3): p. 159-64.
17. Herbst, R.S., J.V. Heymach, and S.M. Lippman, Lung Cancer. New England Journal of Medicine, 2008. 359(13): p. 1367-1380.
18. Nichols, K.E., et al., Germ-line p53 mutations predispose to a wide spectrum of early-onset cancers. Cancer Epidemiol Biomarkers Prev, 2001. 10(2): p. 83-7.

19. Hwang, S.J., et al., Lung cancer risk in germline p53 mutation carriers: association between an inherited cancer predisposition, cigarette smoking, and cancer risk. Hum Genet, 2003. 113(3): p. 238-43.

20. Sekido, Y., K.M. Fong, and J.D. Minna, Molecular genetics of lung cancer. Annu Rev Med, 2003. 54: p. 73-87.

21. Ji, H., et al., LKB1 modulates lung cancer differentiation and metastasis. Nature, 2007. 448(7155): p. 807-810.

22. Amos, C.I., et al., Genome-wide association scan of tag SNPs identifies a susceptibility locus for lung cancer at 15q25.1. Nat Genet, 2008. 40(5): p. 616-622.

23. Bell, D.W., et al., Increased prevalence of EGFR-mutant lung cancer in women and in East Asian populations: analysis of estrogen-related polymorphisms. Clin Cancer Res, 2008. 14(13): p. 4079-84.

24. Tsao, A.S., et al., Clinicopathologic characteristics of the EGFR gene mutation in non-small cell lung cancer. J Thorac Oncol, 2006. 1(3): p. 231-9.

25. Lynch, T.J., et al., Activating Mutations in the Epidermal Growth Factor Receptor Underlying Responsiveness of Non–Small-Cell Lung Cancer to Gefitinib. New England Journal of Medicine, 2004. 350(21): p. 2129-2139.

26. Sordella, R., et al., Gefitinib-Sensitizing EGFR Mutations in Lung Cancer Activate Anti-Apoptotic Pathways. Science, 2004. 305(5687): p. 1163-1167.

27. Hoffman, P.C., A.M. Mauer, and E.E. Vokes, Lung cancer. The Lancet, 2000. 355(9202): p. 479-485.

28. Patel, A.M., D.G. Davila, and S.G. Peters, Paraneoplastic syndromes associated with lung cancer. Mayo Clin Proc, 1993. 68(3): p. 278-87.

29. Mulshine, J.L. and D.C. Sullivan, Lung Cancer Screening. New England Journal of Medicine, 2005. 352(26): p. 2714-2720.

30. Weng, E., et al., Accuracy and Clinical Impact of Mediastinal Lymph Node Staging with FDG-PET Imaging in Potentially Resectable Lung Cancer. American Journal of Clinical Oncology, 2000. 23(1): p. 47-52.

31. Wahbah, M., et al., Changing trends in the distribution of the histologic types of lung cancer: a review of 4,439 cases. Annals of Diagnostic Pathology, 2007. 11(2): p. 89-96.

32. Morgensztern, D., et al., Trends in Stage Distribution for Patients with Non-small Cell Lung Cancer: A National Cancer Database Survey. Journal of Thoracic Oncology, 2010. 5(1): p. 29-33 10.1097/JTO.0b013e3181c5920c.

33. Mountain, C.F. and C.M. Dresler, Regional lymph node classification for lung cancer staging. Chest, 1997. 111(6): p. 1718-23.

34. Postoperative radiotherapy in non-small-cell lung cancer: systematic review and meta-analysis of individual patient data from nine randomised controlled trials. The Lancet, 1998. 352(9124): p. 257-263.

35. Cisplatin-Based Adjuvant Chemotherapy in Patients with Completely Resected Non–Small-Cell Lung Cancer. New England Journal of Medicine, 2004. 350(4): p. 351-360.

36. Dillman, R.O., et al., A Randomized Trial of Induction Chemotherapy plus High-Dose Radiation versus Radiation Alone in Stage III Non-Small-Cell Lung Cancer. New England Journal of Medicine, 1990. 323(14): p. 940-945.

37. Dillman, R.O., et al., Improved Survival in Stage III Non-Small-Cell Lung Cancer: Seven-Year Follow-up of Cancer and Leukemia Group B (CALGB) 8433 Trial. Journal of the National Cancer Institute, 1996. 88(17): p. 1210-1215.

38. Pritchard, R.S. and S.P. Anthony, Chemotherapy plus radiotherapy compared with radiotherapy alone in the treatment of locally advanced, unresectable, non-small-cell lung cancer. A meta-analysis. Ann Intern Med, 1996. 125(9): p. 723-9.

39. Schiller, J.H., et al., Comparison of Four Chemotherapy Regimens for Advanced Non–Small-Cell Lung Cancer. New England Journal of Medicine, 2002. 346(2): p. 92-98.

40. Noda, K., et al., Irinotecan plus Cisplatin Compared with Etoposide plus Cisplatin for Extensive Small-Cell Lung Cancer. New England Journal of Medicine, 2002. 346(2): p. 85-91.

41. Pignon, J.-P., et al., A Meta-Analysis of Thoracic Radiotherapy for Small-Cell Lung Cancer. New England Journal of Medicine, 1992. 327(23): p. 1618-1624.

42. Steeg, P.S. and D. Theodorescu, Metastasis: a therapeutic target for cancer. Nat Clin Prac Oncol, 2008. 5(4): p. 206-219.

43. Chambers, A.F., A.C. Groom, and I.C. MacDonald, Metastasis: Dissemination and growth of cancer cells in metastatic sites. Nat Rev Cancer, 2002. 2(8): p. 563-572.

44. Fidler, I.J., The pathogenesis of cancer metastasis: the 'seed and soil' hypothesis revisited. Nat Rev Cancer, 2003. 3(6): p. 453-458.

45. Egeblad, M. and Z. Werb, New functions for the matrix metalloproteinases in cancer progression. Nat Rev Cancer, 2002. 2(3): p. 161-174.

46. Friedl, P. and K. Wolf, Tumour-cell invasion and migration: diversity and escape mechanisms. Nat Rev Cancer, 2003. 3(5): p. 362-374.

47. Valastyan, S. and Robert A. Weinberg, Tumor Metastasis: Molecular Insights and Evolving Paradigms. Cell, 2011. 147(2): p. 275-292.

48. Hanahan, D. and J. Folkman, Patterns and Emerging Mechanisms of the Angiogenic Switch during Tumorigenesis. Cell, 1996. 86(3): p. 353-364.

49. Gimbrone Jr, M.A., et al., Tumor dormancy in vivo by prevention of neovascularization. Journal of Experimental Medicine, 1972. 136(2): p. 261-276.

50. Carmeliet, P. and R.K. Jain, Principles and mechanisms of vessel normalization for cancer and other angiogenic diseases. Nat Rev Drug Discov, 2011. 10(6): p. 417-27.

51. Gupta, G.P., et al., Mediators of vascular remodelling co-opted for sequential steps in lung metastasis. Nature, 2007. 446(7137): p. 765-770.

52. Nagrath, S., et al., Isolation of rare circulating tumour cells in cancer patients by microchip technology. Nature, 2007. 450(7173): p. 1235-1239.

53. Stott, S.L., et al., Isolation of circulating tumor cells using a microvortex-generating herringbone-chip. Proceedings of the National Academy of Sciences, 2010.

54. Maheswaran, S., et al., Detection of Mutations in EGFR in Circulating Lung-Cancer Cells. New England Journal of Medicine, 2008. 359(4): p. 366-377.

55. Stott, S.L., et al., Isolation and Characterization of Circulating Tumor Cells from Patients with Localized and Metastatic Prostate Cancer. Science Translational Medicine, 2010. 2(25): p. 25ra23.

56. Yu, M., et al., Circulating breast tumor cells exhibit dynamic changes in epithelial and mesenchymal composition. Science, 2013. 339(6119): p. 580-4.

57. Nieswandt, B., et al., Lysis of Tumor Cells by Natural Killer Cells in Mice Is Impeded by Platelets. Cancer Research, 1999. 59(6): p. 1295-1300.

58. Palumbo, J.S., et al., Platelets and fibrin(ogen) increase metastatic potential by impeding natural killer cell–mediated elimination of tumor cells. Blood, 2005. 105(1): p. 178-185.

59. Gay, L.J. and B. Felding-Habermann, Contribution of platelets to tumour metastasis. Nat Rev Cancer, 2011. 11(2): p. 123-134.

60. Labelle, M., S. Begum, and Richard O. Hynes, Direct Signaling between Platelets and Cancer Cells Induces an Epithelial-Mesenchymal-Like Transition and Promotes Metastasis. Cancer Cell, 2011. 20(5): p. 576-590.

61. Borsig, L., et al., Heparin and cancer revisited: Mechanistic connections involving platelets, P-selectin, carcinoma mucins, and tumor metastasis. Proceedings of the National Academy of Sciences, 2001. 98(6): p. 3352-3357.

62. Labelle, M. and R.O. Hynes, The Initial Hours of Metastasis: The Importance of Cooperative Host–Tumor Cell Interactions during Hematogenous Dissemination. Cancer Discovery, 2012. 2(12): p. 1091-1099.

63. Wang, H., et al., Tumor cell $\alpha 3\beta 1$ integrin and vascular laminin-5 mediate pulmonary arrest and metastasis. The Journal of Cell Biology, 2004. 164(6): p. 935-941.

64. Brown, D.M. and E. Ruoslahti, Metadherin, a cell surface protein in breast tumors that mediates lung metastasis. Cancer Cell, 2004. 5(4): p. 365-374.

65. Al-Mehdi, A.B., et al., Intravascular origin of metastasis from the proliferation of endothelium-attached tumor cells: a new model for metastasis. Nat Med, 2000. 6(1): p. 100-102.

66. Kim, M.-Y., et al., Tumor Self-Seeding by Circulating Cancer Cells. Cell, 2009. 139(7): p. 1315-1326.

67. Kaplan, R.N., et al., VEGFR1-positive haematopoietic bone marrow progenitors initiate the pre-metastatic niche. Nature, 2005. 438(7069): p. 820-827.

68. Qian, B.-Z., et al., CCL2 recruits inflammatory monocytes to facilitate breast-tumour metastasis. Nature, 2011. 475(7355): p. 222-225.

69. Luzzi, K.J., et al., Multistep Nature of Metastatic Inefficiency : Dormancy of Solitary Cells after Successful Extravasation andLimited Survival of Early Micrometastases. Am J Pathol, 1998. 153(3): p. 865-873.

70. Röcken, M., Early tumor dissemination, but late metastasis: insights into tumor dormancy. The Journal of Clinical Investigation, 2010. 120(6): p. 1800-1803.

71. Hüsemann, Y., et al., Systemic Spread Is an Early Step in Breast Cancer. Cancer Cell, 2008. 13(1): p. 58-68.

72. Eyles, J., et al., Tumor cells disseminate early, but immunosurveillance limits metastatic outgrowth, in a mouse model of melanoma. The Journal of Clinical Investigation, 2010. 120(6): p. 2030-2039.

73. Podsypanina, K., et al., Seeding and Propagation of Untransformed Mouse Mammary Cells in the Lung. Science, 2008. 321(5897): p. 1841-1844.

74. Braun, S., et al., Cytokeratin-Positive Cells in the Bone Marrow and Survival of Patients with Stage I, II, or III Breast Cancer. N Engl J Med, 2000. 342(8): p. 525-533.

75. Wang, Y., et al., Gene-expression profiles to predict distant metastasis of lymph-node-negative primary breast cancer. The Lancet. 365(9460): p. 671-679.

76. van 't Veer, L.J., et al., Gene expression profiling predicts clinical outcome of breast cancer. Nature, 2002. 415(6871): p. 530-536.

77. Ramaswamy, S., et al., A molecular signature of metastasis in primary solid tumors. Nat Genet, 2003. 33(1): p. 49-54.

78. Smid, M., et al., Genes associated with breast cancer metastatic to bone. J Clin Oncol, 2006. 24(15): p. 2261-7.

79. Woelfle, U., et al., Molecular signature associated with bone marrow micrometastasis in human breast cancer. Cancer Res, 2003. 63(18): p. 5679-84.

80. Xi, L., et al., Prediction of lymph node metastasis by analysis of gene expression profiles in primary lung adenocarcinomas. Clin Cancer Res, 2005. 11(11): p. 4128-35.

81. Al-Hajj, M., et al., Prospective identification of tumorigenic breast cancer cells. Proceedings of the National Academy of Sciences of the United States of America, 2003. 100(7): p. 3983-3988.

82. Lapidot, T., et al., A cell initiating human acute myeloid leukaemia after transplantation into SCID mice. Nature, 1994. 367(6464): p. 645-648.

83. Singh, S.K., et al., Identification of a cancer stem cell in human brain tumors. Cancer Research, 2003. 63(18): p. 5821-5828.

84. Li, X., et al., Intrinsic resistance of tumorigenic breast cancer cells to chemotherapy. Journal of the National Cancer Institute, 2008. 100(9): p. 672-679.

85. Bao, S., et al., Glioma stem cells promote radioresistance by preferential activation of the DNA damage response. Nature, 2006. 444(7120): p. 756-760.

86. Diehn, M., et al., Association of reactive oxygen species levels and radioresistance in cancer stem cells. Nature, 2009. 458(7239): p. 780-783.

87. Dean, M., T. Fojo, and S. Bates, Tumour stem cells and drug resistance. Nature Reviews Cancer, 2005. 5(4): p. 275-284.

88. Mani, S.A., et al., The Epithelial-Mesenchymal Transition Generates Cells with Properties of Stem Cells. 2008. 133(4): p. 704-715.

89. Gupta, P.B., et al., Identification of Selective Inhibitors of Cancer Stem Cells by High-Throughput Screening. Cell, 2009. 138(4): p. 645-659.

90. Shoushtari, A.N., R.Z. Szmulewitz, and C.W. Rinker-Schaeffer, Metastasis-suppressor genes in clinical practice: lost in translation? Nat Rev Clin Oncol, 2011. 8(6): p. 333-42.

91. Bevilacqua, G., et al., Association of low nm23 RNA levels in human primary infiltrating ductal breast carcinomas with lymph node involvement and other histopathological indicators of high metastatic potential. Cancer Res, 1989. 49(18): p. 5185-90.

92. Takeuchi, T., et al., The membrane-anchored matrix metalloproteinase (MMP) regulator RECK in combination with MMP-9 serves as an informative prognostic indicator for colorectal cancer. Clin Cancer Res, 2004. 10(16): p. 5572-9.

93. Li, J., Inhibition of ovarian cancer metastasis by adeno-associated virus-mediated gene transfer of nm23H1 in an orthotopic implantation model. Cancer Gene Ther., 2006. 13: p. 266-272.

94. Takeda, T., Adenoviral transduction of MRP-1/CD9 and KAI1/CD82 inhibits lymph node metastasis in orthotopic lung cancer model. Cancer Res., 2007. 67: p. 1744-1749.

95. Wu, Y., Src phosphorylation of RhoGDI2 regulates its metastasis suppressor function. Proc. Natl Acad. Sci. USA, 2009. 106: p. 5807-5812.

96. Ouatas, T., D. Halverson, and P.S. Steeg, Dexamethasone and medroxyprogesterone acetate elevate Nm23-H1 metastasis suppressor gene expression in metastatic human breast carcinoma cells: new uses for old compounds. Clin. Cancer Res., 2003. 9: p. 3763-3772.

97. Hartsough, M.T., Elevation of breast carcinoma Nm23-H1 metastasis suppressor gene expression and reduced motility by DNA methylation inhibition. Cancer Res., 2001. 61: p. 2320-2327.

98. Ohtaki, T., Metastasis suppressor gene KiSS-1 encodes peptide ligand of a G-protein-coupled receptor. Nature, 2001. 411: p. 613-617.

99. Boucharaba, A., The type 1 lysophosphatidic acid receptor is a target for therapy in bone metastases. Proc. Natl Acad. Sci. USA, 2006. 103: p. 9643-9648.

100. Mina, L.A. and G.W. Sledge, Jr., Rethinking the metastatic cascade as a therapeutic target. Nat Rev Clin Oncol, 2011. 8(6): p. 325-32.

101. Hodi, F.S., et al., Improved Survival with Ipilimumab in Patients with Metastatic Melanoma. New England Journal of Medicine, 2010. 363(8): p. 711-723.

102. Topalian, S.L., et al., Safety, Activity, and Immune Correlates of Anti–PD-1 Antibody in Cancer. New England Journal of Medicine, 2012. 366(26): p. 2443-2454.

103. Flaherty, K.T., et al., Inhibition of Mutated, Activated BRAF in Metastatic Melanoma. New England Journal of Medicine, 2010. 363(9): p. 809-819.

104. Bollag, G., et al., Clinical efficacy of a RAF inhibitor needs broad target blockade in BRAF-mutant melanoma. Nature, 2010. 467(7315): p. 596-599.

105. Mintz, B. and K. Illmensee, Normal genetically mosaic mice produced from malignant teratocarcinoma cells. Proc Natl Acad Sci U S A, 1975. 72(9): p. 3585-9.

106. Joyce, J.A. and J.W. Pollard, Microenvironmental regulation of metastasis. Nat Rev Cancer, 2009. 9(4): p. 239-252.

107. Paget, S., The Distribution of Secondary Growths in Cancer of the Breast. The Lancet, 1889. 133(3421): p. 571-573.

108. Kang, Y., et al., A multigenic program mediating breast cancer metastasis to bone. Cancer Cell, 2003. 3(6): p. 537-549.

109. Minn, A.J., et al., Genes that mediate breast cancer metastasis to lung. Nature, 2005. 436(7050): p. 518-524.

110. Bos, P.D., et al., Genes that mediate breast cancer metastasis to the brain. Nature, 2009. 459(7249): p. 1005-1009.

111. Nguyen, D.X., P.D. Bos, and J. Massague, Metastasis: from dissemination to organ-specific colonization. Nat Rev Cancer, 2009. 9(4): p. 274-284.

112. Naba, A., et al., The matrisome: in silico definition and in vivo characterization by proteomics of normal and tumor extracellular matrices. Molecular & Cellular Proteomics, 2011.

113. Levental, K.R., et al., Matrix Crosslinking Forces Tumor Progression by Enhancing Integrin Signaling. 2009. 139(5): p. 891-906.

114. Oskarsson, T., et al., Breast cancer cells produce tenascin C as a metastatic niche component to colonize the lungs. Nat Med, 2011. 17(7): p. 867-874.

115. Desgrosellier, J.S. and D.A. Cheresh, Integrins in cancer: biological implications and therapeutic opportunities. Nat Rev Cancer, 2010. 10(1): p. 9-22.

116. Weaver, V.M., et al., Reversion of the Malignant Phenotype of Human Breast Cells in Three-Dimensional Culture and In Vivo by Integrin Blocking Antibodies. J. Cell Biol., 1997. 137(1): p. 231-245.

117. Hynes, R.O., The Extracellular Matrix: Not Just Pretty Fibrils. Science, 2009. 326(5957): p. 1216-1219.

118. Karnoub, A.E., et al., Mesenchymal stem cells within tumour stroma promote breast cancer metastasis. Nature, 2007. 449(7162): p. 557-563.

119. McAllister, S.S., et al., Systemic Endocrine Instigation of Indolent Tumor Growth Requires Osteopontin. Cell, 2008. 133(6): p. 994-1005.

120. Lu, X., et al., VCAM-1 Promotes Osteolytic Expansion of Indolent Bone Micrometastasis of Breast Cancer by Engaging $\alpha 4\beta 1$-Positive Osteoclast Progenitors. Cancer Cell, 2011. 20(6): p. 701-714.

121. Sethi, N., et al., Tumor-Derived Jagged1 Promotes Osteolytic Bone Metastasis of Breast Cancer by Engaging Notch Signaling in Bone Cells. Cancer Cell, 2011. 19(2): p. 192-205.

122. Jones, D.H., et al., Regulation of cancer cell migration and bone metastasis by RANKL. Nature, 2006. 440(7084): p. 692-696.

123. Erler, J.T., et al., Hypoxia-Induced Lysyl Oxidase Is a Critical Mediator of Bone Marrow Cell Recruitment to Form the Premetastatic Niche. Cancer Cell, 2009. 15(1): p. 35-44.

124. Qian, B.-Z. and J.W. Pollard, Macrophage Diversity Enhances Tumor Progression and Metastasis. Cell, 2010. 141(1): p. 39-51.

125. Muller, A., et al., Involvement of chemokine receptors in breast cancer metastasis. Nature, 2001. 410(6824): p. 50-56.

126. Pollard, J.W., Tumour-educated macrophages promote tumour progression and metastasis. Nat Rev Cancer, 2004. 4(1): p. 71-78.

127. Robinson, B.D., et al., Tumor Microenvironment of Metastasis in Human Breast Carcinoma: A Potential Prognostic Marker Linked to Hematogenous Dissemination. Clinical Cancer Research, 2009. 15(7): p. 2433-2441.

128. Wyckoff, J., et al., A paracrine loop between tumor cells and macrophages is required for tumor cell migration in mammary tumors. Cancer Res, 2004. 64(19): p. 7022-9.

129. Goswami, S., et al., Macrophages promote the invasion of breast carcinoma cells via a colony-stimulating factor-1/epidermal growth factor paracrine loop. Cancer Res, 2005. 65(12): p. 5278-83.

130. Wyckoff, J.B., et al., Direct visualization of macrophage-assisted tumor cell intravasation in mammary tumors. Cancer Res, 2007. 67(6): p. 2649-56.

131. Bunt, S.K., et al., Inflammation induces myeloid-derived suppressor cells that facilitate tumor progression. J Immunol, 2006. 176(1): p. 284-90.

132. Cheng, P., et al., Inhibition of dendritic cell differentiation and accumulation of myeloid-derived suppressor cells in cancer is regulated by S100A9 protein. J Exp Med, 2008. 205(10): p. 2235-49.

133. Discher, D.E., D.J. Mooney, and P.W. Zandstra, Growth Factors, Matrices, and Forces Combine and Control Stem Cells. Science, 2009. 324(5935): p. 1673-1677.

134. Geiger, B., J.P. Spatz, and A.D. Bershadsky, Environmental sensing through focal adhesions. Nat Rev Mol Cell Biol, 2009. 10(1): p. 21-33.

135. Thery, M., et al., The extracellular matrix guides the orientation of the cell division axis. Nat Cell Biol, 2005. 7(10): p. 947-953.

136. Kalluri, R., Basement membranes: structure, assembly and role in tumour angiogenesis. Nat Rev Cancer, 2003. 3(6): p. 422-433.

137. Mohammadi, M., S.K. Olsen, and R. Goetz, A protein canyon in the FGF–FGF receptor dimer selects from an à la carte menu of heparan sulfate motifs. Current Opinion in Structural Biology, 2005. 15(5): p. 506-516.

138. Neptune, E.R., et al., Dysregulation of TGF-beta activation contributes to pathogenesis in Marfan syndrome. Nat Genet, 2003. 33(3): p. 407-11.

139. Engel, J., EGF-like domains in extracellular matrix proteins: Localized signals for growth and differentiation? FEBS Letters, 1989. 251(1–2): p. 1-7.

140. Panayotou, G., et al., Domains of laminin with growth-factor activity. Cell, 1989. 56(1): p. 93-101.

141. Mohamed, M.M. and B.F. Sloane, Cysteine cathepsins: multifunctional enzymes in cancer. Nat Rev Cancer, 2006. 6(10): p. 764-775.

142. Giannelli, G., et al., Induction of Cell Migration by Matrix Metalloprotease-2 Cleavage of Laminin-5. Science, 1997. 277(5323): p. 225-228.

143. WESTERMARCK, J. and V.-M. KAHARI, Regulation of matrix metalloproteinase expression in tumor invasion. FASEB J., 1999. 13(8): p. 781-792.

144. Hotary, K.B., et al., Membrane Type I Matrix Metalloproteinase Usurps Tumor Growth Control Imposed by the Three-Dimensional Extracellular Matrix. Cell, 2003. 114(1): p. 33-45.

145. Xu, L. and R.O. Hynes, GPR56 and TG2: possible roles in suppression of tumor growth by the microenvironment. Cell Cycle, 2007. 6(2): p. 160-5.

146. Sasisekharan, R., et al., Roles of heparan-sulphate glycosaminoglycans in cancer. Nat Rev Cancer, 2002. 2(7): p. 521-528.

147. Liu, D., et al., Tumor cell surface heparan sulfate as cryptic promoters or inhibitors of tumor growth and metastasis. Proceedings of the National Academy of Sciences of the United States of America, 2002. 99(2): p. 568-573.

148. Wai, P.Y. and P.C. Kuo, The role of Osteopontin in tumor metastasis. Journal of Surgical Research, 2004. 121(2): p. 228-241.

149. Singhal, H., et al., Elevated plasma osteopontin in metastatic breast cancer associated with increased tumor burden and decreased survival. Clinical Cancer Research, 1997. 3(4): p. 605-611.

150. Patarroyo, M., K. Tryggvason, and I. Virtanen, Laminin isoforms in tumor invasion, angiogenesis and metastasis. Seminars in Cancer Biology, 2002. 12(3): p. 197-207.

151. Reuter, J.A., et al., Modeling Inducible Human Tissue Neoplasia Identifies an Extracellular Matrix Interaction Network Involved in Cancer Progression. Cancer Cell, 2009. 15(6): p. 477-488.

152. Iyengar, P., et al., Adipocyte-derived collagen VI affects early mammary tumor progression in vivo, demonstrating a critical interaction in the tumor/stroma microenvironment. The Journal of Clinical Investigation, 2005. 115(5): p. 1163-1176.

153. Liu, F.-T. and G.A. Rabinovich, Galectins as modulators of tumour progression. Nat Rev Cancer, 2005. 5(1): p. 29-41.

154. Ingber, D.E., Can cancer be reversed by engineering the tumor microenvironment? Seminars in Cancer Biology, 2008. 18(5): p. 356-364.

155. Hynes, R.O., Alteration of cell-surface proteins by viral transformation and by proteolysis. Proc Natl Acad Sci U S A, 1973. 70(11): p. 3170-4.

156. Graham, J.M., et al., The location of proteins labeled by the 125I-lactoperoxidase system in the NIL 8 hamster fibroblast. Cell, 1975. 4(4): p. 353-65.

157. Wartiovaara, J., et al., Distribution of fibroblast surface antigen: association with fibrillar structures of normal cells and loss upon viral transformation. J Exp Med, 1974. 140(6): p. 1522-33.

158. Mautner, V. and R.O. Hynes, Surface distribution of LETS protein in relation to the cytoskeleton of normal and transformed cells. J Cell Biol, 1977. 75(3): p. 743-68.

159. Ali, I.U. and R.O. Hynes, Effects of cytochalasin B and colchicine on attachment of a major surface protein of fibroblasts. Biochim Biophys Acta, 1977. 471(1): p. 16-24.

160. Ali, I.U. and R.O. Hynes, Effects of LETS glycoprotein on cell motility. Cell, 1978. 14(2): p. 439-46.

161. Pierschbacher, M.D. and E. Ruoslahti, Cell attachment activity of fibronectin can be duplicated by small synthetic fragments of the molecule. Nature, 1984. 309(5963): p. 30-3.

162. Gardner, J.M. and R.O. Hynes, Interaction of fibronectin with its receptor on platelets. Cell, 1985. 42(2): p. 439-48.

163. Tamkun, J.W., et al., Structure of integrin, a glycoprotein involved in the transmembrane linkage between fibronectin and actin. Cell, 1986. 46(2): p. 271-82.

164. Hynes, R.O., Integrins: A family of cell surface receptors. Cell, 1987. 48(4): p. 549-554.

165. Hynes, R.O., Integrins: Bidirectional, Allosteric Signaling Machines. Cell, 2002. 110(6): p. 673-687.

166. Strauch, U.G., et al., Integrin alpha E(CD103)beta 7 mediates adhesion to intestinal microvascular endothelial cell lines via an E-cadherin-independent interaction. J Immunol, 2001. 166(5): p. 3506-14.

167. Cepek, K.L., et al., Integrin alpha E beta 7 mediates adhesion of T lymphocytes to epithelial cells. The Journal of Immunology, 1993. 150(8): p. 3459-70.

168. Cepek, K.L., et al., Adhesion between epithelial cells and T lymphocytes mediated by E-cadherin and the alpha E beta 7 integrin. Nature, 1994. 372(6502): p. 190-3.

169. Palecek, S.P., et al., Integrin dynamics on the tail region of migrating fibroblasts. Journal of Cell Science, 1996. 109(5): p. 941-952.

170. Emsley, J., et al., Structural Basis of Collagen Recognition by Integrin α2β1. Cell, 2000. 101(1): p. 47-56.

171. Xiong, J.P., et al., Crystal structure of the extracellular segment of integrin alpha Vbeta3. Science, 2001. 294(5541): p. 339-45.

172. Takagi, J., H.P. Erickson, and T.A. Springer, C-terminal opening mimics 'inside-out' activation of integrin alpha5beta1. Nat Struct Biol, 2001. 8(5): p. 412-6.

173. Calderwood, D.A., et al., The Talin head domain binds to integrin beta subunit cytoplasmic tails and regulates integrin activation. J Biol Chem, 1999. 274(40): p. 28071-4.

174. Calderwood, D.A., et al., The phosphotyrosine binding-like domain of talin activates integrins. J Biol Chem, 2002. 277(24): p. 21749-58.

175. Guo, W. and F.G. Giancotti, Integrin signalling during tumour progression. Nat Rev Mol Cell Biol, 2004. 5(10): p. 816-826.

176. Zutter, M.M., et al., Re-expression of the alpha 2 beta 1 integrin abrogates the malignant phenotype of breast carcinoma cells. Proc Natl Acad Sci U S A, 1995. 92(16): p. 7411-5.

177. Stupack, D.G., et al., Apoptosis of adherent cells by recruitment of caspase-8 to unligated integrins. J. Cell Biol., 2001. 155(3): p. 459-470.

178. Desgrosellier, J.S., et al., An integrin [alpha]v[beta]3-c-Src oncogenic unit promotes anchorage-independence and tumor progression. Nat Med, 2009. 15(10): p. 1163-1169.

179. Friedlander, M., et al., Definition of Two Angiogenic Pathways by Distinct αv Integrins. Science, 1995. 270(5241): p. 1500-1502.

180. Trusolino, L., A. Bertotti, and P.M. Comoglio, A Signaling Adapter Function for α6β4 Integrin in the Control of HGF-Dependent Invasive Growth. Cell, 2001. 107(5): p. 643-654.

181. Miyamoto, S., et al., Integrins can collaborate with growth factors for phosphorylation of receptor tyrosine kinases and MAP kinase activation: roles of integrin aggregation and occupancy of receptors. The Journal of Cell Biology, 1996. 135(6): p. 1633-1642.

182. Caswell, P.T., et al., Rab-coupling protein coordinates recycling of α5β1 integrin and EGFR1 to promote cell migration in 3D microenvironments. The Journal of Cell Biology, 2008. 183(1): p. 143-155.

183. Muller, P.A.J., et al., Mutant p53 Drives Invasion by Promoting Integrin Recycling. 2009. 139(7): p. 1327-1341.

184. Jin, H., et al., A homing mechanism for bone marrow–derived progenitor cell recruitment to the neovasculature. The Journal of Clinical Investigation, 2006. 116(3): p. 652-662.

185. Taverna, D., et al., Increased primary tumor growth in mice null for β3- or β3/β5-integrins or selectins. Proceedings of the National Academy of Sciences of the United States of America, 2004. 101(3): p. 763-768.

186. Chen, Q., Xiang H.F. Zhang, and J. Massagué, Macrophage Binding to Receptor VCAM-1 Transmits Survival Signals in Breast Cancer Cells that Invade the Lungs. Cancer Cell, 2011. 20(4): p. 538-549.

187. Lahlou, H., et al., Mammary epithelial-specific disruption of the focal adhesion kinase blocks mammary tumor progression. Proceedings of the National Academy of Sciences, 2007. 104(51): p. 20302-20307.

188. Pylayeva, Y., et al., Ras- and PI3K-dependent breast tumorigenesis in mice and humans requires focal adhesion kinase signaling. The Journal of Clinical Investigation, 2009. 119(2): p. 252-266.

189. Brooks, P.C., et al., Localization of Matrix Metalloproteinase MMP-2 to the Surface of Invasive Cells by Interaction with Integrin [alpha]v[beta]3. Cell, 1996. 85(5): p. 683-693.

190. Avraamides, C.J., B. Garmy-Susini, and J.A. Varner, Integrins in angiogenesis and lymphangiogenesis. Nat Rev Cancer, 2008. 8(8): p. 604-617.

191. Beer, D.G., et al., Gene-expression profiles predict survival of patients with lung adenocarcinoma. Nat Med, 2002. 8(8): p. 816-824.

192. Zhang, X.H.F., et al., Latent Bone Metastasis in Breast Cancer Tied to Src-Dependent Survival Signals. Cancer Cell, 2009. 16(1): p. 67-78.

193. Nguyen, D.X., et al., WNT/TCF Signaling through LEF1 and HOXB9 Mediates Lung Adenocarcinoma Metastasis. Cell, 2009. 138(1): p. 51-62.

194. Winslow, M.M., et al., Suppression of lung adenocarcinoma progression by Nkx2-1. Nature, 2011. 473(7345): p. 101-104.

195. Boutros, M. and J. Ahringer, The art and design of genetic screens: RNA interference. Nat Rev Genet, 2008. 9(7): p. 554-566.

196. Silva, J.M., et al., Profiling Essential Genes in Human Mammary Cells by Multiplex RNAi Screening. Science, 2008. 319(5863): p. 617-620.

197. Neumann, B., et al., Phenotypic profiling of the human genome by time-lapse microscopy reveals cell division genes. Nature, 2010. 464(7289): p. 721-727.

198. Carpenter, A.E. and D.M. Sabatini, Systematic genome-wide screens of gene function. Nat Rev Genet, 2004. 5(1): p. 11-22.

199. Bleicher, K.H., et al., Hit and lead generation: beyond high-throughput screening. Nat Rev Drug Discov, 2003. 2(5): p. 369-378.

200. Quintavalle, M., et al., A Cell-Based High-Content Screening Assay Reveals Activators and Inhibitors of Cancer Cell Invasion. Sci. Signal., 2011. 4(183): p. ra49-.

201. Swinney, D.C. and J. Anthony, How were new medicines discovered? Nat Rev Drug Discov, 2011. 10(7): p. 507-519.

202. Abraham, V.C., D.L. Taylor, and J.R. Haskins, High content screening applied to large-scale cell biology. Trends in Biotechnology, 2004. 22(1): p. 15-22.

203. Paul, S.M., et al., How to improve R&D productivity: the pharmaceutical industry's grand challenge. Nat Rev Drug Discov, 2010. 9(3): p. 203-214.

204. Dolberg, D.S. and M.J. Bissell, Inability of Rous sarcoma virus to cause sarcomas in the avian embryo. Nature, 1984. 309(5968): p. 552-556.

205. Hendrix, M.J.C., et al., Reprogramming metastatic tumour cells with embryonic microenvironments. Nat Rev Cancer, 2007. 7(4): p. 246-255.

206. Olumi, A.F., et al., Carcinoma-associated Fibroblasts Direct Tumor Progression of Initiated Human Prostatic Epithelium. Cancer Research, 1999. 59(19): p. 5002-5011.

207. Albini, A., et al., A Rapid in Vitro Assay for Quantitating the Invasive Potential of Tumor Cells. Cancer Research, 1987. 47(12): p. 3239-3245.

208. Malik, G., et al., Plasma Fibronectin Promotes Lung Metastasis by Contributions to Fibrin Clots and Tumor Cell Invasion. Cancer Research, 2010. 70(11): p. 4327-4334.

209. White, D.E., et al., Targeted disruption of β1-integrin in a transgenic mouse model of human breast cancer reveals an essential role in mammary tumor induction. Cancer Cell, 2004. 6(2): p. 159-170.

210. Flaim, C.J., S. Chien, and S.N. Bhatia, An extracellular matrix microarray for probing cellular differentiation. Nat Meth, 2005. 2(2): p. 119-125.

211. Flaim, C.J., et al., Combinatorial Signaling Microenvironments for Studying Stem Cell Fate. Stem Cells and Development, 2008. 17(1): p. 29-40.

212. LaBarge, M.A., et al., Human mammary progenitor cell fate decisions are products of interactions with combinatorial microenvironments. Integrative Biology, 2009. 1(1): p. 70-79.

213. Mei, Y., et al., Cell-Compatible, Multicomponent Protein Arrays with Subcellular Feature Resolution. Small, 2008. 4(10): p. 1600-1604.

214. Brafman, D.A., et al., Investigating the role of the extracellular environment in modulating hepatic stellate cell biology with arrayed combinatorial microenvironments. Integrative Biology, 2009. 1(8-9): p. 513-24.

215. Jackson, E.L., et al., Analysis of lung tumor initiation and progression using conditional expression of oncogenic K-ras. Genes & Development, 2001. 15(24): p. 3243-3248.

216. DuPage, M., A.L. Dooley, and T. Jacks, Conditional mouse lung cancer models using adenoviral or lentiviral delivery of Cre recombinase. Nat. Protocols, 2009. 4(8): p. 1064-1072.

217. Perou, C.M., et al., Molecular portraits of human breast tumours. Nature, 2000. 406(6797): p. 747-752.

218. Paik, S., et al., A Multigene Assay to Predict Recurrence of Tamoxifen-Treated, Node-Negative Breast Cancer. New England Journal of Medicine, 2004. 351(27): p. 2817-2826.

219. van de Vijver, M.J., et al., A Gene-Expression Signature as a Predictor of Survival in Breast Cancer. New England Journal of Medicine, 2002. 347(25): p. 1999-2009.

220. Danen, E.H.J. and K.M. Yamada, Fibronectin, integrins, and growth control. Journal of Cellular Physiology, 2001. 189(1): p. 1-13.

221. Humphries, M., K. Olden, and K. Yamada, A synthetic peptide from fibronectin inhibits experimental metastasis of murine melanoma cells. Science, 1986. 233(4762): p. 467-470.

222. Akiyama, S.K., K. Olden, and K.M. Yamada, Fibronectin and integrins in invasion and metastasis. Cancer Metastasis Rev, 1995. 14(3): p. 173-89.

223. Yi, M. and E. Ruoslahti, A fibronectin fragment inhibits tumor growth, angiogenesis, and metastasis. Proceedings of the National Academy of Sciences, 2001. 98(2): p. 620-624.

224. Newton, S., et al., Inhibition of experimental metastasis of human breast-carcinoma cells in athymic nude-mice by anti-alpha(5)beta(1) fibronectin receptor integrin antibodies. Int J Oncol, 1995. 6(5): p. 1063-70.

225. Plantefaber, L.C. and R.O. Hynes, Changes in integrin receptors on oncogenically transformed cells. Cell, 1989. 56(2): p. 281-290.

226. Mitra, A.K., et al., Ligand-independent activation of c-Met by fibronectin and [alpha]5[beta]1-integrin regulates ovarian cancer invasion and metastasis. Oncogene, 2011. 30(13): p. 1566-1576.

227. Nam, J.-M., et al., Breast Cancer Cells in Three-dimensional Culture Display an Enhanced Radioresponse after Coordinate Targeting of Integrin α5β1 and Fibronectin. Cancer Research, 2010. 70(13): p. 5238-5248.

228. Garmy-Susini, B., et al., Integrin α4β1 Signaling Is Required for Lymphangiogenesis and Tumor Metastasis. Cancer Research, 2010. 70(8): p. 3042-3051.

229. Barsky, S.H., et al., Laminin molecular domains which alter metastasis in a murine model. The Journal of Clinical Investigation, 1984. 74(3): p. 843-848.

230. Pouliot, N., E.C. Nice, and A.W. Burgess, Laminin-10 Mediates Basal and EGF-Stimulated Motility of Human Colon Carcinoma Cells via [alpha]3[beta]1 and [alpha]6[beta]4 Integrins. Experimental Cell Research, 2001. 266(1): p. 1-10.

231. Carter, W.G., M.C. Ryan, and P.J. Gahr, Epiligrin, a new cell adhesion ligand for integrin α3β1 in epithelial basement membranes. Cell, 1991. 65(4): p. 599-610.

232. Fukushi, J., I.T. Makagiansar, and W.B. Stallcup, NG2 proteoglycan promotes endothelial cell motility and angiogenesis via engagement of galectin-3 and alpha3beta1 integrin. Mol Biol Cell, 2004. 15(8): p. 3580-90.

233. Hadari, Y.R., et al., Galectin-8 binding to integrins inhibits cell adhesion and induces apoptosis. Journal of Cell Science, 2000. 113(13): p. 2385-2397.

234. Hemler, M.E., et al., Multiple ligand binding functions for VLA-2 (alpha 2 beta 1) and VLA-3 (alpha 3 beta 1) in the integrin family. Cell Differ Dev, 1990. 32(3): p. 229-38.

235. DiPersio, C.M., et al., α3β1 Integrin Is Required for Normal Development of the Epidermal Basement Membrane. The Journal of Cell Biology, 1997. 137(3): p. 729-742.

236. deHart, G.W., K.E. Healy, and J.C.R. Jones, The role of α3β1 integrin in determining the supramolecular organization of laminin-5 in the extracellular matrix of keratinocytes. Experimental Cell Research, 2003. 283(1): p. 67-79.

237. Morini, M., et al., The alpha 3 beta 1 integrin is associated with mammary carcinoma cell metastasis, invasion, and gelatinase B (MMP-9) activity. Int J Cancer, 2000. 87(3): p. 336-42.

238. Melchiori, A., et al., The α3β1 Integrin Is Involved in Melanoma Cell Migration and Invasion. Experimental Cell Research, 1995. 219(1): p. 233-242.

239. Bartolazzi, A., et al., Transformation and tumor progression are frequently associated with expression of the α3/β1 heterodimer in solid tumors. International Journal of Cancer, 1994. 58(4): p. 488-491.

240. Natali, P.G., et al., Integrin expression in cutaneous malignant melanoma: Association of the α3/β1 heterodimer with tumor progression. International Journal of Cancer, 1993. 54(1): p. 68-72.

241. Lamar, J.M., V. Iyer, and C.M. DiPersio, Integrin [alpha]3[beta]1 Potentiates TGF[beta]-Mediated Induction of MMP-9 in Immortalized Keratinocytes. J Invest Dermatol, 2007. 128(3): p. 575-586.

242. Baldwin, G., et al., Tetraspanin CD151 regulates glycosylation of (alpha)3(beta)1 integrin. J Biol Chem, 2008. 283(51): p. 35445-54.

243. Gu, J. and N. Taniguchi, Regulation of integrin functions by N-glycans. Glycoconjugate Journal, 2004. 21(1-2): p. 9-15.

244. Diskin, S., et al., The role of integrin glycosylation in galectin-8-mediated trabecular meshwork cell adhesion and spreading. Glycobiology, 2009. 19(1): p. 29-37.

245. Pocheć, E., et al., Glycosylation profile of integrin changes with melanoma progression. Biochimica et Biophysica Acta (BBA) - Molecular Cell Research, 2003. 1643(1–3): p. 113-123.

246. Janik, M.E., et al., Effect of alpha3beta1 and alphavbeta3 integrin glycosylation on interaction of melanoma cells with vitronectin. Acta Biochim Pol, 2010. 57(1): p. 55-61.

247. Teichberg, V.I., et al., A beta-D-galactoside binding protein from electric organ tissue of Electrophorus electricus. Proceedings of the National Academy of Sciences, 1975. 72(4): p. 1383-1387.

248. de Waard, A., S. Hickman, and S. Kornfeld, Isolation and properties of beta-galactoside binding lectins of calf heart and lung. Journal of Biological Chemistry, 1976. 251(23): p. 7581-7587.

249. Cooper, D.N.W., Galectinomics: finding themes in complexity. Biochimica et Biophysica Acta (BBA) - General Subjects, 2002. 1572(2–3): p. 209-231.

250. Barondes, S.H., et al., Galectins: A family of animal β-galactoside-binding lectins. Cell, 1994. 76(4): p. 597-598.

251. Hughes, R.C., Secretion of the galectin family of mammalian carbohydrate-binding proteins. Biochim Biophys Acta, 1999. 1473(1): p. 172-85.

252. Mehul, B. and R.C. Hughes, Plasma membrane targetting, vesicular budding and release of galectin 3 from the cytoplasm of mammalian cells during secretion. Journal of Cell Science, 1997. 110(10): p. 1169-1178.

253. Ho, M.K. and T.A. Springer, Mac-2, a novel 32,000 Mr mouse macrophage subpopulation-specific antigen defined by monoclonal antibodies. The Journal of Immunology, 1982. 128(3): p. 1221-8.

254. Dumic, J., S. Dabelic, and M. Flögel, Galectin-3: An open-ended story. Biochimica et Biophysica Acta (BBA) - General Subjects, 2006. 1760(4): p. 616-635.

255. Newlaczyl, A.U. and L.-G. Yu, Galectin-3 – A jack-of-all-trades in cancer. Cancer Letters, 2011. 313(2): p. 123-128.

256. Raz, A., G. Pazerini, and P. Carmi, Identification of the Metastasis-associated, Galactoside-binding Lectin as a Chimeric Gene Product with Homology to an IgE-binding Protein. Cancer Research, 1989. 49(13): p. 3489-3493.

257. Massa, S.M., et al., L-29, an endogenous lectin, binds to glycoconjugate ligands with positive cooperativity. Biochemistry, 1993. 32(1): p. 260-267.

258. Ochieng, J., et al., Modulation of the biological functions of galectin-3 by matrix metalloproteinases. Biochimica et Biophysica Acta (BBA) - General Subjects, 1998. 1379(1): p. 97-106.

259. Yoshii, T., et al., Galectin-3 Phosphorylation Is Required for Its Anti-apoptotic Function and Cell Cycle Arrest. Journal of Biological Chemistry, 2002. 277(9): p. 6852-6857.

260. Seetharaman, J., et al., X-ray Crystal Structure of the Human Galectin-3 Carbohydrate Recognition Domain at 2.1-Å Resolution. Journal of Biological Chemistry, 1998. 273(21): p. 13047-13052.

261. Akahani, S., et al., Galectin-3: A Novel Antiapoptotic Molecule with A Functional BH1 (NWGR) Domain of Bcl-2 Family. Cancer Research, 1997. 57(23): p. 5272-5276.

262. Colin Hughes, R., Galectins as modulators of cell adhesion. Biochimie, 2001. 83(7): p. 667-676.

263. Ochieng, J., M.L. Leite-Browning, and P. Warfield, Regulation of Cellular Adhesion to Extracellular Matrix Proteins by Galectin-3. Biochemical and Biophysical Research Communications, 1998. 246(3): p. 788-791.

264. Ochieng, J., et al., Galectin-3 regulates the adhesive interaction between breast carcinoma cells and elastin. Journal of Cellular Biochemistry, 1999. 75(3): p. 505-514.

265. Pesheva, P., et al., Galectin-3 promotes neural cell adhesion and neurite growth. Journal of Neuroscience Research, 1998. 54(5): p. 639-654.

266. Sato, S., I. Burdett, and R.C. Hughes, Secretion of the Baby Hamster Kidney 30-kDa Galactose-Binding Lectin from Polarized and Nonpolarized Cells: A Pathway Independent of the Endoplasmic Reticulum-Golgi Complex. Experimental Cell Research, 1993. 207(1): p. 8-18.

267. Dagher, S.F., J.L. Wang, and R.J. Patterson, Identification of galectin-3 as a factor in pre-mRNA splicing. Proc. Natl Acad. Sci. USA, 1995. 92: p. 1213-1217.

268. Elad-Sfadia, G., et al., Galectin-3 augments K-Ras activation and triggers a Ras signal that attenuates ERK but not phosphoinositide 3-kinase activity. J. Biol. Chem., 2004. 279: p. 34922-34930.

269. Choi, J.H., et al., Inhibition of N-(4-hydroxyphenyl)retinamide-induced apoptosis in breast cancer cells by galectin-3. Cancer Biol. Ther., 2004. 3: p. 447-452.

270. Hoyer, K.K., An anti-apoptotic role for galectin-3 in diffuse large B-cell lymphomas. Am. J. Pathol., 2004. 164: p. 893-902.

271. Takenaka, Y., Nuclear export of phosphorylated galectin-3 regulates its antiapoptotic activity in response to chemotherapeutic drugs. Mol. Cell. Biol., 2004. 24: p. 4395-4406.

272. Honjo, Y., et al., Down-regulation of galectin-3 suppresses tumorigenicity of human breast carcinoma cells. Clin. Cancer Res., 2001. 7: p. 661-668.

273. van den Brule, F.A., Antisense galectin-3 alters thymidine incorporation in human MDA-MB435 breast cancer cells. Int. J. Oncol., 1997. 11: p. 261-264.

274. Califice, S., et al., Dual activities of galectin-3 in human prostate cancer: tumor suppression of nuclear galectin-3 vs tumor promotion of cytoplasmic galectin-3. Oncogene, 2004. 23: p. 7527-7536.

275. Paron, I., Nuclear localization of galectin-3 in transformed thyroid cells: a role in transcriptional regulation. Biochem. Biophys. Res. Commun., 2003. 302: p. 545-553.

276. Kim, H.R., et al., Cell cycle arrest and inhibition of anoikis by galectin-3 in human breast epithelial cells. Cancer Res., 1999. 59: p. 4148-4154.

277. Nangia-Makker, P., Galectin-3 induces endothetial cell morphogenesis and angiogenesis. Am. J. Pathol., 2000. 156: p. 899-909.

278. Furtak, V., F. Hatcher, and J. Ochieng, Galectin-3 mediates the endocytosis of [beta]-1 integrins by breast carcinoma cells. Biochem. Biophys. Res. Commun., 2001. 289: p. 845-850.

279. Danguy, A., I. Camby, and R. Kiss, Galectins and cancer. Biochimica et Biophysica Acta (BBA) - General Subjects, 2002. 1572(2–3): p. 285-293.

280. Pieters, R.J., Inhibition and Detection of Galectins. ChemBioChem, 2006. 7(5): p. 721-728.

281. Khaldoyanidi, S.K., MDA-MB-435 human breast carcinoma cell homo- and heterotypic adhesion under flow conditions is mediated in part by Thomsen-Friedenreich antigen-galectin-3 interactions. J. Biol. Chem., 2003. 278: p. 4127-4134.

282. Levy, Y., et al., Galectin-8 Functions as a Matricellular Modulator of Cell Adhesion. Journal of Biological Chemistry, 2001. 276(33): p. 31285-31295.

283. Nishi, N., Galectin-8 modulates neutrophil function via interaction with integrin alpha M. Glycobiology, 2003. 13: p. 755-763.

284. Dong, S. and R.C. Hughes, Macrophage surface glycoproteins binding to galectin-3 (Mac-2-antigen). Glycoconj J, 1997. 14(2): p. 267-74.

285. Mataresse, P., Galectin-3 overexpression protects from apoptosis by improving cell adhesion properties. Int. J. Cancer, 2000. 85: p. 545-554.

286. Le Marer, N. and R.C. Hughes, Effects of the carbohydrate-binding protein galectin-3 on the invasiveness of human breast carcinoma cells. J. Cell Physiol., 1996. 168: p. 51-58.

287. O'Driscoll, L., Galectin-3 expression alters adhesion, motility and invasion in a lung cell line (DLKP), in vitro. Anticancer Res., 2002. 22: p. 3117-3125.

288. Bresalier, R.S., Metastasis of human colon cancer is altered by modifying expression of the [beta]-galactoside-binding protein galectin 3. Gastroenterology, 1998. 115: p. 287-296.

289. Inufusa, H., Role of galectin-3 in adenocarcinoma liver metastasis. Int. J. Oncol., 2001. 19: p. 913-919.

290. Glinsky, V.V., et al., Synthetic galectin-3 inhibitor increases metastatic cancer cell sensitivity to taxol-induced apoptosis in vitro and in vivo. Neoplasia, 2009. 11(9): p. 901-9.

291. Jackson, E.L., et al., The Differential Effects of Mutant p53 Alleles on Advanced Murine Lung Cancer. Cancer Research, 2005. 65(22): p. 10280-10288.

292. Takenaka, Y., T. Fukumori, and A. Raz, Galectin-3 and metastasis. Glycoconjugate Journal, 2002. 19(7): p. 543-549.

293. Bresalier*, R.S., et al., Metastasis of human colon cancer is altered by modifying expression of the β-galactoside-binding protein galectin 3. Gastroenterology, 1998. 115(2): p. 287-296.

294. Yu, L.-G., The oncofetal Thomsen–Friedenreich carbohydrate antigen in cancer progression. Glycoconjugate Journal, 2007. 24(8): p. 411-420.

295. Nagy, N., et al., Galectin-8 expression decreases in cancer compared with normal and dysplastic human colon tissue and acts significantly on human colon cancer cell migration as a suppressor. Gut, 2002. 50(3): p. 392-401.

296. Zick, Y., et al., Role of galectin-8 as a modulator of cell adhesion and cell growth. Glycoconjugate Journal, 2002. 19(7): p. 517-526.

297. Lamar, J.M., Stern, P., Liu, H., Schindler, J.W., Jiang, Z. and Hynes, R.O., The Hippo pathway target, YAP, promotes metastasis through its TEAD interaction domain. Proc. Natl. Acad. Sci. USA, 2012. manuscript in press.

298. Stern, P., et al., A system for Cre-regulated RNA interference in vivo. Proceedings of the National Academy of Sciences, 2008. 105(37): p. 13895-13900.

299. Kim, Y. and A. Varki, Perspectives on the significance of altered glycosylation of glycoproteins in cancer. Glycoconjugate Journal, 1997. 14(5): p. 569-576.

300. Dennis, J.W., M. Granovsky, and C.E. Warren, Glycoprotein glycosylation and cancer progression. Biochimica et Biophysica Acta (BBA) - General Subjects, 1999. 1473(1): p. 21-34.

301. Hakomori, S., Glycosylation defining cancer malignancy: New wine in an old bottle. Proceedings of the National Academy of Sciences, 2002. 99(16): p. 10231-10233.

302. Hakomori, S.-i., Tumor Malignancy Defined by Aberrant Glycosylation and Sphingo(glyco)lipid Metabolism. Cancer Research, 1996. 56(23): p. 5309-5318.

303. Burger, M.M., Surface changes in transformed cells detected by lectins. Fed Proc, 1973. 32(1): p. 91-101.

304. Singh, R. and D. Bandyopadhyay, MUC1: a target molecule for cancer therapy. Cancer Biol Ther, 2007. 6(4): p. 481-6.

305. Taylor-Papadimitriou, J., et al., MUC1 and cancer. Biochimica et Biophysica Acta (BBA) - Molecular Basis of Disease, 1999. 1455(2–3): p. 301-313.

306. Yuan, Z., et al., Down-regulation of MUC1 in cancer cells inhibits cell migration by promoting E-cadherin/catenin complex formation. Biochem Biophys Res Commun, 2007. 362(3): p. 740-6.

307. Lakshminarayanan, V., et al., Immune recognition of tumor-associated mucin MUC1 is achieved by a fully synthetic aberrantly glycosylated MUC1 tripartite vaccine. Proc Natl Acad Sci U S A, 2012. 109(1): p. 261-6.

308. Beatson, R.E., J. Taylor-Papadimitriou, and J.M. Burchell, MUC1 immunotherapy. Immunotherapy, 2010. 2(3): p. 305-27.

309. Tarp, M.A. and H. Clausen, Mucin-type O-glycosylation and its potential use in drug and vaccine development. Biochim Biophys Acta, 2008. 1780(3): p. 546-63.

310. Ueda, K., Glycoproteomic strategies: from discovery to clinical application of cancer carbohydrate biomarkers. Proteomics Clin Appl, 2013.

311. Springer, G.F., Immunoreactive T and Tn epitopes in cancer diagnosis, prognosis, and immunotherapy. J Mol Med (Berl), 1997. 75(8): p. 594-602.

312. Cao, Y., et al., Expression of Thomsen-Friedenreich-related antigens in primary and metastatic colorectal carcinomas. A reevaluation. Cancer, 1995. 76(10): p. 1700-8.

313. Cao, Y., et al., Thomsen-Friedenreich-related carbohydrate antigens in normal adult human tissues: a systematic and comparative study. Histochem Cell Biol, 1996. 106(2): p. 197-207.

314. Goletz, S., et al., Thomsen-Friedenreich antigen: the "hidden" tumor antigen. Adv Exp Med Biol, 2003. 535: p. 147-62.

315. Irazoqui, F.J., et al., Correlative fine specificity of several Thomsen-Friedenreich disaccharide-binding proteins with an effect on tumor cell proliferation. J Biochem, 2001. 130(1): p. 33-7.

316. Springer, G.F., T and Tn, general carcinoma autoantigens. Science, 1984. 224(4654): p. 1198-206.

317. Shigeoka, H., et al., Inhibition of liver metastases from neuraminidase-treated colon 26 cells by an anti-Thomsen-Friedenreich-specific monoclonal antibody. Tumour Biol, 1999. 20(3): p. 139-46.

318. Glinsky, V.V., et al., The Role of Thomsen-Friedenreich Antigen in Adhesion of Human Breast and Prostate Cancer Cells to the Endothelium. Cancer Research, 2001. 61(12): p. 4851-4857.

319. Glinsky, V.V., et al., Intravascular Metastatic Cancer Cell Homotypic Aggregation at the Sites of Primary Attachment to the Endothelium. Cancer Research, 2003. 63(13): p. 3805-3811.

320. Wolf, M.F., et al., Increased expression of Thomsen-Friedenreich antigens during tumor progression in breast cancer patients. Tumour Biol, 1988. 9(4): p. 190-4.

321. MacLean, G.D., et al., Active immunization of human ovarian cancer patients against a common carcinoma (Thomsen-Friedenreich) determinant using a synthetic carbohydrate antigen. J Immunother (1991), 1992. 11(4): p. 292-305.

322. Slovin, S.F., et al., Thomsen-Friedenreich (TF) antigen as a target for prostate cancer vaccine: clinical trial results with TF cluster (c)-KLH plus QS21 conjugate vaccine in patients with biochemically relapsed prostate cancer. Cancer Immunol Immunother, 2005. 54(7): p. 694-702.

323. Ragupathi, G., Carbohydrate antigens as targets for active specific immunotherapy. Cancer Immunol Immunother, 1996. 43(3): p. 152-7.

324. Kurtenkov, O., et al., IgG immune response to tumor-associated carbohydrate antigens (TF, Tn, alphaGal) in patients with breast cancer: impact of neoadjuvant chemotherapy and relation to the survival. Exp Oncol, 2005. 27(2): p. 136-40.

325. Yu, L.-G., et al., Galectin-3 Interaction with Thomsen-Friedenreich Disaccharide on Cancer-associated MUC1 Causes Increased Cancer Cell Endothelial Adhesion. Journal of Biological Chemistry, 2007. 282(1): p. 773-781.

326. Delorge, S., et al., Correlation of galectin-3/galectin-3-binding sites with low differentiation status in head and neck squamous cell carcinomas. Otolaryngol Head Neck Surg, 2000. 122(6): p. 834-41.

327. Bian, C.F., et al., Structural basis for distinct binding properties of the human galectins to Thomsen-Friedenreich antigen. PLoS ONE, 2011. 6(9): p. e25007.

328. Khaldoyanidi, S.K., et al., MDA-MB-435 Human Breast Carcinoma Cell Homo- and Heterotypic Adhesion under Flow Conditions Is Mediated in Part by Thomsen-Friedenreich Antigen-Galectin-3 Interactions. Journal of Biological Chemistry, 2003. 278(6): p. 4127-4134.

329. Reticker-Flynn, N.E., et al., A combinatorial extracellular matrix platform identifies cell-extracellular matrix interactions that correlate with metastasis. Nat Commun, 2012. 3: p. 1122.

330. Functional Glycomics Gateway, in Consortium for Functional Glycomics. 2010.

331. Cárcamo, C., et al., Galectin-8 binds specific β1 integrins and induces polarized spreading highlighted by asymmetric lamellipodia in Jurkat T cells. Experimental Cell Research, 2006. 312(4): p. 374-386.

332. Saravanan, C., et al., Galectin-3 promotes lamellipodia formation in epithelial cells by interacting with complex N-glycans on α3β1 integrin. Journal of Cell Science, 2009. 122(20): p. 3684-3693.

333. Lityńska, A., et al., Differences of alpha3beta1 integrin glycans from different human bladder cell lines. Acta biochimica Polonica, 2000. 47(2): p. 427-434.

334. Bellis, S.L., Variant glycosylation: an underappreciated regulatory mechanism for β1 integrins. Biochimica et Biophysica Acta (BBA) - Biomembranes, 2004. 1663(1–2): p. 52-60.

335. Ju, T., et al., Regulation of protein O-glycosylation by the endoplasmic reticulum–localized molecular chaperone Cosmc. The Journal of Cell Biology, 2008. 182(3): p. 531-542.

336. Wang, Y., et al., Cosmc is an essential chaperone for correct protein O-glycosylation. Proceedings of the National Academy of Sciences, 2010. 107(20): p. 9228-9233.

337. The Cancer Genome Atlas, Lung Carcinoma DNA Copy Number Data. The Cancer Genome Atlas, 2011.

338. Cheever, M.A., et al., The Prioritization of Cancer Antigens: A National Cancer Institute Pilot Project for the Acceleration of Translational Research. Clinical Cancer Research, 2009. 15(17): p. 5323-5337.

339. Hanisch, F.G. and T. Ninkovic, Immunology of O-glycosylated proteins: approaches to the design of a MUC1 glycopeptide-based tumor vaccine. Curr Protein Pept Sci, 2006. 7(4): p. 307-15.

340. Deck, M.B., et al., MHC-Restricted, Glycopeptide-Specific T Cells Show Specificity for Both Carbohydrate and Peptide Residues. The Journal of Immunology, 1999. 162(8): p. 4740-4744.

341. Avci, F.Y., et al., A mechanism for glycoconjugate vaccine activation of the adaptive immune system and its implications for vaccine design. Nat Med, 2011. 17(12): p. 1602-1609.

342. Werdelin, O., M. Meldal, and T. Jensen, Processing of glycans on glycoprotein and glycopeptide antigens in antigen-presenting cells. Proc Natl Acad Sci U S A, 2002. 99(15): p. 9611-3.

343. Gad, M., et al., Characterization of T cell hybridomas raised against a glycopeptide containing the tumor-associated T antigen, (betaGal (1-3) alphaGalNAc-O/Ser). Glycoconj J, 2002. 19(1): p. 59-65.

344. Galli-Stampino, L., et al., T-cell recognition of tumor-associated carbohydrates: the nature of the glycan moiety plays a decisive role in determining glycopeptide immunogenicity. Cancer Res, 1997. 57(15): p. 3214-22.

345. Springer, G.F., P.R. Desai, and I. Banatwala, Blood group MN antigens and precursors in normal and malignant human breast glandular tissue. J Natl Cancer Inst, 1975. 54(2): p. 335-9.

346. Zhao, Q., et al., Circulating Galectin-3 Promotes Metastasis by Modifying MUC1 Localization on Cancer Cell Surface. Cancer Research, 2009. 69(17): p. 6799-6806.

347. Rabinovich, G.A. and M.A. Toscano, Turning 'sweet' on immunity: galectin-glycan interactions in immune tolerance and inflammation. Nat Rev Immunol, 2009. 9(5): p. 338-352.

348. Tlsty, T.D. and L.M. Coussens, TUMOR STROMA AND REGULATION OF CANCER DEVELOPMENT. Annual Review of Pathology: Mechanisms of Disease, 2006. 1(1): p. 119-150.

349. Humphries, M.J., K.M. Yamada, and K. Olden, Investigation of the biological effects of anti-cell adhesive synthetic peptides that inhibit experimental metastasis of B16-F10 murine melanoma cells. The Journal of Clinical Investigation, 1988. 81(3): p. 782-790.

350. Mantovani, A., et al., Cancer-related inflammation. Nature, 2008. 454(7203): p. 436-444.

351. Lin, E.Y., et al., Macrophages regulate the angiogenic switch in a mouse model of breast cancer. Cancer Res, 2006. 66(23): p. 11238-46.

352. De Palma, M., et al., Tie2 identifies a hematopoietic lineage of proangiogenic monocytes required for tumor vessel formation and a mesenchymal population of pericyte progenitors. Cancer Cell, 2005. 8(3): p. 211-26.

353. Nozawa, H., C. Chiu, and D. Hanahan, Infiltrating neutrophils mediate the initial angiogenic switch in a mouse model of multistage carcinogenesis. Proc Natl Acad Sci U S A, 2006. 103(33): p. 12493-8.

354. Coussens, L.M., et al., Inflammatory mast cells up-regulate angiogenesis during squamous epithelial carcinogenesis. Genes Dev, 1999. 13(11): p. 1382-97.

355. Murray, P.J. and T.A. Wynn, Protective and pathogenic functions of macrophage subsets. Nat Rev Immunol, 2011. 11(11): p. 723-37.

356. Mantovani, A. and A. Sica, Macrophages, innate immunity and cancer: balance, tolerance, and diversity. Curr Opin Immunol, 2010. 22(2): p. 231-7.

357. Lin, E.Y., et al., Colony-stimulating factor 1 promotes progression of mammary tumors to malignancy. J Exp Med, 2001. 193(6): p. 727-40.

358. Marigo, I., et al., Tumor-induced tolerance and immune suppression by myeloid derived suppressor cells. Immunol Rev, 2008. 222: p. 162-79.

359. Youn, J.-I., et al., Subsets of Myeloid-Derived Suppressor Cells in Tumor-Bearing Mice. The Journal of Immunology, 2008. 181(8): p. 5791-5802.

360. Yang, L., et al., Abrogation of TGF beta signaling in mammary carcinomas recruits Gr-1+CD11b+ myeloid cells that promote metastasis. Cancer Cell, 2008. 13(1): p. 23-35.

361. Acharyya, S., et al., A CXCL1 Paracrine Network Links Cancer Chemoresistance and Metastasis. Cell, 2012. 150(1): p. 165-178.

362. Qian, B., et al., A distinct macrophage population mediates metastatic breast cancer cell extravasation, establishment and growth. PLoS ONE, 2009. 4(8): p. e6562.

363. Hiratsuka, S., et al., Tumour-mediated upregulation of chemoattractants and recruitment of myeloid cells predetermines lung metastasis. Nat Cell Biol, 2006. 8(12): p. 1369-75.

364. Hiratsuka, S., et al., The S100A8-serum amyloid A3-TLR4 paracrine cascade establishes a pre-metastatic phase. Nat Cell Biol, 2008. 10(11): p. 1349-55.

365. Zlotnik, A., A.M. Burkhardt, and B. Homey, Homeostatic chemokine receptors and organ-specific metastasis. Nat Rev Immunol, 2011. 11(9): p. 597-606.

366. Rabinovich, G.A., et al., Functions of cell surface galectin-glycoprotein lattices. Curr Opin Struct Biol, 2007. 17(5): p. 513-20.

367. Brewer, C.F., M.C. Miceli, and L.G. Baum, Clusters, bundles, arrays and lattices: novel mechanisms for lectin-saccharide-mediated cellular interactions. Curr Opin Struct Biol, 2002. 12(5): p. 616-23.

368. Perillo, N.L., et al., Apoptosis of T cells mediated by galectin-1. Nature, 1995. 378(6558): p. 736-739.

369. Pace, K.E., et al., Restricted receptor segregation into membrane microdomains occurs on human T cells during apoptosis induced by galectin-1. J Immunol, 1999. 163(7): p. 3801-11.

370. Zhu, C., et al., The Tim-3 ligand galectin-9 negatively regulates T helper type 1 immunity. Nat Immunol, 2005. 6(12): p. 1245-52.

371. Garin, M.I., et al., Galectin-1: a key effector of regulation mediated by CD4+CD25+ T cells. Blood, 2007. 109(5): p. 2058-65.

372. Kubach, J., et al., Human CD4+CD25+ regulatory T cells: proteome analysis identifies galectin-10 as a novel marker essential for their anergy and suppressive function. Blood, 2007. 110(5): p. 1550-8.

373. Demetriou, M., et al., Negative regulation of T-cell activation and autoimmunity by Mgat5 N-glycosylation. Nature, 2001. 409(6821): p. 733-9.

374. Chen, I.J., H.L. Chen, and M. Demetriou, Lateral compartmentalization of T cell receptor versus CD45 by galectin-N-glycan binding and microfilaments coordinate basal and activation signaling. J Biol Chem, 2007. 282(48): p. 35361-72.

375. Toscano, M.A., et al., Differential glycosylation of TH1, TH2 and TH-17 effector cells selectively regulates susceptibility to cell death. Nat Immunol, 2007. 8(8): p. 825-34.

376. Demotte, N., et al., Restoring the association of the T cell receptor with CD8 reverses anergy in human tumor-infiltrating lymphocytes. Immunity, 2008. 28(3): p. 414-24.

377. Stillman, B.N., et al., Galectin-3 and galectin-1 bind distinct cell surface glycoprotein receptors to induce T cell death. J Immunol, 2006. 176(2): p. 778-89.

378. Fukumori, T., et al., CD29 and CD7 mediate galectin-3-induced type II T-cell apoptosis. Cancer Res, 2003. 63(23): p. 8302-11.

379. Gauthier, L., et al., Galectin-1 is a stromal cell ligand of the pre-B cell receptor (BCR) implicated in synapse formation between pre-B and stromal cells and in pre-BCR triggering. Proc Natl Acad Sci U S A, 2002. 99(20): p. 13014-9.

380. Rossi, B., et al., Clustering of pre-B cell integrins induces galectin-1-dependent pre-B cell receptor relocalization and activation. J Immunol, 2006. 177(2): p. 796-803.

381. Acosta-Rodriguez, E.V., et al., Galectin-3 mediates IL-4-induced survival and differentiation of B cells: functional cross-talk and implications during Trypanosoma cruzi infection. J Immunol, 2004. 172(1): p. 493-502.

382. Clark, A.G., et al., Multifunctional regulators of cell growth are differentially expressed in anergic murine B cells. Mol Immunol, 2007. 44(6): p. 1274-85.

383. Partridge, E.A., et al., Regulation of cytokine receptors by Golgi N-glycan processing and endocytosis. Science, 2004. 306(5693): p. 120-4.

384. Breuilh, L., et al., Galectin-3 modulates immune and inflammatory responses during helminthic infection: impact of galectin-3 deficiency on the functions of dendritic cells. Infect Immun, 2007. 75(11): p. 5148-57.

385. Barrionuevo, P., et al., A novel function for galectin-1 at the crossroad of innate and adaptive immunity: galectin-1 regulates monocyte/macrophage physiology through a nonapoptotic ERK-dependent pathway. J Immunol, 2007. 178(1): p. 436-45.

386. Vasta, G.R., Roles of galectins in infection. Nat Rev Micro, 2009. 7(6): p. 424-438.

387. Mey, A., et al., The animal lectin galectin-3 interacts with bacterial lipopolysaccharides via two independent sites. J Immunol, 1996. 156(4): p. 1572-7.

388. Sato, S. and J. Nieminen, Seeing strangers or announcing "danger": Galectin-3 in two models of innate immunity. Glycoconjugate Journal, 2002. 19(7-9): p. 583-591.

389. Baum, L.G., et al., Synthesis of an endogeneous lectin, galectin-1, by human endothelial cells is up-regulated by endothelial cell activation. Glycoconj J, 1995. 12(1): p. 63-8.

390. Thijssen, V.L., S. Hulsmans, and A.W. Griffioen, The galectin profile of the endothelium: altered expression and localization in activated and tumor endothelial cells. Am J Pathol, 2008. 172(2): p. 545-53.

391. Fulcher, J.A., et al., Galectin-1 co-clusters CD43/CD45 on dendritic cells and induces cell activation and migration through Syk and protein kinase C signaling. J Biol Chem, 2009. 284(39): p. 26860-70.

392. Hsu, D.K., et al., Endogenous galectin-3 is localized in membrane lipid rafts and regulates migration of dendritic cells. J Invest Dermatol, 2009. 129(3): p. 573-83.

393. Thiemann, S. and L. Baum, The Road Less Traveled: Regulation of Leukocyte Migration Across Vascular and Lymphatic Endothelium by Galectins. Journal of Clinical Immunology, 2011. 31(1): p. 2-9.

394. Sano, H., et al., Human Galectin-3 Is a Novel Chemoattractant for Monocytes and Macrophages. The Journal of Immunology, 2000. 165(4): p. 2156-2164.

395. Sato, S., et al., Role of galectin-3 as an adhesion molecule for neutrophil extravasation during streptococcal pneumonia. J Immunol, 2002. 168(4): p. 1813-22.

396. Colnot, C., et al., Maintenance of granulocyte numbers during acute peritonitis is defective in galectin-3-null mutant mice. Immunology, 1998. 94(3): p. 290-296.

397. Zuberi, R.I., et al., Critical role for galectin-3 in airway inflammation and bronchial hyperresponsiveness in a murine model of asthma. Am J Pathol, 2004. 165(6): p. 2045-53.

398. Hsu, D.K., et al., Targeted Disruption of the Galectin-3 Gene Results in Attenuated Peritoneal Inflammatory Responses. The American Journal of Pathology, 2000. 156(3): p. 1073-1083.

399. Nieminen, J., et al., Role of galectin-3 in leukocyte recruitment in a murine model of lung infection by Streptococcus pneumoniae. J Immunol, 2008. 180(4): p. 2466-73.

400. Bhaumik, P., et al., Galectin-3 facilitates neutrophil recruitment as an innate immune response to a parasitic protozoa cutaneous infection. J Immunol, 2013. 190(2): p. 630-40.

401. Matsushita, N., et al., Requirement of divalent galactoside-binding activity of ecalectin/galectin-9 for eosinophil chemoattraction. J Biol Chem, 2000. 275(12): p. 8355-60.

402. La, M., et al., A novel biological activity for galectin-1: inhibition of leukocyte-endothelial cell interactions in experimental inflammation. Am J Pathol, 2003. 163(4): p. 1505-15.

403. Rabinovich, G.A., et al., Evidence of a role for galectin-1 in acute inflammation. Eur J Immunol, 2000. 30(5): p. 1331-9.

404. Norling, L.V., et al., Inhibitory control of endothelial galectin-1 on in vitro and in vivo lymphocyte trafficking. FASEB J, 2008. 22(3): p. 682-90.

405. Liu, F.T., et al., Expression and function of galectin-3, a beta-galactoside-binding lectin, in human monocytes and macrophages. Am J Pathol, 1995. 147(4): p. 1016-28.

406. Yamaoka, A., et al., A human lectin, galectin-3 (epsilon bp/Mac-2), stimulates superoxide production by neutrophils. The Journal of Immunology, 1995. 154(7): p. 3479-87.

407. Karlsson, A., et al., Galectin-3 activates the NADPH-oxidase in exudated but not peripheral blood neutrophils. Blood, 1998. 91(9): p. 3430-8.

408. Almkvist, J., et al., Lipopolysaccharide-induced gelatinase granule mobilization primes neutrophils for activation by galectin-3 and formylmethionyl-Leu-Phe. Infect Immun, 2001. 69(2): p. 832-7.

409. Feuk-Lagerstedt, E., et al., Identification of CD66a and CD66b as the major galectin-3 receptor candidates in human neutrophils. J Immunol, 1999. 163(10): p. 5592-8.

410. Fernandez, G.C., et al., Galectin-3 and soluble fibrinogen act in concert to modulate neutrophil activation and survival: involvement of alternative MAPK pathways. Glycobiology, 2005. 15(5): p. 519-27.

411. Kuwabara, I. and F.T. Liu, Galectin-3 promotes adhesion of human neutrophils to laminin. J Immunol, 1996. 156(10): p. 3939-44.

412. Stowell, S.R., et al., Differential roles of galectin-1 and galectin-3 in regulating leukocyte viability and cytokine secretion. J Immunol, 2008. 180(5): p. 3091-102.

413. Sano, H., et al., Critical role of galectin-3 in phagocytosis by macrophages. J Clin Invest, 2003. 112(3): p. 389-97.

414. MacKinnon, A.C., et al., Regulation of Alternative Macrophage Activation by Galectin-3. The Journal of Immunology, 2008. 180(4): p. 2650-2658.

415. Fenczik, C.A., et al., Complementation of dominant suppression implicates CD98 in integrin activation. Nature, 1997. 390(6655): p. 81-5.

416. Nishi, N., et al., Galectin-8 modulates neutrophil function via interaction with integrin αM. Glycobiology, 2003. 13(11): p. 755-763.

417. Zhang, G.J. and I. Adachi, Serum interleukin-6 levels correlate to tumor progression and prognosis in metastatic breast carcinoma. Anticancer research, 1999. 19(2B): p. 1427-1432.

418. Blay, J.-Y., et al., Serum Level of Interleukin 6 as a Prognosis Factor in Metastatic Renal Cell Carcinoma. Cancer Research, 1992. 52(12): p. 3317-3322.

419. Nakashima, J., et al., Serum Interleukin 6 as a Prognostic Factor in Patients with Prostate Cancer. Clinical Cancer Research, 2000. 6(7): p. 2702-2706.

420. Ueda, T., E. Shimada, and T. Urakawa, Serum levels of cytokines in patients with colorectal cancer: Possible involvement of interleukin-6 and interleukin-8 in hematogenous metastasis. Journal of Gastroenterology, 1994. 29(4): p. 423-429.

421. Campbell, J.P., et al., Stimulation of host bone marrow stromal cells by sympathetic nerves promotes breast cancer bone metastasis in mice. PLoS Biol, 2012. 10(7): p. e1001363.

422. Schneider, J.G., S.R. Amend, and K.N. Weilbaecher, Integrins and bone metastasis: integrating tumor cell and stromal cell interactions. Bone, 2011. 48(1): p. 54-65.

423. Gocheva, V., et al., IL-4 induces cathepsin protease activity in tumor-associated macrophages to promote cancer growth and invasion. Genes Dev, 2010. 24(3): p. 241-55.

424. Mohamed, M.M., et al., Interleukin-6 Increases Expression and Secretion of Cathepsin B by Breast Tumor-Associated Monocytes. Cellular Physiology and Biochemistry, 2010. 25(2-3): p. 315-324.

425. Balan, V., P. Nangia-Makker, and A. Raz, Galectins as Cancer Biomarkers. Cancers, 2010. 2(2): p. 592-610.

426. Radisky, D.C., Epithelial-mesenchymal transition. Journal of Cell Science, 2005. 118(19): p. 4325-4326.

427. Kalluri, R. and R.A. Weinberg, The basics of epithelial-mesenchymal transition. The Journal of Clinical Investigation, 2009. 119(6): p. 1420-1428.

428. Thiery, J.P. and J.P. Sleeman, Complex networks orchestrate epithelial-mesenchymal transitions. Nat Rev Mol Cell Biol, 2006. 7(2): p. 131-142.

429. Yang, J. and R.A. Weinberg, Epithelial-Mesenchymal Transition: At the Crossroads of Development and Tumor Metastasis. Developmental Cell, 2008. 14(6): p. 818-829.

430. Thiery, J.P., Epithelial-mesenchymal transitions in tumour progression. Nat Rev Cancer, 2002. 2(6): p. 442-454.

431. Wu, Y. and B.P. Zhou, New insights of epithelial-mesenchymal transition in cancer metastasis. Acta Biochim Biophys Sin (Shanghai), 2008. 40(7): p. 643-50.

432. Gunasinghe, N.P., et al., Mesenchymal-epithelial transition (MET) as a mechanism for metastatic colonisation in breast cancer. Cancer Metastasis Rev, 2012. 31(3-4): p. 469-78.

433. Yang, J., et al., Twist, a Master Regulator of Morphogenesis, Plays an Essential Role in Tumor Metastasis. Cell, 2004. 117(7): p. 927-939.

434. Park, S.-M., et al., The miR-200 family determines the epithelial phenotype of cancer cells by targeting the E-cadherin repressors ZEB1 and ZEB2. Genes & Development, 2008. 22(7): p. 894-907.

435. Kudo-Saito, C., et al., Cancer Metastasis Is Accelerated through Immunosuppression during Snail-Induced EMT of Cancer Cells. Cancer Cell, 2009. 15(3): p. 195-206.

436. Munger, J.S., et al., Interactions between growth factors and integrins: latent forms of transforming growth factor-beta are ligands for the integrin alphavbeta1. Mol Biol Cell, 1998. 9(9): p. 2627-38.

437. Loeys, B.L., et al., Aneurysm syndromes caused by mutations in the TGF-beta receptor. N Engl J Med, 2006. 355(8): p. 788-98.

438. Elenbaas, B., et al., Human breast cancer cells generated by oncogenic transformation of primary mammary epithelial cells. Genes & Development, 2001. 15(1): p. 50-65.

439. Zuk, A. and E.D. Hay, Expression of β1 integrins changes during transformation of avian lens epithelium to mesenchyme in collagen gels. Developmental Dynamics, 1994. 201(4): p. 378-393.

440. Maschler, S., et al., Tumor cell invasiveness correlates with changes in integrin expression and localization. 2005. 24(12): p. 2032-2041.

441. Mamuya, F.A. and M.K. Duncan, aV integrins and TGF-beta-induced EMT: a circle of regulation. J Cell Mol Med, 2012. 16(3): p. 445-55.

442. Kim, K.K., et al., Epithelial cell α3β1 integrin links β-catenin and Smad signaling to promote myofibroblast formation and pulmonary fibrosis. The Journal of Clinical Investigation, 2009. 119(1): p. 213-224.

443. Alisson-Silva, F., et al., Increase of o-glycosylated oncofetal fibronectin in high glucose-induced epithelial-mesenchymal transition of cultured human epithelial cells. PLoS ONE, 2013. 8(4): p. e60471.

444. Guan, F., K. Handa, and S.-i. Hakomori, Specific glycosphingolipids mediate epithelial-to-mesenchymal transition of human and mouse epithelial cell lines. Proceedings of the National Academy of Sciences, 2009. 106(18): p. 7461-7466.

445. Park, J.H., et al., Polypeptide N-acetylgalactosaminyltransferase 6 disrupts mammary acinar morphogenesis through O-glycosylation of fibronectin. Neoplasia, 2011. 13(4): p. 320-6.

446. Zhang, H., et al., Engagement of I-Branching β-1, 6-N-Acetylglucosaminyltransferase 2 in Breast Cancer Metastasis and TGF-β Signaling. Cancer Research, 2011. 71(14): p. 4846-4856.

447. Lorke, D. and P. Moller, The early appearance of fibronectin in the course of metastatic tumor growth in lymph nodes. J Cancer Res Clin Oncol, 1985. 109(1): p. 65-71.

448. Maniotis, A.J., et al., Vascular channel formation by human melanoma cells in vivo and in vitro: vasculogenic mimicry. Am J Pathol, 1999. 155(3): p. 739-52.

449. Humphries, M.J., K. Olden, and K.M. Yamada, A synthetic peptide from fibronectin inhibits experimental metastasis of murine melanoma cells. Science, 1986. 233(4762): p. 467-70.

450. Ruoslahti, E., Fibronectin and its integrin receptors in cancer. Adv Cancer Res, 1999. 76: p. 1-20.

451. Clark, E.A., et al., Genomic analysis of metastasis reveals an essential role for RhoC. Nature, 2000. 406(6795): p. 532-535.

452. Gumireddy, K., et al., In vivo selection for metastasis promoting genes in the mouse. Proceedings of the National Academy of Sciences, 2007. 104(16): p. 6696-6701.

453. Schwartz, R.E., et al., ECM array reveals unique ECM combinations that support pluripotency and clarifies the role of ECM driven signaling in Stem Cell Pluripotency. Submitted, 2013.

454. Yu, M.K., J. Park, and S. Jon, Targeting strategies for multifunctional nanoparticles in cancer imaging and therapy. Theranostics, 2012. 2(1): p. 3-44.

455. Keefe, A.D., S. Pai, and A. Ellington, Aptamers as therapeutics. Nat Rev Drug Discov, 2010. 9(7): p. 537-550.

456. Peletskaya, E.N., et al., Identification of peptide sequences that bind the Thomsen-Friedenreich cancer-associated glycoantigen from bacteriophage peptide display libraries. Mol Divers, 1996. 2(1-2): p. 13-8.

457. Peletskaya, E.N., et al., Characterization of peptides that bind the tumor-associated Thomsen-Friedenreich antigen selected from bacteriophage display libraries. J Mol Biol, 1997. 270(3): p. 374-84.

458. Glinsky, V.V., et al., Effects of Thomsen-Friedenreich Antigen-specific Peptide P-30 on β-Galactoside-mediated Homotypic Aggregation and Adhesion to the Endothelium of MDA-MB-435 Human Breast Carcinoma Cells. Cancer Research, 2000. 60(10): p. 2584-2588.

459. Landon, L., et al., Combinatorial Evolution of High-Affinity Peptides That Bind to the Thomsen-Friedenreich Carcinoma Antigen. Journal of Protein Chemistry, 2003. 22(2): p. 193-204.

460. Ruoslahti, E., S.N. Bhatia, and M.J. Sailor, Targeting of drugs and nanoparticles to tumors. The Journal of Cell Biology, 2010. 188(6): p. 759-768.

461. Rudin, M. and R. Weissleder, Molecular imaging in drug discovery and development. Nat Rev Drug Discov, 2003. 2(2): p. 123-131.

462. Tempany Cc, M.B.J., Advances in biomedical imaging. JAMA, 2001. 285(5): p. 562-567.

463. Harisinghani, M.G., et al., Noninvasive Detection of Clinically Occult Lymph-Node Metastases in Prostate Cancer. New England Journal of Medicine, 2003. 348(25): p. 2491-2499.

464. Ghosh, D., et al., M13-templated magnetic nanoparticles for targeted in vivo imaging of prostate cancer. Nat Nano, 2012. 7(10): p. 677-682.

465. Massoud, T.F. and S.S. Gambhir, Molecular imaging in living subjects: seeing fundamental biological processes in a new light. Genes & Development, 2003. 17(5): p. 545-580.

466. Strong, V., et al., Laparoscopic Adrenalectomy for Isolated Adrenal Metastasis. Annals of Surgical Oncology, 2007. 14(12): p. 3392-3400.

467. Pastorino, U., et al., Long-term results of lung metastasectomy: Prognostic analyses based on 5206 cases. The Journal of Thoracic and Cardiovascular Surgery, 1997. 113(1): p. 37-49.

468. MacDermed, D.M., R.R. Weichselbaum, and J.K. Salama, A rationale for the targeted treatment of oligometastases with radiotherapy. Journal of Surgical Oncology, 2008. 98(3): p. 202-206.

469. Weichselbaum, R.R. and S. Hellman, Oligometastases revisited. Nat Rev Clin Oncol, 2011. 8(6): p. 378-382.